2016-05-01

Micro-CT Inspection of Impact Damage in Carbon/Epoxy Rods

Lindsey Charlene Cahoon
Brigham Young University

Micro-CT Inspection of Impact Damage in Carbon/Epoxy Rods

Lindsey Charlene Cahoon

A thesis submitted to the faculty of
Brigham Young University
in partial fulfillment of the requirements for the degree of

Master of Science

David W. Jensen, Chair
Paul W. Richards
David T. Fullwood

Department of Civil and Environmental Engineering

Brigham Young University

May 2016

ABSTRACT

Micro-CT Inspection of Impact Damage in Carbon/Epoxy Rods

Lindsey Charlene Cahoon
Department of Civil and Environmental Engineering, BYU
Master of Science

Various configurations of unidirectional carbon/epoxy composite rods were impacted radially, inspected using micro-CT scanning equipment, and tested in axial compression to measure the residual strength after impact. This data was used to correlate the relationship between impact energy, residual strength, and the peak crack area and total crack volume along the length of the specimens. These specimens represent local members of open three-dimensional composite lattice structures (e.g., based on isogrid or IsoTruss® geometries) that are continuously fabricated using advanced three-dimensional braiding techniques. The specimens were radially impacted with 2.5 J (1.9 ft-lbs), 5.0 J (3.7 ft-lbs), 7.5 J (5.6 ft-lbs), 10 J (7.4 ft-lb), 15 J (11 ft-lbs), and 20 J (15 ft-lbs) of energy, and compared to undamaged control specimens. The unidirectional core specimens were 8 mm (5/16") in diameter and were consolidated with various sleeve configurations and materials. Sleeves differed in types (bi-directional braided sleeves or unidirectional spiral wraps), nominal sleeve coverage of the core fibers (full or half), and sleeve material (Nomex Thread or Dunstone Hi-Shrink Tape). The unsupported length of the specimens used in this research was 50.8 mm (2") to ensure a strength-controlled compression failure rather than a failure due to buckling.

After impact, the specimens were scanned using a micro-CT scanner at resolutions of 50 and 35 microns and subsequently tested in axial compression. The micro-CT scan images were analyzed to measure the crack areas along the specimen. From this analysis, the peak crack area and total crack volume along the length of the specimen was calculated. Similar to past research, as the impact energy increases, the residual compression-strength-after-impact decreases. As the impact energy increases, specimens with shrink tape sleeves had the largest increase in peak crack area and overall crack volume while specimens with full spiral sleeves had the lowest increase in peak crack area and overall crack volume. A bimodal increase is evident in the peak crack area and total crack volume over the length of the specimen where specimens impacted at 15 J (11 ft-lbs) showed the highest peak crack area across all sleeve types. There is a slight correlation between the increase in peak crack area and overall crack volume and the decrease in residual compression strength after impact. Shrink Tape, while yielding a higher quality specimen with greater compression strength prior to impact, did not protect the specimens against damage due to impact as well as other sleeve types. This was shown by the large decrease in residual compression strength after impact and increase in peak crack area and overall crack volume as the impact energy increased.

Keywords: Micro-CT, carbon/epoxy, impact, residual strength, NDI

ACKNOWLEDGEMENTS

I would like to thank all of the people who have supported me through this process. The members of my committee, especially Dr. David Jensen, who provided guidance and support throughout this whole process, thank-you for your patience and the opportunity to be a part of this research. I gratefully acknowledge the support of the University of Utah, who provided the micro-CT scanner used in this research. Additional technical support and assistance was offered by Dave Anderson, Rodney Mayo, and Samer Merchant.

I would also like to thank my committee for the time they spent reviewing and helping me to submit a high quality thesis. I appreciate the other student employees of the Center for Advanced Structural Composites who helped throughout this process. Their assistance was invaluable and saved me countless hours. A special thanks to all Brigham Young University faculty and staff who assisted in my graduate education.

I would also like to gratefully acknowledge my family and friends for their moral support along the way; especially for my husband Nathan for his help, patience, and love throughout the entire process. This has been an incredible experience for me academically, professionally, and personally and I owe thanks to my Heavenly Father for the blessing of this opportunity.

TABLE OF CONTENTS

LIST OF TABLES

LIST OF FIGURES

1 INTRODUCTION

The damage tolerance of unidirectional carbon composite rods wrapped with various sleeve types has been examined using nondestructive methods. These elements represent the local members of open 3-dimensional lattice structures, such as based on IsoTruss®, IsoBeam™, or isogrid technologies [1], using a continuous manufacturing process. When impacted, the compression strengths of these members are affected differently according to sleeve type, sleeve coverage, and sleeve material. This research applied nondestructive inspection methods to quantify the damage caused by impact and correlate the damage level with the residual compression strength of the members, which in turn helps to predict the local response of IsoTruss structures when impacted during use. Though there have been tests done to determine the residual Compression Strength After (radial) Impact (CSAI), there has been no attempt to quantify the degree of damage caused by impact. This research expands on the work conducted by Allen [2] and Sika [3] by using micro computed tomography (micro-CT) scanning equipment to quantify the damage caused by impact and how it correlates with CSAI and other methods of calculating damage.

1.1 Description of IsoTruss Grid Structure

IsoTruss structures offer a lightweight and efficient alternative to typical steel, wood, aluminum, and even other traditional composite structures [3]. The unique geometry of the

IsoTruss not only poses an advantage when it comes to inspection, but also enables tremendous support to axial, torsional, and flexural loads. The IsoTruss is composed of longitudinal and helical members. Typical orientations with joints for the longitudinal and helical members are illustrated in Figure 1.1. The members of the IsoTruss structure are composed of transversely isotropic composite tows consolidated with sleeves. In IsoTruss structures, axial loads are carried primarily by the longitudinal members, while torsional loads are carried by the helical members. Helical members also increase the overall stiffness of the structure by reducing the un-braced length of the longitudinal members, which can be susceptible to buckling [2] [4].

Figure 1.1 Example of a Typical IsoTruss Structure

1.2 Related Research

IsoTruss structures have been studied in a variety of applications using several geometric variations and materials. The equations used in IsoTruss analysis were documented by Kesler [5] and Winkel [6]. The nomenclature and geometric definitions of IsoTruss structures were defined by Scoresby [7] and McCune [8]. Kesler [9] showed how automated processes could be used to manufacture complex IsoTruss geometries. Kesler also showed that by increasing the number of

braiders, the scatter in stiffness and strength can be significantly decreased. Also, compression failure has been shown to absorb significantly more energy than buckling failure. Stoutis [9] tested primarily undamaged pultruded carbon/epoxy rods under compression in a similar method to the compression tests completed for this thesis. Stoutis observed that the primary failure mode of the undamaged specimens was micro buckling. Sleeves were used in this research to confine the core fibers and minimize the effects of micro buckling. Hansen [10] used different sleeve types to consolidate core fibers. The resulting increase in stiffness and strength of the specimens was a significant improvement. Hansen's specimens were also undamaged, which lead to the conclusion that braided sleeves exhibited a more consistent strength and stiffness than other sleeve types. In Wisnom's research [11] carbon fiber rods were post-wrapped with aramid sleeves and tested for residual CSAI.

The research performed in this thesis used Nomex Thread and Shrink Tape sleeves to consolidate the core fibers, and these sleeves were applied prior to curing the composite materials in the core. The sleeves improve performance by confining the cores and preventing splitting of the core fibers. The current research on the CSAI of carbon/epoxy composites complements the previous CSAI research on basalt/epoxy composites by Allen [2], the research on the CSAI of carbon/epoxy and fiberglass/epoxy composites by Sika [3], and buckling strength research of longer members on basalt, carbon, and fiberglass fiber/epoxy composites conducted by Embley [4].

Conclusions from related research by Sika [3] [12] are as follows:

1. Co-curing dry fiber over unidirectional fiber/epoxy composites effectively consolidates the core materials.

2. When undamaged, the ultimate compression strength and compression stiffness are virtually unaffected by sleeve type (braid or spiral) and coverage (half or full), as demonstrated by Hansen [13], for carbon/epoxy composites with carbon/epoxy braided sleeves.
3. Increasing aramid sleeve coverage increases the damage tolerance of carbon fiber and fiberglass epoxy composite elements.
4. Not surprisingly, ultimate compression strength and compression stiffness after impact decrease with increasing impact energy levels.

Considerable research has been performed using non-destructive methods to quantify the damage due to impact of composites. Bull [14] compared multi-scale 3-dimensional x-ray tomographic inspection techniques for assessing impact damage in carbon fiber composites. In this study, synchrotron radiation computed tomography (SRCT) and computed laminography (SRCL) offer scans with the highest image quality, allowing damage micromechanisms to be studied. Wright [15] used high-resolution SRCT to show the role of intra-laminar cracks and delamination in localizing fiber fractures. While SRCT provide scans with the higher image quality, Bull [14] showed that micro-CT was found to offer efficient routine assessment of damage at mesoscopic and macroscopic levels in engineering-scale test coupons and relatively high spatial resolutions on trimmed-down samples.

Micro-CT offers valuable detail for understanding the three-dimensional macroscopic and mesoscopic extent of impact damage with reliable detection of the extent of cracks being illustrated. Micro-CT also offers scan volumes up to tens of centimeters, capturing entire impact sites in a single scan. Crupi [16] used micro-CT scans to analyze the effect of the low-velocity impact response for laminated composites including PVC foam sandwiches, aluminum foam, and

honeycomb sandwiches. The scans were able to show the failure mode and the internal damage of the impacted composites. The non-destructive analysis for this research used micro-CT to determine the behavior and distribution of the internal damage (i.e., cracks) and to correlate this damage with the residual strength of impacted specimens.

1.3 **Scope of Investigation**

The focus of this research was to assess the internal damage caused by radial impact to individual unidirectional carbon fiber members with various consolidation sleeves. This information was obtained by using a micro-CT scanner. These scans show internal cracks along the length of the specimen which were quantified and correlated with the reduction in compression strength of the specimens. Specifically, this research answers the following design questions about carbon fiber/epoxy composite rods under axial compression after radial impact:

- How much damage is introduced in cylindrical unidirectional carbon/epoxy composites at various levels of impact energy ranging up to 20 J (15 ft-lbs)?
- Can the extent of damage be adequately represented by peak crack area and/or overall crack volume from a micro-CT scan?
- How does sleeve configuration affect the damage (as quantified by peak crack area and/or overall crack volume) caused by the radial impact?
- How well does the extent of damage (as quantified by micro-CT scans) in cylindrical unidirectional carbon/epoxy composite rods after impact correlate with residual compression strength?
- How well do specimens consolidated using Nomex Thread resist damage compared to specimens consolidated with Kevlar?

- How well do specimens consolidated using Shrink Tape resist damage compared to specimens consolidated with Kevlar?

To answer these questions, unidirectional carbon fiber epoxy composite rods with different sleeve types and patterns were fabricated, impacted with various energy levels, scanned with a micro-CT scanner, and tested in axial compression. The unidirectional core specimens were 8 mm (5/16") in diameter and the unsupported length of the specimens were 50.8 mm (2") to ensure a strength-controlled compression failure rather than a failure due to buckling. Specimens were consolidated with various sleeve configurations and materials. Sleeves differed in type (bi-directional braided sleeves or unidirectional spiral wraps), nominal sleeve coverage of the core fibers (full or half), and sleeve material (Nomex Thread or Dunstone Hi-Shrink Tape). Specimens were radially impacted about mid-length with impact energy levels of 2.5 J (1.9 ft-lbs), 5.0 J (3.7 ft-lbs), 7.5 J (5.6 ft-lbs), 10 J (7.4 ft-lbs), 15 J (11 ft-lbs), and 20 J (15 ft-lbs). Specimens were scanned using a micro-CT scanner at resolutions of 35 and 50 microns. The micro-CT scan images were used to quantify the peak crack area and overall crack volume along the length of the specimens. The specimens were tested in axial compression to determine the CSAI. This data was compared to correlate internal damage, impact, and residual strength.

1.4 **Thesis Overview**

The experimental approach and data reduction procedure are described in Chapter Two. Chapter Three contains the test results for the micro-CT images for each test configuration. Chapter Four summarizes the averages for the micro-CT test data. Chapter Five contains the test results for each test configuration for the compression testing of the samples. Chapter Six summarizes the averages for the compression test results. Chapters Seven and Eight discusses the test results for all tested materials and correlates the impact, micro-CT inspection and residual

strength of the carbon epoxy rods and Chapter Nine summarizes the final conclusions and provides recommendations.

2 EXPERIMENTAL APPROACH

This chapter details the test variables, manufacturing process, specimen preparation, and testing procedure used in this research.

2.1 Experimental Variables

Variables examined in this research include sleeve type, sleeve coverage, sleeve material, impact energy, and micro-CT scan resolution.

2.1.1 Specimen Geometry

The specimen diameter was based on previous research completed by Sika [3] who used a diameter of 8 mm (5/16 in) [3]. This diameter equates to a cross-sectional area of 50.3 mm^2 (0.0779 in^2). Sika's research was based on 79 tows of 12-k carbon fiber. Since this research used a larger tow size of 24-k carbon fiber, however, in order to obtain the same 8 mm (5/16 in) diameter, a total of 40 carbon/epoxy tows were used. Preliminary tests by Allen [2] determined the critical length of 50.8 mm (2.0 in) long specimens to be used in the current research. This unsupported length of carbon fiber epoxy composite rods ensured compression failure, rather than buckling. To allow room for bonding in end caps, an additional 38 mm (1.5 in) was added to the specimens' unsupported length. The total specimen length was therefore, 88.9 mm (3.5 in).

2.1.2 Core Materials

Unidirectional carbon/epoxy prepreg tows were selected for the specimen core material. The resulting unidirectional rods were consolidated with either Nomex Thread or Shrink Tape sleeves which were applied prior to curing. A list of each of the core materials, manufacturers, and type is shown in Table 2.1. The nominal mechanical properties for the core material are shown in Tables 2.2 [17].

Table 2.1 Core Material Specifications

Material	Manufacturer	Material Specification	Filament Diameter [in (µm)]	Filament Count per Tow
Carbon Fiber	Toray	T700SC-24K-50C	2.8E -04 (7.0)	24,000
Epoxy (Pre-Preg)	TCR Composites	UF3369-100	-	-

Table 2.2 Nominal Mechanical Properties of Core Material

Material	Modulus of Elasticity [Msi (GPa)]	Tensile Strength [ksi (MPa)]	Compressive Strength [ksi (MPa)]
T700/UF3369 Carbon/Epoxy Composite	20.0 (138)	370 (2551)	111 (765)

2.1.3 Consolidation Sleeve Materials

The two consolidation sleeve materials tested were Nomex Thread (size 415) and 1.3 cm (1/2”) wide strips of Dunstone Hi-Shrink Tape. Table 2.3 lists the nominal mechanical properties for the consolidation materials [18] [19]. The choice to use Nomex Thread rather than Kevlar, which was used in previous research, was based primarily on the extent of fraying that occurs in Kevlar during the manufacturing process. Nomex Thread is heat resistant and doesn’t fray. The only downside with the Nomex Thread was its low ultimate tensile strength. During the

manufacturing process, particularly for the braided sleeve, the thread broke repeatedly, requiring the thread to be retied. This resulted in a geometric inconsistency (i.e., bump) along the length of the specimen.

The other sleeve material used was a Dunstone Hi-Shrink Tape. In order to use the IsoTruss® machine to continuously apply the shrink tape sleeve, the bobbins were modified to dispense the Shrink Tape evenly without wrinkling the tape. The modified bobbin is shown in Figure 2.1.

Table 2.3 Mechanical Properties of Consolidation Materials

Material	Thickness [in]	Ultimate Tensile Strength [lbs]	Shrinkage [%]
Nomex Thread	0.0247	30.0	0
Dunstone Hi-Shrink Tape	0.005	-	20

Figure 2.1 Original Bobbin Used to Apply Thread (left); Bobbin Modification to Apply Shrink Tape Sleeve Shown with Shrink Tape (middle); and, Green Ribbon (right) to Improve Visualization

2.1.4 Sleeve Type and Coverage

The sleeve type was either bi-directional (asymmetric) braid wrap or unidirectional spiral wrap. Sleeve coverage ranged nominally from full to half. Figure 2.2 shows all five sleeve configurations (full spiral, half spiral, shrink tape, full braid, and half braid). In this research, specimens without sleeves were not considered, since the sleeves were needed to consolidate the specimens.

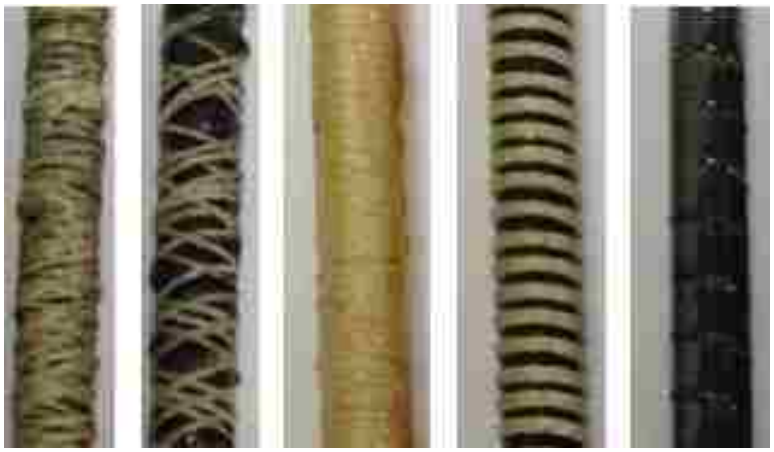

Figure 2.2 Sleeve Configurations (left to right): Full Spiral, Half Spiral, Shrink Tape, Full Braid and Half Braid

2.1.5 Impact Energy

For comparison purposes, the same impact energy levels that Allen [2] and Sika [3] used were repeated in this research. To better understand the internal damage that occurs as impact energy increases, however, a few more energy levels were added. The impact energies used were 2.5 J (1.9 ft-lbs), 5.0 J (3.7 ft-lbs), 7.5 J (5.6 ft-lbs), 10 J (7.4 ft-lbs), 15 J (11 ft-lbs), and 20 J (15 ft-lbs).

2.1.6 Test Matrix

The different test variables resulted in a total of thirty-five possible configurations, summarized in Table 2.4. Nominally, five specimens of each configuration were tested, for a total of 175 test specimens.

Table 2.4 Test Matrix

Material	Diameter [mm (in)]	Sleeve Type	Sleeve Coverage	Impact Energy [J (ft-lbs)]
Carbon	8 (5/16)	Braid	Full	0 (0.0)
				2.5 (1.9)
				5 (3.7)
				7.5 (5.6)
				10 (7.4)
				15 (11)
				20 (15)
			Half	0 (0.0)
				2.5 (1.9)
				5 (3.7)
				7.5 (5.6)
				10 (7.4)
				15 (11)
				20 (15)
		Spiral	Full	0 (0.0)
				2.5 (1.9)
				5 (3.7)
				7.5 (5.6)
				10 (7.4)
				15 (11)
				20 (15)
			Half	0 (0.0)
				2.5 (1.9)
				5 (3.7)
				7.5 (5.6)
				10 (7.4)
				15 (11)
				20 (15)
		Shrink Tape		0 (0.0)
				2.5 (1.9)
				5 (3.7)
				7.5 (5.6)
				10 (7.4)
				15 (11)
				20 (15)

2.2 Specimen Manufacturing

The specimens were fabricated on an advanced three-dimensional, prototype braiding machine developed specifically for the manufacture of IsoTruss, IsoBeam™ and isogrid type composite lattice structures (see Figure 2.3). For a complete and detailed report outlining the manufacturing method, creation of sleeve patterns, and consolidation, refer to Allen [2]. The member was kept in constant tension while cured in an in-line oven.

Figure 2.3: Test Specimen Being Manufactured on Prototype IsoTruss Machine

2.3 Final Specimen Preparation

This section contains a summary of the specimen preparation procedure. The steps were similar to research previously conducted by Sika [3], Allen [2], and Embley [4].

2.3.1 Specimen Cutting

Test materials were manufactured in approximately 1.2 m (4 ft) lengths. The specimens were cut to their proper length with a diamond-coated cutting blade, using a Leco CM-10 cutoff machine shown in Figure 2.4. The Leco Spectrum System 2000, was used to create a flat end

surface together with a special sanding fixture attachment. The attachment ensured a proper vertical alignment of specimens to polishing surface as shown in Figure 2.4.

Figure 2.4 Specimen Preparation Equipment: Cutting Jig with Diamond Tip Blade (left); and, Polisher with Vertical Aligning Attachment (right).

2.3.2 Label Notation

To improve statistical validity, a random number generator was used to assign the specimen's impact energy levels and testing order. Each specimen was labeled in the [N-FS2-5-10-35] notation. This example denotes a Nomex Thread [N] forming a full [F] spiral [S] wrap, fabricated in the 2nd batch [2], fifth specimen in the batch [5], impacted with 10 J (7.4 ft-lbs) of energy [10], and micro-CT scanned with a resolution of 35 microns [35]. The complete details of this notation (number and letter designation) for each of the test variables are listed in Table 2.5.

Table 2.5 Specimen Label Notation Convention

Sleeve Material	Nomex Thread	**N**
	Shrink Tape	**ST**
Sleeve Coverage	Full	**F**
	Half	**H**
Sleeve Type	Braid	**B**
	Spiral	**S**
Specimen Batch	Number	**1-5**
Specimen	Number	**1-10**
Impact Energy	0.0 J (0.0 ft-lbs)	**0**
	2.5 J (1.9 ft-lbs)	**2.5**
	5.0 J (3.7 ft-lbs)	**5**
	7.5 J (5.6 ft-lbs)	**7.5**
	10 J (7.4 ft-lbs)	**10**
	15 J (11 ft-lbs)	**15**
	20 J (15 ft-lbs)	**20**

2.4 Test Procedures

This section summarizes the impact, micro-CT, and compression test procedures. The impact and compression test procedures were conducted similarly to that of research by Allen [2], Embley [4], and Sika [3]. The micro-CT scanning procedure was first introduced in the current research.

2.4.1 Impact Test Procedure

Impact tests were performed using the Dynatup® 8200 drop weight impact test machine shown in Figure 2.5. Different levels of impact energy were achieved by adjusting the drop weight and height. The total impact energy provides a basis for comparison with the internal damage of the inflicted specimens from the micro-CT scans.

Figure 2.5: Dynatup(R) 8200 Drop Weight Impact Test Machine

Specimens were clamped in blocks fixed to a steel plate and radially impacted at mid-length with a cylindrical tup. The specimens were not bonded in end caps prior to impact as done in previous research because the end caps would have inhibited the readings from the micro-CT scan. The ends of the specimens were covered in two layers of masking tape, however, to help cushion the impact on the ends and prevent damage from occurring outside of the mid-point of the sample. The ends were clamped on the ends by v-blocks thus resulting in fixed-end conditions. This is a highly conservative approach compared to practical applications. Typically, three-dimensional lattice structures are comparatively flexible and dissipate impact energy through vibrations, resulting in less local damage to members at the site of impact.

2.4.2 Micro-CT Scanning Procedure

Several methods of non-destructive imaging were tested in preparation for this research including magnetic resonance imaging (MRI), X-ray, and micro-CT scanning. Because the specimens were solid, the hydrogen was too tightly bound and so there was no image that could be seen using an MRI. Though cracks could be seen using an X-ray, only one slice of the sample could be seen with each scan. A CT scanner uses x-rays and a series of detectors that rotate continuously around a patient. A General Electric EVS-RS9 micro-CT was used in this research because it allowed for three-dimensional internal visualization of the specimens. The micro-CT had a large area 165 mm X-ray camera and it incorporates a high-resolution 14-bit x-ray imaging detector with 4064 x 4064 pixels [20]. There were three available resolutions for the micro-CT scanner: 100 microns, 50 microns, and 35 microns. Three of the five specimens of each configuration were tested using the micro-CT scanner. Two of the three specimens were tested at 50 microns and one was tested at 35 microns. Each scan provided 1984 images of the cross-section along the length of the specimen. A random number generator was used to determine which specimens were tested at which resolution. Typical impacted specimens scanned at 50 and 35 micron resolutions are shown in Figures 2.6 and 2.7, respectively. While the 35 micron images are higher quality than the 50 micron scans, they also take longer to scan and for this analysis, the increase in image quality did not increase the accuracy of the crack area measurements.

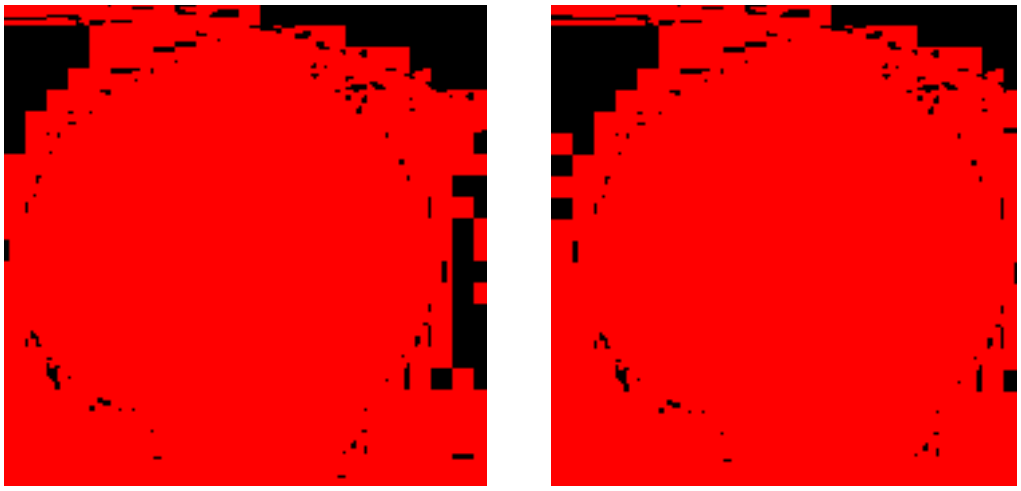

Figure 2.6 Axial View of Impacted Specimens: A) 50 Micron Resolution (left) B) 35 Micron Resolution (right)

In order to measure the crack area, the axial view of the specimen was first converted into a binary image where the black area indicated cracks. The number of black pixels was calculated and converted into an area. The peak crack area was the maximum area along the length of the specimen. These images were also used to quantify the overall crack volume by integrating the crack area along the length of each specimen. Figure 2.8 illustrates the steps in the process for calculating the crack area at that particular slice for a specimen scanned with 35 micro resolution.

Figure 2.7 Procedure for Quantifying Damage based on Micro-CT Scans: Initial Image (left); Binary Image (center); and, Crack Area (right)

2.4.3 Area, Fiber Volume, and Void Fraction Measurements

The micro-CT scanned images were used to determine the average cross-sectional areas of the samples. The cross-sectional areas were measured at three separate locations along the length of each specimen and averaged. These measurements were similar to the cross-sectional areas obtained using the Leco Olympus SZX12 microscope and Pax-it software. The cross-sectional areas for each specimen using the microscope and the micro-CT scanned images are listed in Appendix B.

To evaluate the effectiveness of the IsoTruss machine in producing quality members, fiber volume percentages were measured optically using the Leco Olympus GX51 microscope and Pax-it software. This software enabled 50X magnified pictures of the ends of each specimen to be recorded. Measurements were taken on one specimen from each batch for each sleeve configuration. The measurements were taken at three separate locations on each end of the specimen. A table summarizing the fiber volumes for the different configurations is provided in Appendix C, along with typical images used to obtain measurements. The void ratio was measured using the Leco Olympus SZX12 microscope and the Pax-it software for each batch of each configuration. Table 2.6 summarizes the average fiber volumes and void ratios for each sleeve configuration. A table summarizing the void ratio for the different specimens is in Appendix C.

Table 2.6 Average Void Ratios and Fiber Volume Fractions for Each Sleeve Types

Sleeve Type	Void Ratio [%]	Fiber Volume Fraction [%]
Full Braid	0.06	64.5
Half Braid	0.09	63.2
Full Spiral	0.04	62.0
Half Spiral	0.08	63.3
Shrink Tape	0.04	66.0

2.4.4 Compression Test Sample Preparation

Steel caps were bonded to each end of the specimens using Loctite 5-minute epoxy. End caps prevented splaying of the ends of each specimen when compressed; and allowed proper alignment in the test fixture by creating an even surface for uniform load distribution. A setting fixture specifically designed for this research was used to vertically align the specimens when bonding the end caps. Excess epoxy was cleaned off the ends using the Leco Spectrum System 2000 polishing machine.

2.4.5 Compression Test Procedure

Compression tests were performed on an 89 kN (20 kip) Instron Model 1321 universal testing machine, as shown in Figure 2.9. The test specimen receptacles were designed specifically to hold the end caps, making it quick and easy to align each specimen. The receptacles were clamped into the machine and tungsten-carbide pucks were used between the receptacles and the specimens to eliminate repeated use damage and to ensure uniform load introduction. The specimens were loaded at a stroke-controlled rate of 1.27 mm/min (0.05 in/min) as done in previous research [3]. Refer to Appendix A for a picture of each specimen after failure.

Figure 2.8: Instron Test Machine: Full Instron Test Machine (top left); Extensometer Attached to Specimen (center); and, Specimen Being Held by Test Specimen Receptacles (right)

2.5 **Data Reduction and Statistical Analysis**

This section details the data reduction and statistical analysis that was used on the compression test data. Natrella noted that “the argument for exclusion is that when a "good" measurement is excluded we simply lose some of the relevant information, with consequent decrease in precision and the introduction of some bias (both being theoretically computable); whereas, when a truly anomalous measurement is included it vitiates our results, biasing both the final average and the estimate of precision by unknown, and generally unknowable, amounts” [21]. For this purpose, Chauvenet’s criterion was used in prior research by Embley [4], Allen [2] and Sika [3], and was applied to identify which, if any, tests should be considered as outliers and therefore be excluded from the averages. This criterion provides an envelope based on a 1/2n probability, which is calculated using a specified ratio based on the number of samples (1.54 and 1.65 for 4 and 5 samples, respectively) in conjunction with the overall average, and standard deviation.

A range of probable values representing 90% reliability with 95% confidence are shown for the average stress-strain curves and the average ultimate strengths of each test configuration. Details of this statistical analysis procedure, including equations for computation of the lower and upper limit envelopes, were documented in previous related research by Embley [4].

3 MICRO-CT SCAN RESULTS

3.1 Overview

Detailed results for each of the thirty test configurations scanned using the micro-CT scanner are illustrated in this chapter. The undamaged specimens were not scanned. Tables summarizing the peak crack area and overall crack volume for each test configuration are followed by plots of the crack area as a function of the position relative to the impact location. The crack areas were averaged across the point of impact.

3.2 Full Braid Micro-CT Scan Results

Micro-CT scan results for full braid specimens impacted at 2.5 J (1.9 ft-lbs) are summarized in Table 3.1 and the corresponding crack area curves are shown in Figure 3.1.

Table 3.1 Peak Crack Area and Crack Volume of Full Braid, 2.5 J (1.9 ft-lbs) Impact

Specimen I.D.	Peak Crack Area [mm^2 (10^3 in^2)]		Crack Volume [mm^3 (10^3 in^3)]	
N-FB-5-1-2.5	0.27	(0.41)	22.6	(1.38)
N-FB-4-10-2.5	1.65	(2.56)	15.7	(0.96)
N-FB-4-3-2.5	0.09	(0.13)	2.40	(0.14)
Average 2.5 J	0.58	(0.90)	10.1	(0.61)

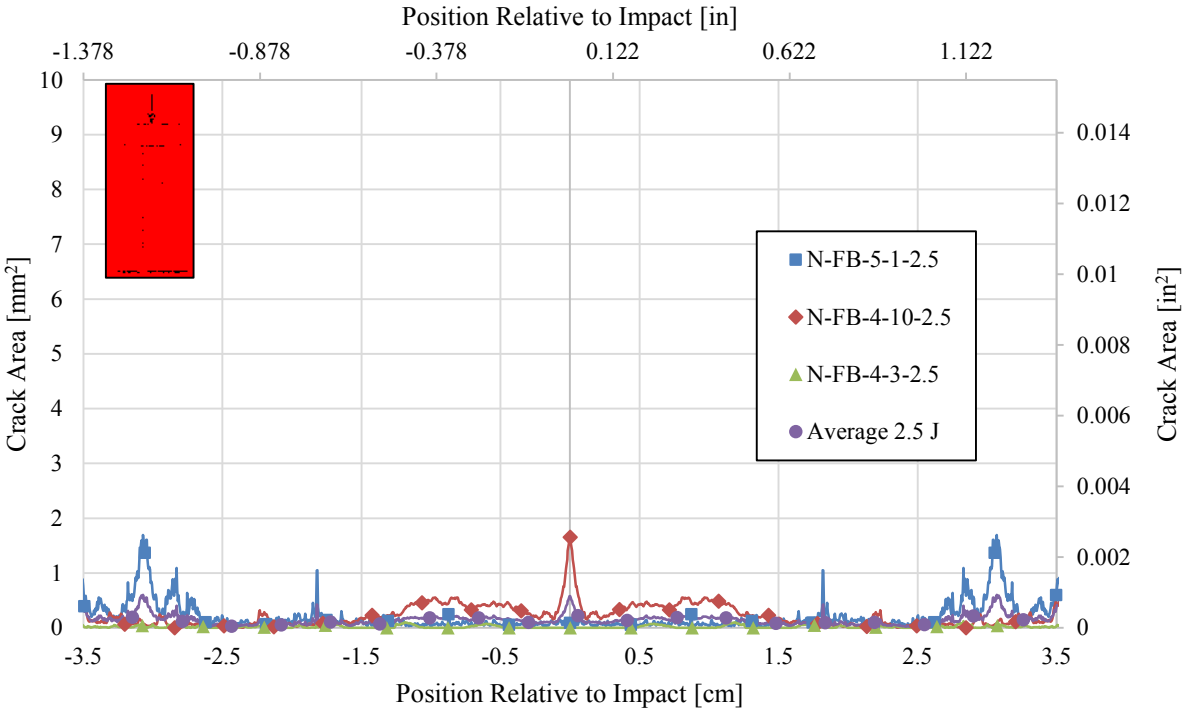

Figure 3.1 Average Crack Area as a Function of Distance from the Point of Impact for Full Braid, 2.5 J (1.9 ft-lbs) Impact

Micro-CT scan results for full braid specimens impacted at 5.0 J (3.7 ft-lbs) are summarized in Table 3.2 and the corresponding crack area curves are shown in Figure 3.2. Micro-CT scan results for full braid specimens impacted at 7.5 J (5.6 ft-lbs) are summarized in Table 3.3 and the corresponding crack area curves are shown in Figure 3.3.

Table 3.2 Peak Crack Area and Crack Volume of Full Braid, 5.0 J (3.7 ft-lbs) Impact

Specimen I.D.	Peak Crack Area [mm² (10^3 in²)]		Crack Volume [mm³ (10^3 in³)]	
N-FB-1-2-5.0	3.53	(5.46)	21.1	(1.28)
N-FB-4-4-5.0	0.03	(0.04)	8.16	(0.50)
N-FB-4-8-5.0	4.05	(6.27)	45.5	(2.78)
Average 5.0 J	2.51	(3.89)	19.7	(1.20)

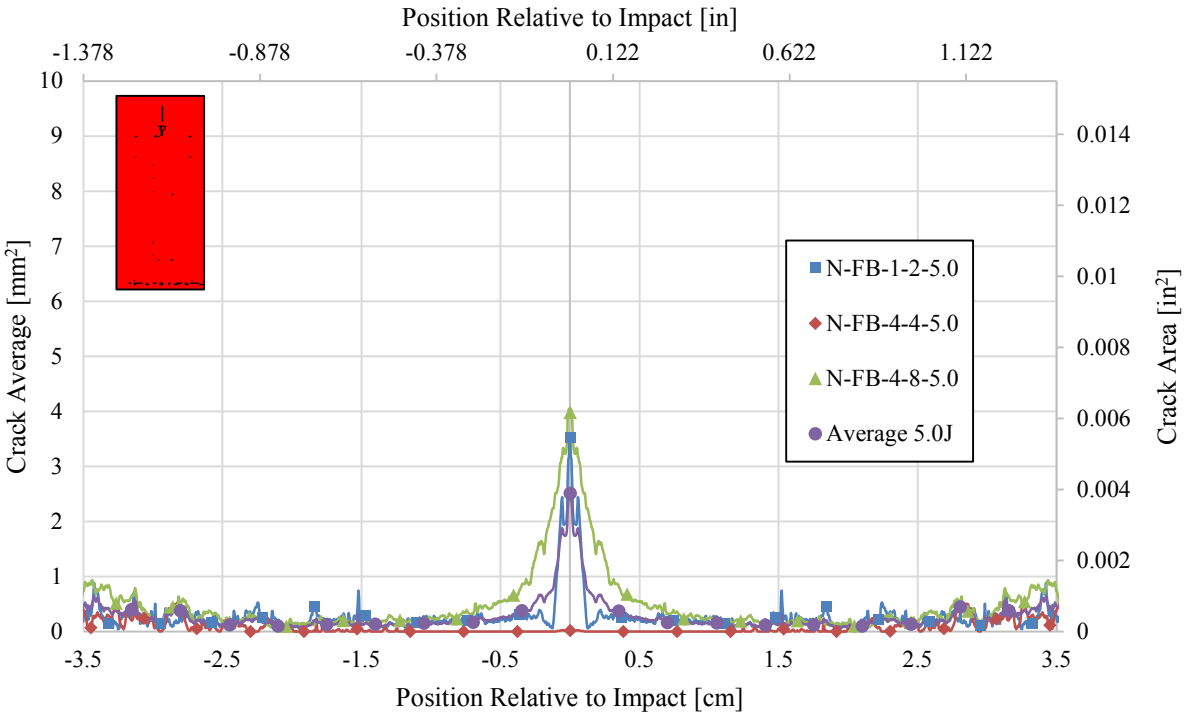

Figure 3.2 Average Crack Area as a Function of Distance from the Point of Impact for Full Braid, 5.0 J (3.7 ft-lbs) Impact

Table 3.3 Peak Crack Area and Crack Volume of Full Braid, 7.5 J (5.6 ft-lbs) Impact

Specimen I.D.	Peak Crack Area [mm^2 (10^3 in^2)]		Crack Volume [mm^3 (10^3 in^3)]	
N-FB-3-1-7.5	2.04	(3.17)	27.3	(1.67)
N-FB-1-4-7.5	4.33	(6.72)	65.3	(3.99)
N-FB-2-3-7.5	0.19	(0.29)	7.65	(0.47)
Average 7.5 J	2.12	(3.28)	26.6	(1.62)

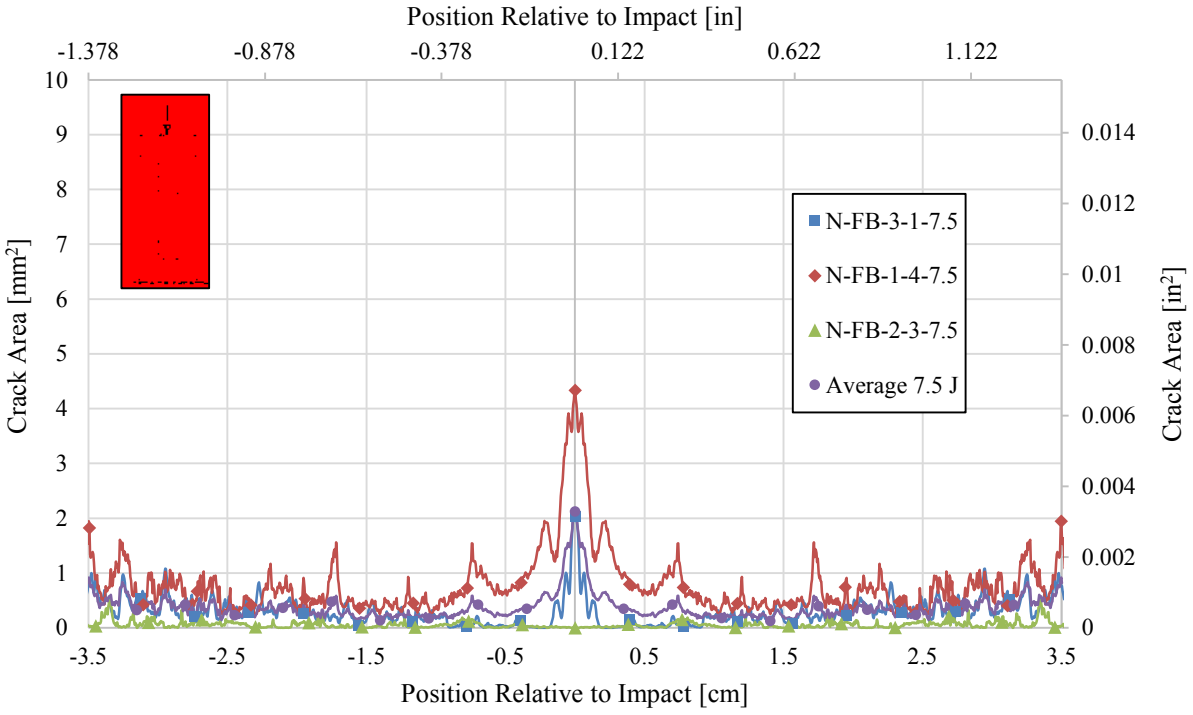

Figure 3.3 Average Crack Area as a Function of Distance from the Point of Impact for Full Braid, 7.5 J (5.6 ft-lbs) Impact

Micro-CT scan results for full braid specimens impacted at 10 J (7.4 ft-lbs) are summarized in Table 3.4 and the corresponding crack area curves are shown in Figure 3.4. Micro-CT scan results for full braid specimens impacted at 15 J (11 ft-lbs) are summarized in Table 3.5 and the corresponding crack area curves are shown in Figure 3.5.

Table 3.4 Peak Crack Area and Crack Volume of Full Braid, 10 J (7.4 ft-lbs) Impact

Specimen I.D.	Peak Crack Area [mm² (10^3 in²)]		Crack Volume [mm³ (10^3 in³)]	
N-FB-1-6-10.0	2.03	(3.14)	32.8	(2.00)
N-FB-3-8-10.0	0.74	(1.14)	30.1	(1.84)
N-FB-5-2-10.0	1.68	(2.60)	8.57	(0.52)
Average 10 J	1.48	(2.30)	18.6	(1.14)

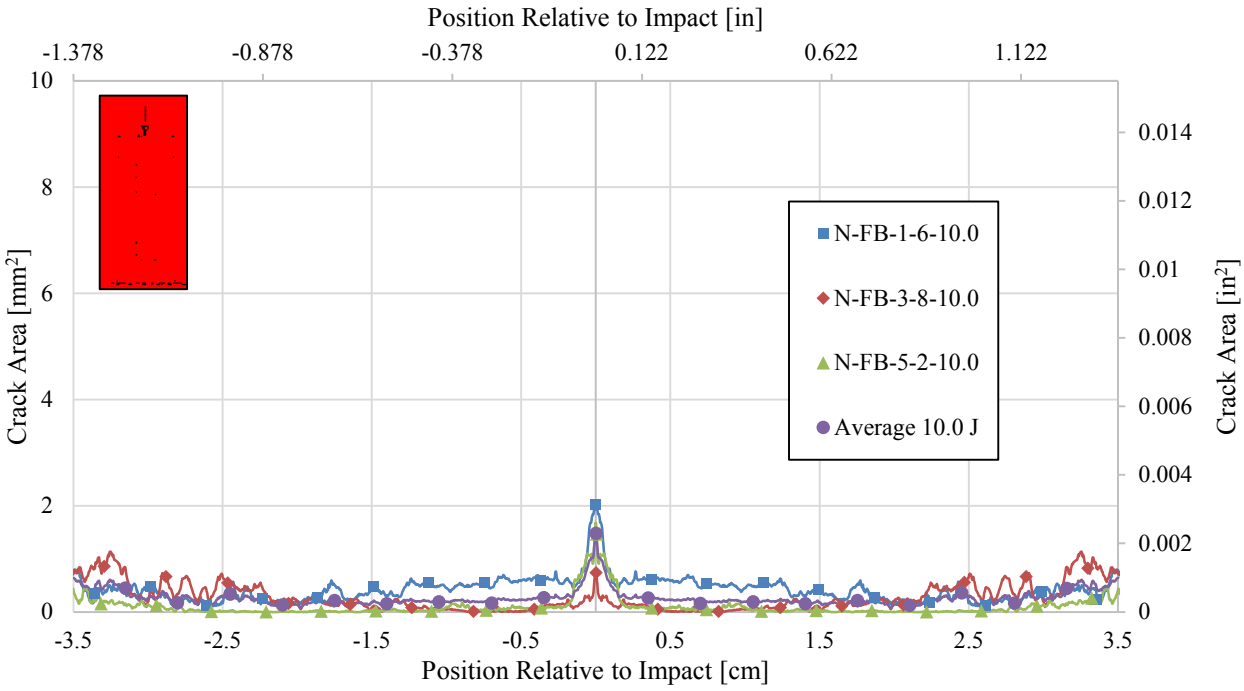

Figure 3.4 Average Crack Area as a Function of Distance from the Point of Impact for Full Braid, 10 J (7.4 ft-lbs) Impact

Table 3.5 Peak Crack Area and Crack Volume of Full Braid, 15 J (11 ft-lbs) Impact

Specimen I.D.	Peak Crack Area [mm^2 (10^3 in^2)]		Crack Volume [mm^3 (10^3 in^3)]	
N-FB-2-4-15.0	8.37	(13.0)	30.9	(1.89)
N-FB-2-1-15.0	4.24	(6.57)	77.4	(4.72)
N-FB-2-6-15.0	0.44	(0.68)	5.85	(0.36)
Average 15 J	4.35	(6.74)	37.2	(2.27)

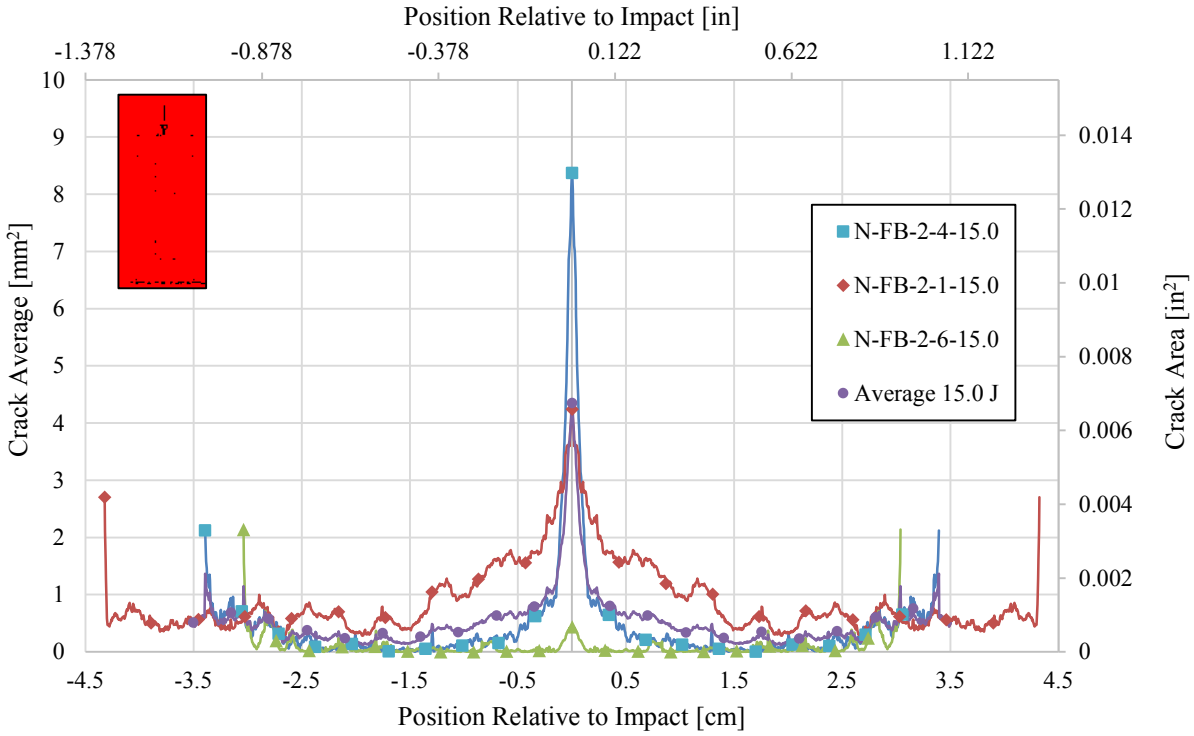

Figure 3.5 Average Crack Area as a Function of Distance from the Point of Impact for Full Braid, 15 J (11 ft-lbs) Impact

Micro-CT scan results for full braid specimens impacted at 20 J (15 ft-lbs) are summarized in Table 3.6 and the corresponding crack area curves are shown in Figure 3.6.

Table 3.6 Peak Crack Area and Crack Volume of Full Braid, 20 J (15 ft-lbs) Impact

Specimen I.D.	Peak Crack Area [mm² (10^3 in²)]		Crack Volume [mm³ (10^3 in³)]	
N-FB-4-2-20.0	5.91	(9.16)	154.9	(9.45)
N-FB-3-5-20.0	3.33	(5.16)	23.9	(1.46)
N-FB-3-6-20.0	2.26	(3.50)	121.9	(7.44)
Average 20 J	3.83	(5.94)	93.9	(5.73)

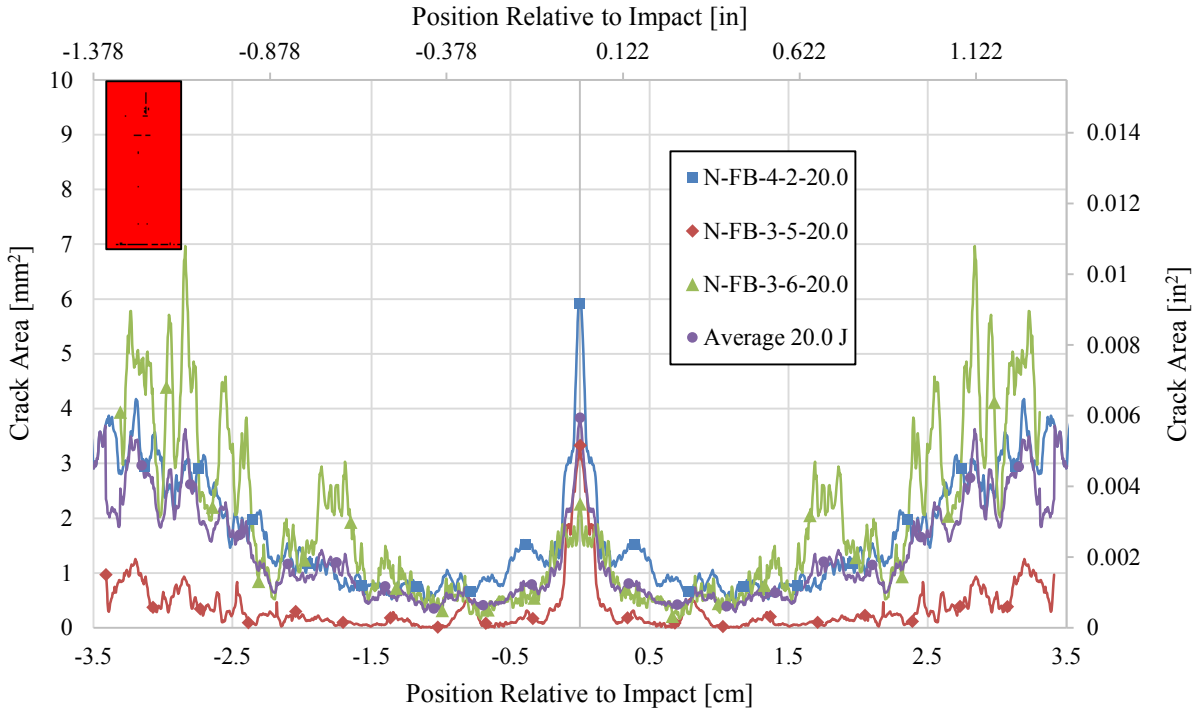

Figure 3.6 Average Crack Area as a Function of Distance from the Point of Impact for Full Braid, 20 J (15 ft-lbs) Impact

3.3 Half Braid Micro-CT Scan Results

The micro-CT scan results for half braid specimens impacted with 2.5 J (1.9 ft-lbs) are summarized in Table 5.7 and the corresponding crack area curves are shown in Figure 5.7.

Table 3.7 Peak Crack Area and Crack Volume of Half Braid, 2.5 J (1.9 ft-lbs) Impact

Specimen I.D.	Peak Crack Area [mm² (10^3 in²)]		Crack Volume [mm³ (10^3 in³)]	
N-HB-1-2-2.5	0.06	(0.10)	0.35	(0.02)
N-HB-1-7-2.5	0.47	(0.73)	5.26	(0.32)
N-HB-1-8-2.5	1.45	(2.25)	9.67	(0.59)
Average 2.5 J	0.55	(0.85)	5.09	(0.31)

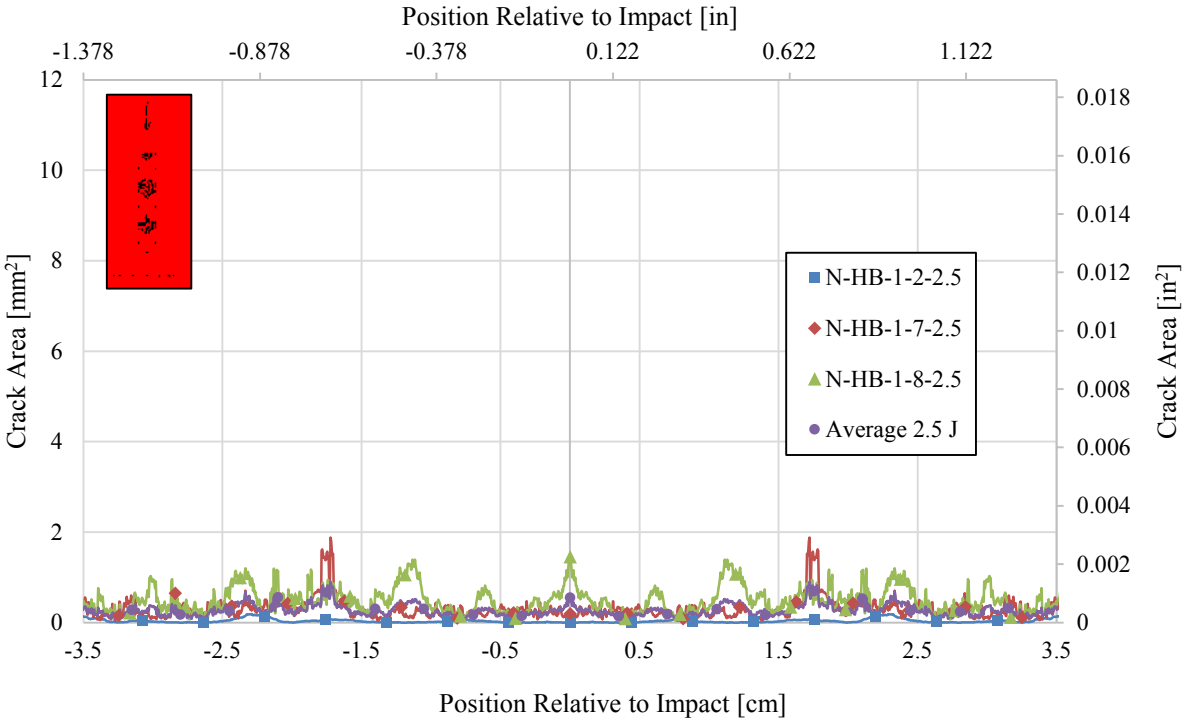

Figure 3.7 Average Crack Area as a Function of Distance from the Point of Impact for Half Braid, 2.5 J (1.9 ft-lbs) Impact

The micro-CT scan results for half braid specimens impacted with 5.0 J (3.7 ft-lbs) are summarized in Table 3.8 and the corresponding crack area curves are shown in Figure 3.8. The micro-CT scan results for half braid specimens impacted with 7.5 J (5.6 ft-lbs) are summarized in Table 3.9 and the corresponding crack area curves are shown in Figure 3.9.

Table 3.8 Peak Crack Area and Crack Volume of Half Braid, 5.0 J (3.7 ft-lbs) Impact

Specimen I.D.	Peak Crack Area [mm^2	(10^3 in^2)]	Crack Volume [mm^3	(10^3 in^3)]
N-HB-1-10-5.0	0.82	(1.27)	3.73	(0.23)
N-HB-2-2-5.0	0.76	(0.62)	10.2	(2.26)
N-HB-2-4-5.0	1.46	(2.26)	6.02	(0.37)
Average 5.0 J	1.00	(1.54)	6.66	(0.41)

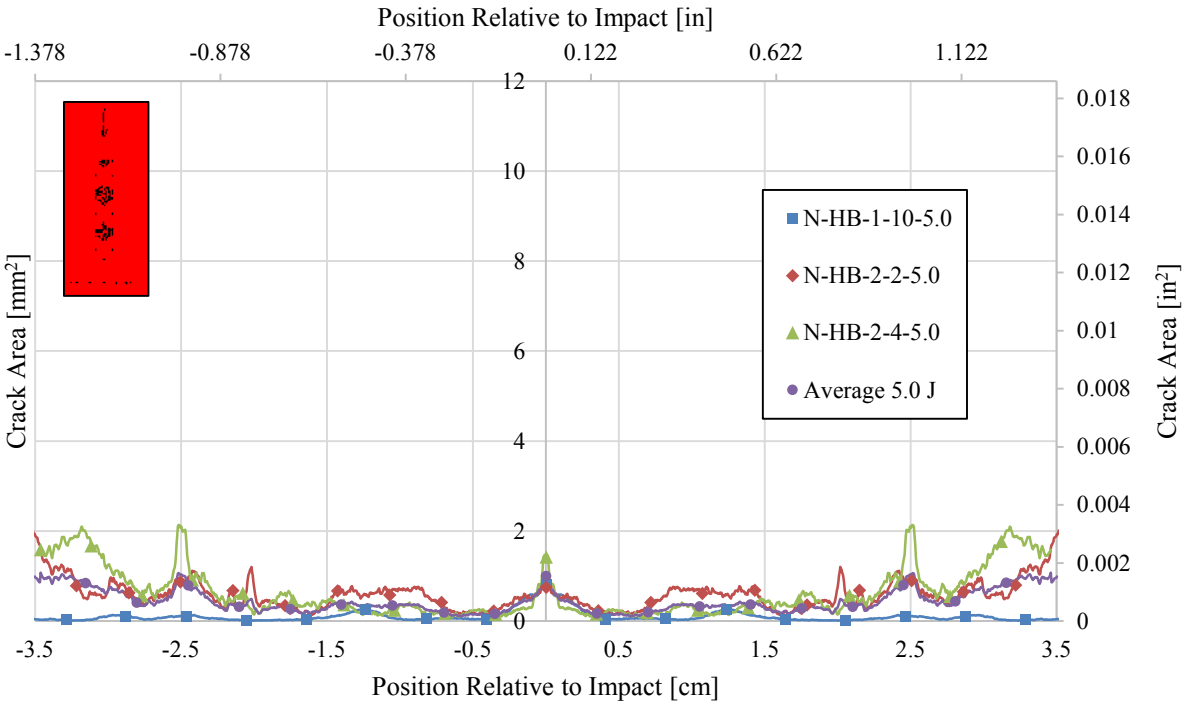

Figure 3.8 Average Crack Area as a Function of Distance from the Point of Impact for Half Braid, 5.0 J (3.7 ft-lbs) Impact

Table 3.9 Peak Crack Area and Crack Volume of Half Braid, 7.5 J (5.6 ft-lbs) Impact

Specimen I.D.	Peak Crack Area [mm² (10^3 in²)]		Crack Volume [mm³ (10^3 in³)]	
N-HB-1-9-7.5	1.63	(2.53)	12.6	(0.77)
N-HB-2-6-7.5	1.57	(2.43)	12.7	(0.77)
N-HB-3-11-7.5	2.60	(4.02)	12.9	(0.79)
Average 7.5 J	1.93	(3.00)	12.7	(0.78)

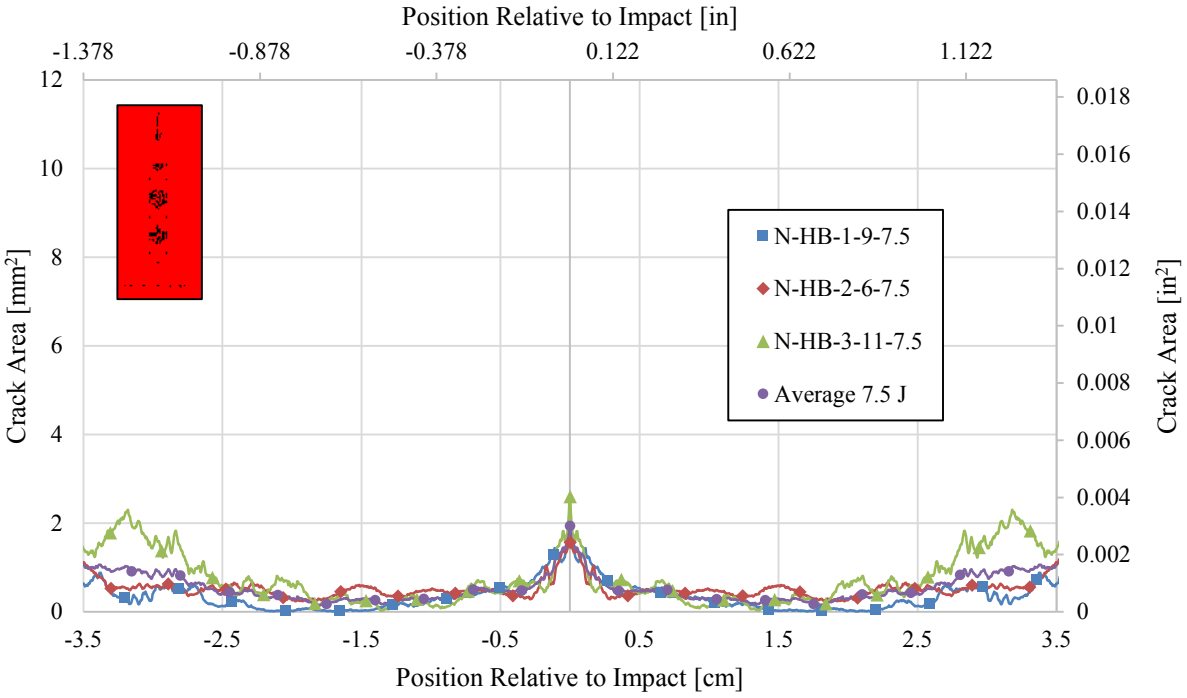

Figure 3.9 Average Crack Area as a Function of Distance from the Point of Impact for Half Braid, 7.5 J (5.6 ft-lbs) Impact

The micro-CT scan results for half braid specimens impacted with 10 J (7.4 ft-lbs) are summarized in Table 3.10 and the corresponding crack area curves are shown in Figure 3.10. The micro-CT scan results for half braid specimens impacted with 15 J (11 ft-lbs) are summarized in Table 3.11 and the corresponding crack area curves are shown in Figure 3.11.

Table 3.10 Peak Crack Area and Crack Volume of Half Braid, 10 J (7.4 ft-lbs) Impact

Specimen I.D.	Peak Crack Area [mm^2 (10^3 in^2)]		Crack Volume [mm^3 (10^3 in^3)]	
N-HB-1-5-10.0	2.98	(4.61)	16.0	(0.97)
N-HB-1-6-10.0	3.19	(4.94)	26.5	(1.62)
N-HB-2-3-10.0	3.31	(5.12)	16.1	(0.98)
Average 10 J	3.16	(4.89)	19.5	(1.19)

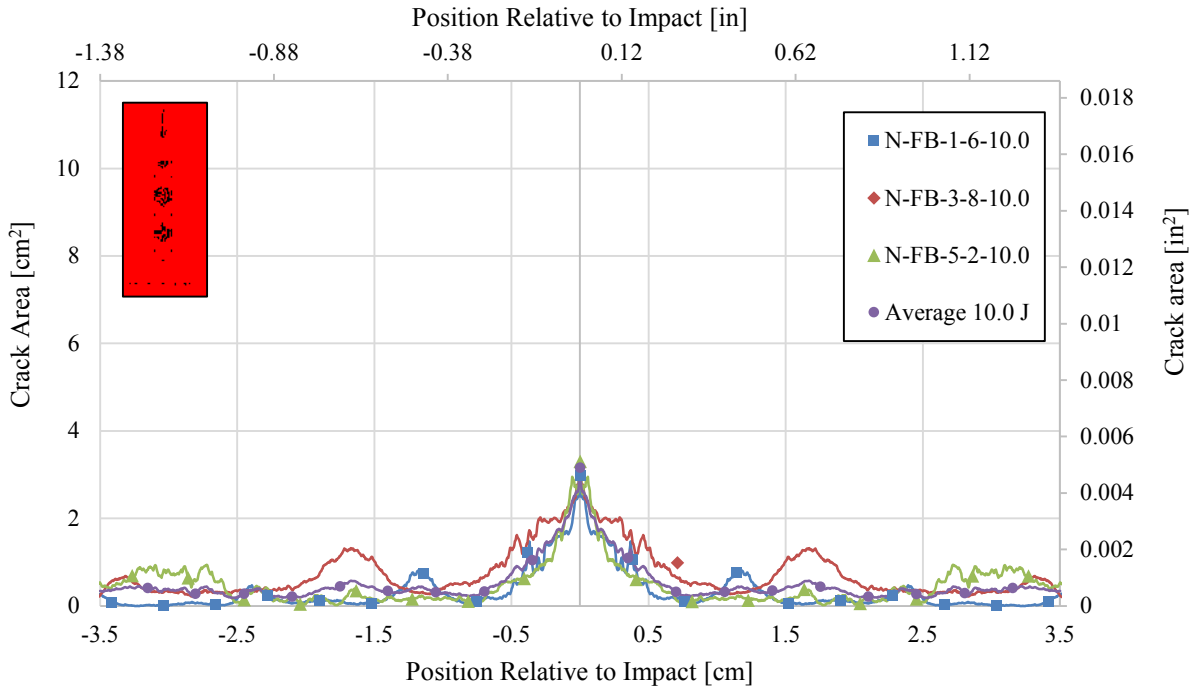

Figure 3.10 Average Crack Area as a Function of Distance from the Point of Impact for Half Braid, 10 J (7.4 ft-lbs) Impact

Table 3.11 Peak Crack Area and Crack Volume of Half Braid, 15 J (11 ft-lbs) Impact

Specimen I.D.	Peak Crack Area [mm² (10^3 in²)]		Crack Volume [mm³ (10^3 in³)]	
N-HB-2-1-15.0	4.31	(6.68)	15.6	(0.95)
N-HB-4-2-15.0	11.0	(17.0)	95.0	(5.80)
N-HB-3-3-15.0	4.45	(6.90)	23.3	(1.42)
Average 15 J	6.58	(10.2)	44.7	(2.72)

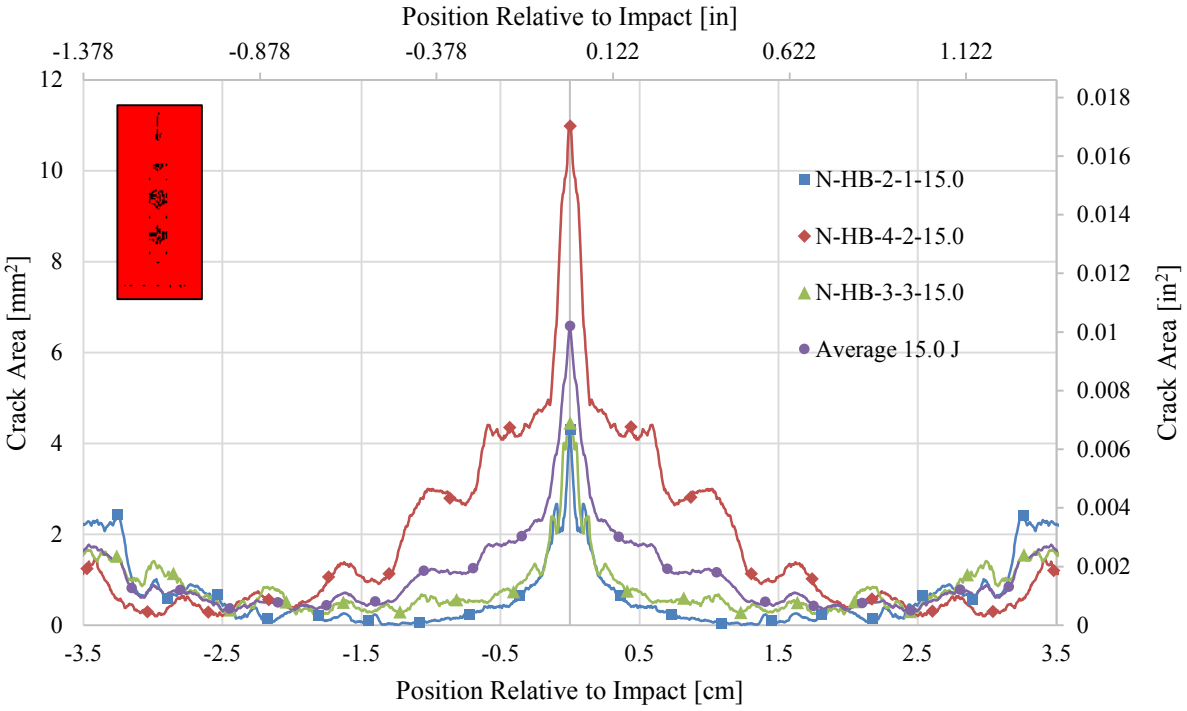

Figure 3.11 Average Crack Area as a Function of Distance from the Point of Impact for Half Braid, 15 J (11 ft-lbs) Impact

The micro-CT scan results for half braid specimens impacted with 20 J (15 ft-lbs) are summarized in Table 3.12 and the corresponding crack area curves are shown in Figure 3.12.

Table 3.12 Peak Crack Area and Crack Volume of Half Braid, 20 J (15 ft-lbs) Impact

Specimen I.D.	Peak Crack Area [mm² (10^3 in²)]		Crack Volume [mm³ (10^3 in³)]	
N-HB-1-3-20.0	4.76	(7.38)	34.2	(2.09)
N-HB-2-7-20.0	3.31	(5.13)	23.3	(1.42)
N-HB-4-5-20.0	8.80	(13.6)	96.1	(5.87)
Average 20 J	5.50	(8.53)	51.2	(3.12)

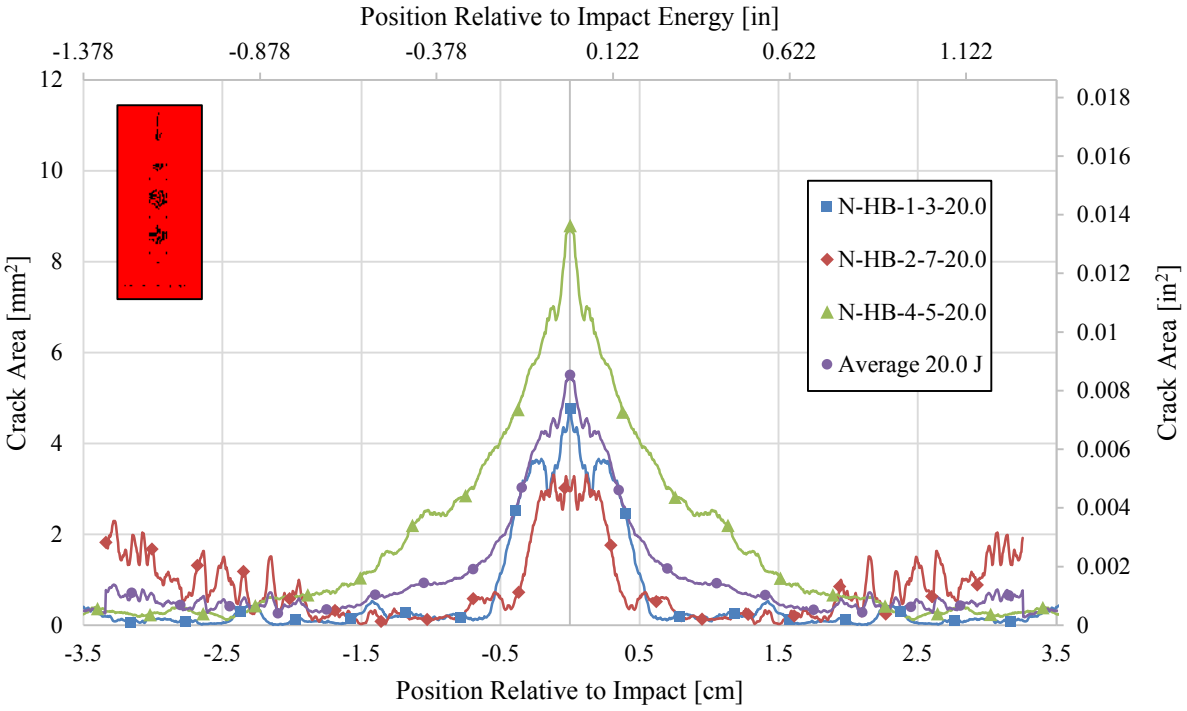

Figure 3.12 Average Crack Area as a Function of Distance from the Point of Impact for Half Braid, 20 J (15 ft-lbs) Impact

3.4 Full Spiral Micro-CT Scan Results

The micro-CT scan results for full spiral specimens impacted with 2.5 J (1.9 ft-lbs) are summarized in Table 3.13 and the corresponding crack area curves are shown in Figure 3.13.

Table 3.13 Peak Crack Area and Crack Volume of Full Spiral, 2.5 J (1.9 ft-lbs) Impact

Specimen I.D.	Peak Crack Area [mm^2]	(10^3 in^2)]	Crack Volume [mm^3]	(10^3 in^3)]
N-FS-3-1-2.5	0.35	(0.54)	6.01	(0.37)
N-FS-3-5-2.5	0.48	(0.74)	5.23	(0.32)
N-FS-3-8-2.5	0.35	(0.55)	6.02	(0.37)
Average 2.5 J	0.32	(0.50)	5.75	(0.35)

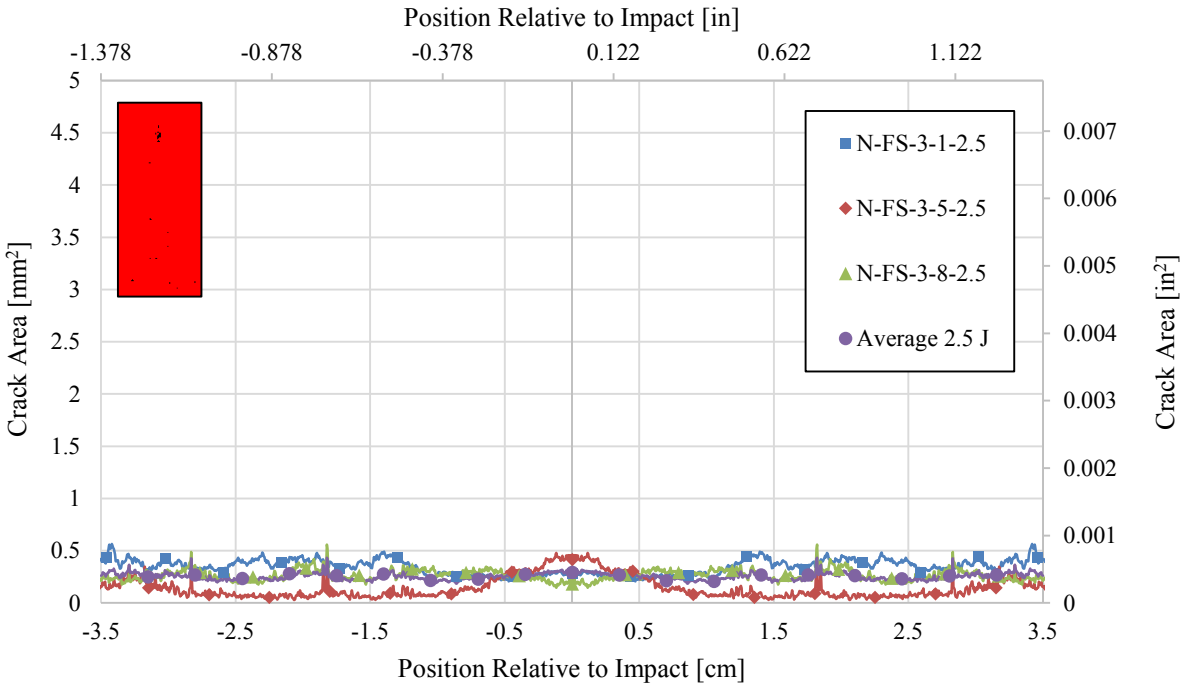

Figure 3.13 Average Crack Area as a Function of Distance from the Point of Impact for Full Spiral, 2.5 J (1.9 ft-lbs) Impact

The micro-CT scan results for full spiral specimens impacted with 5.0 J (3.7 ft-lbs) are summarized in Table 3.14 and the corresponding crack area curves are shown in Figure 3.14. The micro-CT scan results for full spiral specimens impacted with 7.5 J (5.6 ft-lbs) are summarized in Table 3.15 and the corresponding crack area curves are shown in Figure 3.15.

Table 3.14 Peak Crack Area and Crack Volume of Full Spiral, 5.0 J (3.7 ft-lbs) Impact

Specimen I.D.	Peak Crack Area [mm^2 (10^3 in^2)]		Crack Volume [mm^3 (10^3 in^3)]	
N-FS-1-8-5.0	0.96	(1.48)	14.3	(0.87)
N-FS-2-2-5.0	1.67	(2.58)	31.1	(1.90)
N-FS-4-3-5.0	0.58	(0.90)	7.07	(0.43)
Average 5.0 J	1.02	(1.59)	17.5	(1.07)

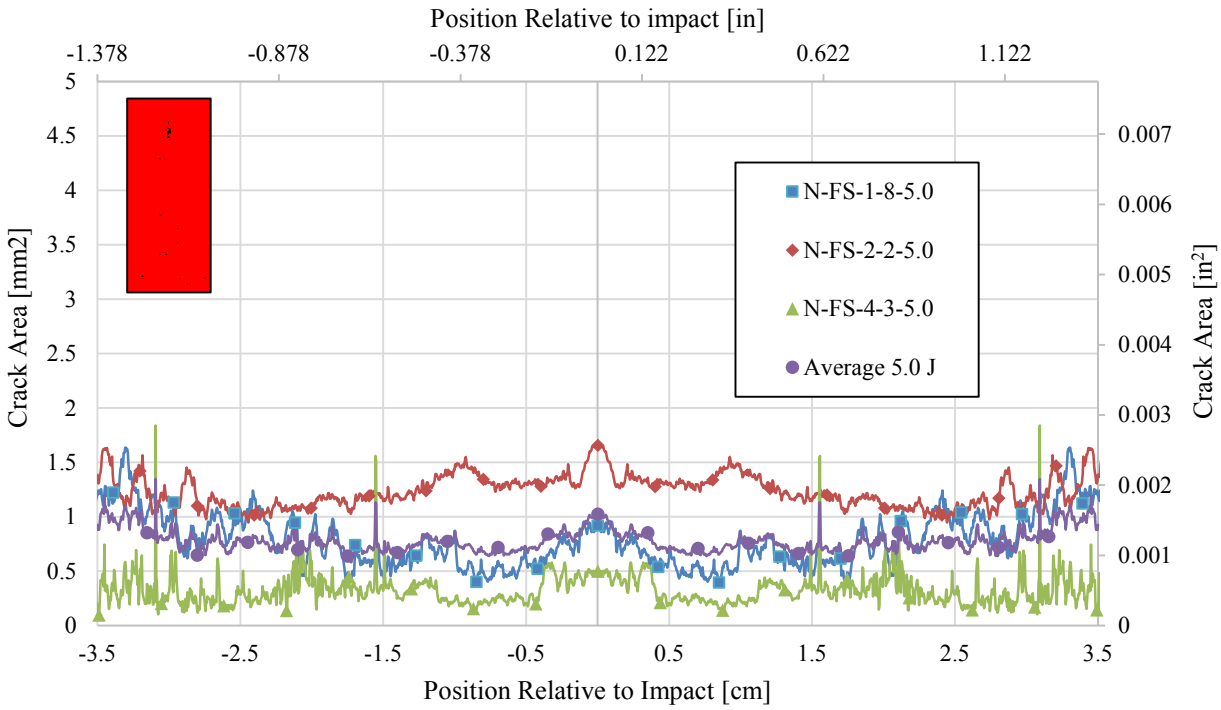

Figure 3.14 Average Crack Area as a Function of Distance from the Point of Impact for Full Spiral, 5.0 J (3.7 ft-lbs) Impact

Table 3.15 Peak Crack Area and Crack Volume of Full Spiral, 7.5 J (5.6 ft-lbs) Impact

Specimen I.D.	Peak Crack Area [mm^2 (10^3 in^2)]		Crack Volume [mm^3 (10^3 in^3)]	
N-FS-1-3-7.5	1.41	(2.19)	21.9	(1.34)
N-FS-1-10-7.5	0.26	(0.40)	3.31	(0.20)
N-FS-4-5-7.5	0.28	(0.44)	1.98	(0.12)
Average 7.5 J	0.60	(0.94)	9.06	(0.55)

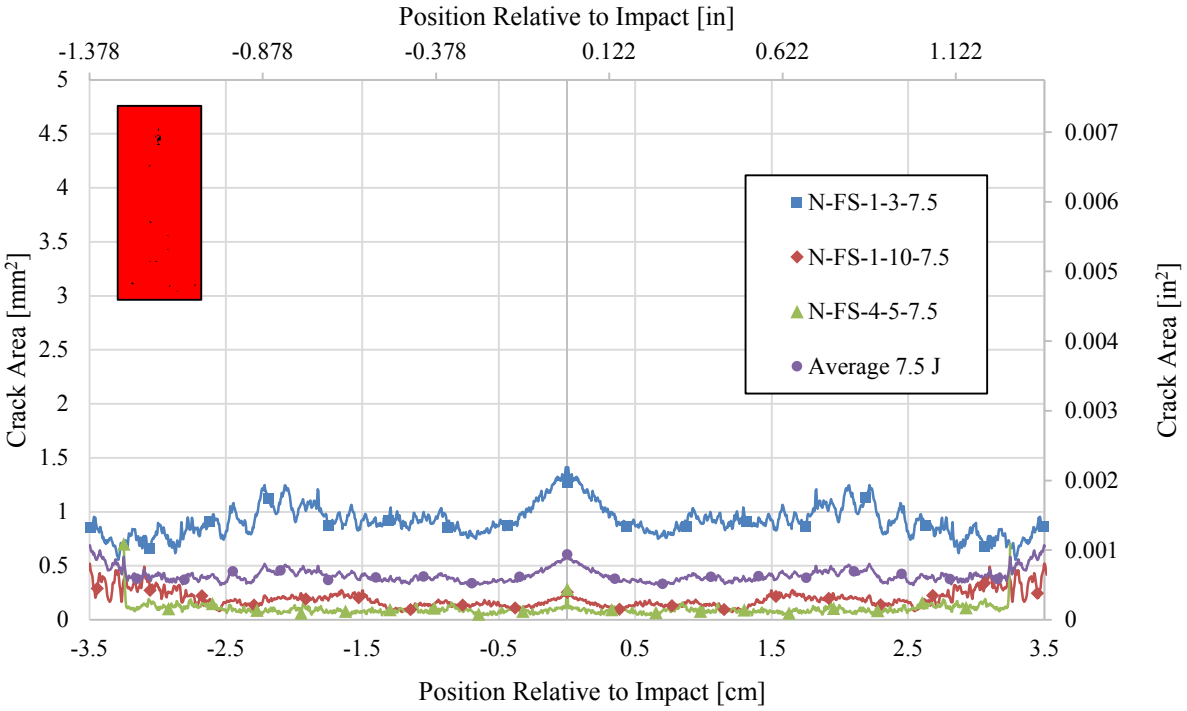

Figure 3.15 Average Crack Area as a Function of Distance from the Point of Impact for Full Spiral, 7.5 J (5.6 ft-lbs) Impact

The micro-CT scan results for full spiral specimens impacted with 10 J (7.4 ft-lbs) are summarized in Table 3.16 and the corresponding crack area curves are shown in Figure 3.16. The micro-CT scan results full spiral specimens impacted with 15 J (11 ft-lbs) are summarized in Table 3.17 and the corresponding crack area curves are shown in Figure 3.17.

Table 3.16 Peak Crack Area and Crack Volume of Full Spiral, 10 J (7.4 ft-lbs) Impact

Specimen I.D.	Peak Crack Area [mm²	(10³ in²)]	Crack Volume [mm³	(10³ in³)]
N-FS-2-9-10.0	1.61	(2.50)	20.0	(1.22)
N-FS-3-2-10.0	1.40	(2.17)	26.0	(1.58)
N-FS-1-9-10.0	0.76	(1.17)	13.6	(0.83)
Average 10 J	1.23	(1.91)	19.8	(1.21)

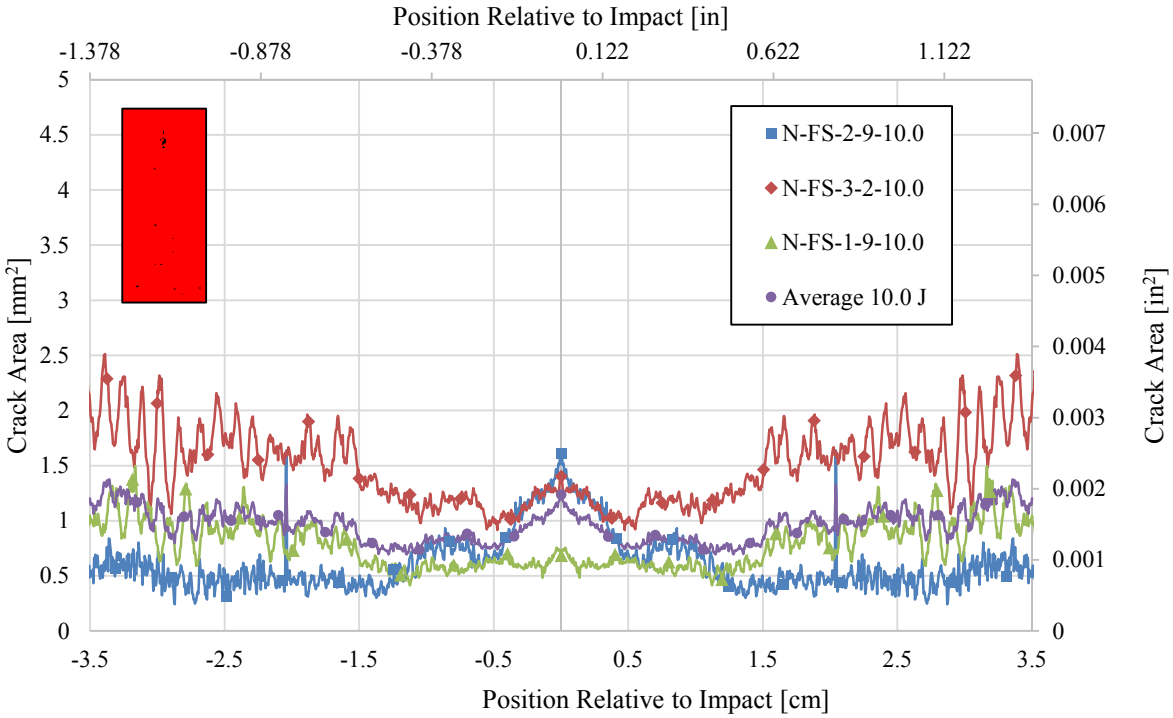

Figure 3.16 Average Crack Area as a Function of Distance from the Point of Impact for Full Spiral, 10 J (7.4 ft-lbs) Impact

Table 3.17 Peak Crack Area and Crack Volume of Full Spiral, 15 J (11 ft-lbs) Impact

Specimen I.D.	Peak Crack Area [mm^2	(10^3 in^2)]	Crack Volume [mm^3	(10^3 in^3)]
N-FS-1-4-15.0	2.33	(3.61)	35.4	(2.16)
N-FS-2-1-15.0	1.71	(2.66)	27.6	(1.68)
N-FS-3-4-15.0	1.50	(2.33)	24.2	(1.47)
Average 15 J	1.73	(2.68)	29.0	(1.77)

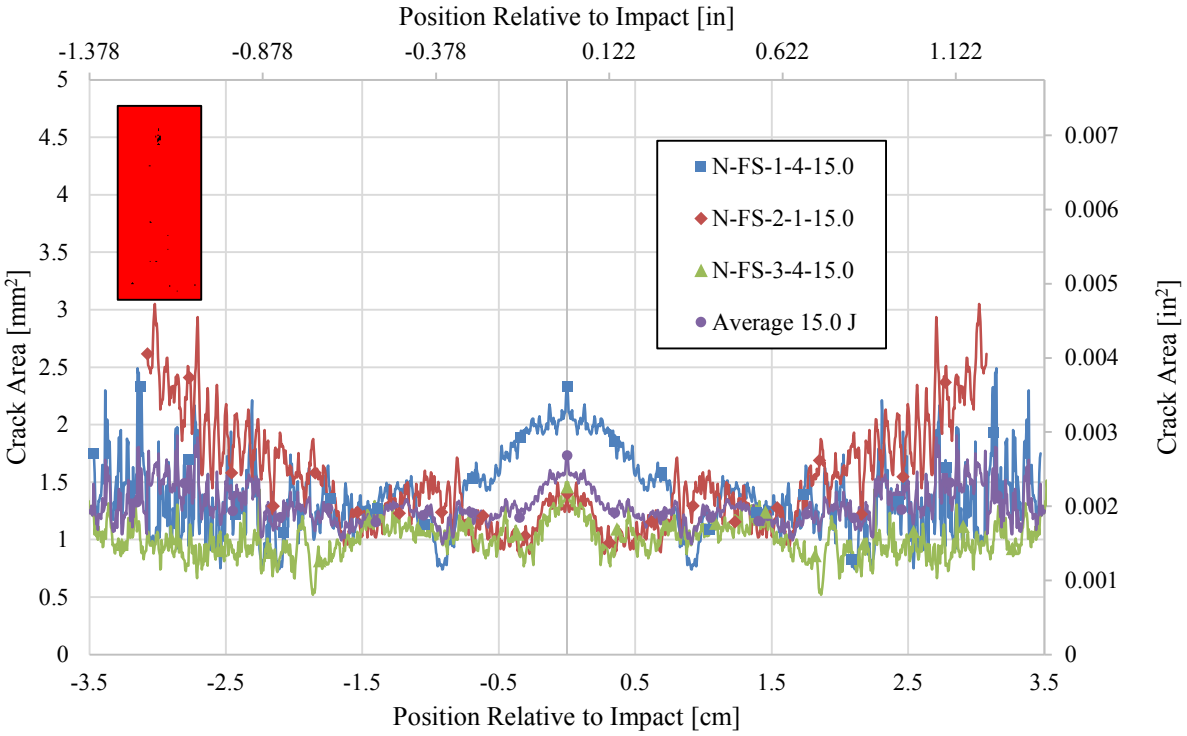

Figure 3.17 Average Crack Area as a Function of Distance from the Point of Impact for Full Spiral, 15 J (11 ft-lbs) Impact

The micro-CT scan results for full spiral specimens impacted with 20 J (15 ft-lbs) are summarized in Table 3.18 and the corresponding crack area curves are shown in Figure 3.18.

Table 3.18 Peak Crack Area and Crack Volume of Full Spiral, 20 J (15 ft-lbs) Impact

Specimen I.D.	Peak Crack Area [mm^2 (10^3 in^2)]		Crack Volume [mm^3 (10^3 in^3)]	
N-FS-1-1-20.0	1.49	(2.31)	8.52	(0.52)
N-FS-1-6-20.0	1.31	(2.03)	20.3	(1.24)
N-FS-2-8-20.0	0.90	(1.40)	17.4	(1.06)
Average 20 J	1.19	(1.85)	15.4	(0.94)

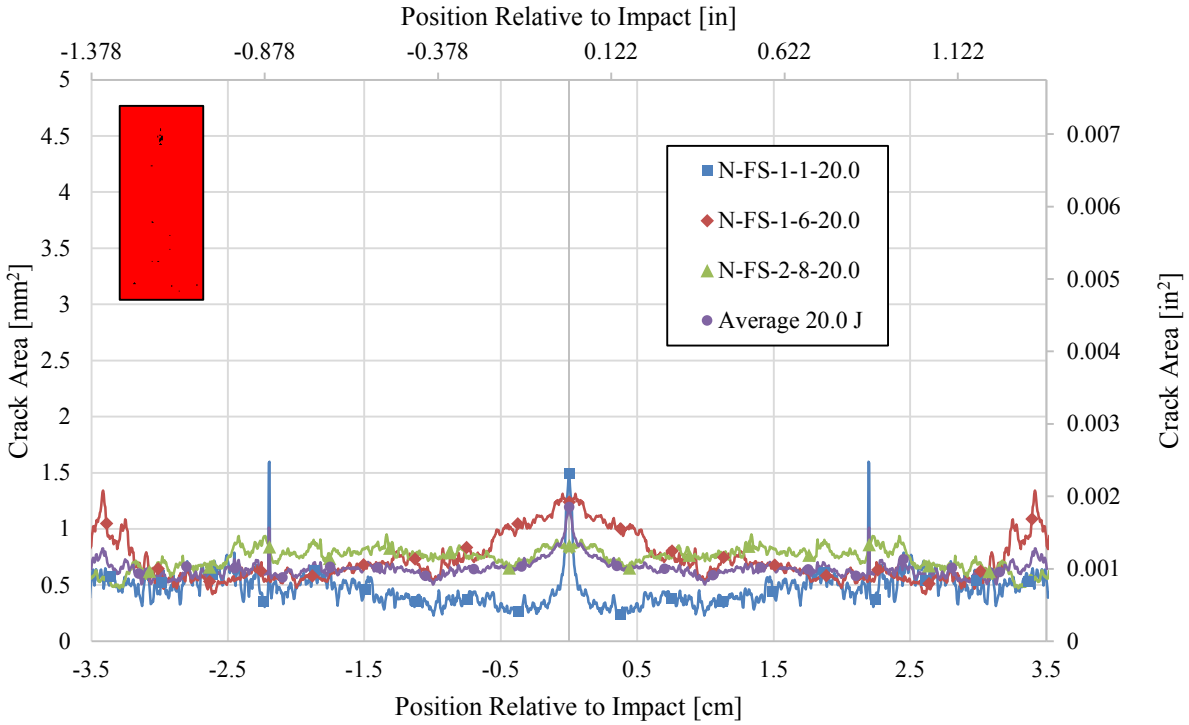

Figure 3.18 Average Crack Area as a Function of Distance from the Point of Impact for Full Spiral, 20 J (15 ft-lbs) Impact

3.5 Half Spiral Micro-CT Scan Results

The micro-CT scan results for half spiral specimens impacted with 2.5 J (1.9 ft-lbs) are summarized in Table 3.19 and the corresponding crack area curves are shown in Figure 3.19.

Table 3.19 Peak Crack Area and Crack Volume of Half Spiral, 2.5 J (1.9 ft-lbs) Impact

Specimen I.D.	Peak Crack Area [mm² (10³ in²)]		Crack Volume [mm³ (10³ in³)]	
N-HS-4-4-2.5	1.00	(1.55)	0.07	(0.005)
N-HS-4-3-2.5	1.12	(1.74)	0.06	(0.003)
N-HS-4-8-2.5	0.99	(1.53)	0.03	(0.002)
Average 2.5 J	0.61	(0.94)	0.03	(0.002)

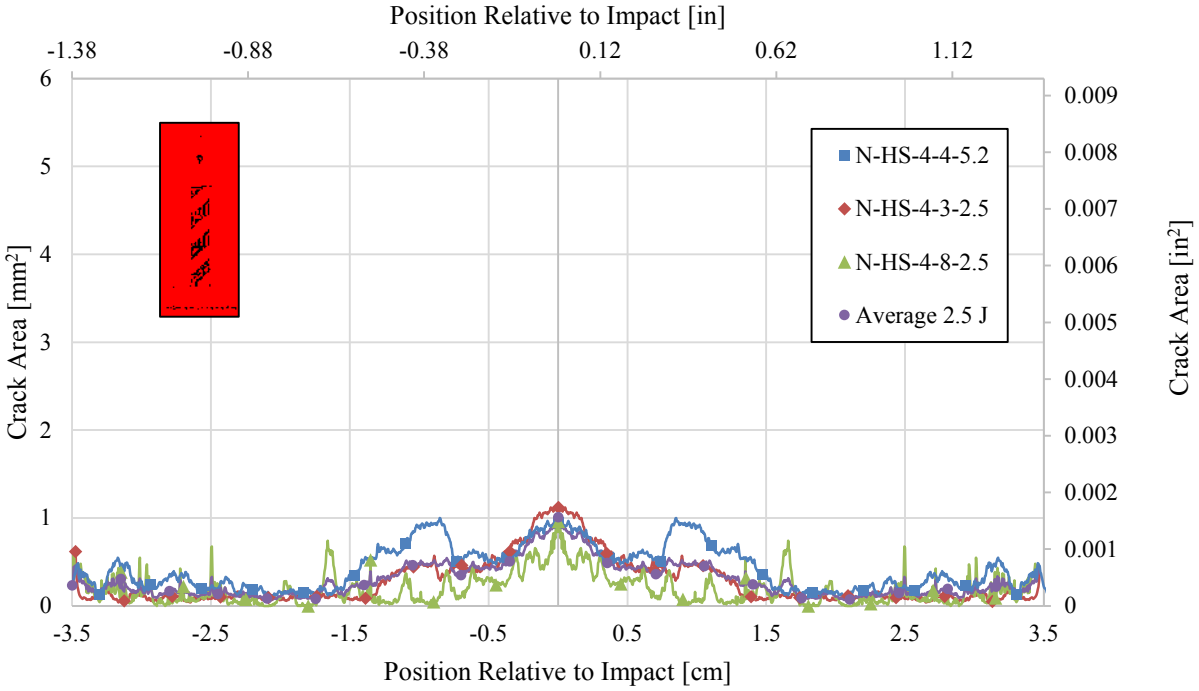

Figure 3.19 Average Crack Area as a Function of Distance from the Point of Impact for Half Spiral, 2.5 J (1.9 ft-lbs) Impact

The micro-CT scan results for half spiral specimens impacted with 5.0 J (3.7 ft-lbs) are summarized in Table 3.20 and the corresponding crack area curves are shown in Figure 3.20. The micro-CT scan results for half spiral specimens impacted with 7.5 J (5.6 ft-lbs) are summarized in Table 3.21 and the corresponding crack area curves are shown in Figure 3.21.

Table 3.20 Peak Crack Area and Crack Volume of Half Spiral, 5.0 J (3.7 ft-lbs) Impact

Specimen I.D.	Peak Crack Area [mm^2 (10^3 in^2)]		Crack Volume [mm^3 (10^3 in^3)]	
N-HS-3-4-5.0	1.93	(2.99)	0.16	(0.009)
N-HS-3-7-5.0	2.59	(4.02)	0.10	(0.006)
N-HS-4-5-5.0	0.30	(0.46)	0.01	(0.0009)
Average 5.0 J	0.96	(1.49)	0.05	(0.003)

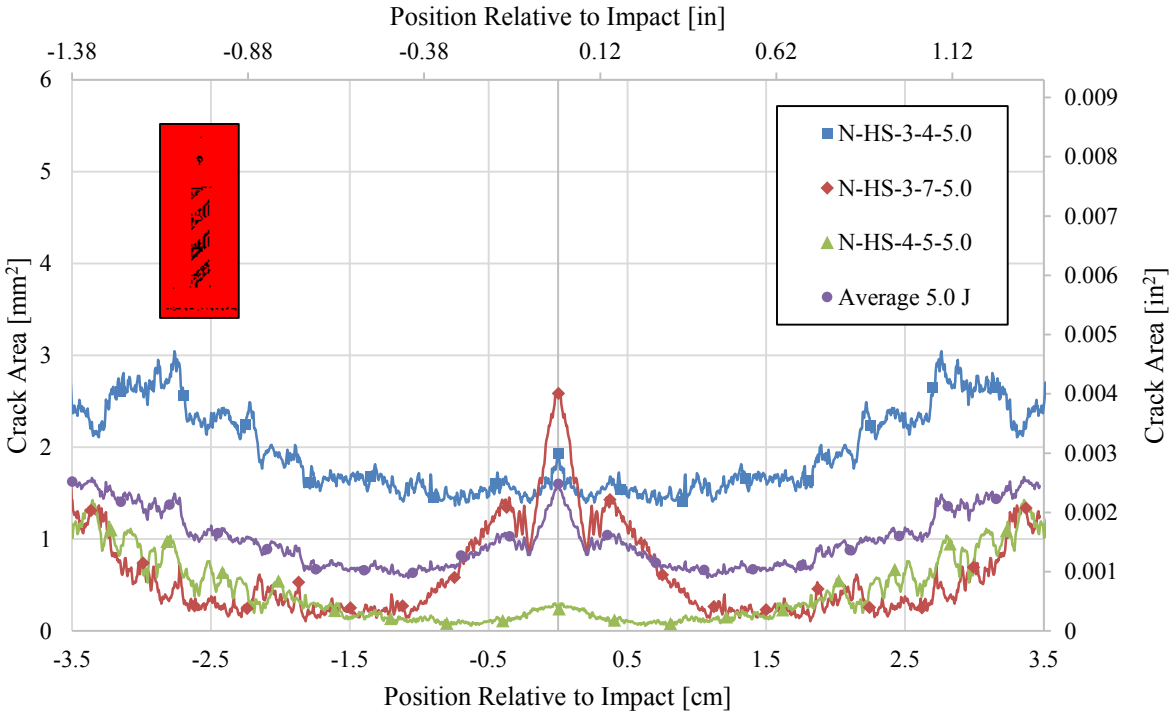

Figure 3.20 Average Crack Area as a Function of Distance from the Point of Impact for Half Spiral, 5.0 J (3.7 ft-lbs) Impact

Table 3.21 Peak Crack Area and Crack Volume of Half Spiral, 7.5 J (5.6 ft-lbs) Impact

Specimen I.D.	Peak Crack Area [mm^2 (10^3 in^2)]		Crack Volume [mm^3 (10^3 in^3)]	
N-HS-3-3-7.5	2.76	(4.28)	0.13	(0.008)
N-HS-4-2-7.5	0.15	(0.23)	0.11	(0.0006)
N-HS-2-9-7.5	0.72	(1.12)	0.03	(0.002)
Average 7.5 J	0.72	(1.12)	0.03	(0.002)

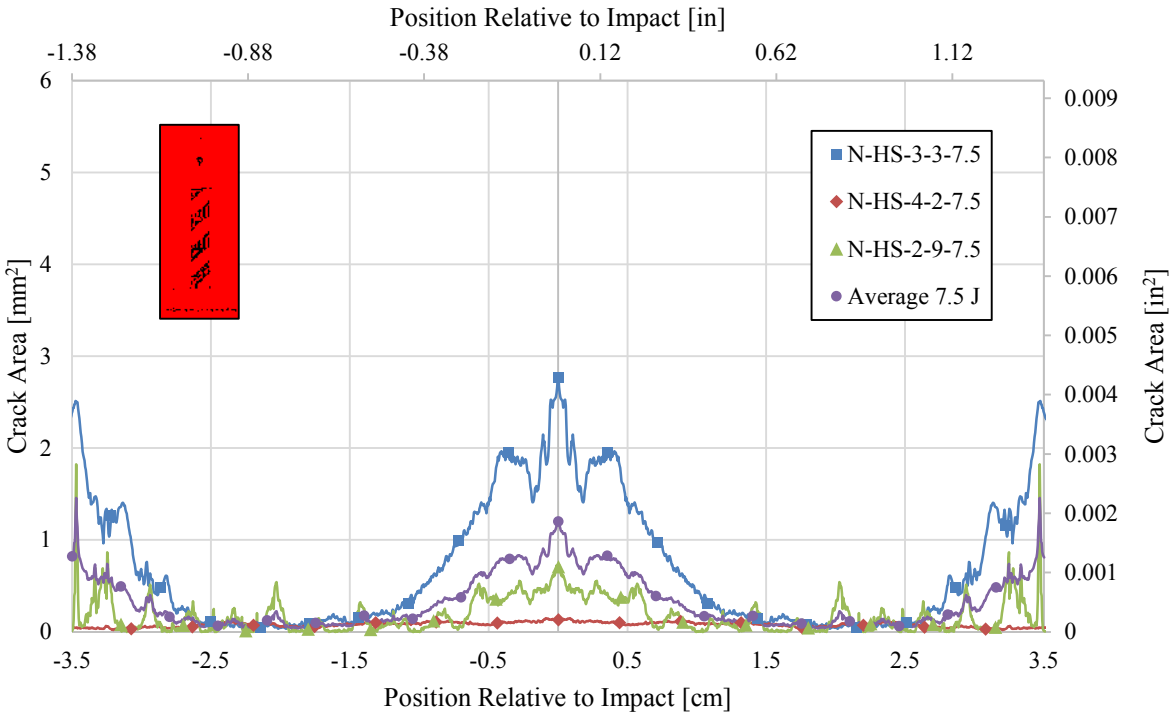

Figure 3.21 Average Crack Area as a Function of Distance from the Point of Impact for Half Spiral, 7.5 J (5.6 ft-lbs) Impact

The micro-CT scan results for half spiral specimens impacted with 10 J (7.4 ft-lbs) are summarized in Table 3.22 and the corresponding crack area curves are shown in Figure 3.22. The micro-CT scan results for half spiral specimens impacted with 15 J (11 ft-lbs) are summarized in Table 3.23 and the corresponding crack area curves are shown in Figure 3.23.

Table 3.22 Peak Crack Area and Crack Volume of Half Spiral, 10 J (7.4 ft-lbs) Impact

Specimen I.D.	Peak Crack Area [mm² (10^3 in²)]		Crack Volume [mm³ (10^3 in³)]	
N-HS-2-4-10.0	2.52	(3.90)	0.18	(0.01)
N-HS-3-10-10.0	1.38	(2.14)	0.09	(0.005)
N-HS-4-1-10.0	0.48	(0.74)	0.008	(0.0005)
Average 10 J	0.87	(1.35)	0.06	(0.003)

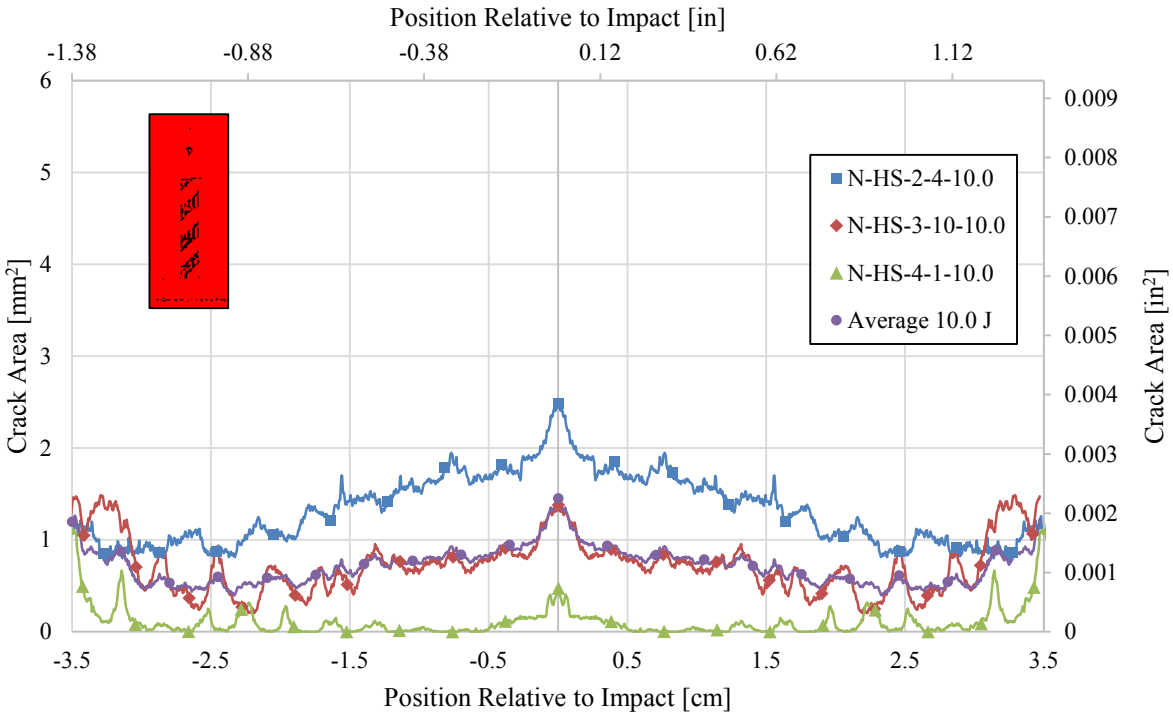

Figure 3.22 Average Crack Area as a Function of Distance from the Point of Impact for Half Spiral, 10 J (7.4 ft-lbs) Impact

Table 3.23 Peak Crack Area and Crack Volume of Half Spiral, 15 J (15 ft-lbs) Impact

Specimen I.D.	Peak Crack Area [mm^2 (10^3 in^2)]		Crack Volume [mm^3 (10^3 in^3)]	
N-HS-3-2-15.0	5.24	(8.12)	0.26	(0.02)
N-HS-2-3-15.0	0.48	(0.74)	0.02	(0.002)
N-HS-1-10-15.0	4.70	(7.29)	0.23	(0.014)
Average 15 J	2.09	(3.24)	0.10	(0.006)

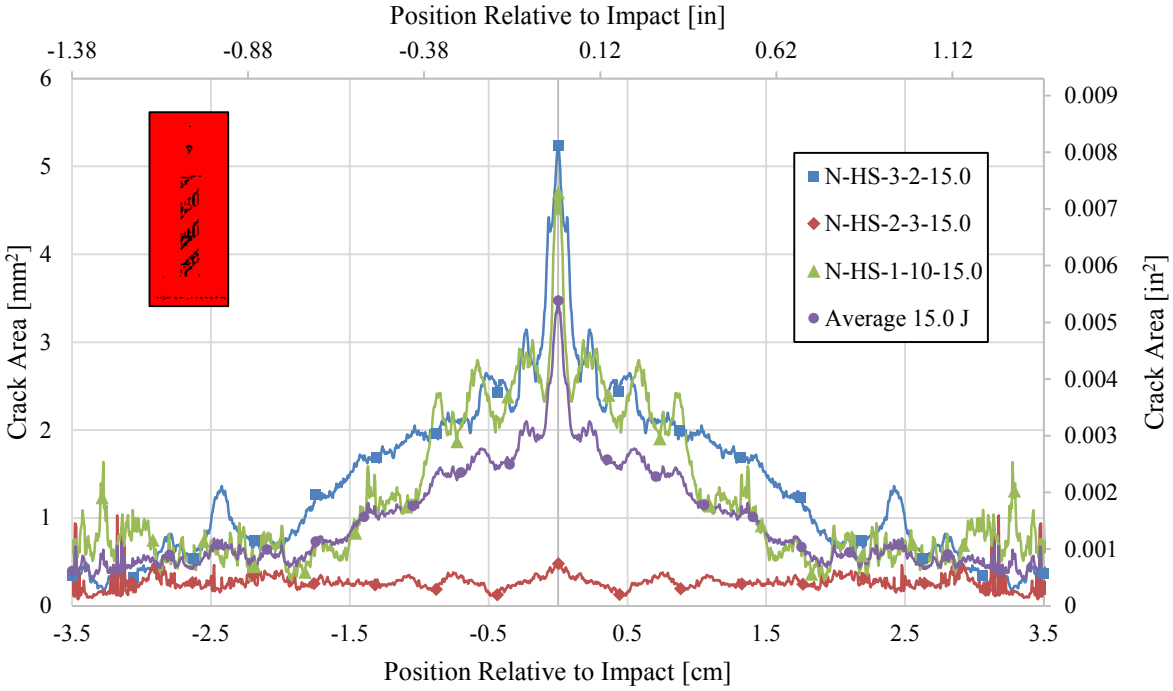

Figure 3.23 Average Crack Area as a Function of Distance from the Point of Impact for Half Spiral, 15 J (11 ft-lbs) Impact

The micro-CT scan results for half spiral specimens impacted with 20 J (15 ft-lbs) are summarized in Table 3.24 and the corresponding crack area curves are shown in Figure 3.24.

Table 3.24 Peak Crack Area and Crack Volume of Half Spiral, 20 J (15 ft-lbs) Impact

Specimen I.D.	Peak Crack Area [mm² (10^3 in²)]		Crack Volume [mm³ (10^3 in³)]	
N-HS-1-2-20.0	3.81	(5.91)	0.22	(0.01)
N-HS-1-9-20.0	0.79	(1.22)	0.05	(0.003)
N-HS-2-5-20.0	2.78	(4.31)	0.15	(0.009)
Average 20 J	1.46	(2.27)	0.08	(0.005)

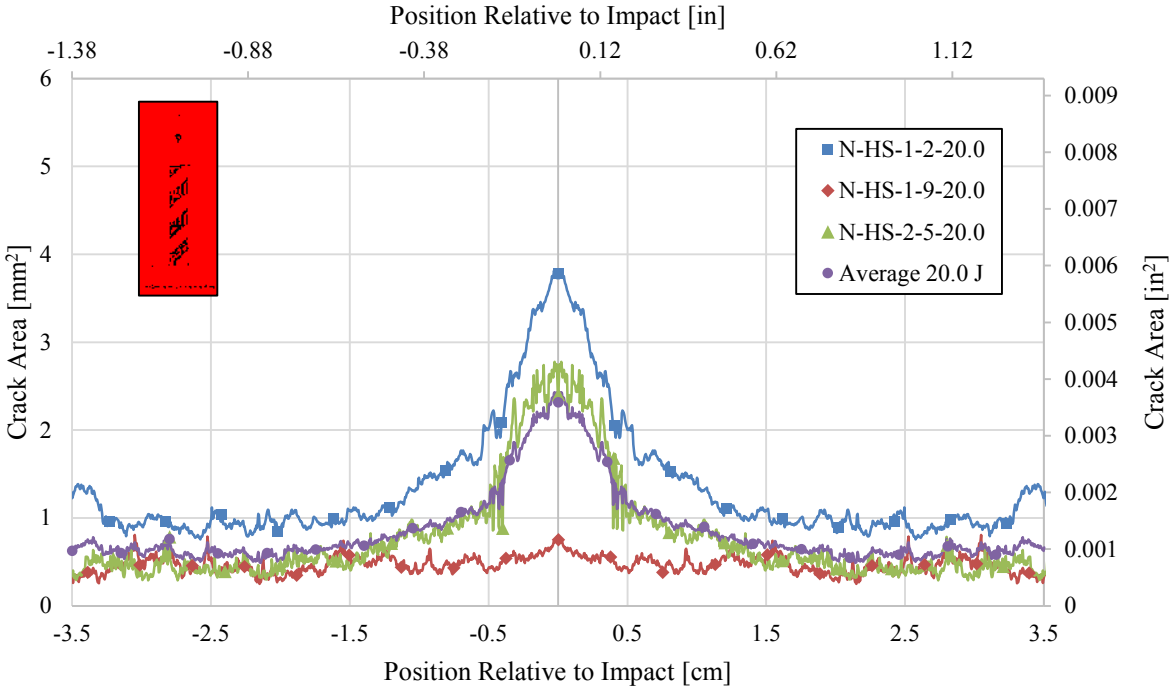

Figure 3.24 Average Crack Area as a Function of Distance from the Point of Impact for Half Spiral, 20 J (15 ft-lbs) Impact

3.6 Shrink Tape Micro-CT Scan Results

The micro-CT scan results for shrink tape specimens impacted with 2.5 J (1.9 ft-lbs) are summarized in Table 3.25 and the corresponding crack area curves are shown in Figure 3.25.

Table 3.25 Peak Crack Area and Crack Volume of Shrink Tape, 2.5 J (1.9 ft-lbs) Impact

Specimen I.D.	Peak Crack Area [mm^2 (10^3 in^2)]		Crack Volume [mm^3 (10^3 in^3)]	
ST-2-1-2.5	0.42	(0.65)	2.51	(0.15)
ST-2-11-2.5	1.17	(1.82)	10.7	(0.65)
ST-3-3-2.5	0.69	(1.07)	7.89	(0.48)
Average 2.5 J	0.62	(0.96)	7.04	(0.43)

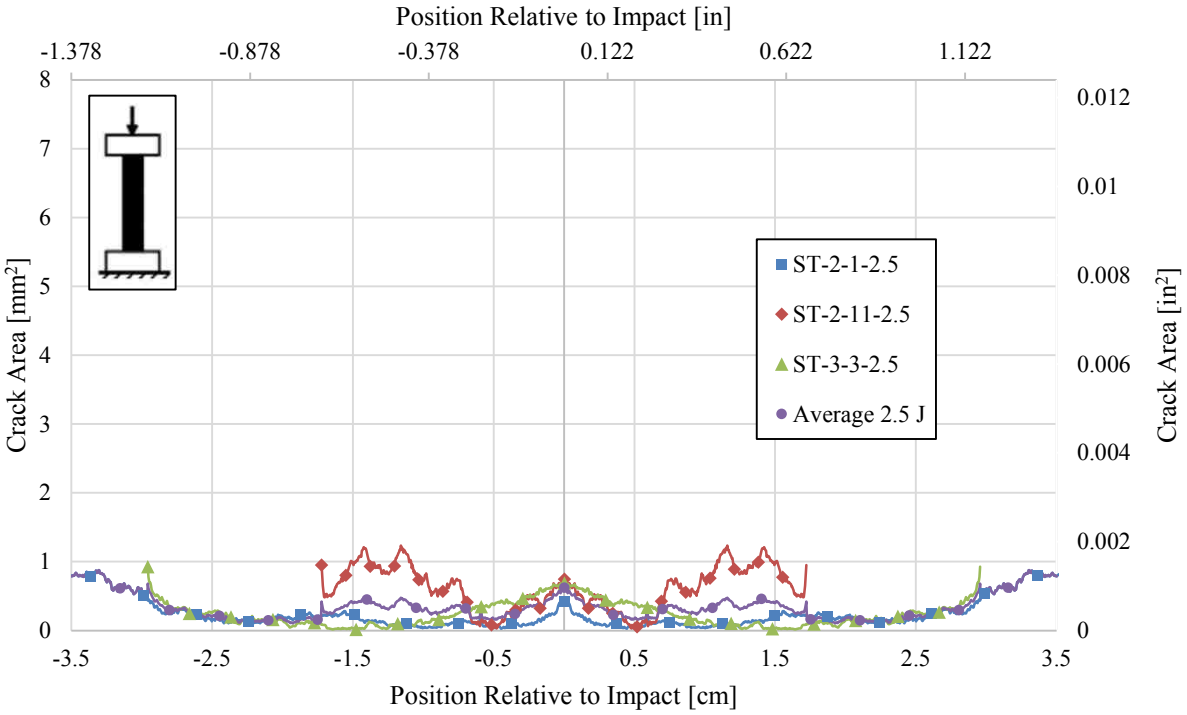

Figure 3.25 Average Crack Area as a Function of Distance from the Point of Impact for Shrink Tape, 2.5 J (1.9 ft-lbs) Impact

The micro-CT scan results for half spiral specimens impacted with 5.0 J (3.7 ft-lbs) are summarized in Table 3.26 and the corresponding crack area curves are shown in Figure 3.26. The micro-CT scan results for half spiral specimens impacted with 7.5 J (5.6 ft-lbs) are summarized in Table 3.27 and the corresponding crack area curves are shown in Figure 3.27.

Table 3.26 Peak Crack Area and Crack Volume of Shrink Tape, 5.0 J (3.7 ft-lbs) Impact

Specimen I.D.	Peak Crack Area [mm² (10^3 in²)]		Crack Volume [mm³ (10^3 in³)]	
ST-1-7-5.0	1.76	(2.72)	14.0	(0.85)
ST-3-6-5.0	2.11	(3.27)	33.2	(2.02)
ST-3-11-5.0	1.41	(2.19)	11.3	(0.69)
Average 5.0 J	1.76	(2.72)	19.5	(1.19)

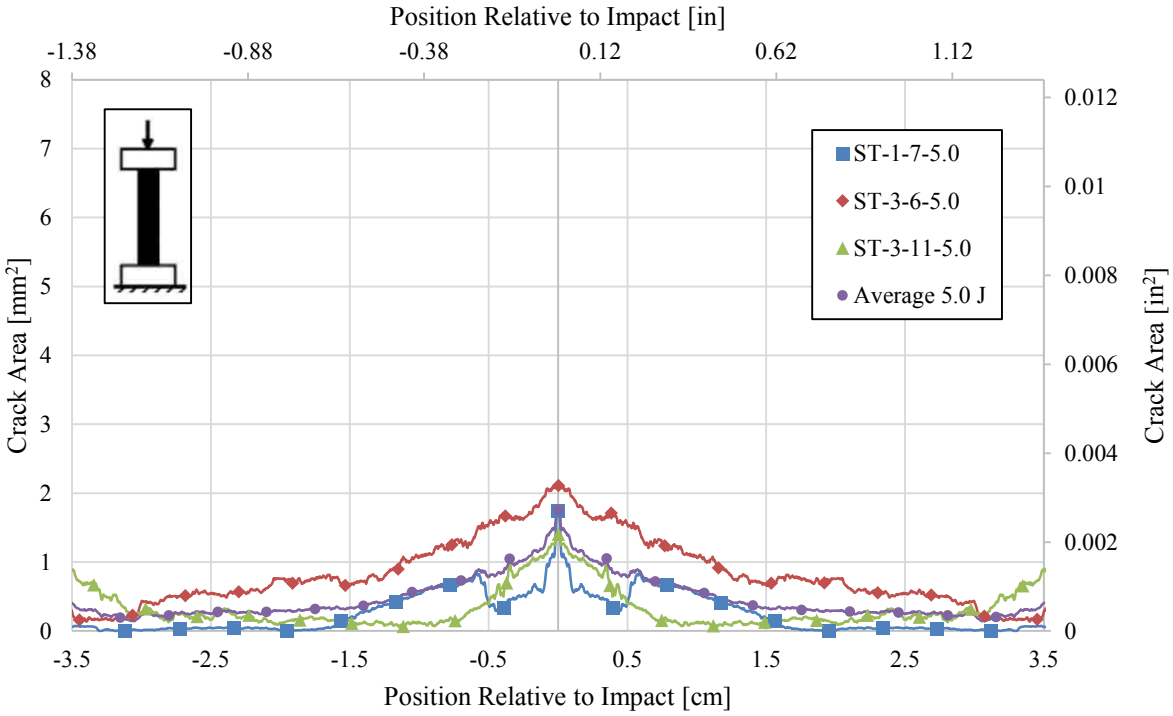

Figure 3.26 Average Crack Area as a Function of Distance from the Point of Impact for Shrink Tape, 5.0 J (3.7 ft-lbs) Impact

Table 3.27 Peak Crack Area and Crack Volume of Shrink Tape, 7.5 J (5.6 ft-lbs) Impact

Specimen I.D.	Peak Crack Area [mm² (10^3 in²)]		Crack Volume [mm³ (10^3 in³)]	
ST-2-2-7.5	3.08	(4.77)	35.6	(2.17)
ST-2-5-7.5	3.35	(5.20)	40.9	(2.50)
ST-3-9-7.5	2.90	(4.49)	27.6	(1.68)
ST-2-8-7.5	3.27	(5.06)	25.3	(1.54)
Average 7.5 J	3.17	(4.92)	31.3	(1.91)

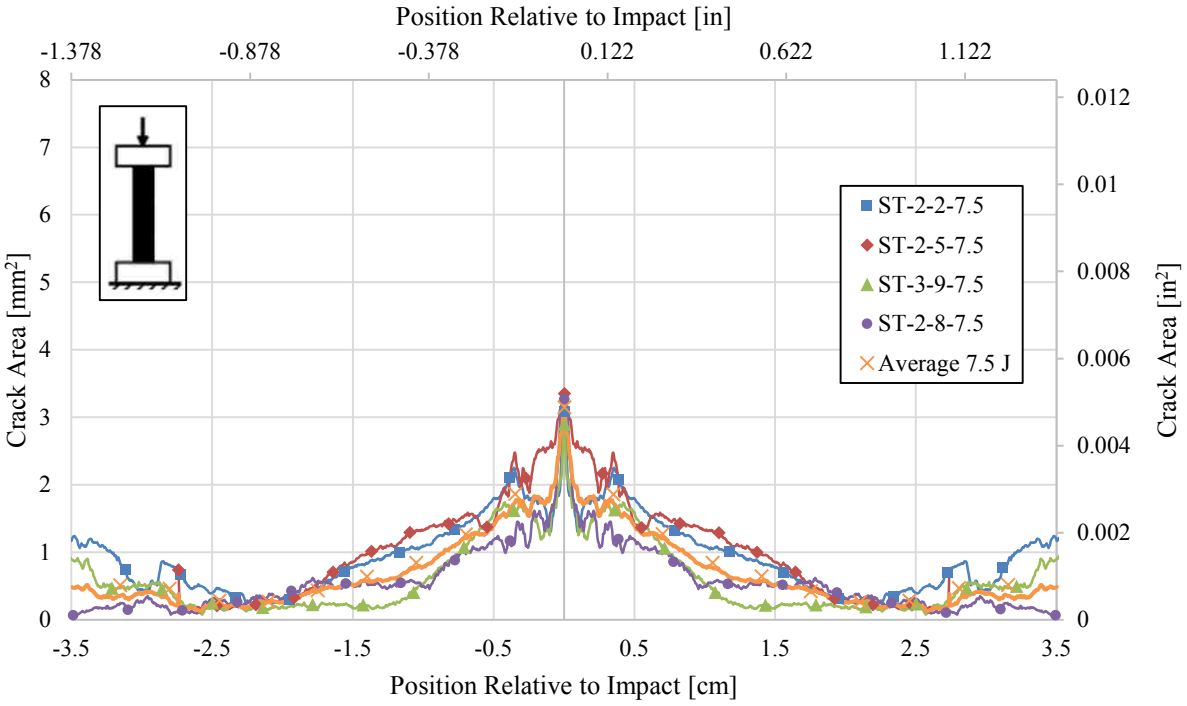

Figure 3.27 Average Crack Area as a Function of Distance from the Point of Impact for Shrink Tape, 7.5 J (5.6 ft-lbs) Impact

The micro-CT scan results for half spiral specimens impacted with 10 J (7.4 ft-lbs) are summarized in Table 3.28 and the corresponding crack area curves are shown in Figure 3.28. The micro-CT scan results for half spiral specimens impacted with 15 J (11 ft-lbs) are summarized in Table 3.29 and the corresponding crack area curves are shown in Figure 3.29.

Table 3.28 Peak Crack Area and Crack Volume of Shrink Tape, 10 J (7.4 ft-lbs) Impact

Specimen I.D.	Peak Crack Area [mm² (10^3 in²)]		Crack Volume [mm³ (10^3 in³)]	
ST-1-3-10.0	1.95	(3.03)	34.3	(2.09)
ST-3-4-10.0	4.51	(6.98)	60.6	(3.70)
ST-1-4-10.0	2.65	(4.10)	31.3	(1.91)
Average 10 J	3.01	(4.67)	42.1	(2.57)

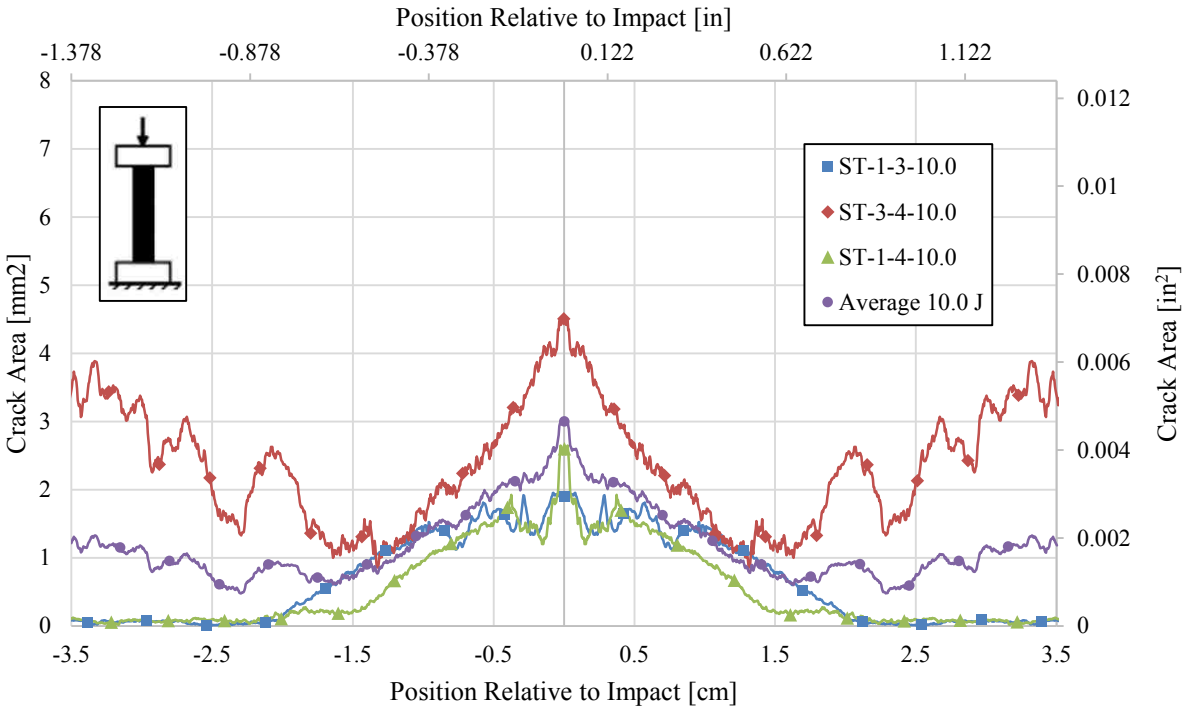

Figure 3.28 Average Crack Area as a Function of Distance from the Point of Impact for Shrink Tape, 10 J (7.4 ft-lbs) Impact, Carbon Specimen.

Table 3.29 Peak Crack Area and Crack Volume of Shrink Tape, 15 J (11 ft-lbs) Impact

Specimen I.D.	Peak Crack Area [mm^2 (10^3 in^2)]		Crack Volume [mm^3 (10^3 in^3)]	
ST-3-7-15.0	6.31	(9.78)	69.1	(4.22)
ST-1-8-15.0	4.02	(6.23)	37.5	(2.29)
ST-4-10-15.0	6.49	(10.1)	61.0	(3.72)
Average 15 J	5.61	(8.69)	55.9	(3.41)

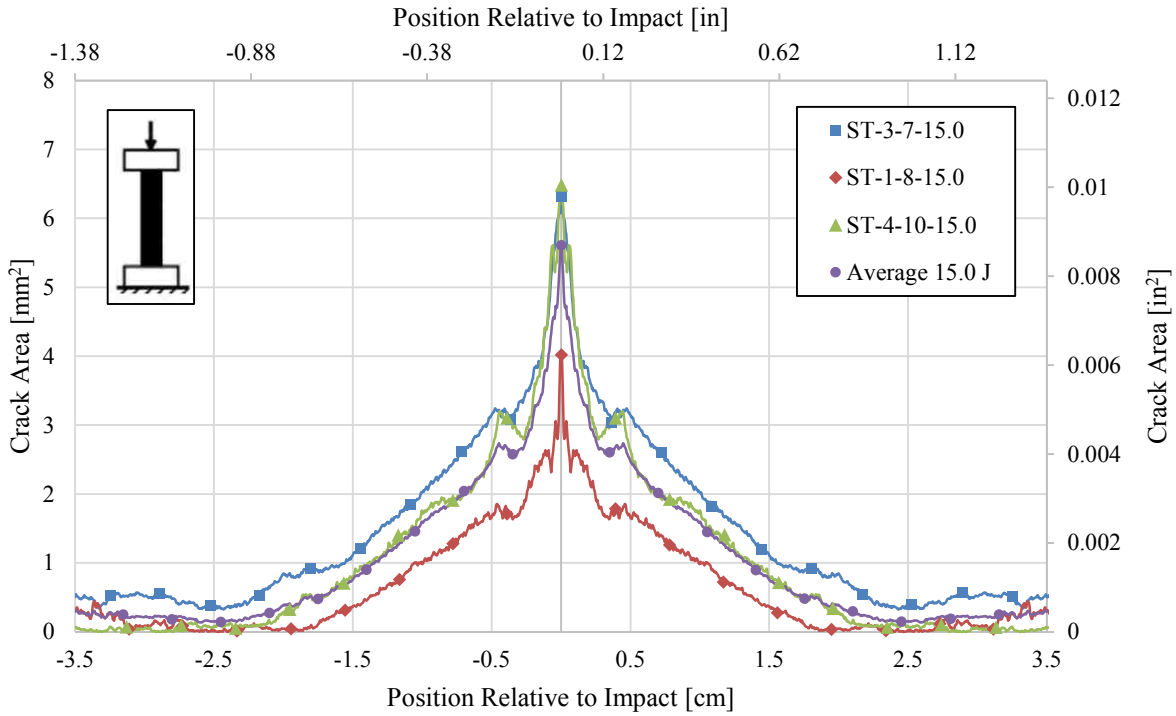

Figure 3.29 Average Crack Area as a Function of Distance from the Point of Impact for Shrink Tape, 15 J (11 ft-lbs) Impact

The micro-CT scan results for half spiral specimens impacted with 20 J (15 ft-lbs) are summarized in Table 3.30 and the corresponding crack area curves are shown in Figure 3.30.

Table 3.30 Peak Crack Area and Crack Volume of Shrink Tape, 20 J (15 ft-lbs) Impact

Specimen I.D.	Peak Crack Area [mm² (10^3 in²)]		Crack Volume [mm³ (10^3 in³)]	
ST-1-10-20.0	5.43	(8.41)	50.2	(3.07)
ST-4-2-20.0	7.12	(11.0)	117	(7.17)
ST-2-9-20.0	2.81	(4.35)	42.4	(2.58)
Average 20 J	5.06	(7.84)	70.0	(4.27)

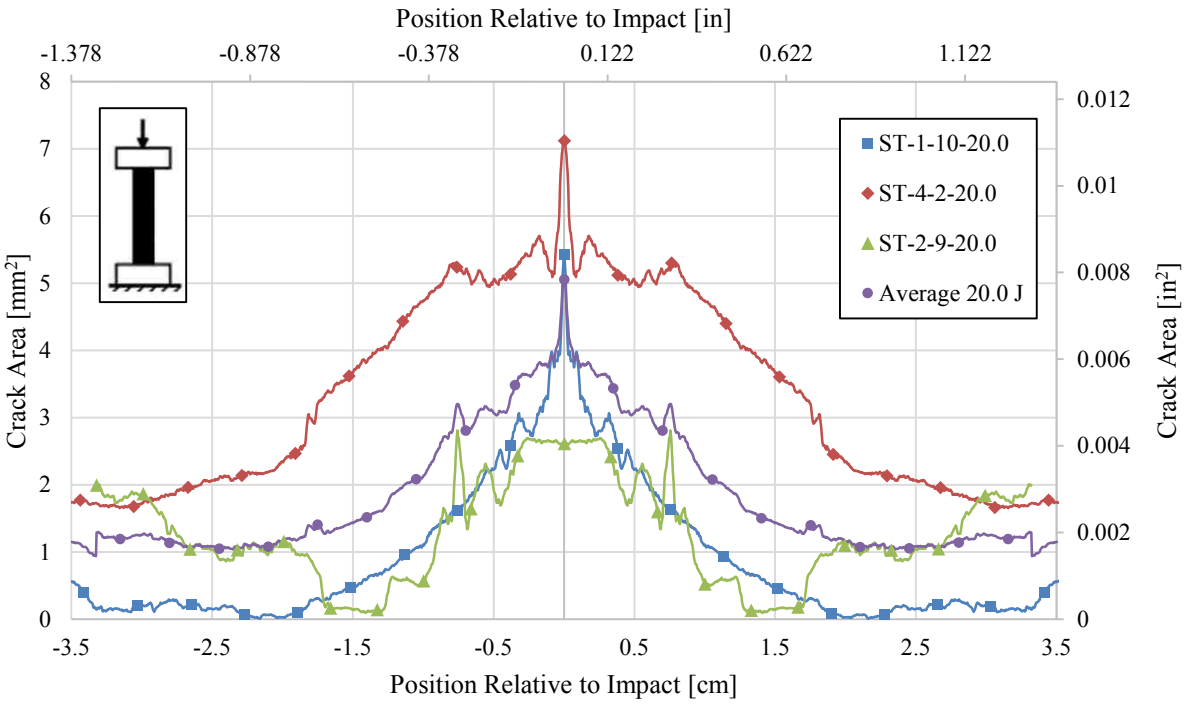

Figure 3.30 Average Crack Area as a Function of Distance from the Point of Impact for Shrink Tape, 20 J (15 ft-lbs) Impact

4 MICRO-CT CONFIGURATION AVERAGES

This chapter summarizes the average micro-CT curves and compares peak crack area and crack volume with the residual strength and impact energy for each of the specimen configurations. All thirty average curves, one for each configuration, area compared to show the overall trend of how crack area and overall crack volume compare to residual strength and impact energy. The influence of impact energy on crack area for each sleeve types and configurations is illustrated as well as the influence of sleeve type and coverage for each impact level. The influence of sleeve type and impact energy for different coverage and sleeve material is also exhibited in this chapter.

In order to get a general sense of how impact energy effects crack area and crack volume, Figure 4.1 shows the average crack area curves for the thirty configurations (five sleeve types at each impact energy level). Figures 4.2 and 4.3 show the ultimate residual compressive stress compared with the peak crack area and the crack volume respectively. For all sleeve configurations, there was a significant increase in peak crack area and crack volume due to impact damage. The peak crack area occurs roughly at the point of impact and dissipates along the length of the specimen.

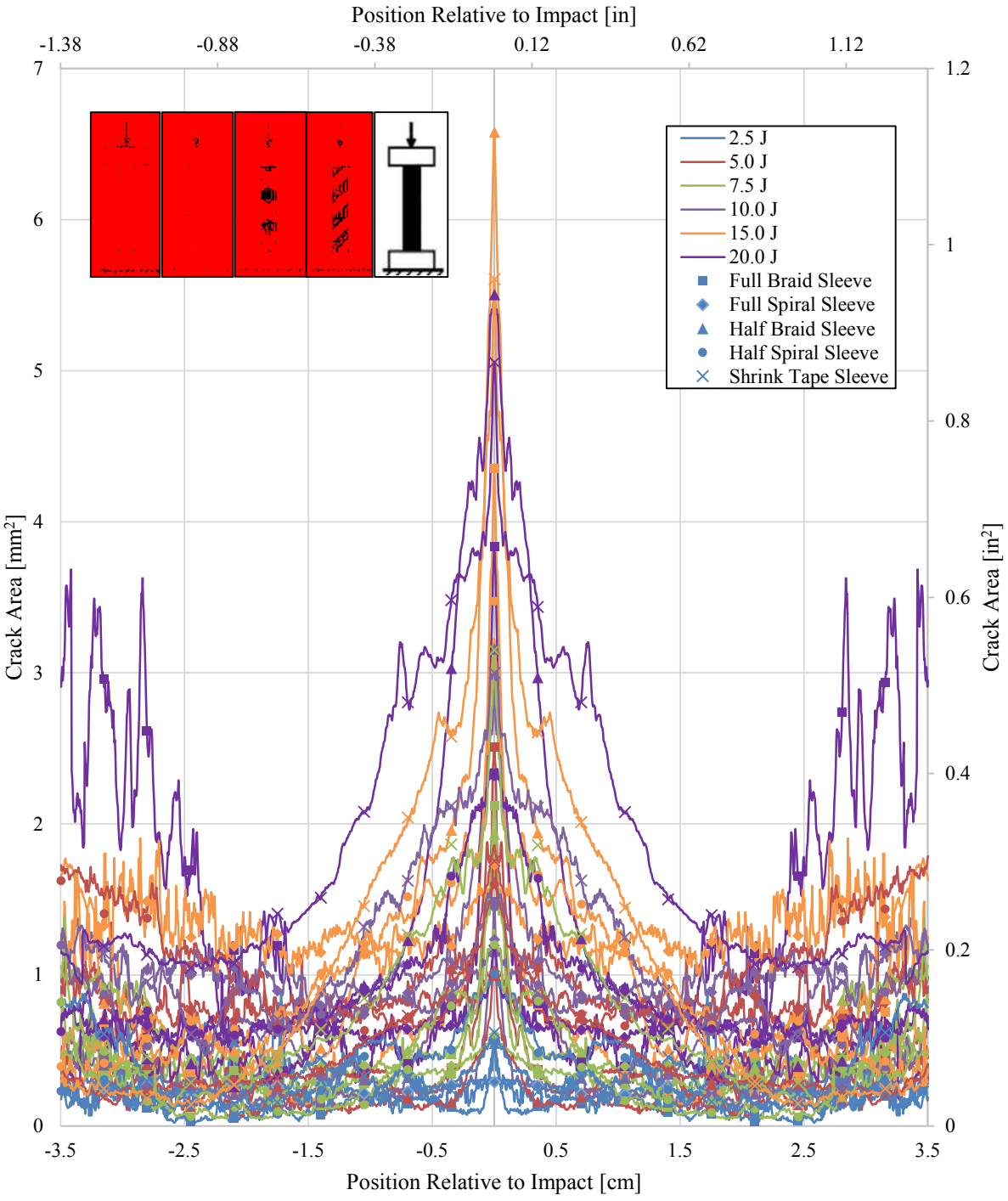

Figure 4.1 Average Crack Area as a Function of Distance from the Point of Impact for All Sleeve Types

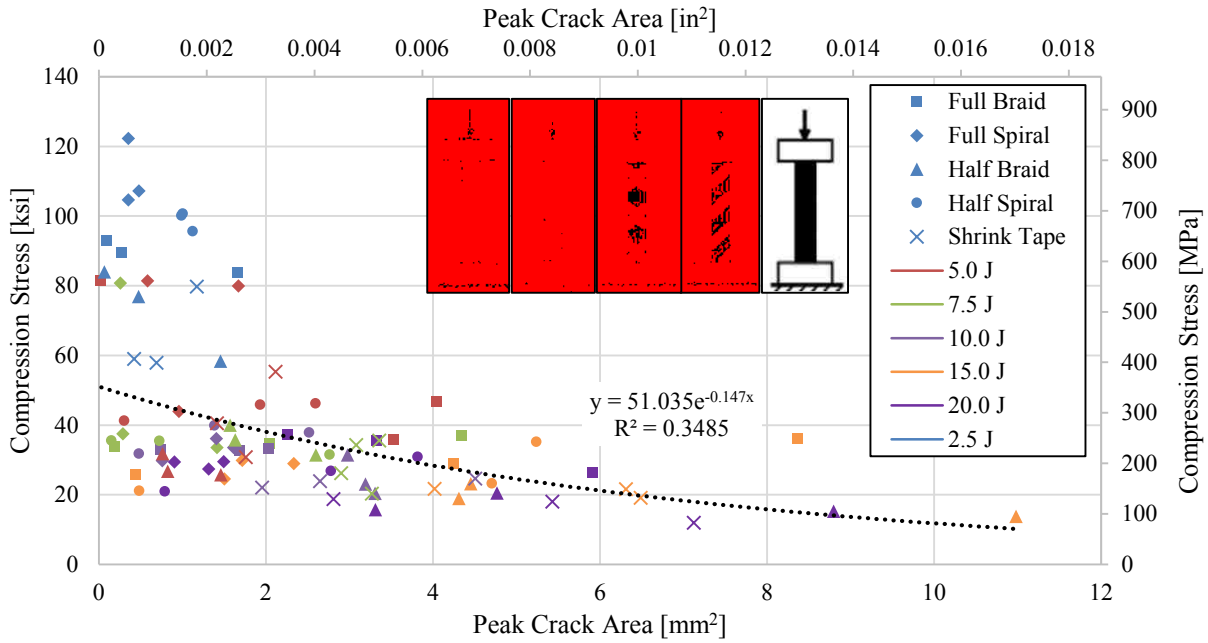

Figure 4.2 Peak Crack Area vs. Ultimate Compressive Stress for All Sleeve Types

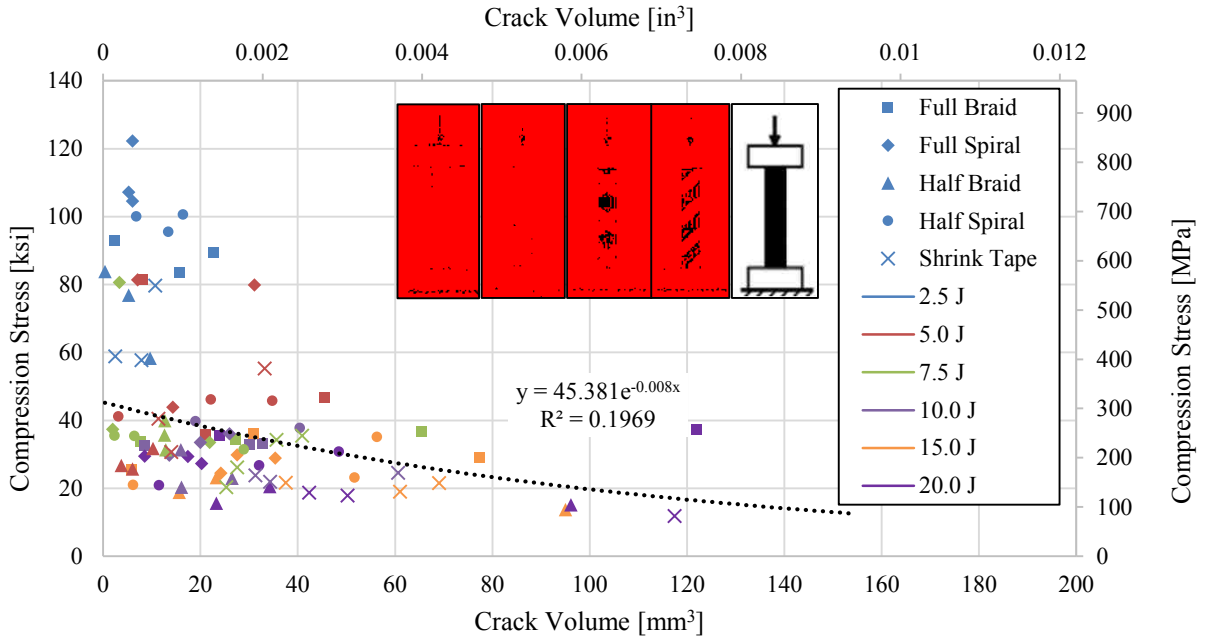

Figure 4.3 Overall Crack Volume vs. Ultimate Compressive Stress for All Sleeve Types

4.1 Configuration Micro-CT Curves

Crack area curves for full braid, half braid, full spiral, half spiral, and shrink tape configurations are shown in Figure 4.4, Figure 4.7, Figure 4.10, Figure 4.13, and Figure 4.16, respectively. The peak crack area and overall crack volume increase with increasing impact energy for each configuration. The peak crack area and overall crack volume compared with the ultimate residual compressive stress for full braid, half braid, full spiral, half spiral, and shrink tape are shown in Figure 4.5, 4.6, 4.8, 4.9, 4.11, 4.12, 4.14, 4.15, 4.17, and 4.18, respectively. In Figure 4.7 there are large crack areas near the ends of the average specimen impacted with 20 J (15 ft-lbs). This may have occurred because of shockwaves that caused the constrained ends to have micro-cracks form in the ends of the specimens.

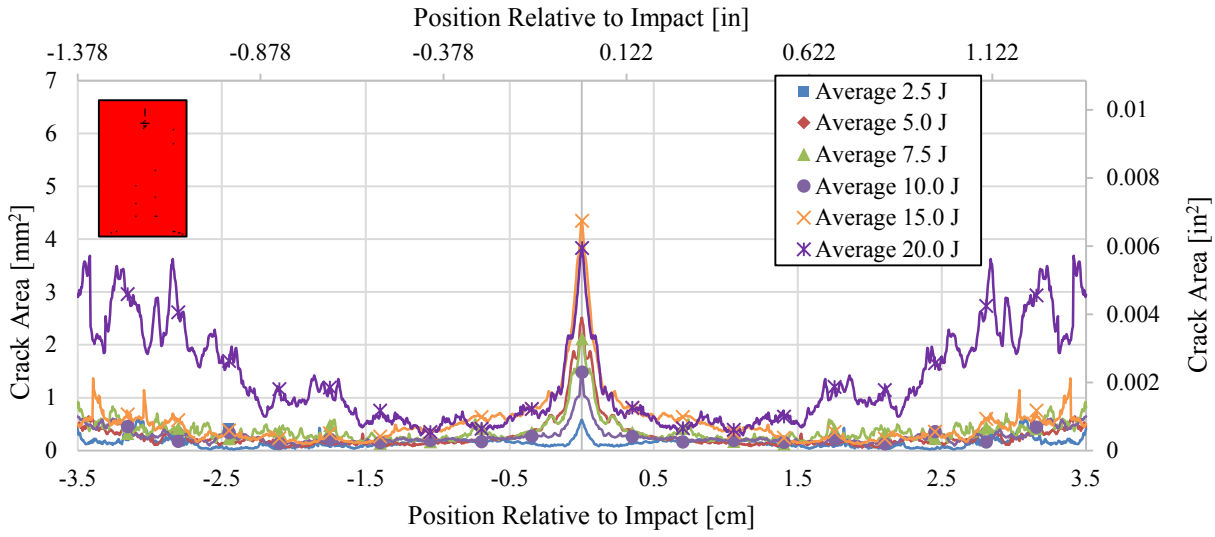

Figure 4.4 Average Crack Area as a Function of Distance from the Point of Impact for Full Braid Sleeve Types

Table 4.1 Peak Crack Area and Overall Crack Volume for Full Braid Sleeve Types

Impact Energy		Peak Crack Area		Overall Crack Volume	
[J	(ft-lbs)]	mm^2	(10^3 in^2)	mm^3	(10^3 in^3)
2.5	(1.9)	0.58	0.90	10.11	0.62
5.0	(3.7)	2.51	3.89	19.73	1.20
7.5	(5.6)	2.12	3.28	26.56	1.62
10	(7.4)	1.48	2.30	18.65	1.14
15	(11)	4.35	6.74	37.19	2.27
20	(14.8)	3.83	5.94	93.86	5.73

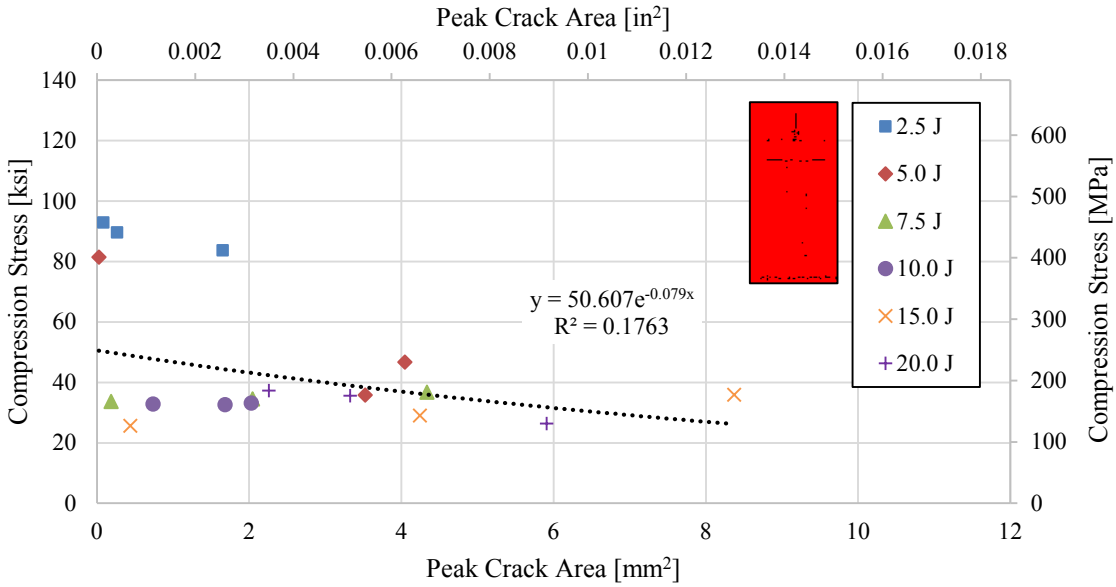

Figure 4.5 Peak Crack Area vs. Ultimate Compressive Stress Full Braid Sleeve Types

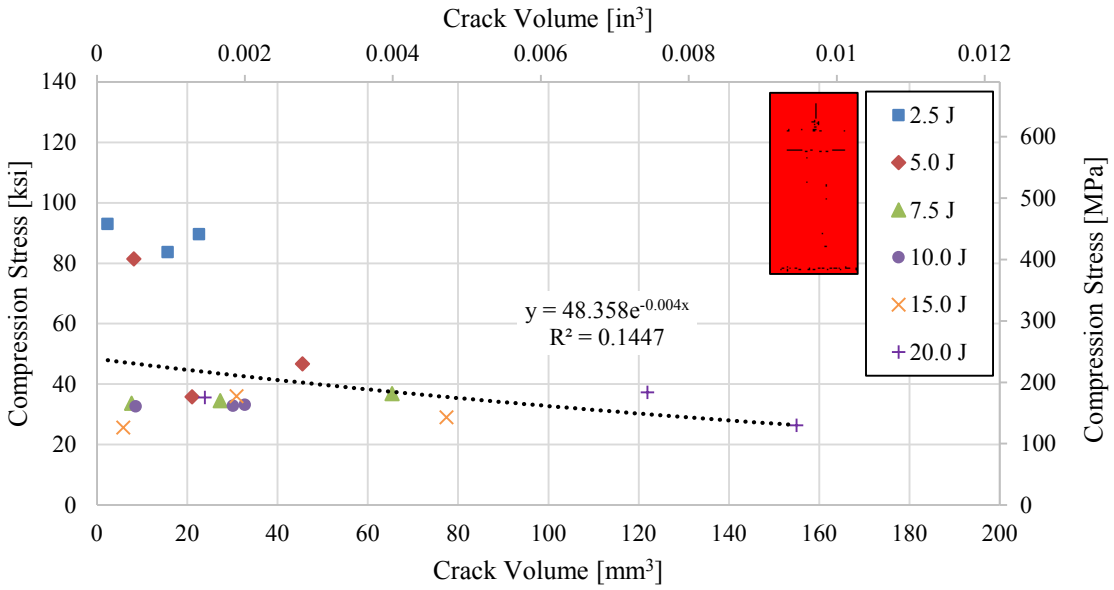

Figure 4.6 Overall Crack Volume vs. Ultimate Compressive Stress Full Braid Sleeve Types

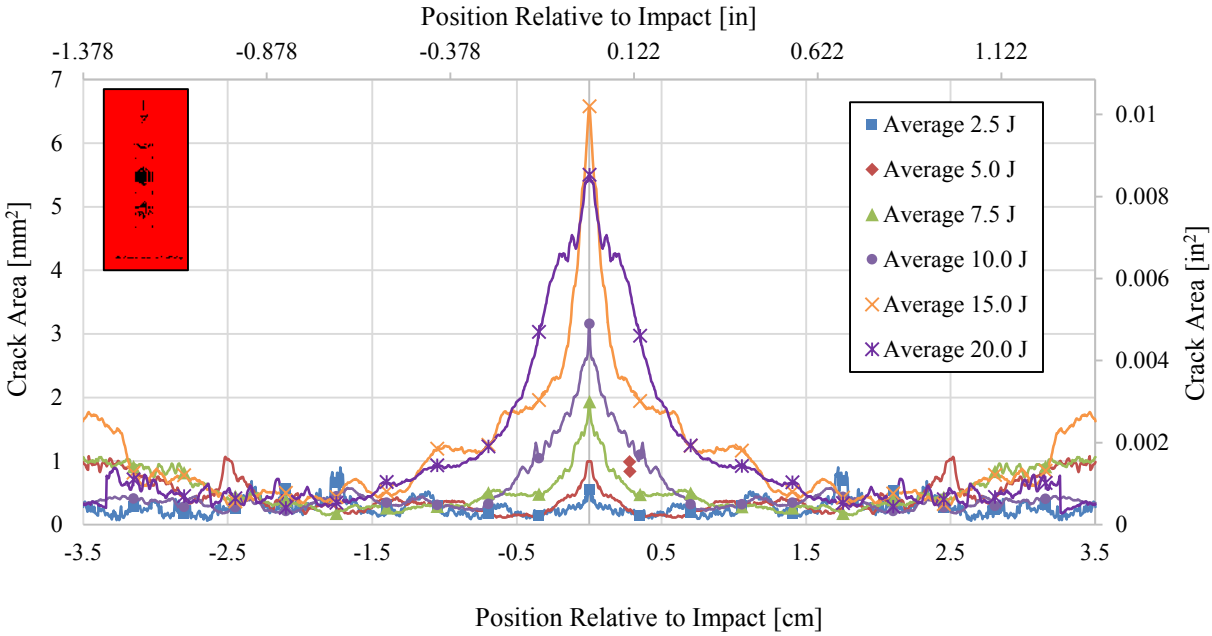

Figure 4.7 Average Crack Area as a Function of Distance from the Point of Impact for Half Braid Sleeve Types

Table 4.2 Peak Crack Area and Overall Crack Volume for Half Braid Sleeve Types

Impact Energy		Peak Crack Area		Overall Crack Volume	
[J	(ft-lbs)]	mm^2	$(10^3\ in^2)$	mm^3	$(10^3\ in^3)$
2.5	(1.9)	0.55	0.85	5.09	0.31
5.0	(3.7)	5.0	1.55	6.66	0.41
7.5	(5.6)	7.5	3.00	12.72	0.78
10	(7.4)	10.0	4.89	19.54	1.19
15	(11)	15.0	10.2	44.65	2.72
20	(14.8)	20.0	8.53	51.21	3.12

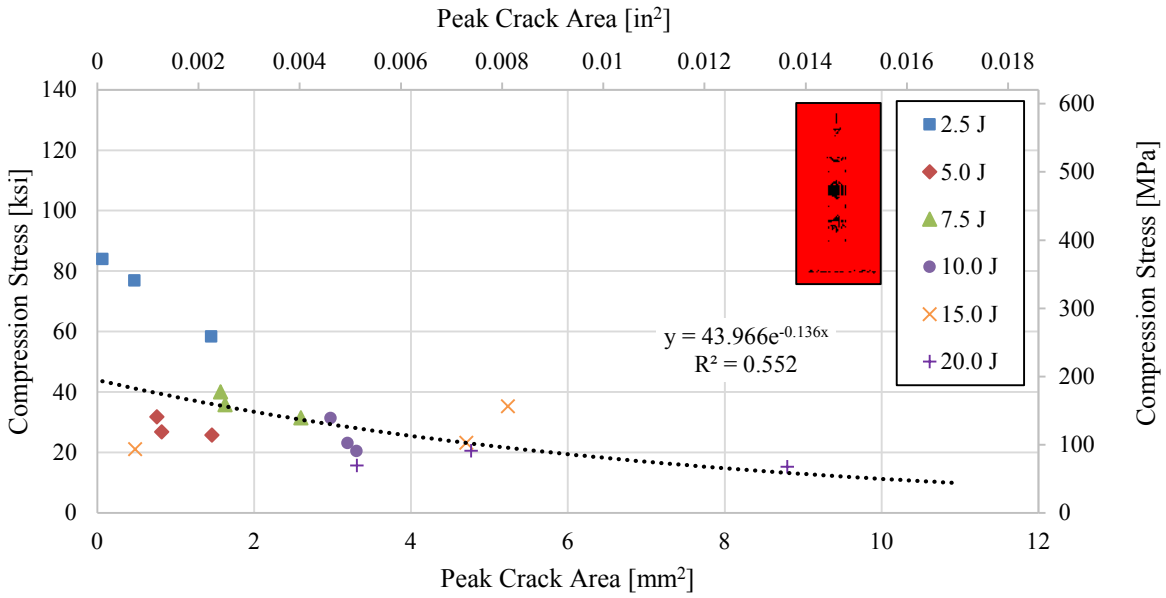

Figure 4.8 Peak Crack Area vs. Ultimate Compressive Stress Half Braid Sleeve Types

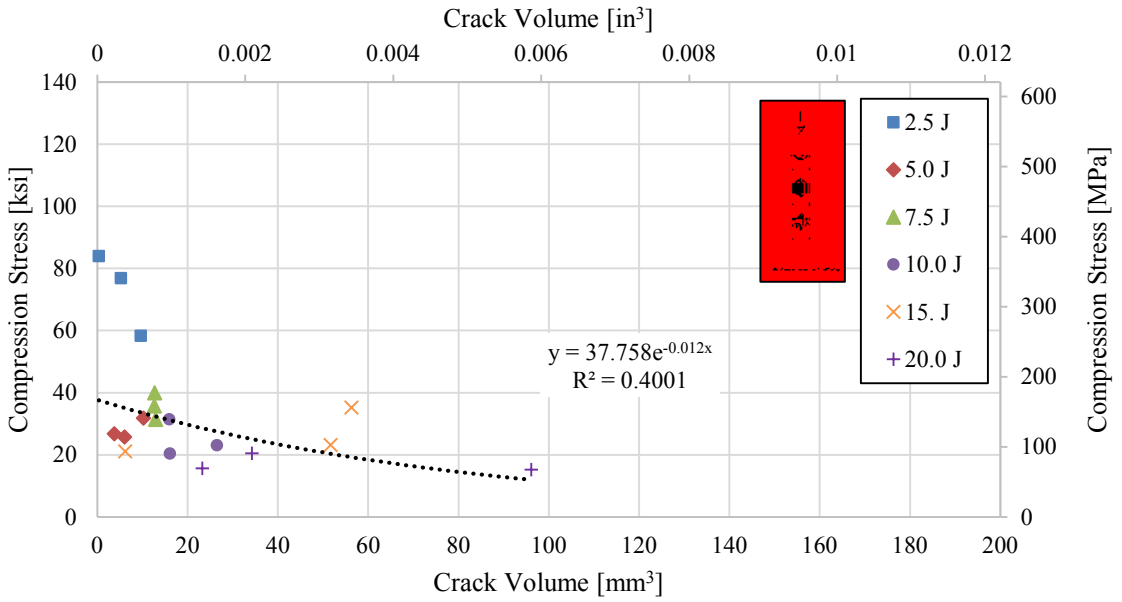

Figure 4.9 Overall Crack Volume vs. Ultimate Compressive Stress Half Braid Sleeve Types

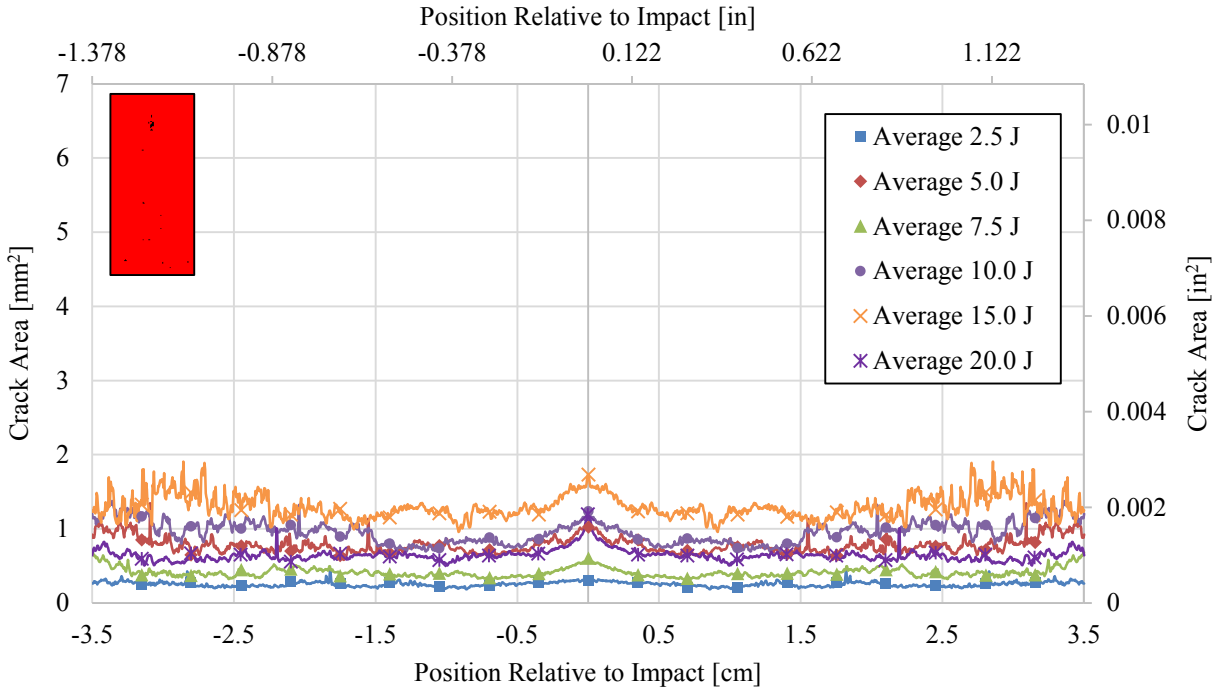

Figure 4.10 Average Crack Area as a Function of Distance from the Point of Impact for Full Spiral Sleeve Types

Table 4.3 Peak Crack Area and Overall Crack Volume for Full Spiral Sleeve Types

Impact Energy		Peak Crack Area		Overall Crack Volume	
[J	(ft-lbs)]	mm^2	(10^3 in^2)	mm^3	(10^3 in^3)
2.5	(1.9)	0.32	0.50	5.75	0.35
5.0	(3.7)	1.02	1.59	17.50	1.07
7.5	(5.6)	0.60	0.94	9.06	0.55
10	(7.4)	1.23	1.91	19.85	1.21
15	(11)	1.73	2.68	29.04	1.77
20	(14.8)	1.19	1.85	15.40	0.94

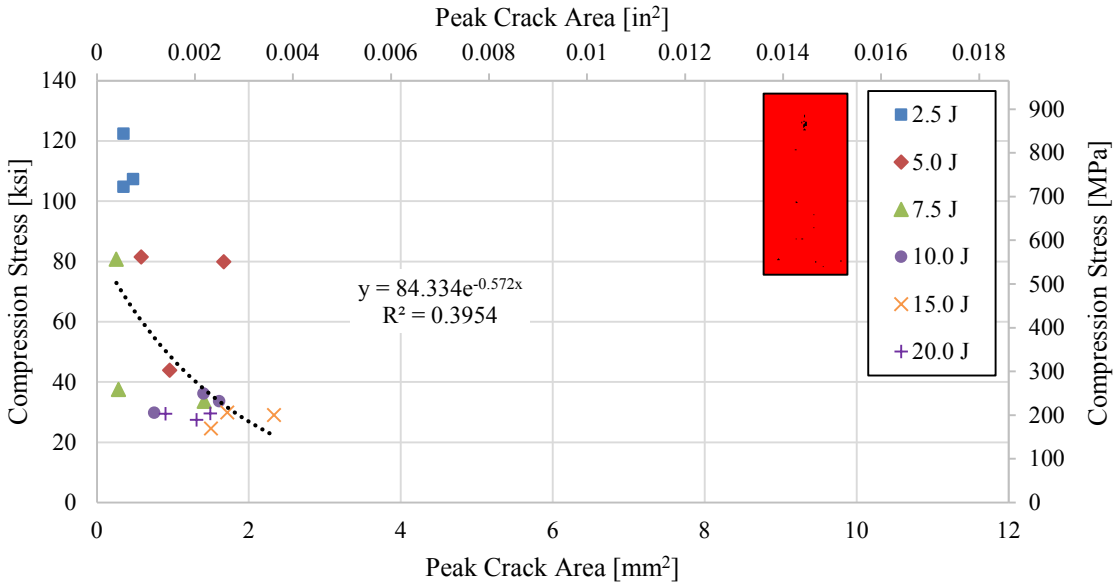

Figure 4.11 Peak Crack Area vs. Ultimate Compressive Stress Full Spiral Sleeve Types

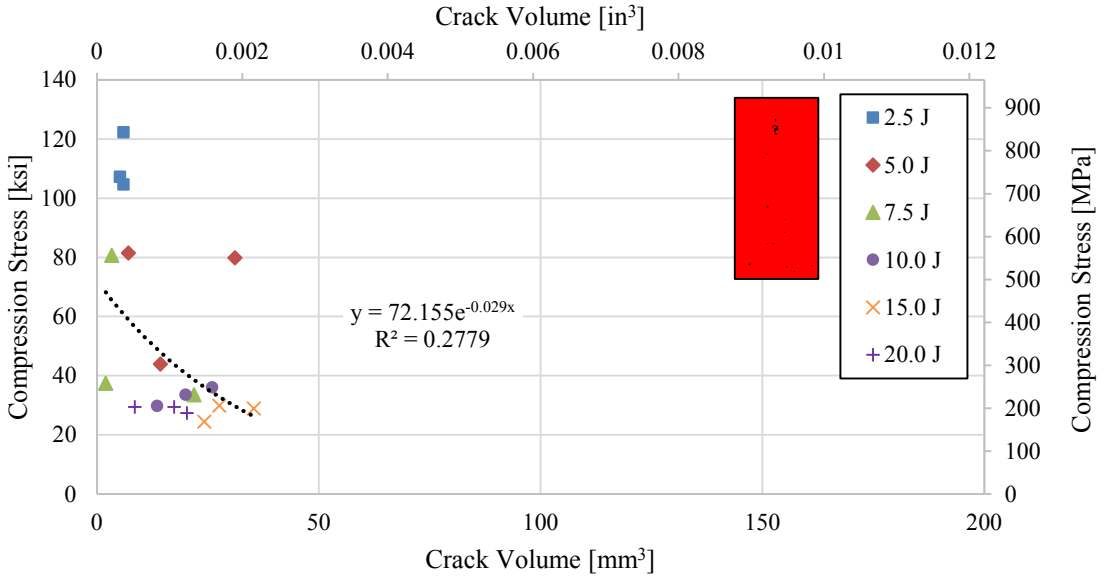

Figure 4.12 Overall Crack Volume vs. Ultimate Compressive Stress Full Spiral Sleeve Types

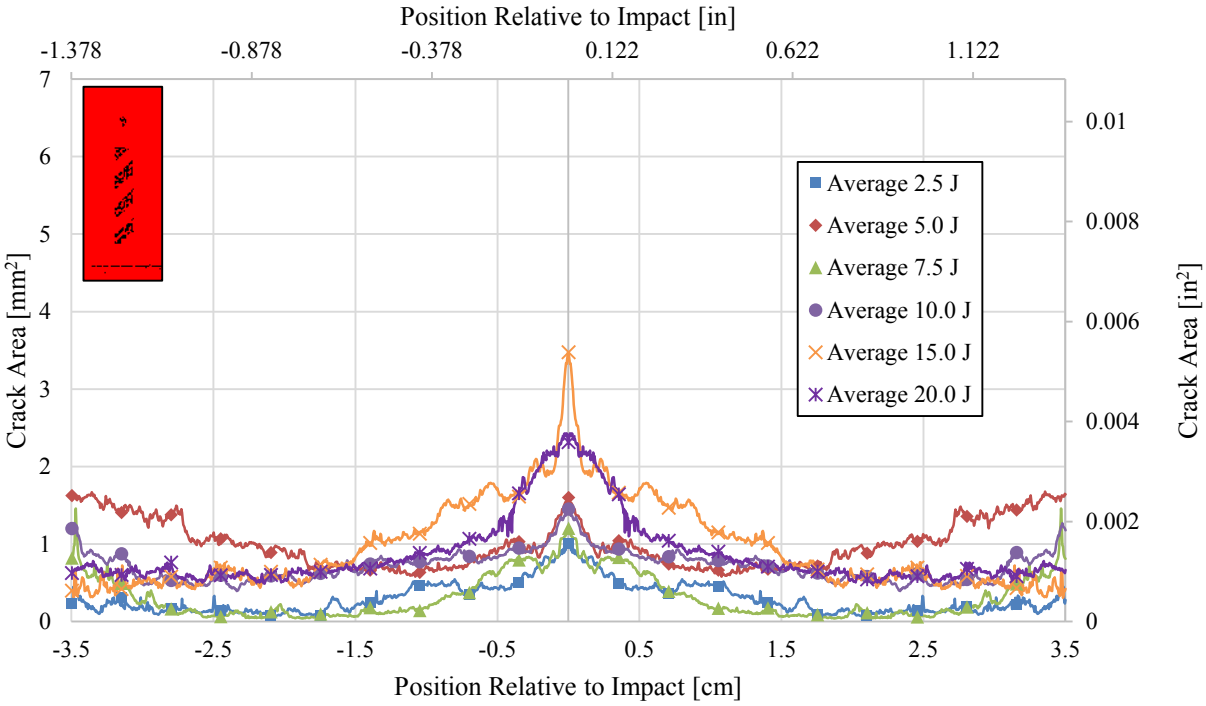

Figure 4.13 Average Crack Area as a Function of Distance from the Point of Impact for Half Spiral Sleeve Types

Table 4.4 Peak Crack Area and Overall Crack Volume for Half Spiral Sleeve Types.

Impact Energy		Peak Crack Area		Overall Crack Volume	
[J	(ft-lbs)]	mm^2	(10^3 in^2)	mm^3	(10^3 in^3)
2.5	(1.9)	1.01	1.56	12.2	0.75
5.0	(3.7)	1.60	2.48	20.0	1.22
7.5	(5.6)	1.20	1.86	12.6	0.77
10	(7.4)	1.45	2.25	20.4	1.25
15	(11)	3.47	5.38	38.1	2.32
20	(14.8)	2.43	3.77	30.7	1.87

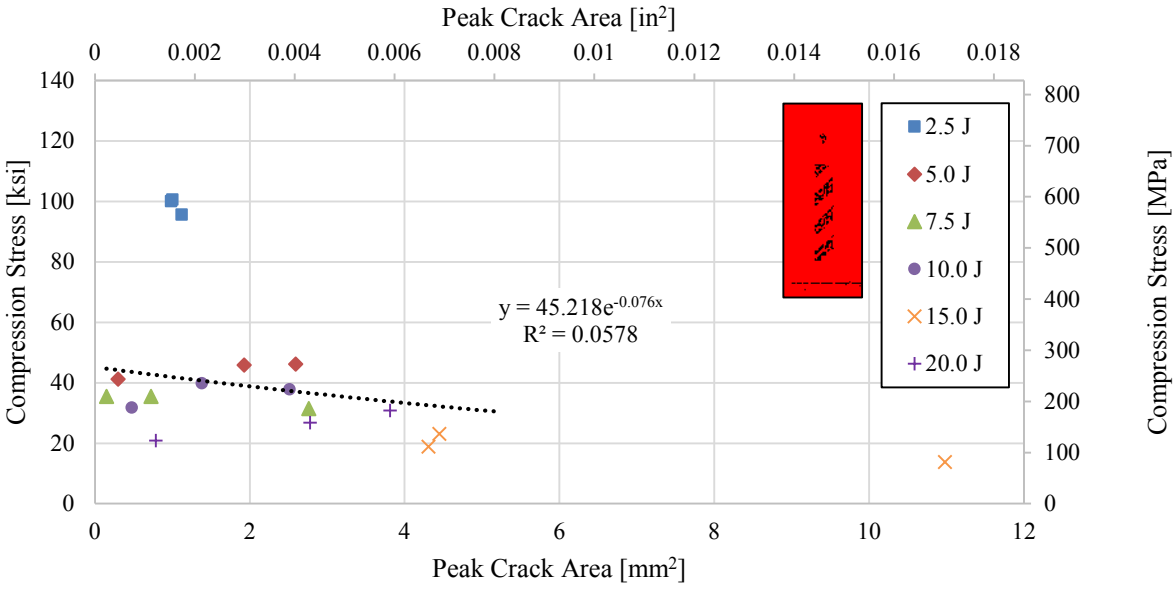

Figure 4.14 Peak Crack Area vs. Ultimate Compressive Stress Half Spiral Sleeve Types

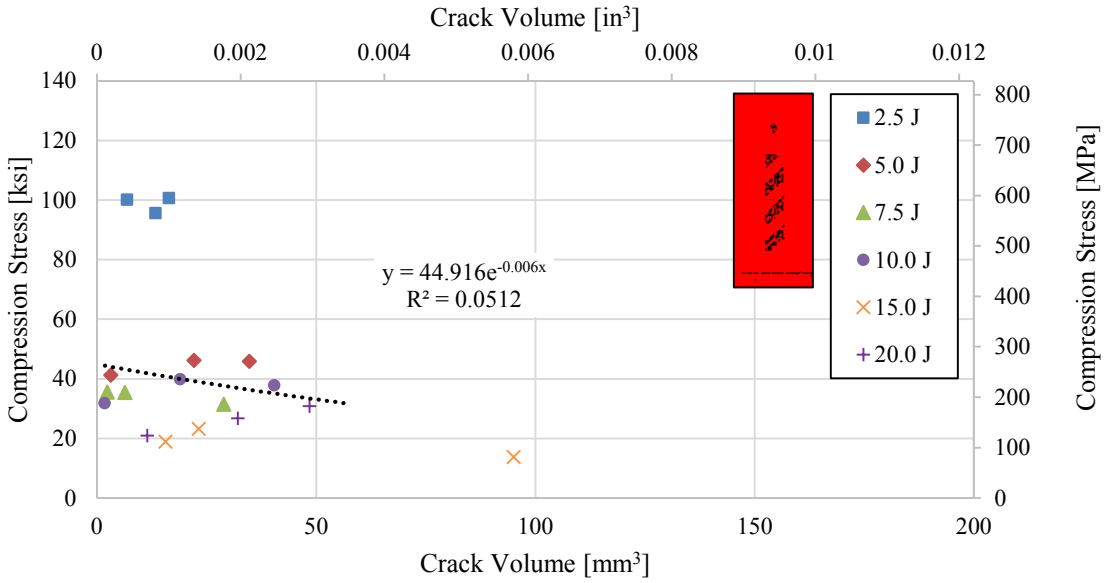

Figure 4.15 Overall Crack Volume vs. Ultimate Compressive Stress Half Spiral Sleeve Types

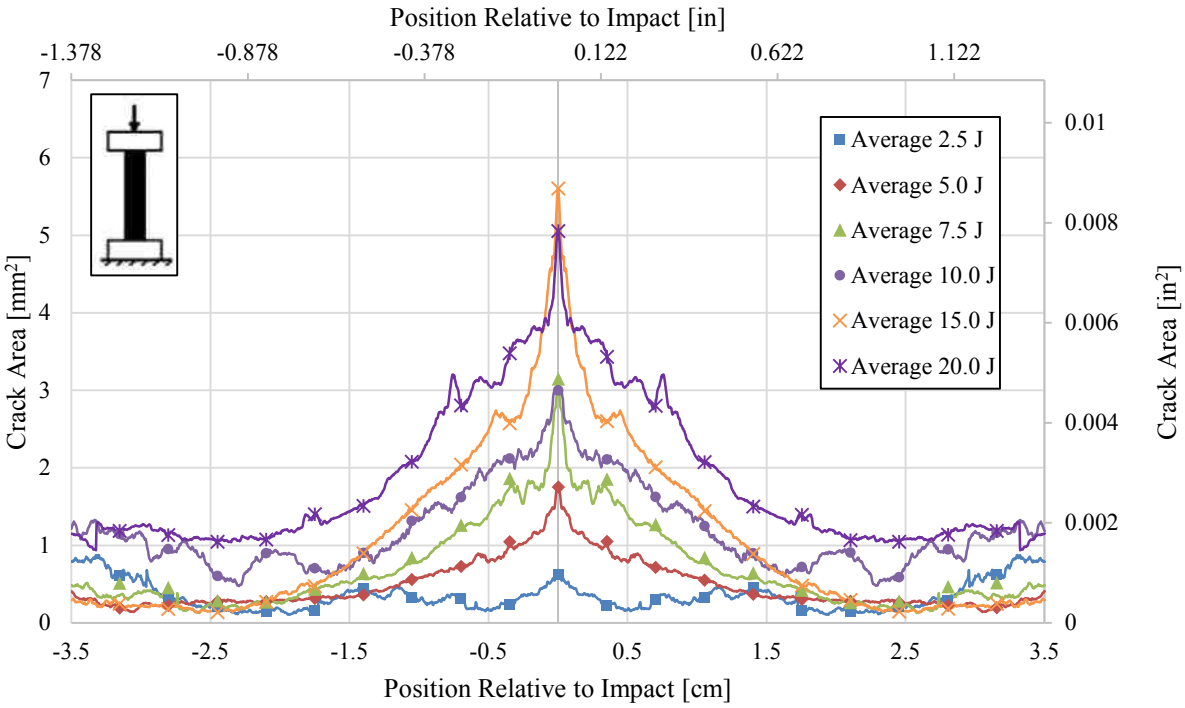

Figure 4.16 Average Crack Area as a Function of Distance from the Point of Impact for Shrink Tape Sleeve Types

Table 4.5 Peak Crack Area and Overall Crack Volume for Shrink Tape Sleeves

Impact Energy		Peak Crack Area		Overall Crack Volume	
[J	(ft-lbs)]	mm^2	(10^3 in^2)	mm^3	(10^3 in^3)
2.5	(1.9)	0.62	(0.96)	7.04	(0.43)
5.0	(3.7)	1.76	(2.72)	19.5	(1.19)
7.5	(5.6)	3.17	(4.92)	31.3	(1.91)
10	(7.4)	3.01	(4.67)	42.1	(2.57)
15	(11)	5.61	(8.69)	55.9	(3.41)
20	(14.8)	5.06	(7.84)	70.0	(4.27)

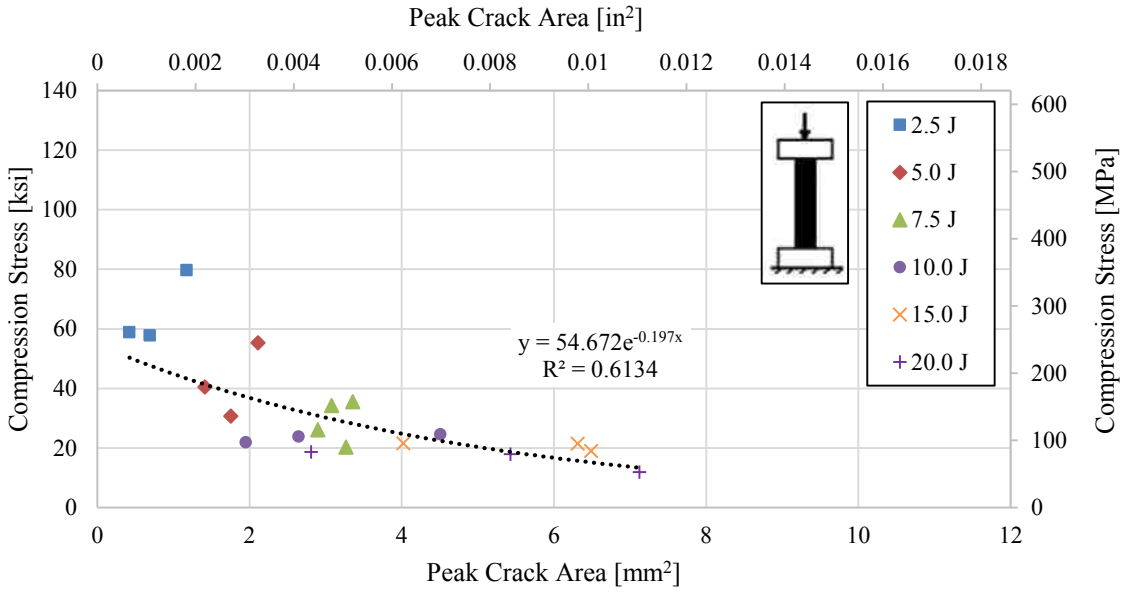

Figure 4.17 Peak Crack Area vs. Ultimate Compressive Stress for Shrink Tape Sleeve Types

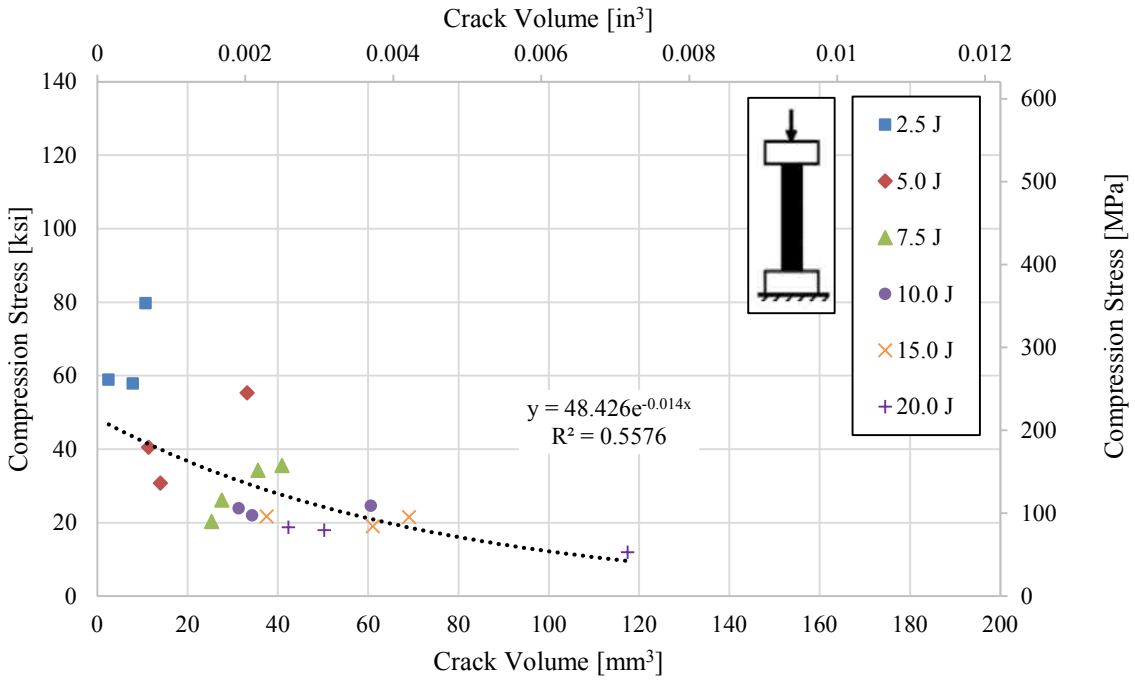

Figure 4.18 Overall Crack Volume vs. Ultimate Compressive Stress Shrink Tape Sleeve Types

The trend lines for each of the various sleeve configurations of the peak crack area and overall crack volume vs. the ultimate compressive stress are shown in Figures 4.19 and 4.20, respectively. The trend lines show a large drop in compression stress for full spiral with a small increase in crack area while the other sleeves have a more gradual slope. A similar trend can be seen with overall crack volume with the exception of full braid sleeves which exhibit a large decrease in compressive stress with a small increase in crack volume. This indicates that for full sleeves, a small quantity of cracks can have a large impact on the residual strength of a member.

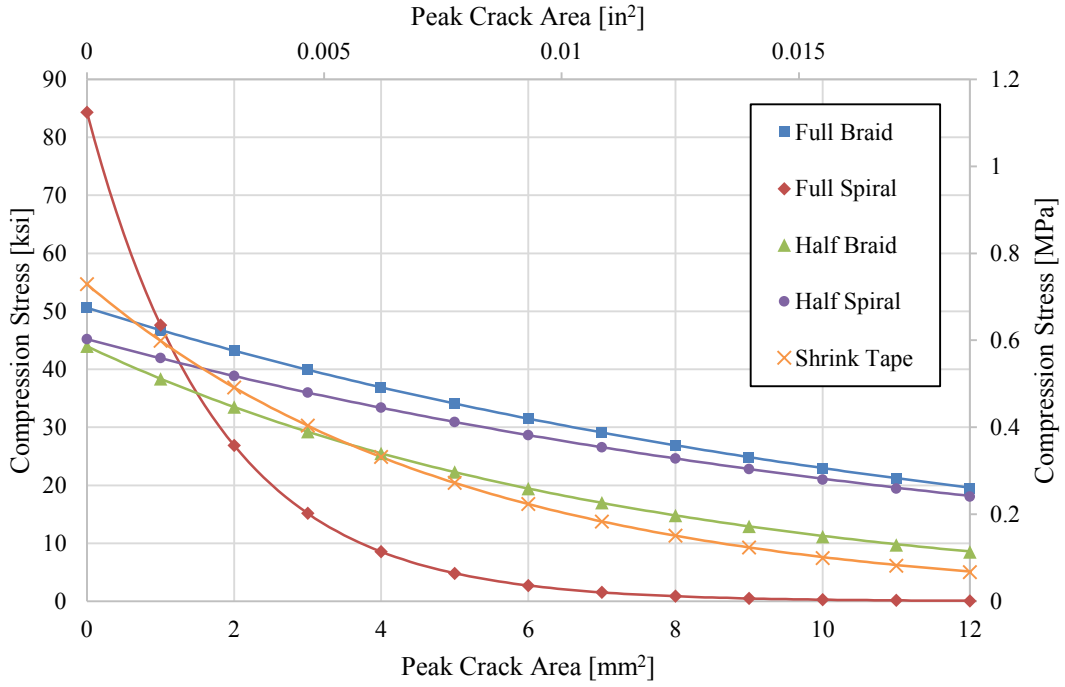

Figure 4.19 Trend Lines of Each Sleeve Configuration for Peak Crack Area vs. Ultimate Compressive Stress

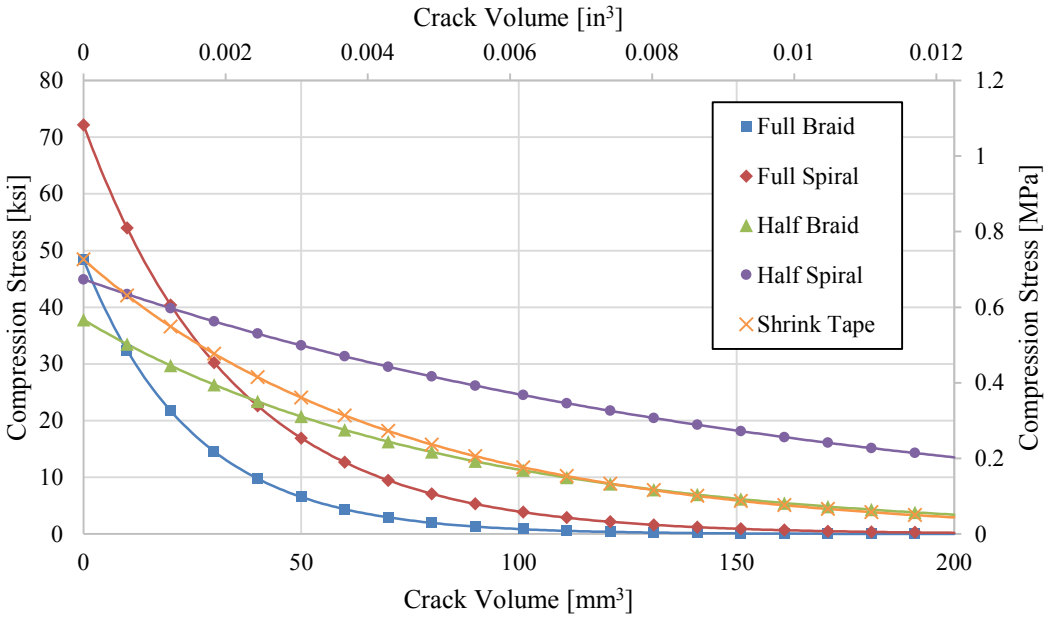

Figure 4.20 Trend Lines of Each Sleeve Configuration for Overall Crack Volume vs. Ultimate Compressive Stress

4.2 Influence of Impact Energy

The influence of sleeve type and coverage for different impact levels (2.5 J, 5.0 J, 7.5 J, 10 J, 15 J (11 ft-lbs), and 20 J (15 ft-lbs)) are illustrated in Figures 4.21 through 4.38, respectively. Sleeve type and coverage make no significant difference in crack area for low-impacted specimens as exemplified by Figure 4.7.

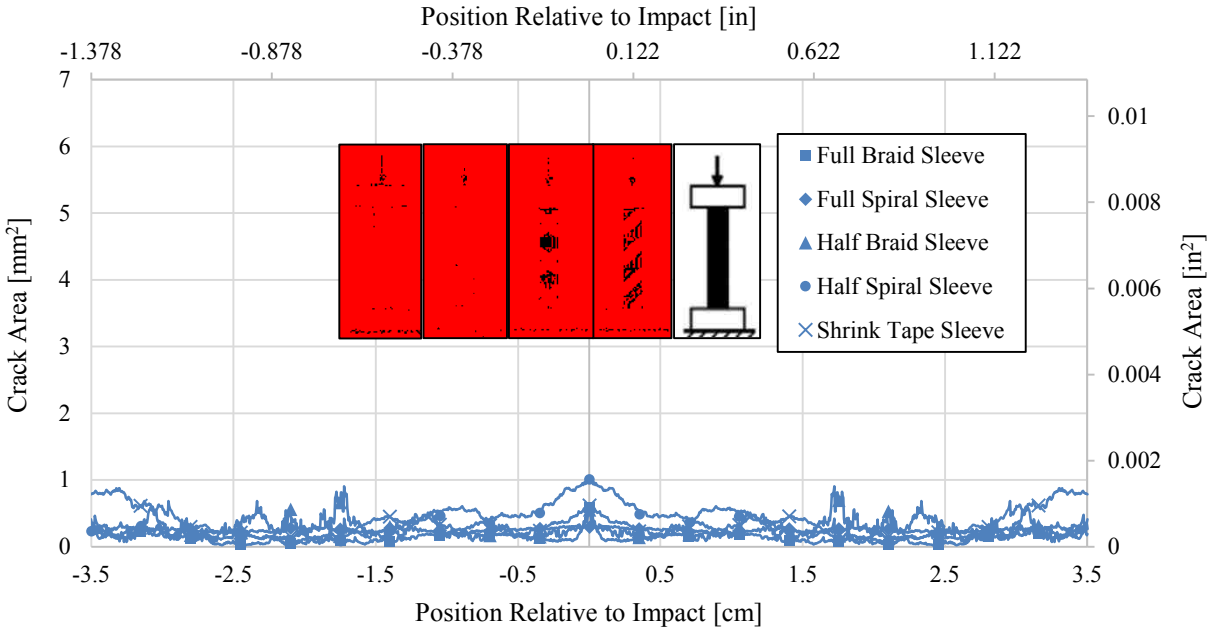

Figure 4.21 Average Crack Area as a Function of Distance from the Point of Impact for 2.5 J (1.9 ft-lbs) Impacted Specimens

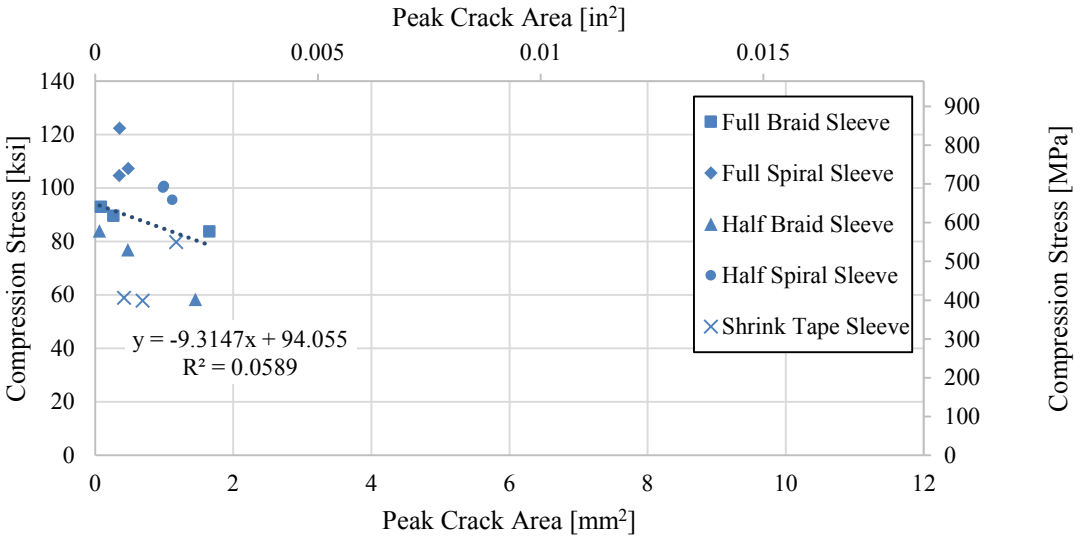

Figure 4.22 Peak Crack Area vs. Ultimate Compressive Stress for 2.5 J (1.9 ft-lbs) Impact Energy

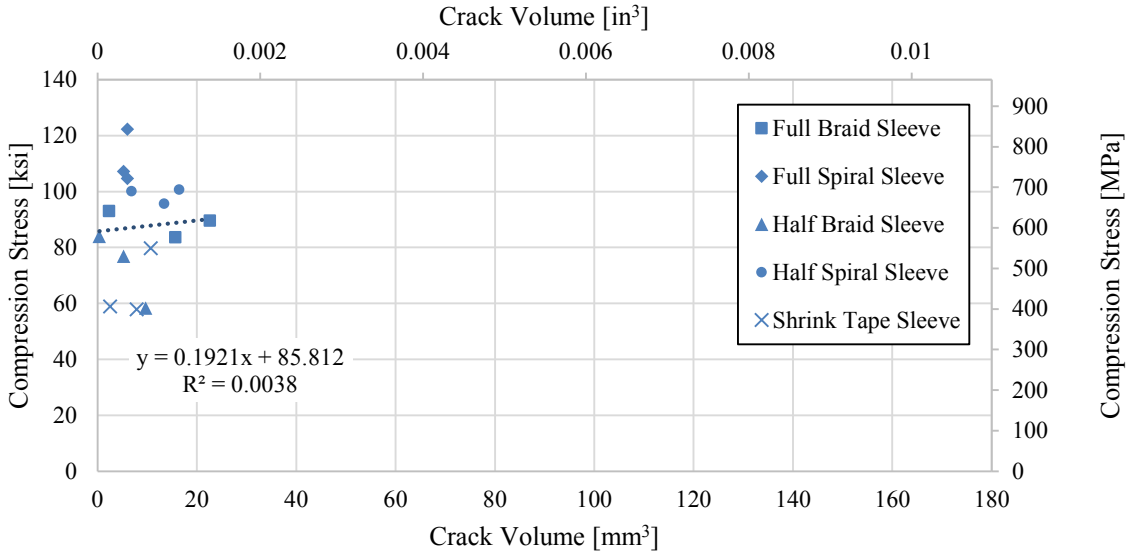

Figure 4.23 Overall Crack Volume vs. Ultimate Compressive Stress for 2.5 J (1.9 ft-lbs) Impact Energy

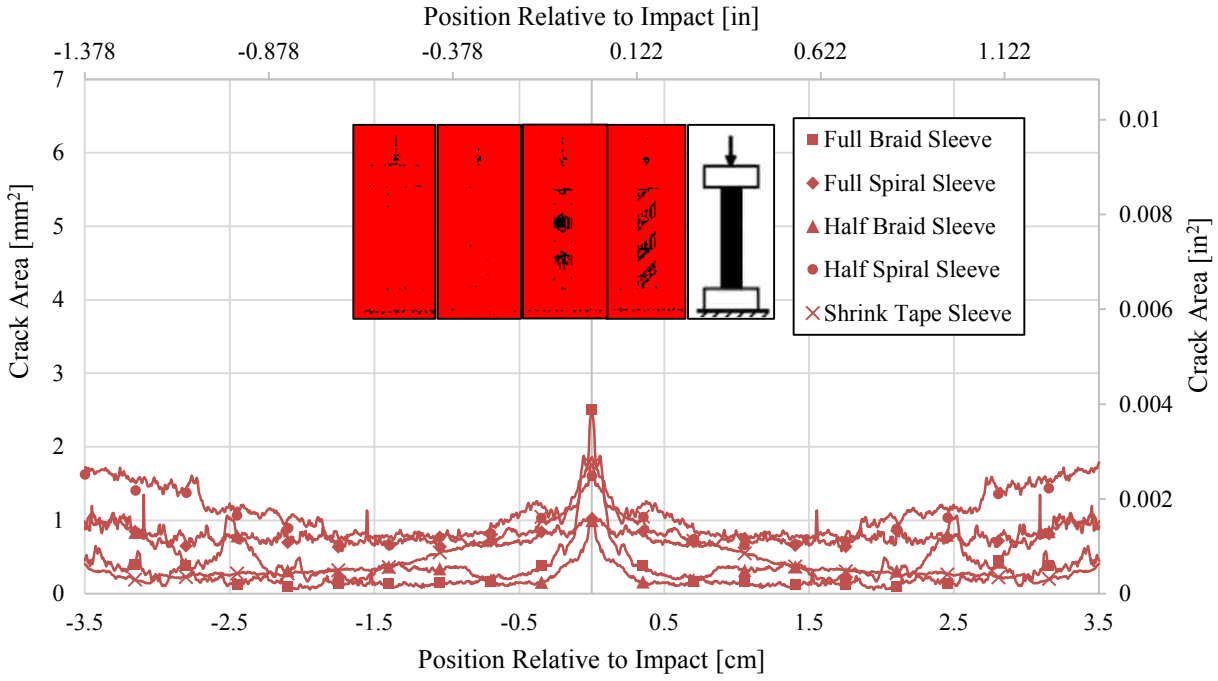

Figure 4.24 Average Crack Area as a Function of Distance from the Point of Impact for 5.0 J (3.7 ft-lbs) Impacted Specimens

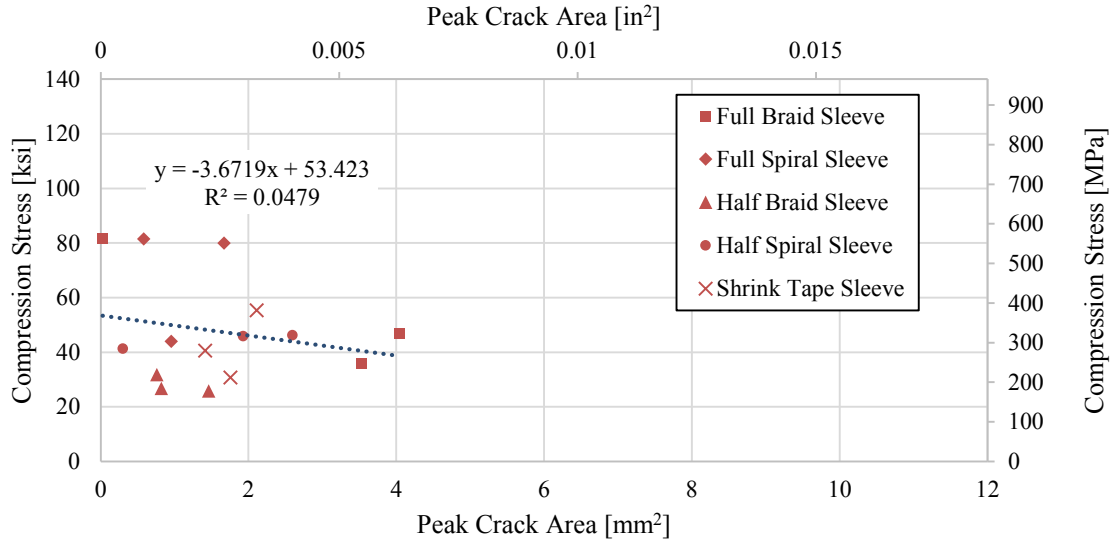

Figure 4.25 Peak Crack Area vs. Ultimate Compressive Stress for 5.0 J (3.7 ft-lbs) Impacted Specimens

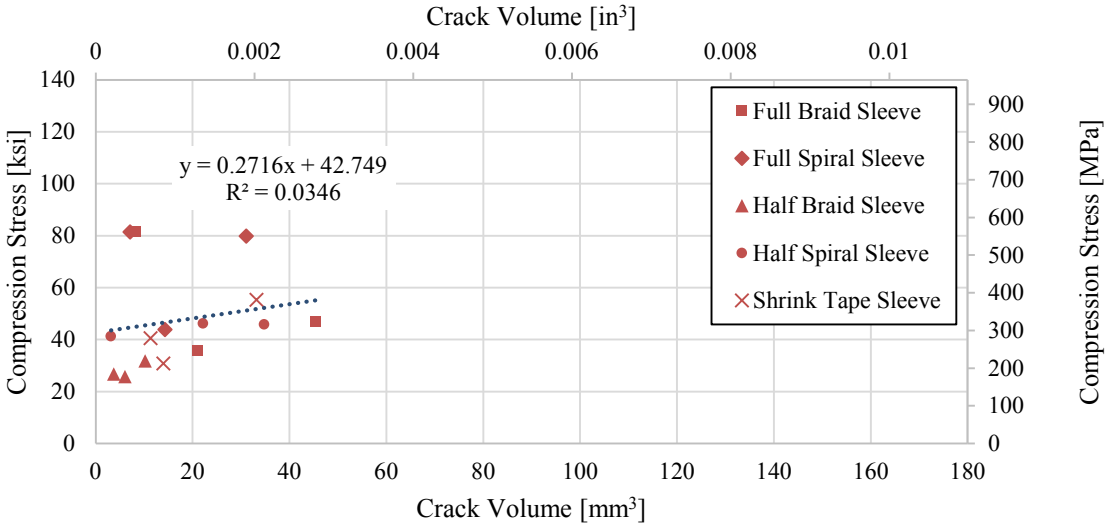

Figure 4.26 Overall Crack Volume vs. Ultimate Compressive Stress for 5.0 J (3.7 ft-lbs) Impacted Specimens

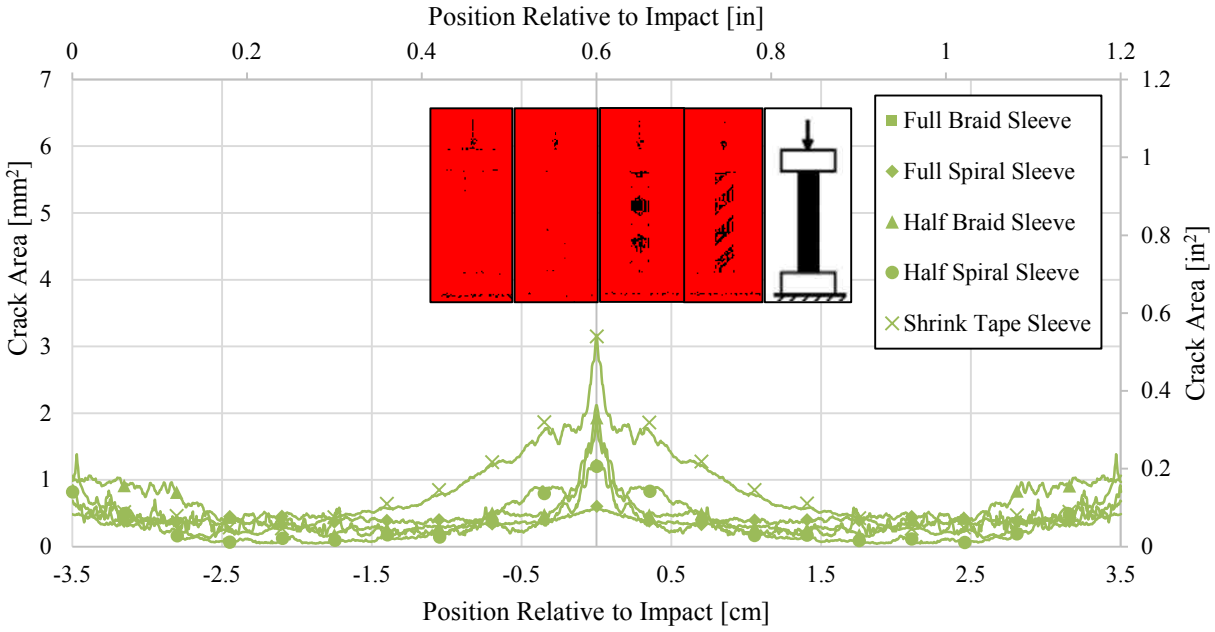

Figure 4.27 Average Crack Area as a Function of Distance from the Point of Impact for 7.5 J (5.6 ft-lbs) Impacted Specimens

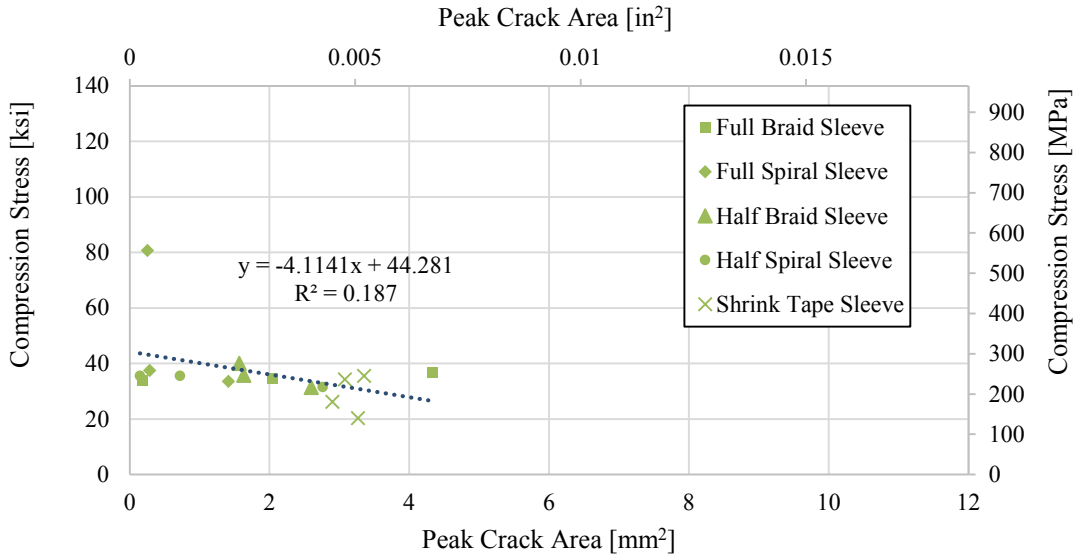

Figure 4.28 Peak Crack Area vs. Ultimate Compressive Stress for 7.5 J (5.6 ft-lbs) Impacted Specimens

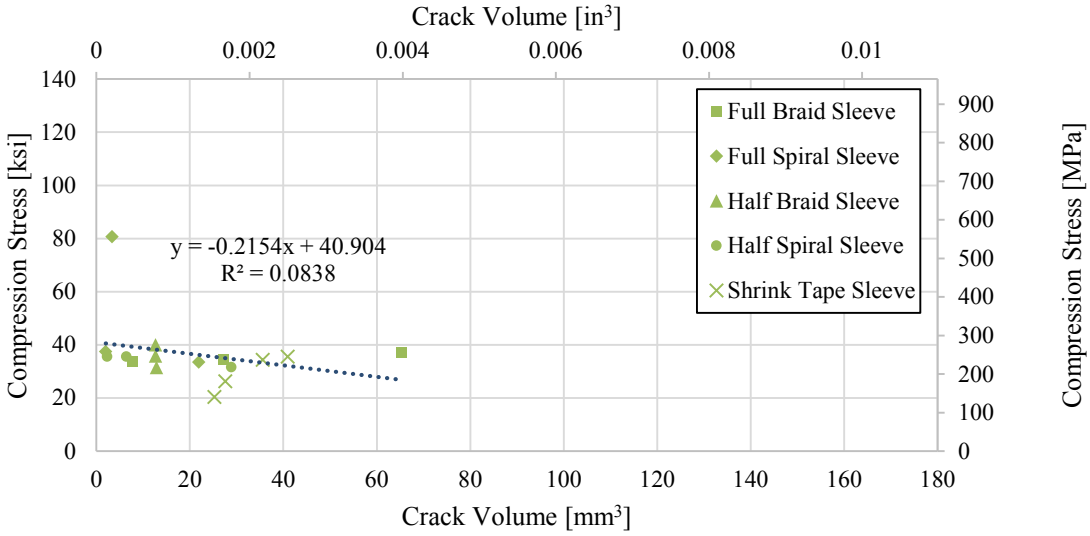

Figure 4.29 Overall Crack Volume vs. Ultimate Compressive Stress for 7.5 J (5.6 ft-lbs) Impacted Specimens

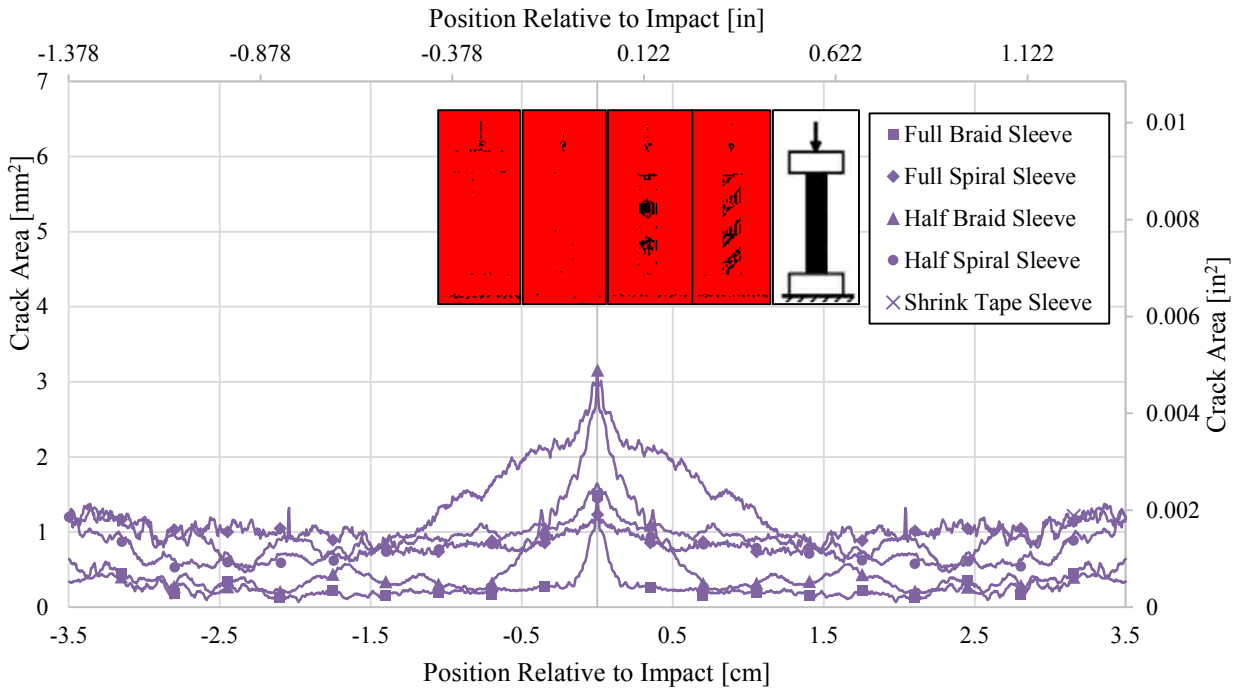

Figure 4.30 Average Crack Area as a Function of Distance from the Point of Impact for 10 J (7.4 ft-lbs) Impacted Specimens

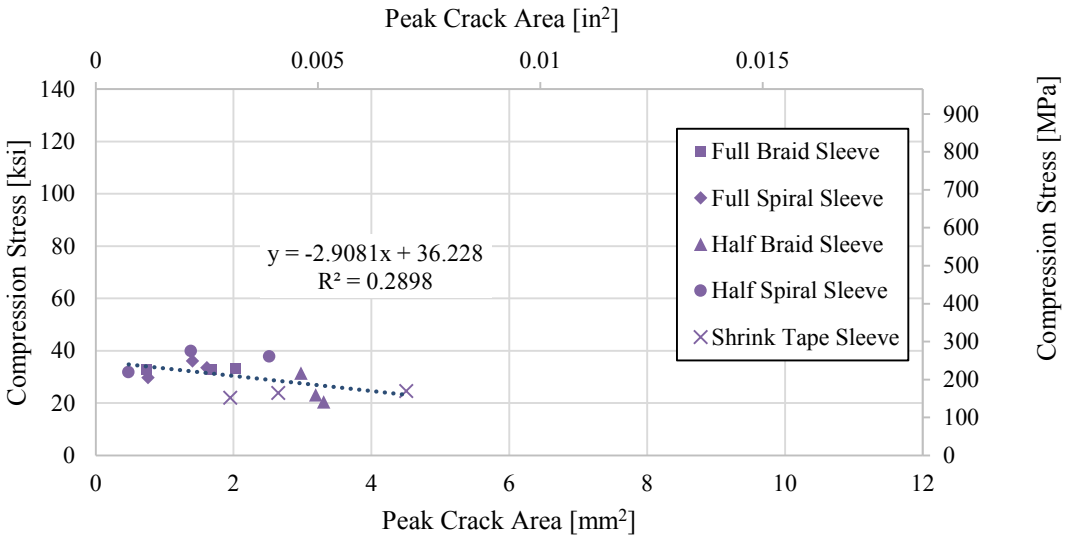

Figure 4.31 Peak Crack Area vs. Ultimate Compressive Stress for 10 J (7.4 ft-lbs) Impacted Specimens

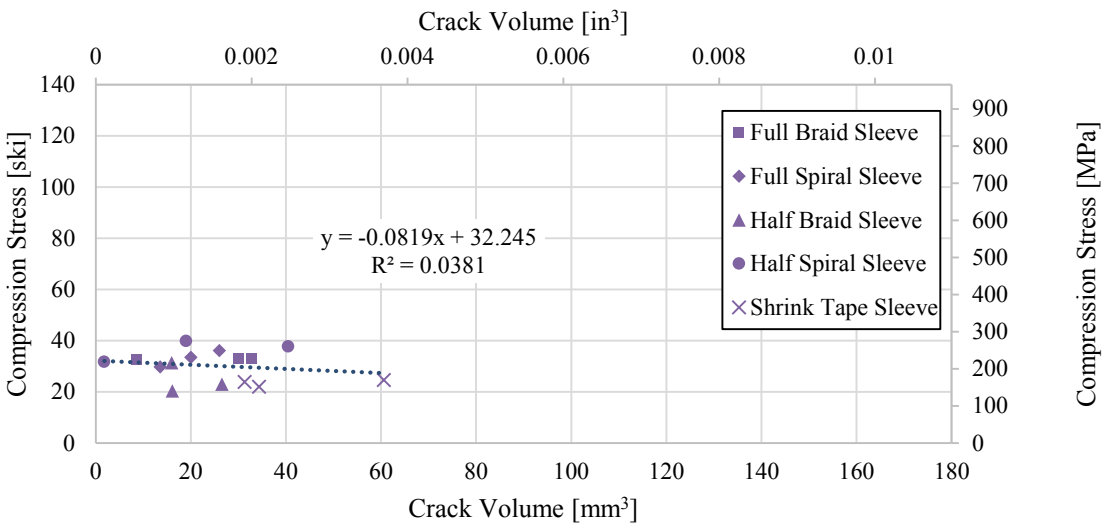

Figure 4.32 Overall Crack Volume vs. Ultimate Compressive Stress for 10 J (7.4 ft-lbs) Impacted Specimens

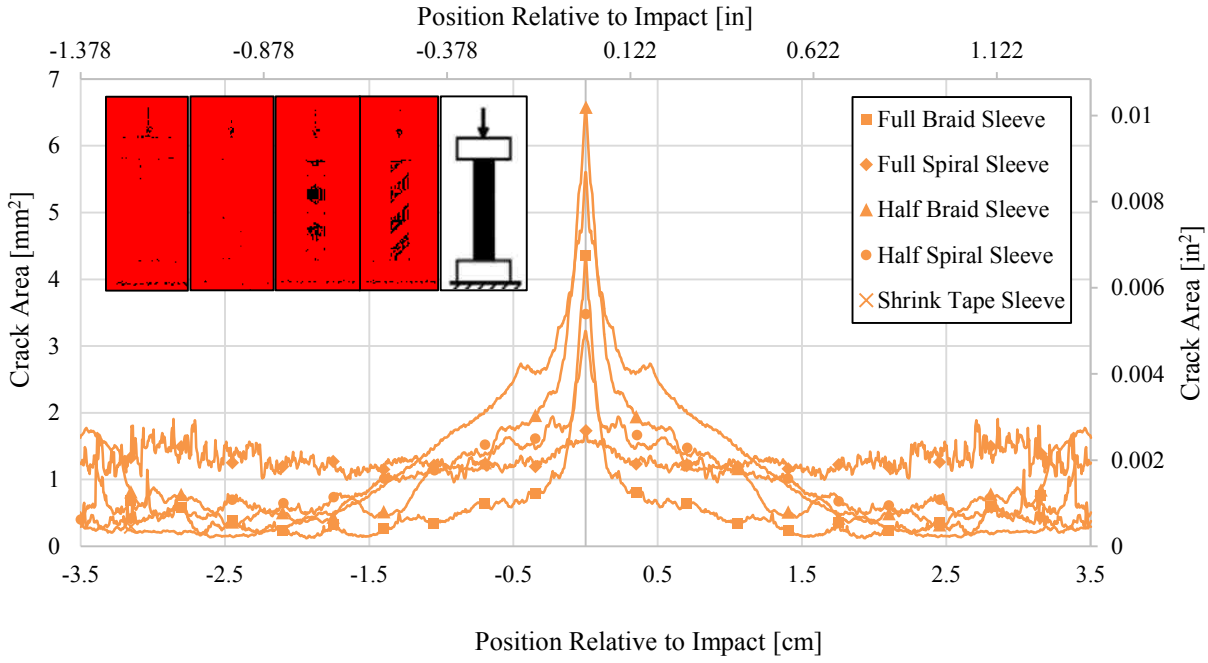

Figure 4.33 Average Crack Area as a Function of Distance from the Point of Impact for 15 J (11 ft-lbs) Impacted Specimens

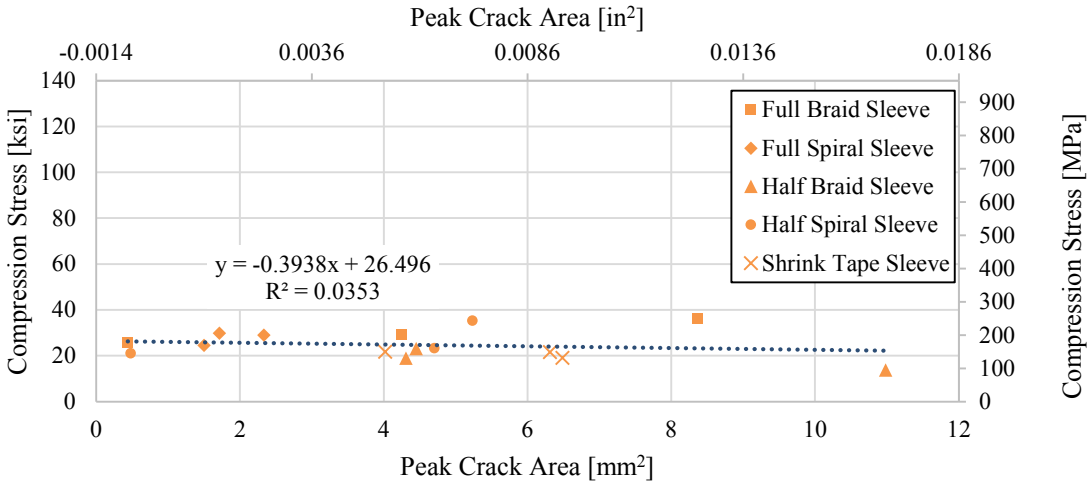

Figure 4.34 Peak Crack Area vs. Ultimate Compressive Stress for 15 J (11 ft-lbs) Impacted Specimens

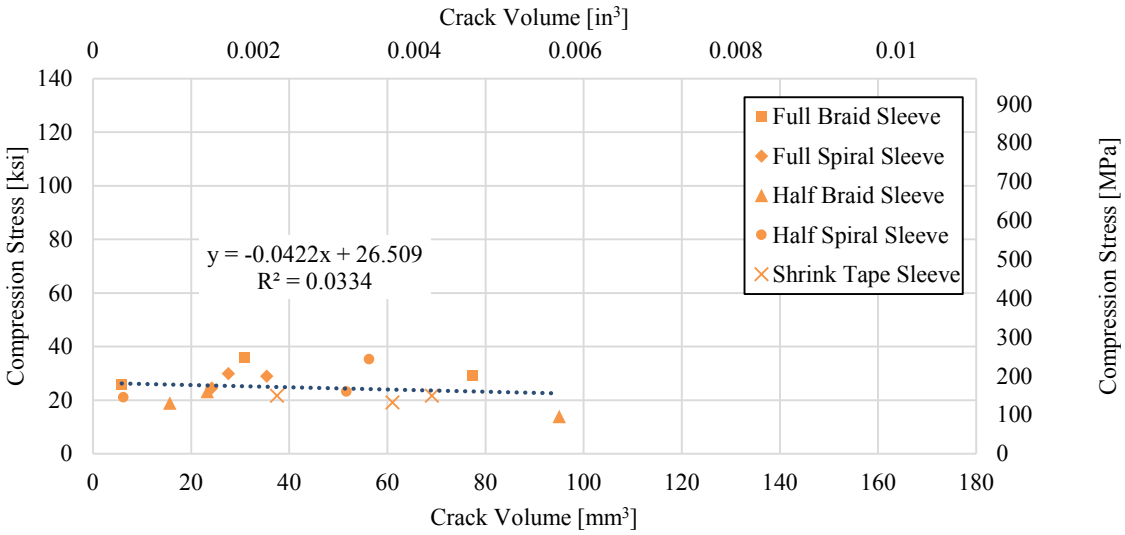

Figure 4.35 Overall Crack Volume vs. Ultimate Compressive Stress for 15 J (11 ft-lbs) Impacted Specimens

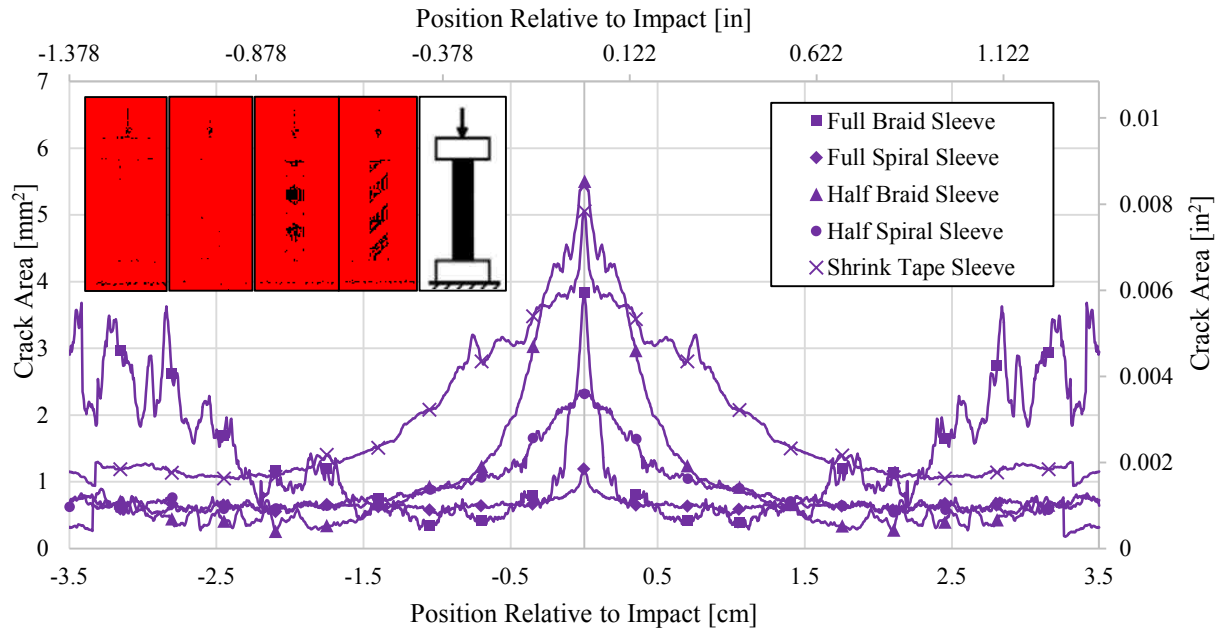

Figure 4.36 Average Crack Area as a Function of Distance from the Point of Impact for 20 J (15 ft-lbs) Impacted Specimens

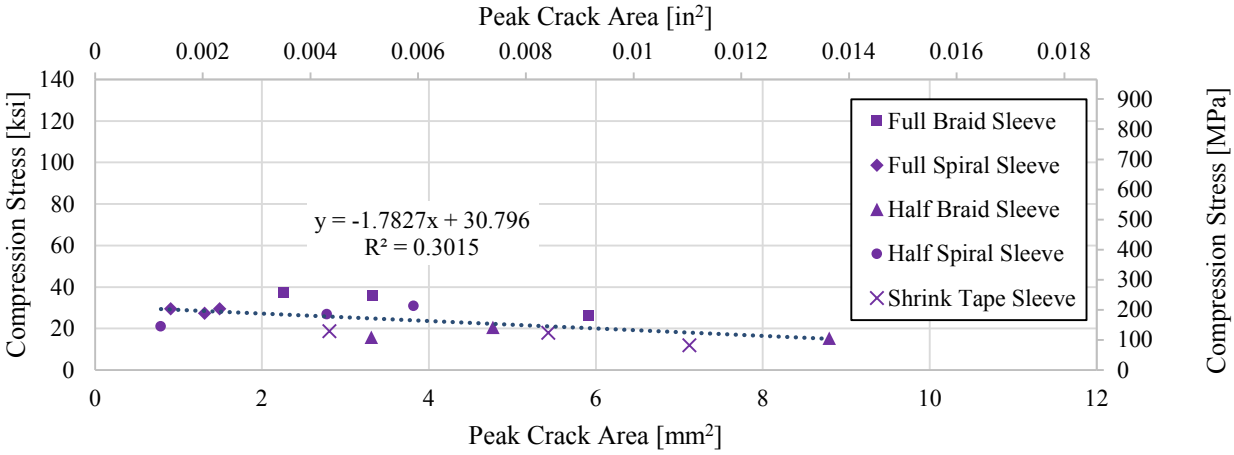

Figure 4.37 Peak Crack Area vs. Ultimate Compressive Stress for 20 J (15 ft-lbs) Impacted Specimens

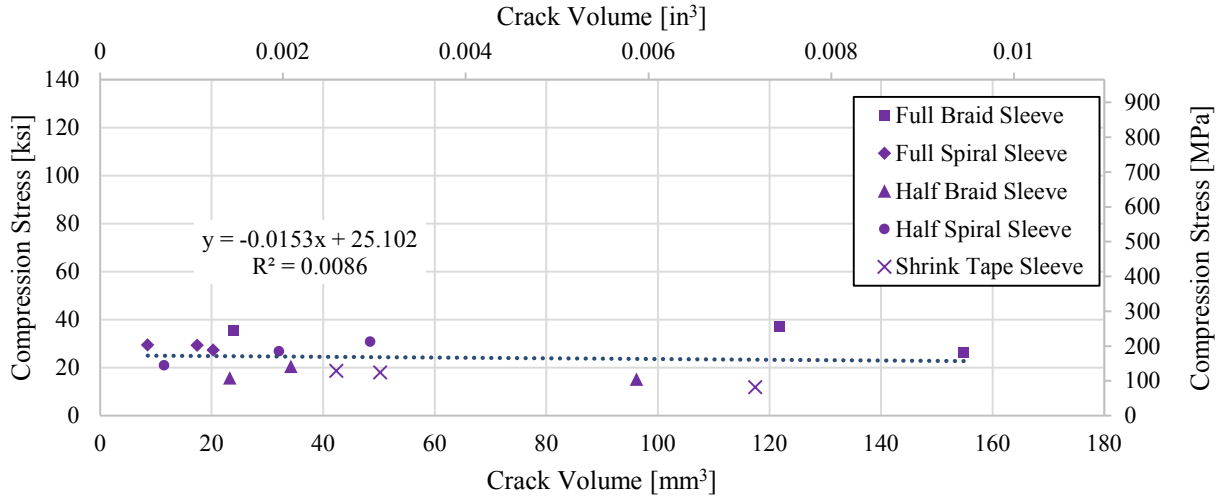

Figure 4.38 Overall Crack Volume vs. Ultimate Compressive Stress for 20 J (15 ft-lbs) Impacted Specimens

4.3 Influence of Sleeve Type and Impact Energy for Different Coverage

Figure 4.37-4.42 show the influence of sleeve type and impact energy for different coverage (full coverage and half coverage). Figures 4.15, 4.16, 4.18, and 4.19 show the peak crack area and the overall crack volume compared with the ultimate residual stress for full coverage and half coverage, respectively.

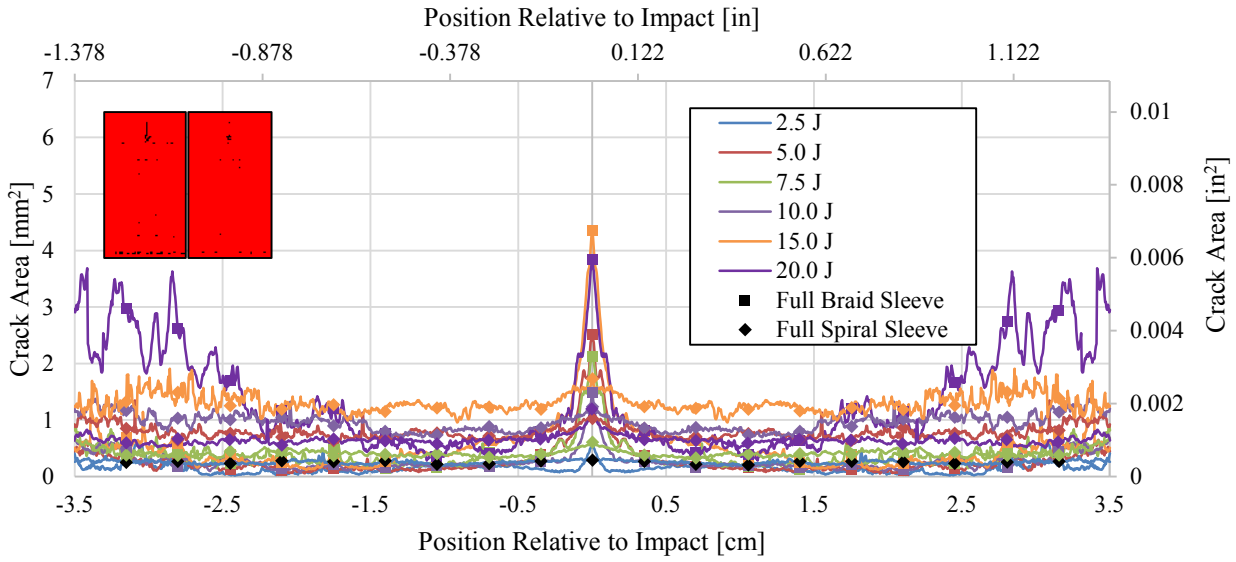

Figure 4.39 Average Crack Area as a Function of Distance from the Point of Impact for All Full Coverage Sleeves

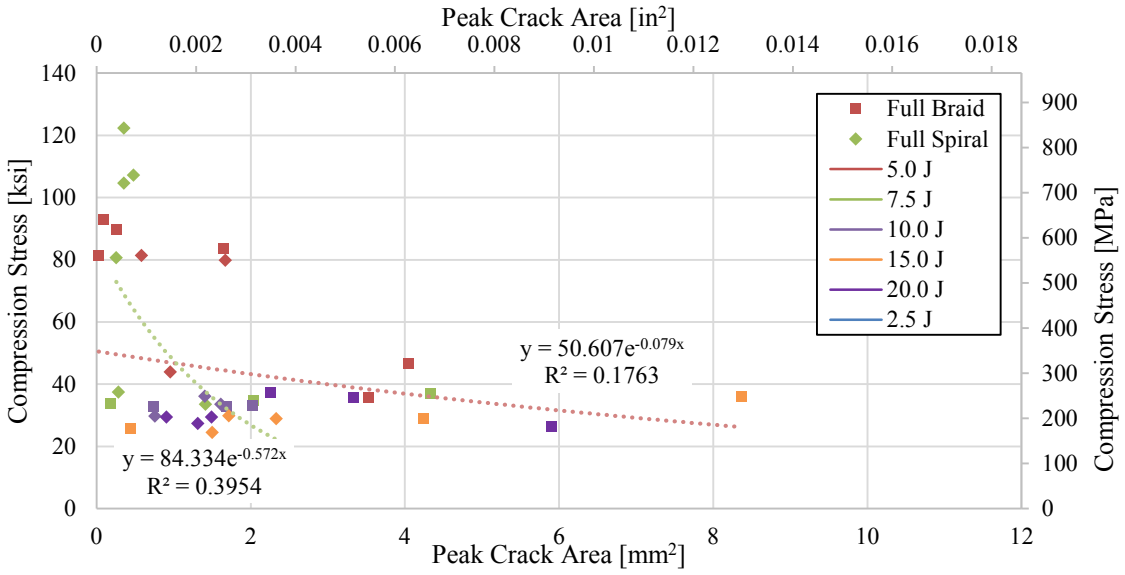

Figure 4.40 Peak Crack Area vs. Ultimate Compressive Stress for Full Coverage Sleeves.

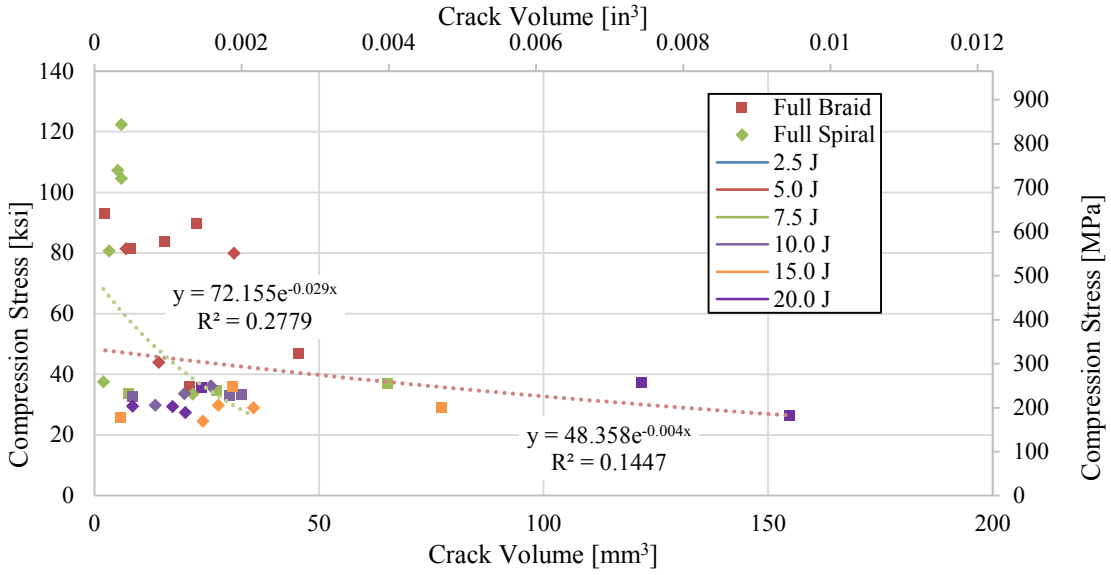

Figure 4.41 Overall Crack Volume vs. Ultimate Compressive Stress for Full Coverage Sleeve Types

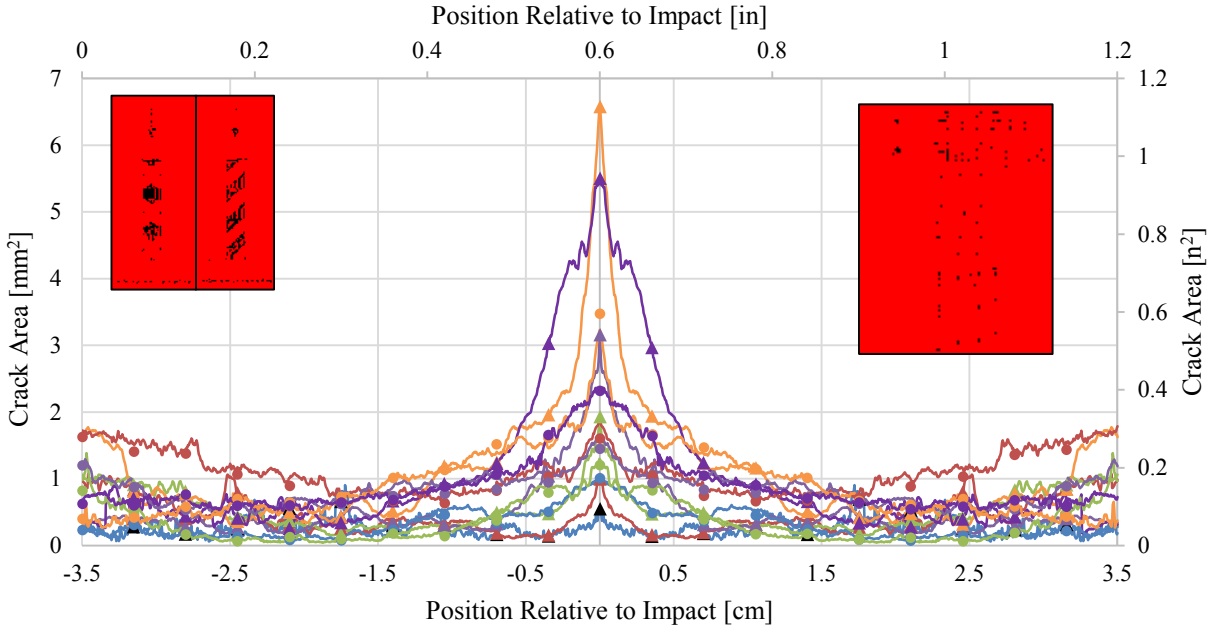

Figure 4.42 Average Crack Area as a Function of Distance from the Point of Impact for Half Coverage Sleeves

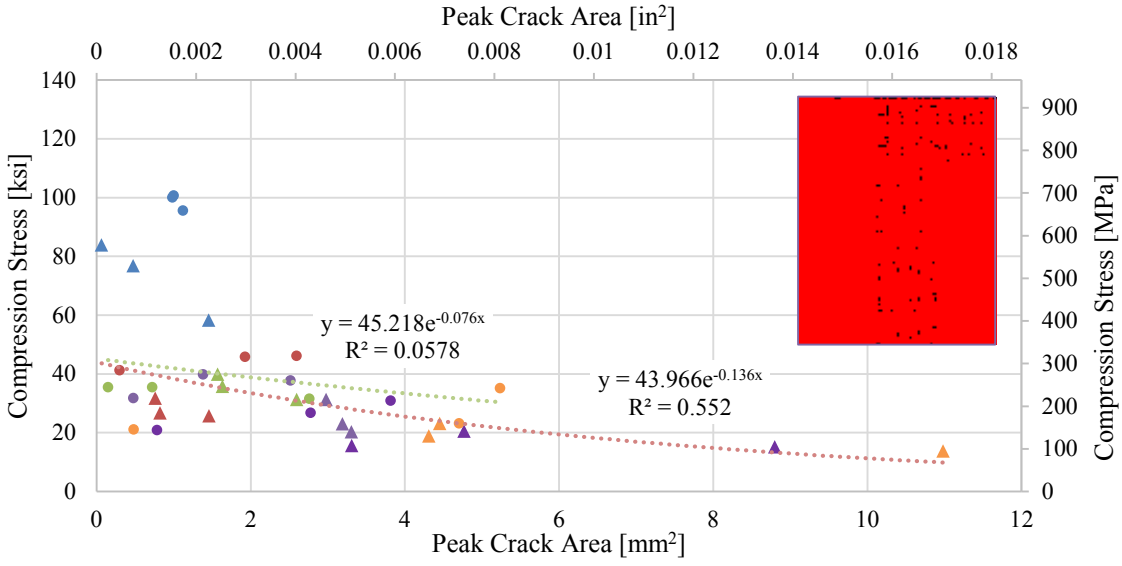

Figure 4.43 Peak Crack Area vs. Ultimate Compressive Stress for Half Coverage Sleeve Type

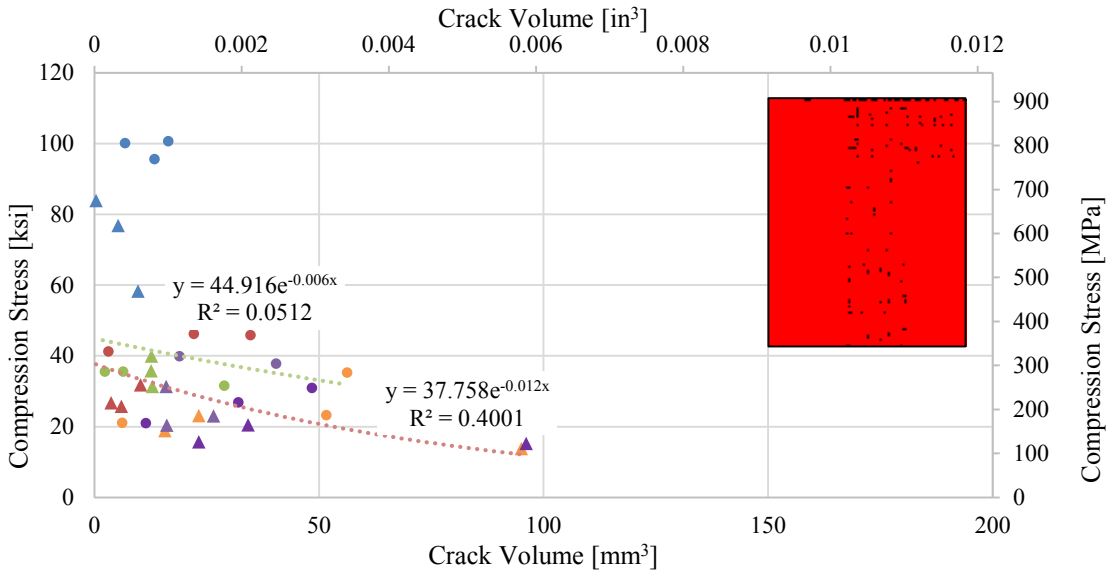

Figure 4.44 Overall Crack Volume vs. Ultimate Compressive Stress Half Coverage Sleeve Types

4.4 Influence of Coverage and Impact Levels for Different Sleeve Types

The final two plots, Figure 4.43-4.48, show the influence of coverage and impact levels for different sleeve types (braid and spiral).

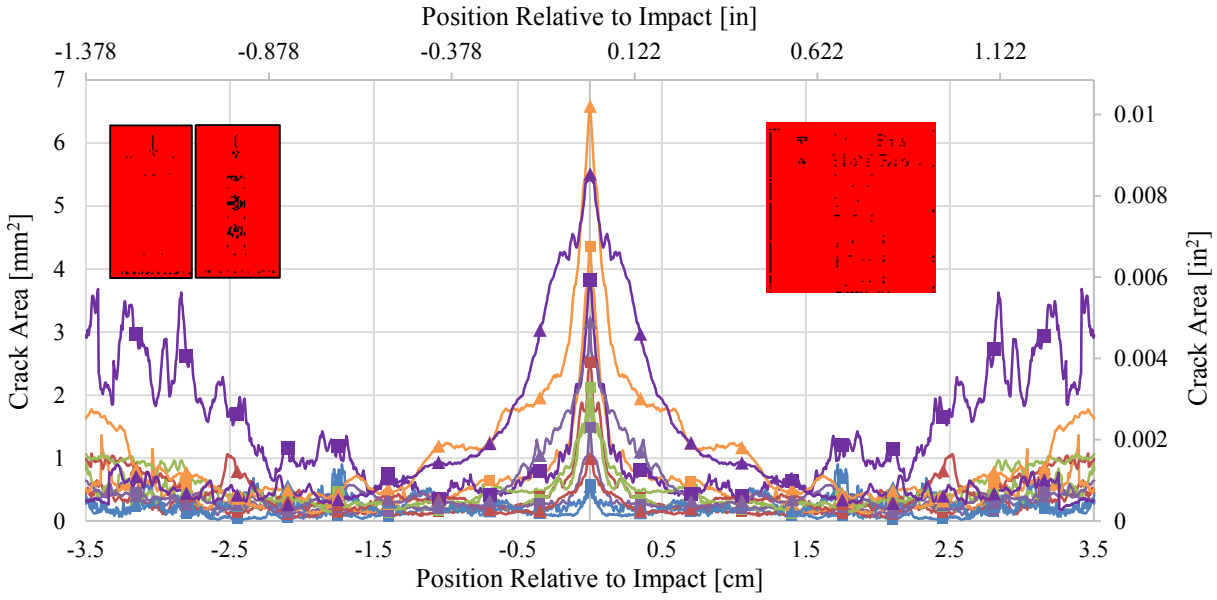

Figure 4.45 Average Crack Area as a Function of Distance from the Point of Impact for Braided Sleeves

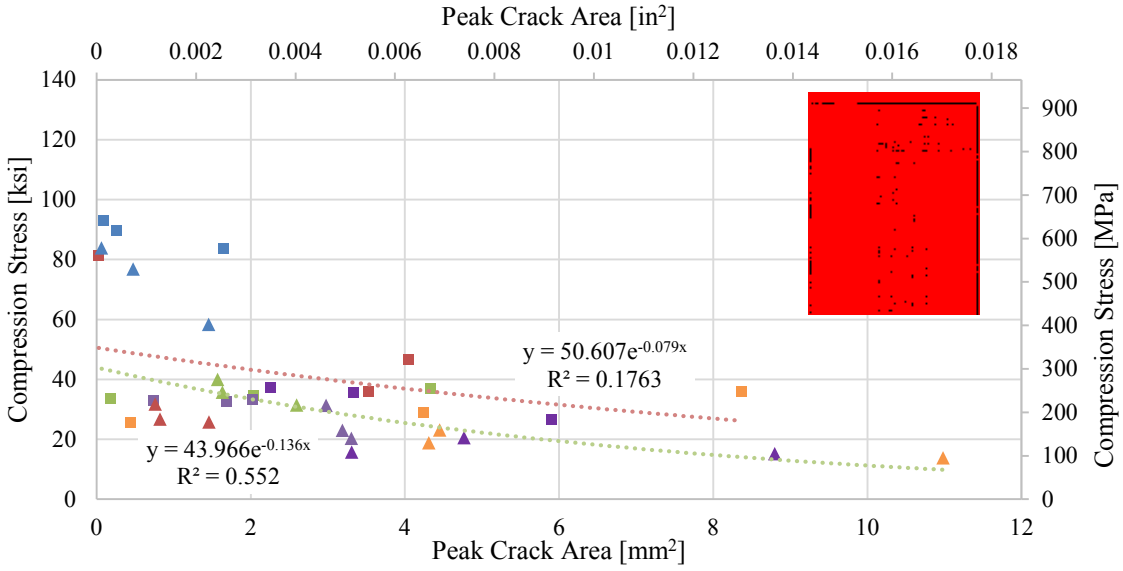

Figure 4.46 Peak Crack Area vs. Ultimate Compressive Stress for Braided Sleeves

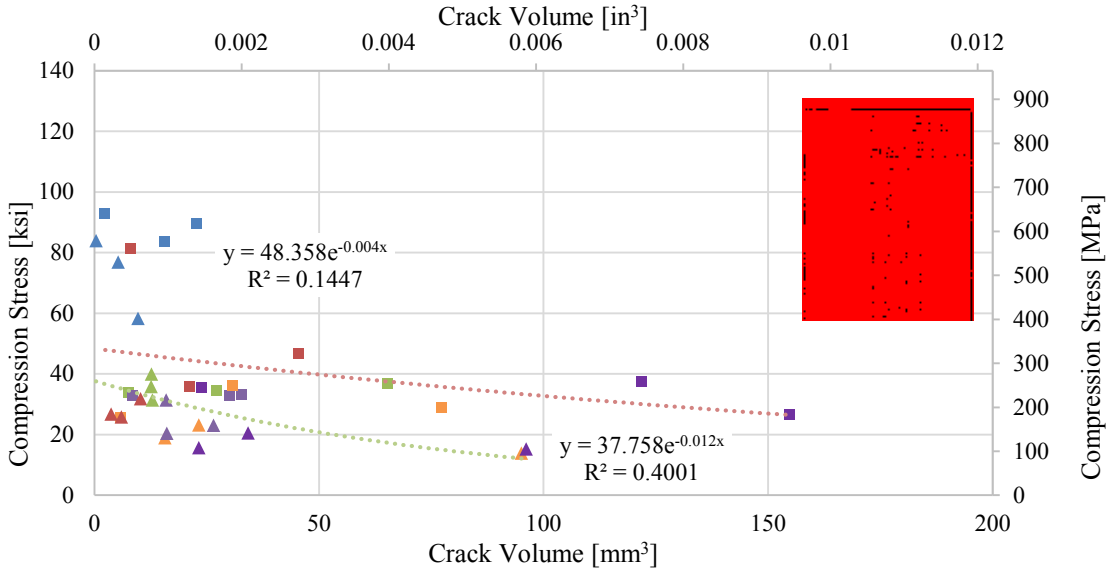

Figure 4.47 Overall Crack Volume vs. Ultimate Compressive Stress for Braided Sleeves.

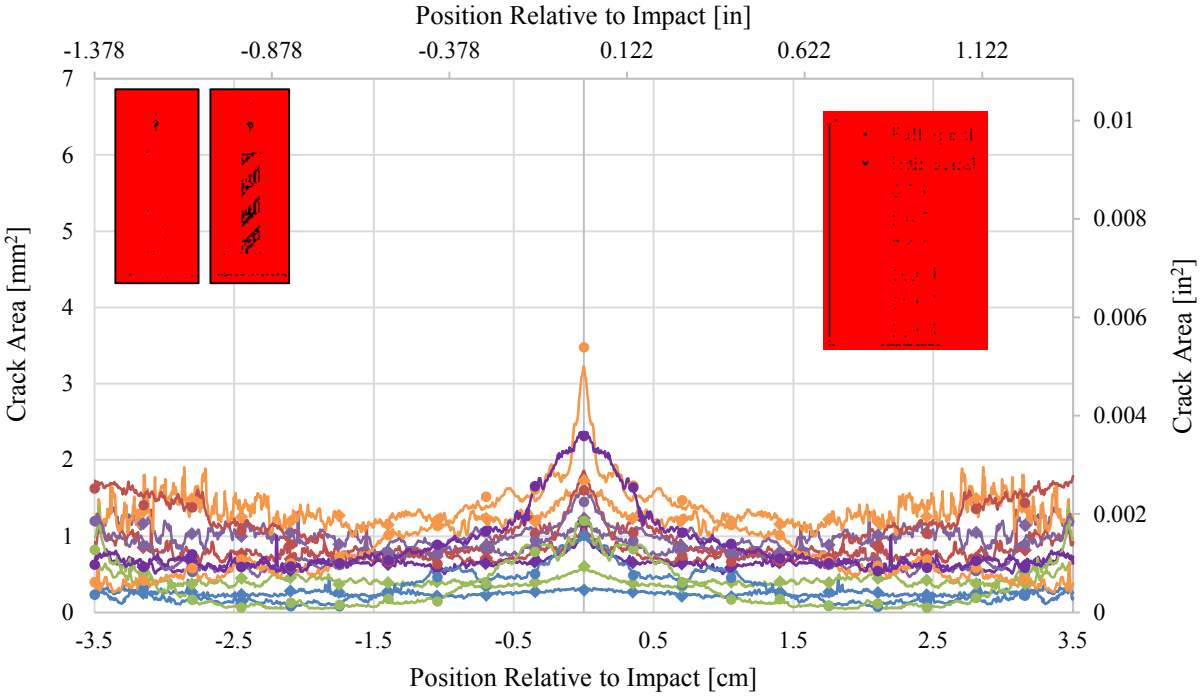

Figure 4.48 Average Crack Area as a Function of Distance from the Point of Impact for Spiral Sleeves

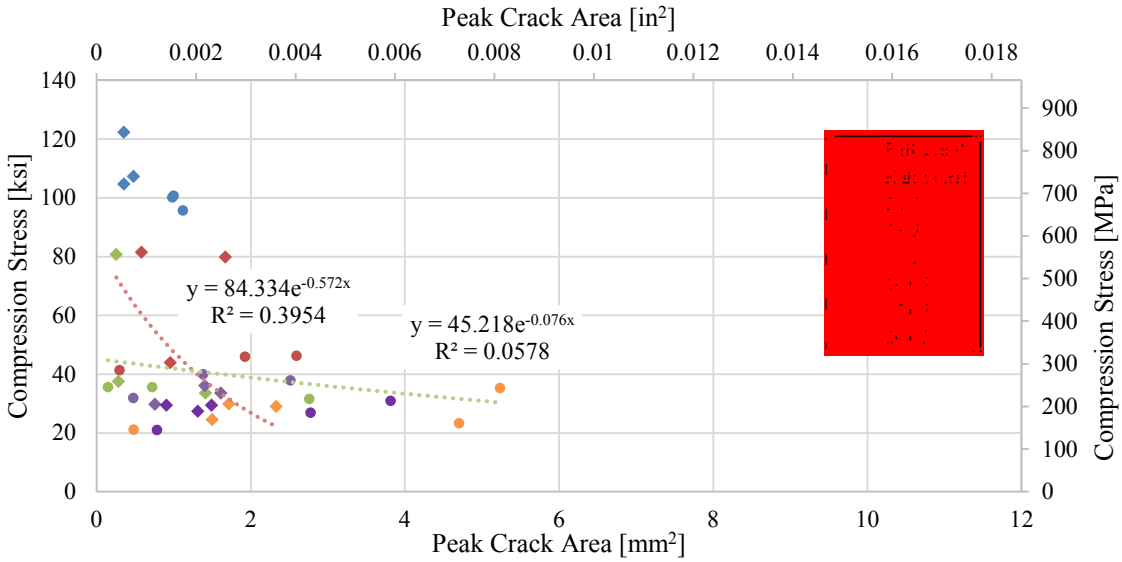

Figure 4.49 Peak Crack Area vs. Ultimate Compressive Stress for Spiral Sleeves

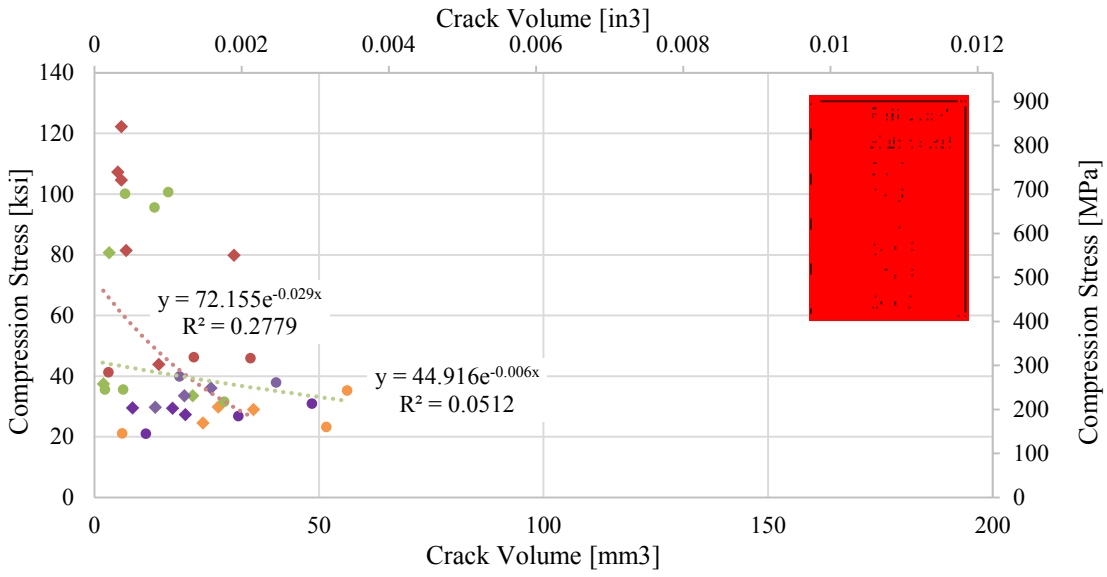

Figure 4.50 Overall Crack Volume vs. Ultimate Compressive Stress for Spiral Sleeves

4.5 Summary

In general, as impact energy increases, the peak crack area and overall crack volume increase. As the peak crack area and overall crack volume increase, the residual strength decreases. Typically, the peak crack area and overall crack volume for all sleeve types for 15 J (11 ft-lbs) is higher than for 20 J (15 ft-lbs). Shrink Tape has the lowest damage tolerance with the largest increase in peak crack area and overall crack volume as impact energy increases. One interesting observation is that there is a large drop in compression stress for full spiral with a small increase in crack area while the other sleeves have a more gradual slope.

5 COMPRESSION TEST RESULTS

5.1 Overview

Detailed compression test results for each of the thirty-five test configurations along with the statistical analysis procedures used in this research are illustrated in this chapter. Tables that summarize average values (compression Young's modulus, compression strain at ultimate strength, and ultimate compression strength) for each test configuration are followed by their respective stress-strain curve plots. After compression failure, the specimens started failing in crushing which is not meaningful and so the stress-strain curves were truncated at the point of maximum stress for a cleaner plot presentation. In the plots, 90% reliability and 95% confidence envelopes are shown to illustrate ranges where data was ultimately discarded as outliers. The envelope was truncated at the lowest strain at ultimate stress value. If the lower limit of the envelope is not present, then it means that the lower limit is negative. The average stress-strain curves end at the point where the third from the last curve ends. The average curve is extended to the average of the maximum stress and strain as maximum stress. The horizontal and vertical lines at the point of average maximum stress and strain represent one standard deviation. The following sections include compression test results for full braid, half braid, full spiral, half spiral, and shrink tape specimens.

5.2 Full Braid Compression Test Results

Test results for undamaged full braid specimens are summarized in Table 5.1 and the stress-strain curves are shown in Figure 5.1. Unfortunately, one of the undamaged full braid specimens was lost at some point in the testing process and so there is only data for four specimens. After the initial test for full braid carbon/epoxy specimens with no impact, the compression modulus of specimen N-FB-1-5-0 was lower than the Chauvenet minimum. Specimen N-FB-1-5-0 was an outlier and was therefore excluded from the final data set. Test results for full braid carbon/epoxy specimens impacted at 2.5 J (1.9 ft-lbs) are summarized in Table 5.2 and the stress-strain curves are shown in Figure 5.2.

Table 5.1 Summary of Compression Properties of Full Braid, Non-Impacted Specimens

Specimen I.D.	Cross Sectional Area		Ultimate Compression Strength		Strain at Ultimate Strength	Initial Compression Stiffness	
	[mm^2	(in^2)]	[MPa	(ksi)]	[10^3 με]	[GPa	(10^6 psi)]
N-FB-1-5-0.0*	52.15	(0.084)	320.4	(46.5)	1.93	190.3+	(27.6)+
N-FB-3-4-0.0	51.22	(0.079)	605.8	(87.9)	1.53	394.5	(57.2)
N-FB-3-7-0.0	51.22	(0.079)	740.2	(107.4)	2.01	379.6	(55.1)
N-FB-4-7-0.0	52.94	(0.083)	676.6	(98.1)	1.78	417.4	(60.5)
Average	51.88	(0.08)	585.8	(85.0)	1.81	345.5	(50.1)
Std. Dev.	0.83	(0.00)	185.2	(26.9)	0.21	90.6	(15.2)
Average	51.79	(0.08)	674.2	(97.8)	1.77	397.2	(57.6)
Std. Dev.	1.00	(0.00)	67.2	(9.8)	0.24	19.0	(2.8)
Chauvenet Limit	53.17	(0.08)	767.0	(111.2)	2.10	423.4	(61.4)
	50.42	(0.08)	581.4	(84.3)	1.44	370.9	(53.8)

*Specimen eliminated using Chauvenet's criterion; italicized values not included in final average or standard deviation.
+ Properties used to eliminate specimen.

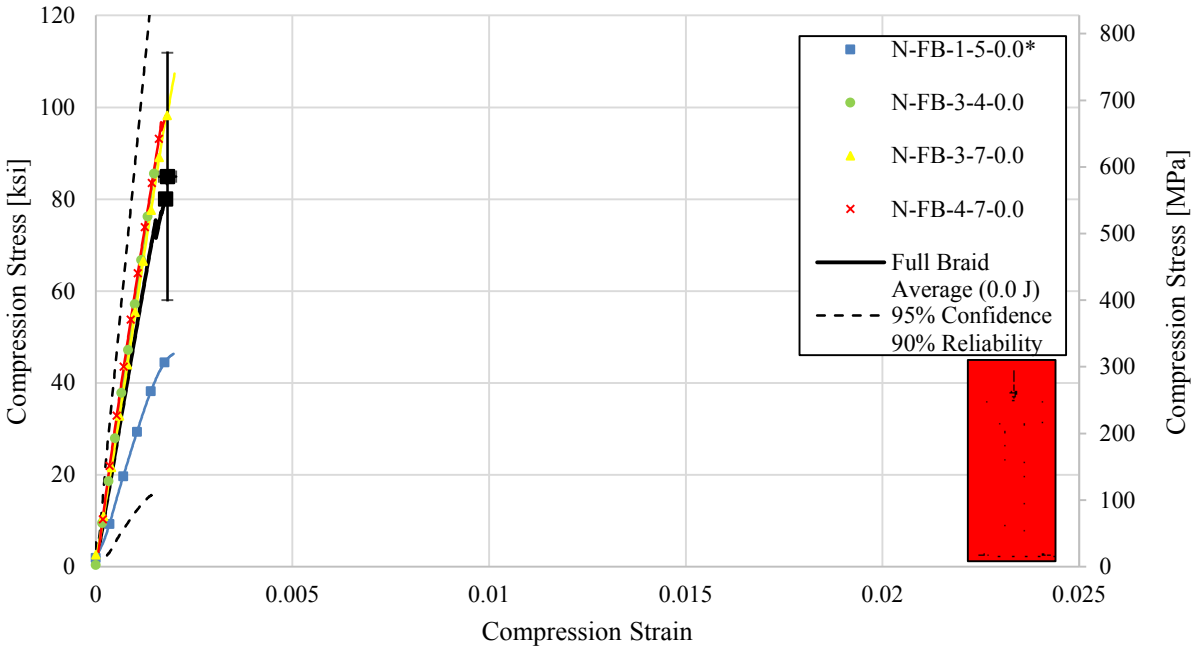

Figure 5.1 Stress-Strain Curves for Full Braid, Non-Impacted Specimens

Table 5.2 Summary of Compression Properties of Full Braid, 2.5 J (1.9 ft-lbs) Impacted Specimens

Specimen I.D.	Cross Sectional Area		Ultimate Compression Strength		Strain at Ultimate Strength	Initial Compression Stiffness	
	[mm^2]	(in^2)]	[MPa]	(ksi)]	[10^3 με]	[GPa	(10^6 psi)]
N-FB-4-1-2.5	52.94	(0.083)	449.3	(65.2)	1.05	447.8	(65.0)
N-FB-4-3-2.5	52.94	(0.083)	640.8	(92.9)	1.54	437.0	(63.4)
N-FB-4-6-2.5	52.94	(0.083)	754.4	(109.4)	1.96	416.9	(60.5)
N-FB-4-10-2.5	52.94	(0.083)	576.7	(83.6)	1.19	505.2	(73.3)
N-FB-5-1-2.5	52.44	(0.087)	617.5	(89.6)	1.32	487.0	(70.6)
Average	52.84	(0.084)	607.7	(88.1)	1.41	458.8	(66.5)
Std. Dev.	0.23	(0.00)	110.4	(16.0)	0.35	36.4	(5.3)
Chauvenet	53.22	(0.08)	789.9	(114.6)	2.00	518.9	(75.3)
Limit	52.47	(0.08)	425.6	(61.7)	0.83	398.7	(57.8)

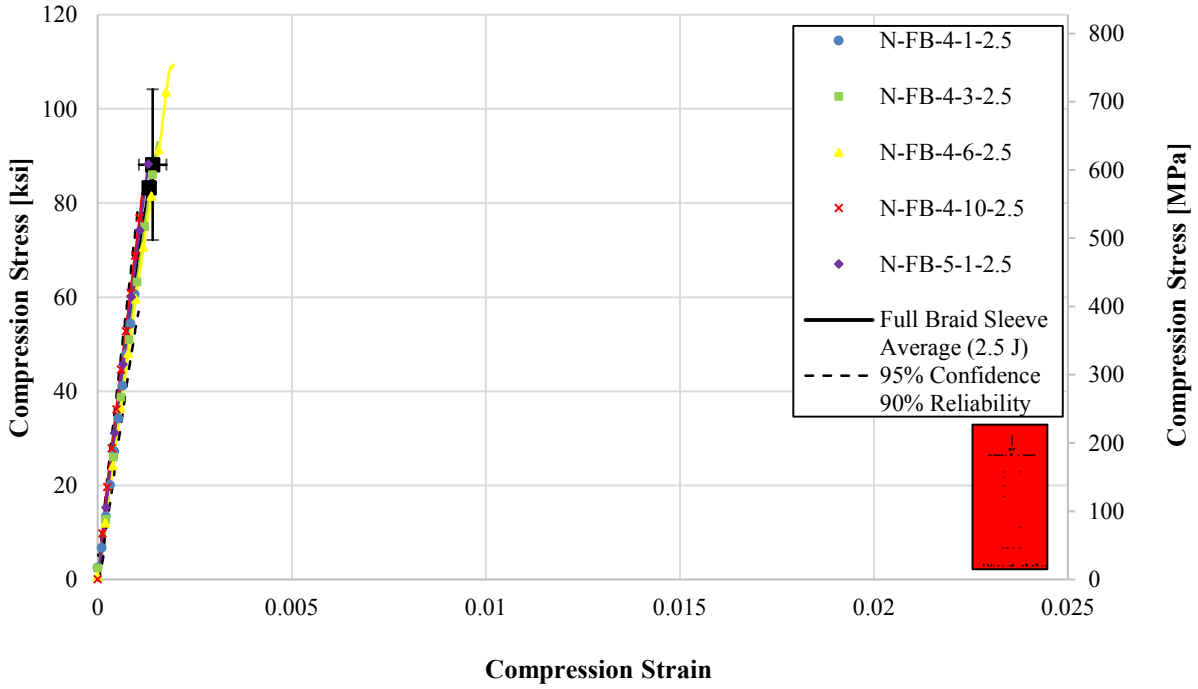

Figure 5.2 Stress-Strain Curves for Full Braid, 2.5 J (1.9 ft-lbs) Impacted Specimens

Test results for full braid carbon/epoxy specimens impacted at 5.0 J (3.7 ft-lbs) are summarized in Table 5.3 and the stress-strain curves are shown in Figure 5.3. Unfortunately, one of the 5.0 J (1.9 ft-lbs) full braid specimens was lost at some point in the testing process and so there is only data for four specimens. Test results for full braid carbon/epoxy specimens impacted at 7.5 J (5.6 ft-lbs) are summarized in Table 5.4 and the stress-strain curves are shown in Figure 5.4. After the initial test for full braid carbon/epoxy specimens with 7.5 J (5.6 ft-lbs) of impact energy, the ultimate compression strength of specimen N-FB-2-2-7.5 was higher than the Chauvenet maximum. Specimen N-FB-2-2-7.5 was an outlier and was therefore excluded from the final data set.

Table 5.3 Summary of Compression Properties of Full Braid, 5.0 J (3.7 ft-lbs) Impacted Specimens

Specimen I.D.	Cross Sectional Area		Ultimate Compression Strength		Strain at Ultimate Strength	Initial Compression Stiffness	
	[mm^2	(in^2)]	[MPa]	(ksi)]	[10^3 με]	[GPa	(10^6 psi)]
N-FB-1-2-5.0	52.15	(0.084)	247.0	(35.8)	1.64	160.5	(23.3)
N-FB-4-4-5.0	52.94	(0.083)	561.4	(81.4)	1.91	362.4	(52.6)
N-FB-4-8-5.0	52.94	(0.083)	322.4	(46.8)	1.96	189.1	(27.4)
N-FB-4-9-5.0	52.94	(0.083)	412.5	(59.8)	1.57	350.2	(50.8)
Average	52.75	(0.083)	385.8	(56.0)	1.77	265.6	(38.5)
Std. Dev.	0.40	(0.00)	135.2	(19.6)	0.19	105.5	(15.3)
Chauvenet	53.35	(0.08)	594.1	(86.2)	2.06	428.1	(62.1)
Limit	52.14	(0.08)	177.6	(25.8)	1.48	103.1	(15.0)

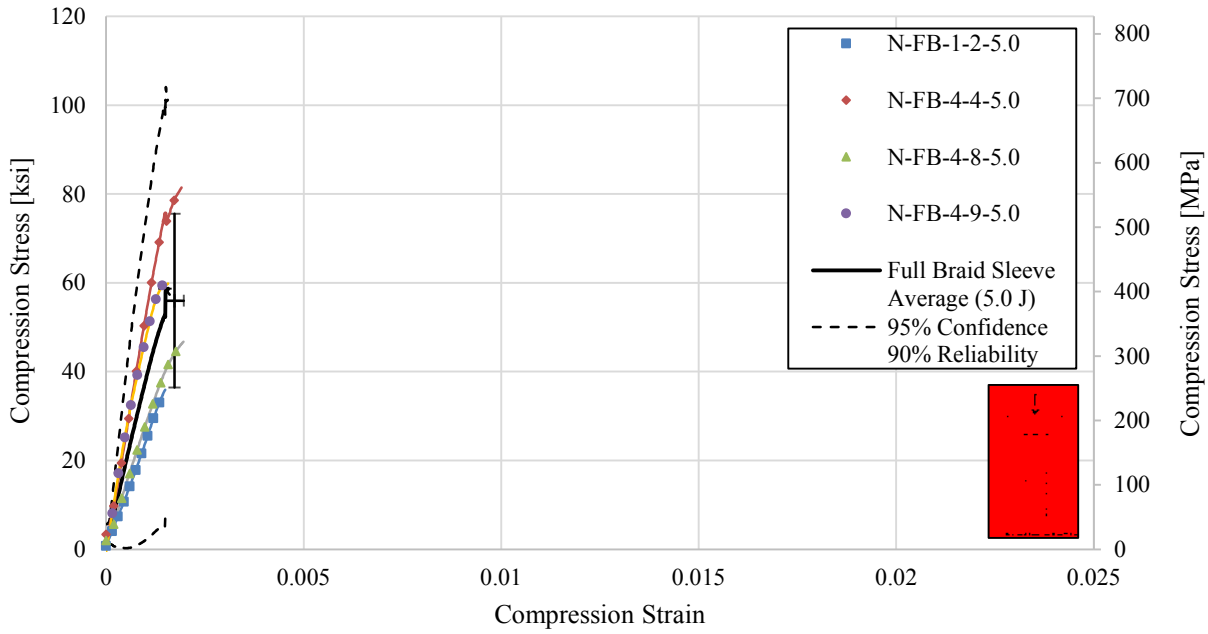

Figure 5.3 Stress-Strain Curves for Full Braid, 5.0 J (3.7 ft-lbs) Impacted Specimens

Table 5.4 Summary of Compression Properties of Full Braid, 7.5 J (5.6 ft-lbs) Impacted Specimens

Specimen I.D.	Cross Sectional Area		Ultimate Compression Strength		Strain at Ultimate Strength	Initial Compression Stiffness	
	[mm^2	(in^2)]	[MPa]	(ksi)]	[10^3 με]	[GPa	(10^6 psi)]
N-FB-1-3-7.5	52.15	(0.084)	238.4	(34.6)	2.00	159.0	(23.1)
N-FB-1-4-7.5	52.15	(0.084)	253.9	(36.8)	2.64	130.1	(18.9)
*N-FB-2-2-7.5**	*53.00*	*(0.087)*	*292.2+*	*(42.4)+*	*10.50*	*203.1*	*(29.5)*
N-FB-2-3-7.5	53.00	(0.087)	232.3	(33.7)	8.14	41.9	(6.1)
N-FB-3-1-7.5	51.22	(0.079)	238.1	(34.5)	1.26	279.3	(40.5)
Average	52.30	(0.084)	251.0	(36.4)	4.91	162.7	(23.6)
Std. Dev.	0.74	(0.00)	24.4	(3.5)	4.14	87.9	(12.7)
Average	52.13	(0.083)	240.7	(34.9)	3.51	152.5	(22.1)
Std Dev.	0.73	(0.00)	9.3	(1.3)	3.14	98.0	(14.2)
Chauvenet Limit	53.25	(0.08)	254.9	(37.0)	8.34	303.6	(44.0)
	51.01	(0.08)	226.4	(32.8)	-1.32	1.6	(0.2)

*Specimen eliminated using Chauvenet's criterion; italicized values not included in final average or standard deviation.
+ Properties used to eliminate specimen.

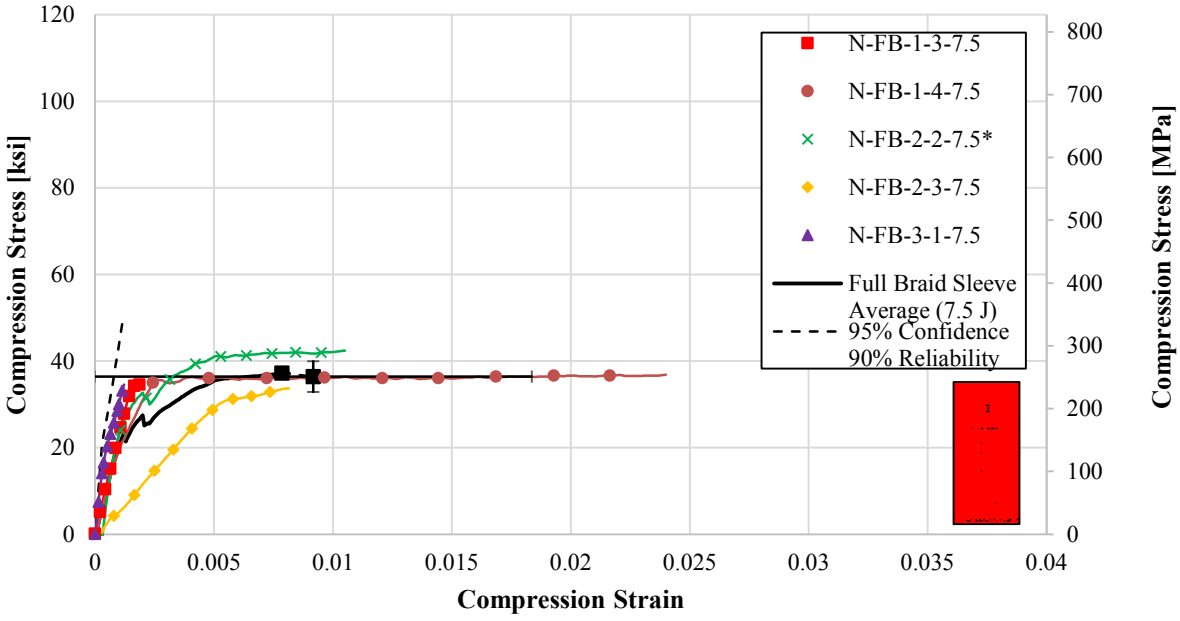

Figure 5.4 Stress-Strain Curves for Full Braid, 7.5 J (5.6 ft-lbs) Impacted Specimens

Test results for full braid carbon/epoxy specimens impacted at 10 J (7.4 ft-lbs) are summarized in Table 5.5 and the stress-strain curves are shown in Figure 5.5. After the initial test for full braid carbon/epoxy specimens with 10 J (7.4 ft-lbs) impact, the ultimate compression strength of specimen N-FB-2-5-10.0 was lower than the Chauvenet minimum. Specimen N-FB-2-5-10.0 was an outlier and was therefore excluded from the final data set. Test results for full braid carbon/epoxy specimens impacted at 15 J (11 ft-lbs) are summarized in Table 5.6 and the stress-strain curves are shown in Figure 5.6. The stress-strain curve for specimen N-FB-2-6-15.0 of the full braid carbon/epoxy specimens impacted at 15 J (11 ft-lbs) fell 11.5% outside of Chauvenet's envelope. Specimen N-FB-2-6-15.0 was an outlier and was therefore excluded from the final data set.

Table 5.5 Summary of Compression Properties of Full Braid, 10 J (7.4 ft-lbs) Impacted Specimens

Specimen I.D.	Cross Sectional Area		Ultimate Compression Strength		Strain at Ultimate Strength	Initial Compression Stiffness	
	[mm^2	(in^2)]	[MPa]	(ksi)]	[10^3 με]	[GPa	(10^6 psi)]
N-FB-1-6-10.0	52.15	(0.084)	228.5	(33.1)	0.34	428.1	(62.1)
*N-FB-2-5-10.0**	*53.00*	*(0.087)*	*211.3+*	*(30.6+)*	*20.79*	*46.2*	*(6.7)*
N-FB-3-2-10.0	51.22	(0.079)	228.3	(33.1)	16.79	52.3	(7.6)
N-FB-3-8-10.0	51.22	(0.079)	226.4	(32.8)	2.79	223.8	(32.5)
N-FB-5-2-10.0	52.44	(0.087)	224.9	(32.6)	12.14	49.3	(7.2)
Average	52.0	(0.832)	223.9	(32.5)	10.57	159.9	(23.2)
Std. Dev.	0.8	(0.0)	7.2	(1.0)	8.81	167.9	(24.4)
Average	51.8	(0.823)	227.0	(32.9)	8.01	188.4	(27.3)
Std. Dev.	0.6	(0.0)	1.7	(0.2)	7.78	179.4	(26.0)
Chauvenet Limit	53.29	(0.08)	235.8	(34.2)	25.11	437.0	(63.4)
	50.72	(0.08)	212.0	(30.7)	-3.98	-117.1	(-17.0)

*Specimen eliminated using Chauvenet's criterion; italicized values not included in final average or standard deviation.
+ Properties used to eliminate specimen.

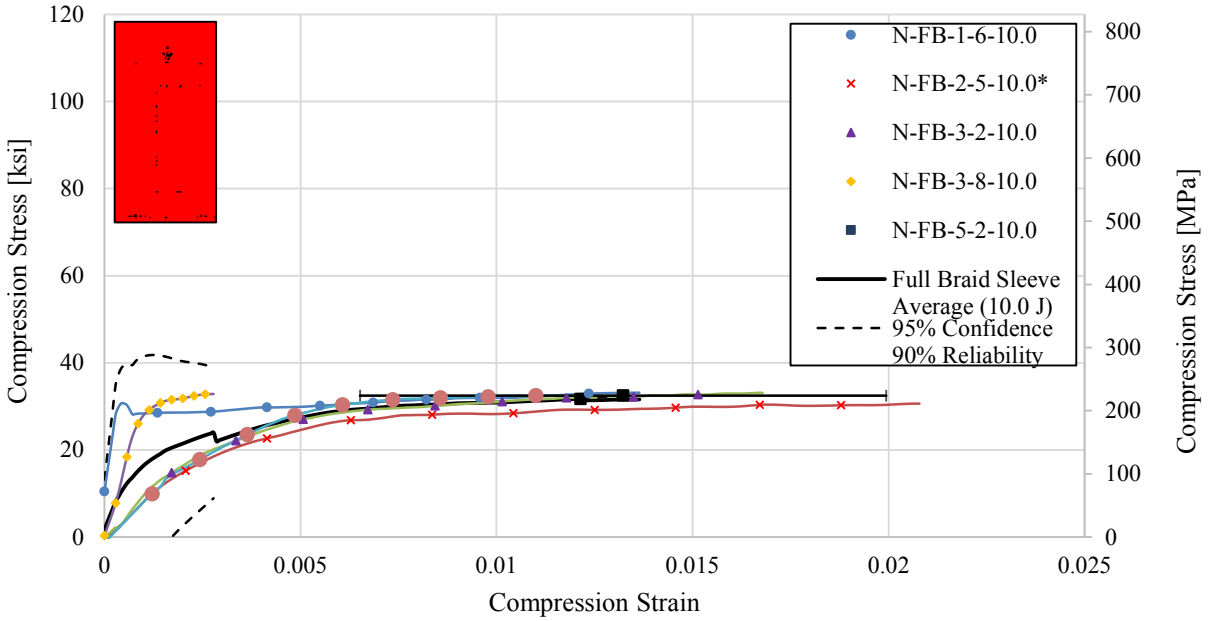

Figure 5.5 Stress-Strain Curves for Full Braid, 10 J (7.4 ft-lbs) Impacted Specimens

Table 5.6 Summary of Compression Properties of Full Braid, 15 J (11 ft-lbs) Impacted Specimens

Specimen I.D.	Cross Sectional Area		Ultimate Compression Strength		Strain at Ultimate Strength	Initial Compression Stiffness	
	[mm^2	(in^2)]	[MPa]	(ksi)]	[10^3 με]	[GPa	(10^6 psi)]
N-FB-2-1-15.0	53.00	(0.087)	200.0	(29.0)	10.21	332.7	(48.3)
N-FB-2-4-15.0	53.00	(0.087)	248.1	(36.0)	14.71	176.0	(25.5)
N-FB-2-6-15.0	53.00	(0.087)	176.8	(25.6)	9.86	93.2	(13.5)
N-FB-3-3-15.0	51.22	(0.079)	226.2	(32.8)	26.64	60.1	(8.7)
N-FB-4-5-15.0	52.94	(0.083)	185.3	(26.9)	5.86	88.8	(12.9)
Average	52.63	(0.084)	207.3	(30.1)	13.46	150.2	(21.8)
Std. Dev.	0.79	(0.00)	29.5	(4.3)	8.01	110.8	(16.1)
Chauvenet	53.93	(0.08)	256.0	(37.1)	26.67	333.0	(48.3)
Limit	51.33	(0.08)	158.6	(23.0)	0.24	-32.6	(-4.73)

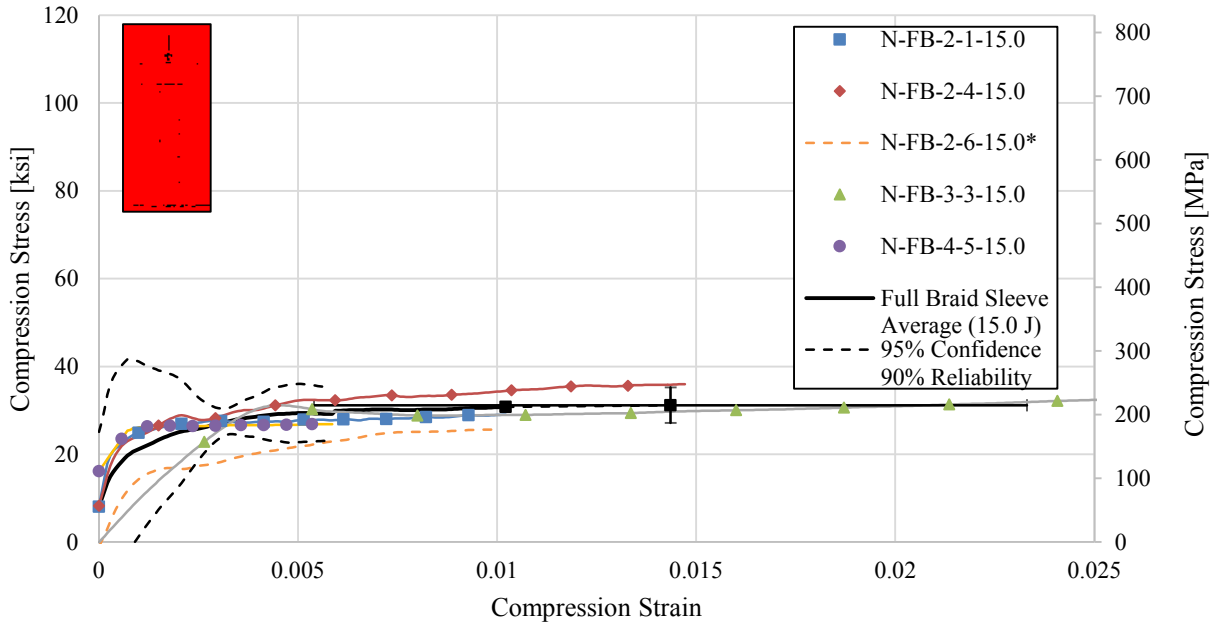

Figure 5.6 Stress-Strain Curves for Full Braid, 15 J (11 ft-lbs) Impacted Specimens

Test results for full braid carbon/epoxy specimens impacted at 20 J (15 ft-lbs) are summarized in Table 5.7 and the stress-strain curves are shown in Figure 5.7.

Table 5.7 Summary of Compression Properties of Full Braid, 20 J (15 ft-lbs) Impacted Specimens

Specimen I.D.	Cross Sectional Area		Ultimate Compression Strength		Strain at Ultimate Strength	Initial Compression Stiffness	
	[mm^2]	(in^2)]	[MPa]	(ksi)]	[10^3 με]	[GPa	(10^6 psi)]
N-FB-1-5-20.0	52.15	(0.084)	184.7	(26.8)	7.79	157.1	(22.8)
N-FB-3-5-20.0	51.22	(0.079)	245.3	(35.6)	7.50	229.6	(33.3)
N-FB-3-6-20.0	51.22	(0.079)	256.9	(37.3)	19.36	122.3	(17.7)
N-FB-3-9-20.0	51.22	(0.079)	139.9	(20.3)	22.50	27.0	(3.9)
N-FB-4-2-20.0	52.94	(0.083)	182.3	(26.4)	6.43	81.5	(11.8)
Average	51.75	(0.081)	201.8	(29.3)	12.71	123.5	(17.9)
Std. Dev.	0.78	(0.00)	48.6	(7.0)	7.60	76.6	(11.1)
Chauvenet	53.04	(0.08)	282.0	(40.9)	25.25	249.9	(36.2)
Limit	50.46	(0.08)	121.7	(17.7)	0.18	-2.9	(-0.4)

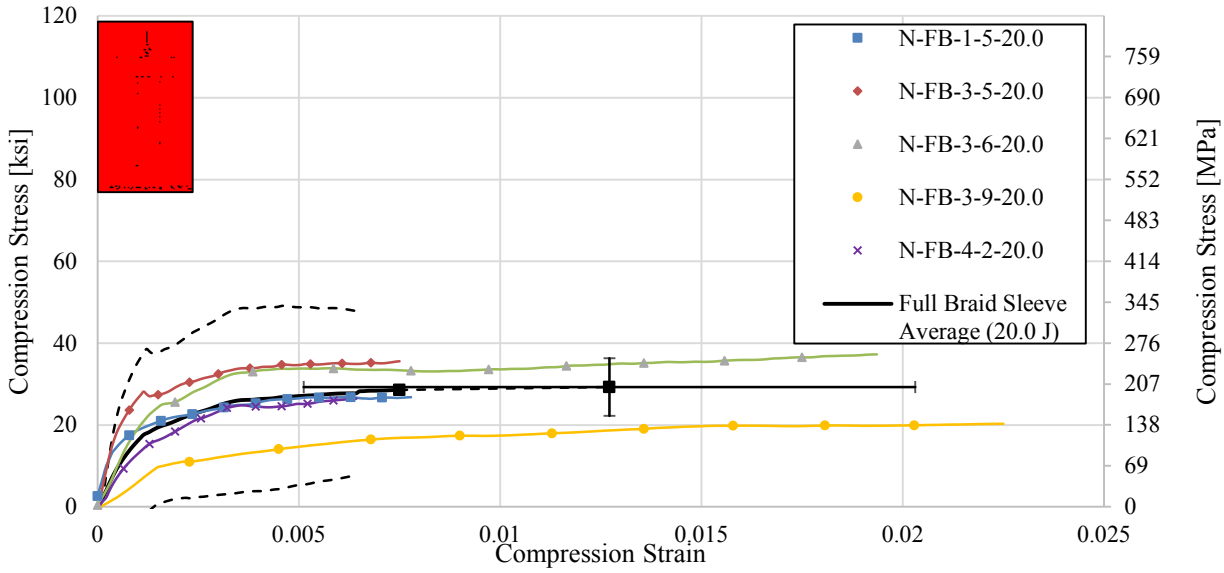

Figure 5.7 Stress-Strain Curves for Full Braid, 20 J (15 ft-lbs) Impacted Specimens

5.3 Half Braid Compression Test Results

The test results for undamaged half braid carbon/epoxy specimens are summarized in Table 5.8 and the stress-strain curves are shown in Figure 5.8. The test results half braid carbon/epoxy specimens impacted with 2.5 J (1.9 ft-lbs) are summarized in Table 5.9 and the stress-strain curves are shown in Figure 5.9.

Table 5.8 Summary of Compression Properties of Half Braid, No Impact Specimens

Specimen I.D.	Cross Sectional Area		Ultimate Compression Strength		Strain at Ultimate Strength	Initial Compression Stiffness	
	[mm^2]	(in^2)]	[MPa]	(ksi)]	[10^3 με]	[GPa	(10^6 psi)]
N-HB-2-5-0.0	54.15	(0.083)	494.4	(71.7)	0.96	602.4	(87.4)
N-HB-3-2-0.0	52.43	(0.082)	519.8	(75.4)	1.45	331.8	(48.1)
N-HB-3-5-0.0	52.43	(0.082)	692.0	(100.4)	1.06	627.4	(91.0)
N-HB-3-6-0.0	52.43	(0.082)	625.3	(90.7)	1.24	532.6	(77.2)
N-HB-4-1-0.0	52.91	(0.086)	642.8	(93.2)	1.73	421.5	(61.1)
Average	52.87	(0.083)	594.9	(86.3)	1.29	503.1	(73.0)
Std. Dev.	0.75	(0.00)	84.2	(12.2)	0.31	124.7	(18.1)
Chauvenet	54.10	(0.08)	733.9	(106.4)	1.80	708.9	(102.8)
Limit	51.64	(0.08)	455.8	(66.1)	0.78	297.4	(43.1)

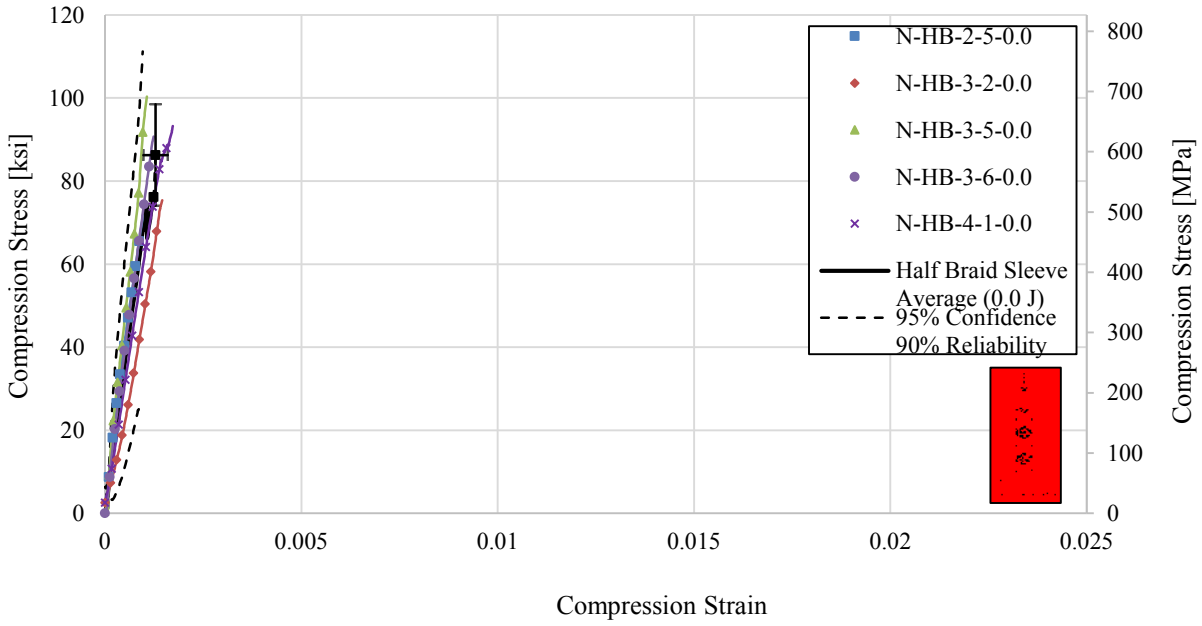

Figure 5.8 Stress-Strain Curves for Half Braid, Non-Impacted Specimens

Table 5.9 Summary of Compression Properties of Half Braid, 2.5 J (1.9 ft-lbs) Impacted Specimens

Specimen I.D.	Cross Sectional Area		Ultimate Compression Strength		Strain at Ultimate Strength	Initial Compression Stiffness	
	[mm^2	(in^2)]	[MPa]	(ksi)]	[10^3 με]	[GPa	(10^6 psi)]
N-HB-1-2-2.5	52.15	(0.080)	578.6	(83.9)	1.71	398.1	(57.7)
N-HB-1-7-2.5	52.15	(0.080)	530.1	(76.9)	1.43	334.7	(48.5)
N-HB-1-8-2.5	52.15	(0.080)	402.2	(58.3)	0.70	504.7	(73.2)
N-HB-3-7-2.5	52.43	(0.082)	626.8	(90.9)	1.44	466.8	(67.7)
N-HB-4-3-2.5	52.91	(0.086)	299.8	(43.5)	1.35	295.6	(42.9)
Average	52.36	(0.082)	487.5	(70.7)	1.33	400.0	(58.0)
Std. Dev.	0.33	(0.00)	134.2	(19.5)	0.37	87.5	(12.7)
Chauvenet Limit	52.91	(0.08)	708.9	(102.8)	1.94	544.3	(79.0)
	51.80	(0.08)	266.1	(38.6)	0.71	255.7	(37.1)

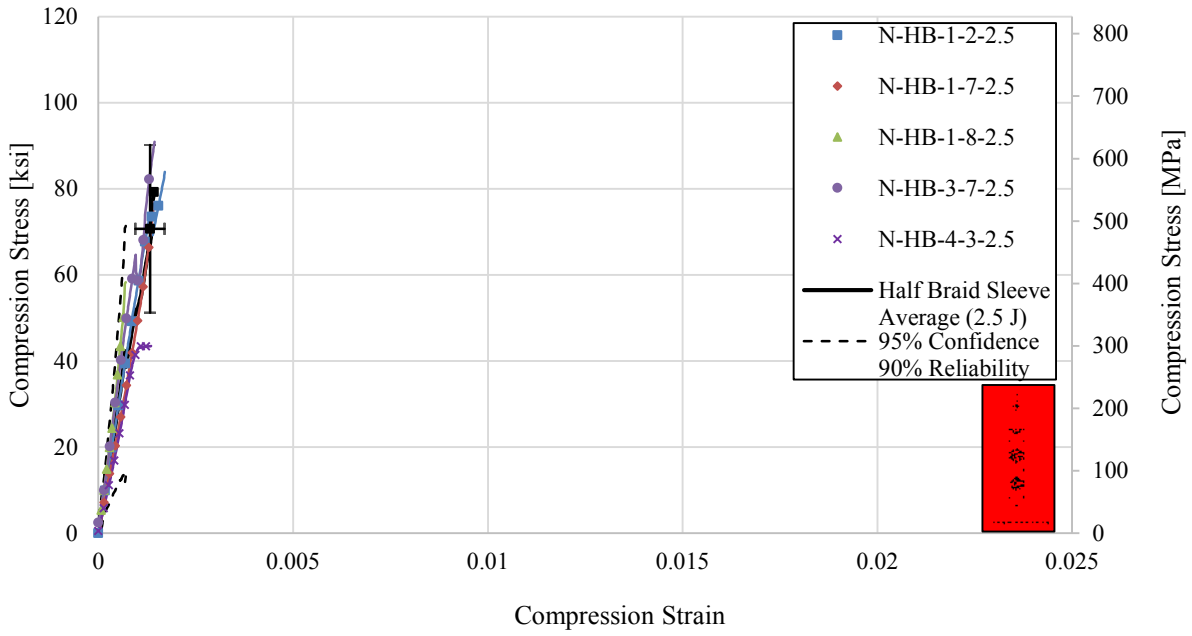

Figure 5.9 Stress-Strain Curves for Half Braid, 2.5 J (1.9 ft-lbs) Impacted Specimens

The test results half braid carbon/epoxy specimens impacted with 5.0 J (3.7 ft-lbs) are summarized in Table 5.10 and the stress-strain curves are shown in Figure 5.10. The test results half braid carbon/epoxy specimens impacted with 7.5 J (5.6 ft-lbs) are summarized in Table 5.11 and the stress-strain curves are shown in Figure 5.11. After the initial test for half braid carbon/epoxy specimens with 5.0 J (3.7 ft-lbs) impact, the ultimate compression modulus of specimen N-HB-1-10-5.0 was higher than the Chauvenet maximum. Specimen N-HB-1-10-5.0 was an outlier and was therefore excluded from the final data set. The stress-strain curve for Specimen N-HB-1-4-5.0 of the full braid carbon/epoxy specimens impacted at 5.0 J (3.7 ft-lbs) fell 11.8% outside of Chauvenet's envelope. Specimen N-HB-1-4-5.0 was an outlier and was therefore excluded from the final data set.

Table 5.10 Summary of Compression Properties of Half Braid, 5.0 J (3.7 ft-lbs) Impacted Specimens

Specimen I.D.	Cross Sectional Area		Ultimate Compression Strength		Strain at Ultimate Strength	Initial Compression Stiffness	
	[mm^2	(in^2)]	[MPa]	(ksi)]	[10^3 με]	[GPa	(10^6 psi)]
N-HB-1-1-5.0	52.15	(0.080)	184.4	(26.8)	2.07	117.2	(17.0)
N-HB-1-4-5.0	52.15	(0.080)	233.7	(33.9)	1.50	159.2	(23.1)
N-HB-1-10-5.0*	52.15	(0.080)	299.5	(43.4)	1.64	270.9+	(39.3)+
N-HB-2-2-5.0	54.15	(0.083)	219.3	(31.8)	1.93	133.3	(19.3)
N-HB-2-4-5.0	54.15	(0.083)	177.6	(25.8)	2.07	112.8	(16.4)
Average	52.95	(0.081)	222.9	(32.3)	1.84	158.7	(23.0)
Std. Dev.	1.10	(0.00)	48.8	(7.1)	0.26	65.3	(9.5)
Average	53.15	(0.082)	203.8	(29.6)	1.89	130.6	(18.9)
Std. Dev.	1.16	(0.00)	27.1	(3.9)	0.27	21.0	(3.0)
Chauvenet Limit	54.76	(0.08)	303.4	(44.0)	2.27	266.4	(38.6)
	51.14	(0.08)	142.4	(20.7)	1.41	50.9	(7.4)

*Specimen eliminated using Chauvenet's criterion; italicized values not included in final average or standard deviation.
+ Properties used to eliminate specimen.

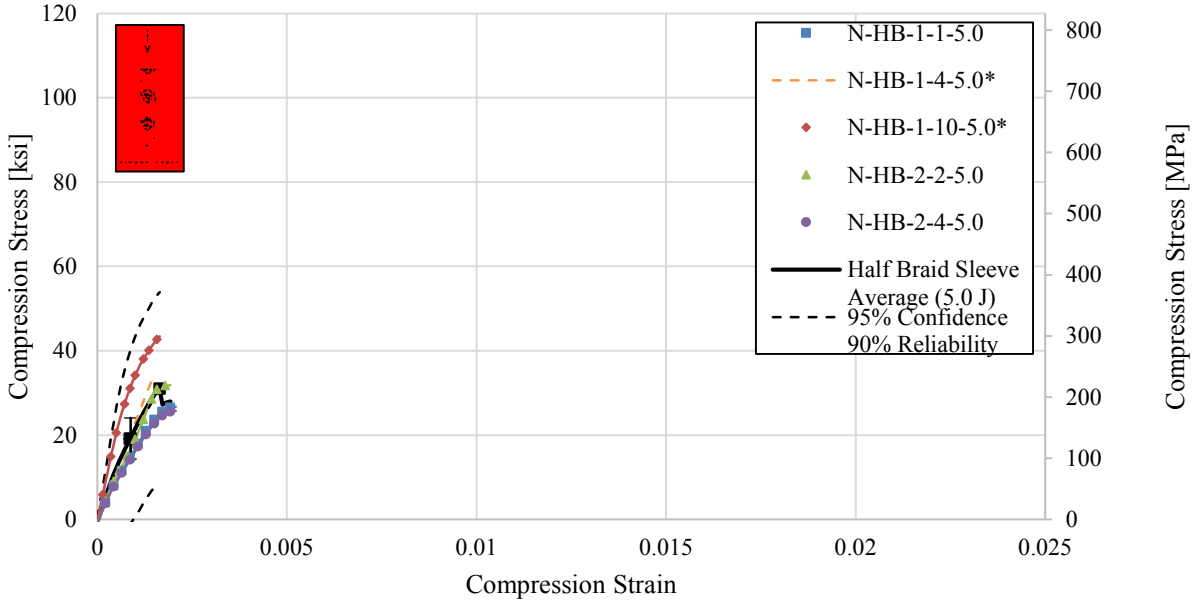

Figure 5.10 Stress-Strain Curves for Half Braid, 5.0 J (3.7 ft-lbs) Impacted Specimens

Table 5.11 Summary of Compression Properties of Half Braid, 7.5 J (5.6 ft-lbs) Impacted Specimens

Specimen I.D.	Cross Sectional Area		Ultimate Compression Strength		Strain at Ultimate Strength	Initial Compression Stiffness	
	[mm^2	(in^2)]	[MPa]	(ksi)]	[10^3 με]	[GPa	(10^6 psi)]
N-HB- 1-8-7.5	52.15	(0.080)	246.6	(35.8)	1.07	347.6	(50.4)
N-HB-2-6-7.5	54.15	(0.083)	275.7	(40.0)	0.86	302.9	(43.9)
N-HB-3-4-7.5	52.43	(0.082)	209.3	(30.4)	4.29	66.3	(9.6)
N-HB-3-9-7.5	52.43	(0.082)	229.3	(33.3)	4.36	80.7	(11.7)
N-HB-3-11-7.5	52.43	(0.082)	216.5	(31.4)	0.43	605.9	(87.9)
Average	52.72	(0.082)	235.5	(34.2)	2.20	280.7	(40.7)
Std. Dev.	0.81	(0.00)	26.6	(3.9)	1.95	221.8	(32.2)
Chauvenet	54.05	(0.08)	279.3	(40.5)	5.42	646.6	(93.8)
Limit	51.38	(0.08)	191.6	(27.8)	-1.02	-85.3	(-12.4)

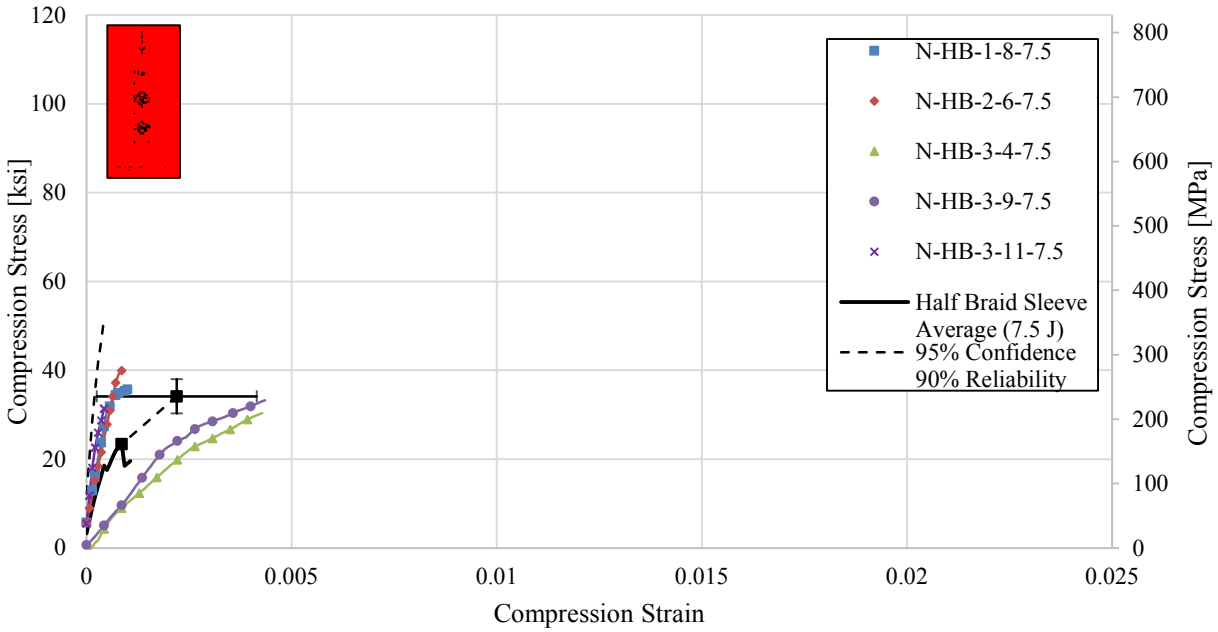

Figure 5.11 Stress-Strain Curves for Half Braid, 7.5 J (5.6 ft-lbs) Impacted Specimens

The test results half braid specimens impacted with 10 J (7.4 ft-lbs) are summarized in Table 5.12 and the stress-strain curves are shown in Figure 5.12. The stress-strain curve for specimen N-HB-1-5-10.0 of the half braid carbon/epoxy specimens impacted at 10 J (7.4 ft-lbs)

fell 80% outside of Chauvenet's envelope. Specimen N-HB-1-5-10.0 was an outlier and was therefore excluded from the final data set. The test results half braid specimens impacted with 15 J (11 ft-lbs) are summarized in Table 5.13 and the stress-strain curves are shown in Figure 5.13.

Table 5.12 Summary of Compression Properties of Half Braid, 10 J (7.4 ft-lbs) Impacted Specimens

Speicmen I.D.	Cross Sectional Area		Ultimate Compression Strength		Strain at Ultimate Strength	Initial Compression Stiffness	
	[mm^2	(in^2)]	[MPa]	(ksi)]	[10^3 με]	[GPa	(10^6 psi)]
N-HB-1-5-10.0	52.15	(0.080)	216.4	(31.4)	0.29	196.7	(28.5)
N-HB-1-6-10.0	52.15	(0.080)	159.0	(23.1)	0.43	275.4	(39.9)
N-HB-1-11-10.0	52.15	(0.080)	234.8	(34.1)	2.29	147.1	(21.3)
N-HB-2-3-10.0	54.15	(0.083)	140.5	(20.4)	25.07	71.5	(10.4)
N-HB-4-4-10.0	52.91	(0.086)	183.0	(26.5)	1.86	236.6	(34.3)
Average	52.70	(0.082)	186.7	(27.1)	5.99	185.4	(26.9)
Std. Dev.	0.88	(0.00)	39.1	(5.7)	10.70	79.5	(11.5)
Chauvenet	54.15	(0.08)	251.2	(36.4)	23.65	316.7	(45.9)
Limit	51.25	(0.08)	122.2	(17.7)	-11.68	54.3	(7.9)

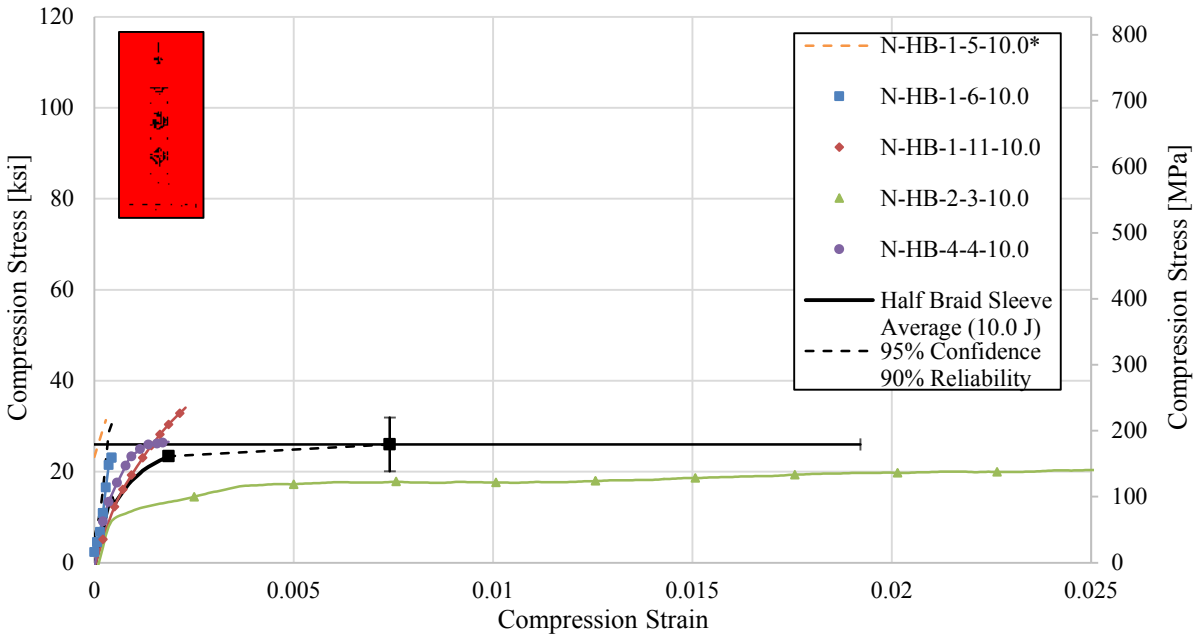

Figure 5.12 Stress-Strain Curves for Half Braid, 10 J (7.4 ft-lbs) Impacted Specimens

Table 5.13 Summary of Compression Properties of Half Braid, 15 J (11 ft-lbs) Impacted Specimens

Specimen I.D.	Cross Sectional Area		Ultimate Compression Strength		Strain at Ultimate Strength	Initial Compression Stiffness	
	[mm^2	(in^2)]	[MPa]	(ksi)]	[10^3 με]	[GPa	(10^6 psi)]
N-HB-2-1-15.0	54.15	(0.083)	130.2	(18.9)	2.07	93.6	(13.6)
N-HB-2-8-15.0	54.15	(0.083)	117.9	(17.1)	6.71	56.7	(8.2)
N-HB-3-1-15.0	52.43	(0.082)	125.1	(18.1)	3.00	75.6	(11.0)
N-HB-3-3-15.0	52.43	(0.082)	159.7	(23.2)	2.57	150.0	(21.8)
N-HB-4-2-15.0	52.91	(0.086)	95.3	(13.8)	10.29	19.7	(2.9)
Average	53.21	(0.083)	125.6	(18.2)	4.93	79.1	(11.5)
Std. Dev.	0.88	(0.00)	23.3	(3.4)	3.51	48.2	(7.0)
Chauvenet	54.66	(0.08)	164.1	(23.8)	10.72	158.6	(23.0)
Limit	51.77	(0.08)	87.3	(12.7)	-0.87	-0.3	(-0.05)

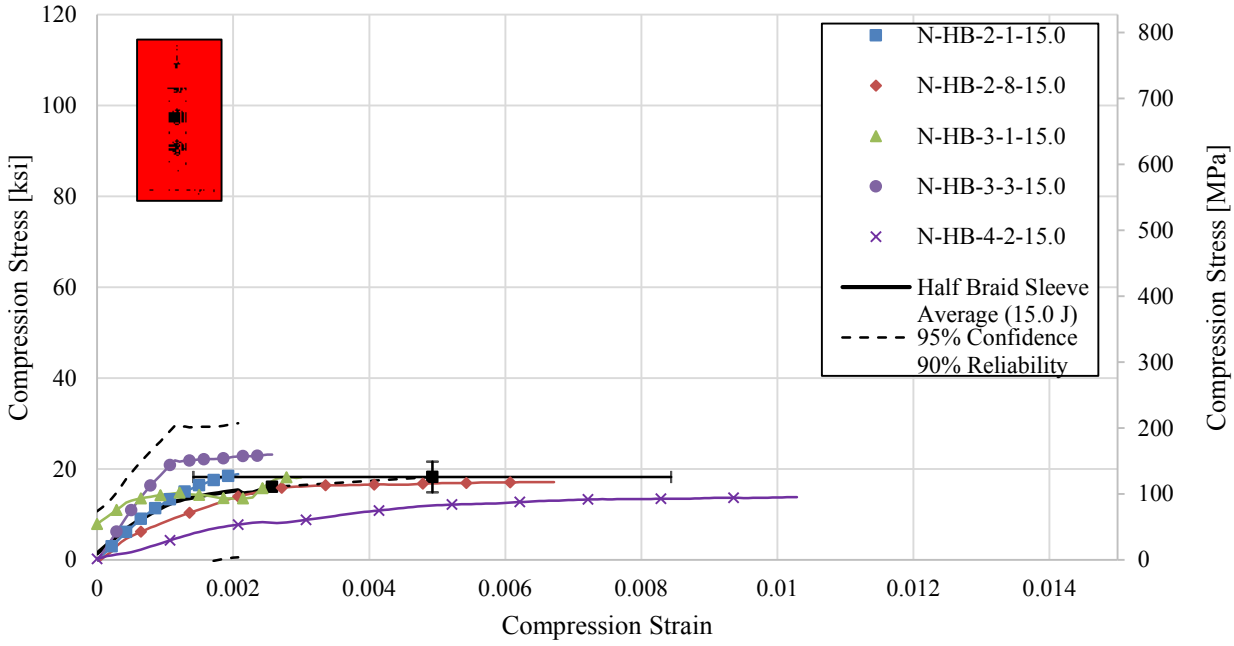

Figure 5.13 Stress-Strain Curves for Half Braid, 15 J (11 ft-lbs) Impacted Specimens

The test results half braid carbon/epoxy specimens impacted with 20 J (15 ft-lbs) are summarized in Table 5.14 and the stress-strain curves are shown in Figure 5.14. After the initial test for half braid carbon/epoxy specimens with 20 J (15 ft-lbs) impact, the ultimate compression modulus of Specimen N-HB-1-3-20.0 was higher than the Chauvenet maximum. The stress-strain curve for Specimen N-HB-1-3-20.0 of the full braid carbon/epoxy specimens impacted at 20 J (15 ft-lbs) fell 47.4% outside of Chauvenet's envelope. Specimen N-HB-1-3-20.0 was an outlier and was therefore excluded from the final data set.

Table 5.14 Summary of Compression Properties of Half Braid, 20 J (15 ft-lbs) Impacted Specimens

Specimen I.D.	Cross Sectional Area		Ultimate Compression Strength		Strain at Ultimate Strength	Initial Compression Stiffness	
	[mm^2	(in^2)]	[MPa]	(ksi)]	[10^3 με]	[GPa	(10^6 psi)]
N-HB-1-3-20.0*	52.15	(0.08)	141.5	(20.5)	6.36	91.2+	(13.2)+
N-HB-2-7-20.0	54.15	(0.08)	108.3	(15.7)	6.50	40.5	(5.9)
N-HB-3-8-20.0	52.43	(0.08)	129.7	(18.8)	12.64	15.1	(2.2)
N-HB-3-10-20.0	52.43	(0.08)	102.1	(14.8)	11.07	19.5	(2.8)
N-HB-4-5-20.0	52.91	(0.08)	105.0	(15.2)	11.93	26.9	(3.9)
Average	52.81	(0.08)	117.3	(17.0)	9.70	38.6	(5.6)
Std. Dev.	0.80	(0.00)	17.3	(2.5)	3.04	30.9	(4.5)
Average	52.98	(0.08)	111.3	(16.1)	10.54	25.5	(3.7)
Std. Dev.	0.81	(0.00)	12.6	(1.8)	2.77	11.1	(1.6)
Chauvenet Limit	54.13	(0.08)	145.9	(21.2)	14.71	89.7	(13.0)
	51.50	(0.08)	88.7	(12.9)	4.69	-12.4	(-1.8)

*Specimen eliminated using Chauvenet's criterion; italicized values not included in final average or standard deviation.
+ Properties used to eliminate specimen.

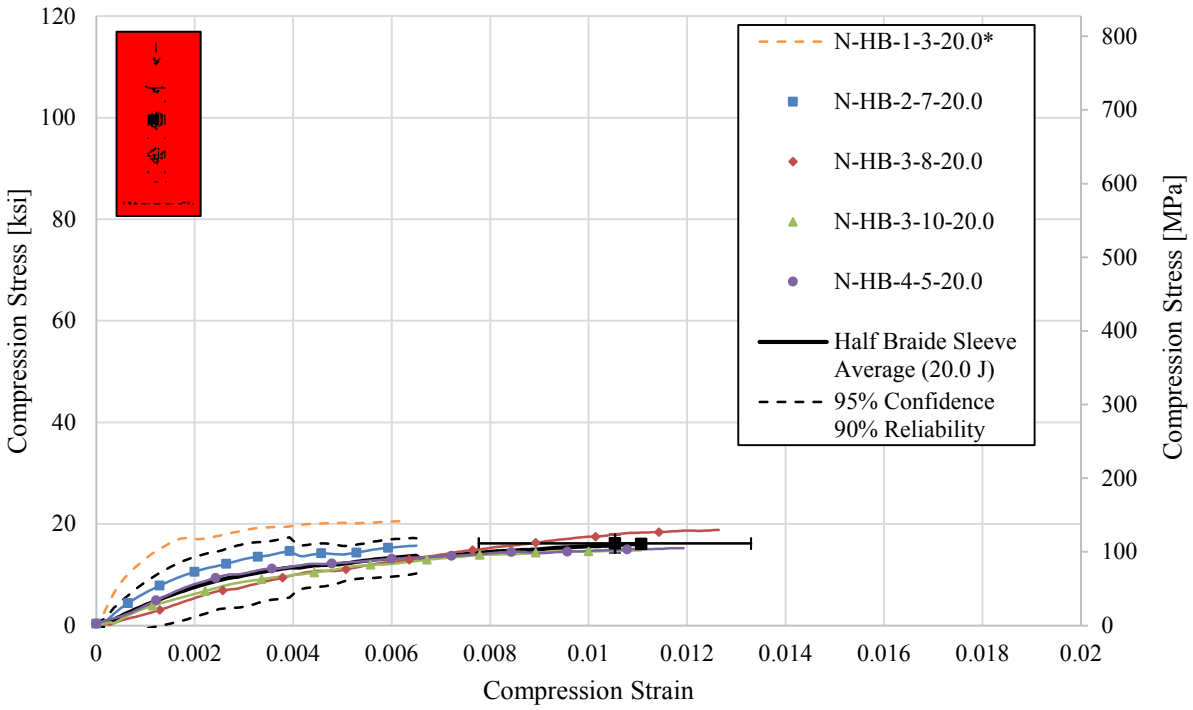

Figure 5.14 Stress-Strain Curves for Half Braid, 20 J (15 ft-lbs) Impacted Specimens

5.4 Full Spiral Compression Test Results

The test results for undamaged full spiral carbon/epoxy specimens are summarized in Table 5.15 and the stress-strain curves are shown in Figure 5.15. Unfortunately, two of the undamaged full braid specimens was lost at some point in the testing process and so there is only data for three specimens. The test results full spiral specimens impacted with 2.5 J (1.9 ft-lbs) are summarized in Table 5.16 and the stress-strain curves are shown in Figure 5.16. After the initial test for full spiral specimens with 2.5 J (1.9 ft-lbs), the ultimate compression strength of Specimen N-FS-3-8-2.5 was higher than the Chauvenet maximum. Specimen N-FS-3-8-2.5 was an outlier and was therefore excluded from the final data set.

Table 5.15 Summary of Compression Properties of Full Spiral, No Impact Specimens

Specimen I.D.	Cross Sectional Area		Ultimate Compression Strength		Strain at Ultimate Strength	Initial Compression Stiffness	
	[mm^2]	(in^2)]	[MPa]	(ksi)]	[10^3 με]	[GPa	(10^6 psi)]
N-FS-2-3-0.0	59.78	(0.090)	684.2	(99.2)	14.57	496.6	(72.0)
N-FS-2-6-0.0	59.78	(0.090)	256.5	(37.2)	5.57	506.9	(73.5)
N-FS-4-4-0.0	59.06	(0.089)	815.9	(118.3)	22.61	359.9	(52.2)
Average	59.54	(0.09)	585.5	(84.9)	14.25	454.5	(65.9)
Std. Dev.	0.42	(0.00)	292.5	(42.4)	8.52	82.1	(11.9)
Chauvenet	60.11	(0.08)	989.1	(143.5)	26.01	567.7	(65.9)
Limit	58.96	(0.08)	181.9	(26.39)	2.49	341.2	(11.9)

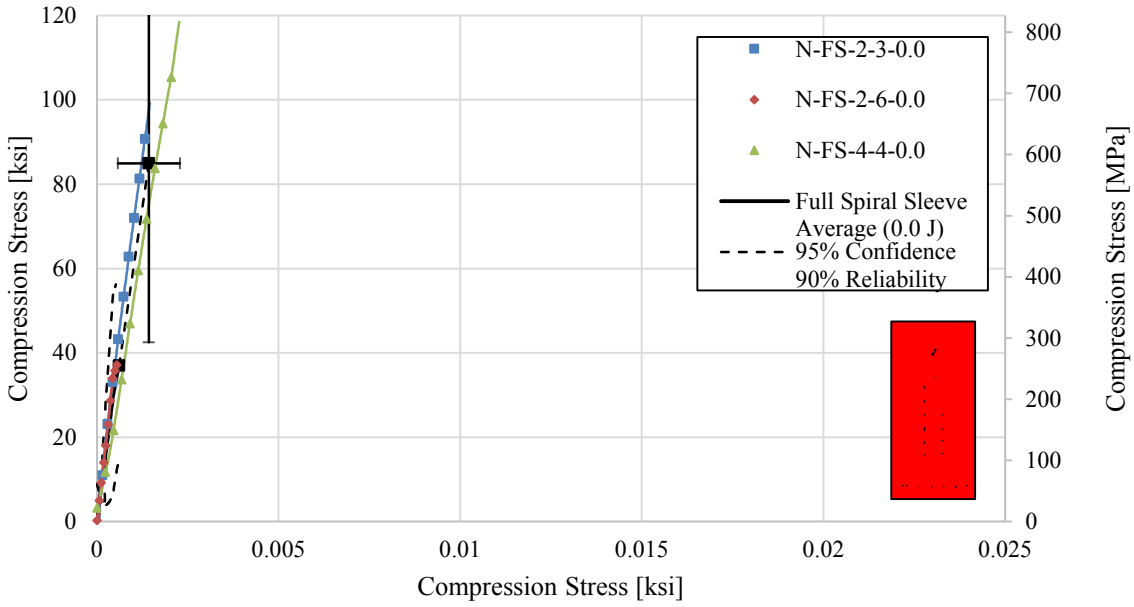

Figure 5.15 Stress-Strain Curves for Full Spiral, Non-Impacted Specimens

Table 5.16 Summary of Compression Properties of Full Spiral, 2.5 J (1.9 ft-lbs) Impacted Specimens

Specimen I.D.	Cross Sectional Area		Ultimate Compression Strength		Strain at Ultimate Strength	Initial Compression Stiffness	
	[mm^2	(in^2)]	[MPa]	(ksi)]	[10^3 με]	[GPa	(10^6 psi)]
N-FS-3-1-2.5	59.97	(0.090)	721.6	(104.7)	22.36	450	(65.2)
N-FS-3-5-2.5	59.97	(0.090)	739.4	(107.2)	21.93	432	(62.6)
N-FS-3-7-2.5	59.97	(0.090)	754.7	(109.5)	22.14	367	(53.3)
*N-FS-3-8-2.5**	*59.97*	*(0.090)*	*843.2+*	*(122.3)+*	*22.43*	*353*	*(51.2)*
N-FS-3-9-2.5	59.97	(0.090)	717.0	(104.0)	16.07	460	(66.7)
Average	59.97	(0.090)	755.2	(109.1)	20.99	412	(59.8)
Std. Dev.	0.00	(0.00)	51.4	(7.5)	2.75	49	(7.1)
Average	59.97	(0.090)	733.15	(106.3)	20.62	427.09	(61.9)
Std. Dev.	0.00	(0.00)	17.30	(2.51)	3.04	41.51	(6.02)
Chauvenet Limit	59.97	(0.090)	759.8	(110.2)	25.31	491.0	(71.2)
	59.97	(0.090)	706.5	(102.5)	15.94	363.2	(52.7)

*Specimen eliminated using Chauvenet's criterion; italicized values not included in final average or standard deviation.
+ Properties used to eliminate specimen.

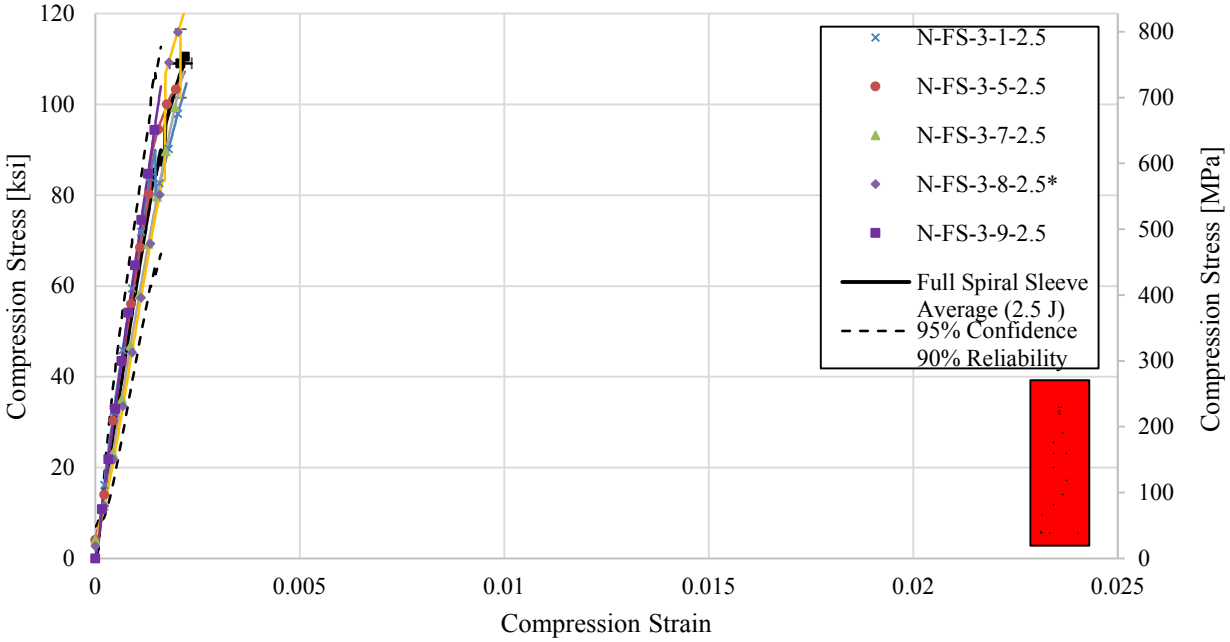

Figure 5.16 Stress-Strain Curves for Full Spiral, 2.5 J (1.9 ft-lbs) Impacted Specimens

The test results full spiral specimens impacted with 5.0 J (3.7 ft-lbs) are summarized in Table 5.17 and the stress-strain curves are shown in Figure 5.17. After the initial test for full spiral specimens with 5.0 J (3.7 ft-lbs) impact, the ultimate compression strength of specimen N-FS-1-8-5.0 was lower than the Chauvenet minimum. Specimen N-FS-1-8-5.0 was an outlier and was therefore excluded from the final data set. The test results full spiral specimens impacted with 7.5 J (5.6 ft-lbs) are summarized in Table 5.18 and the stress-strain curves are shown in Figure 5.18. After the initial test for full spiral specimens with 7.5 J (5.6 ft-lbs) impact, the ultimate compression strength of Specimen N-FS-1-10-7.5 was higher than the Chauvenet maximum. Specimen N-FS-1-10-7.5 was an outlier and was therefore excluded from the final data set.

Table 5.17 Summary of Compression Properties of Full Spiral, 5.0 J (3.7 ft-lbs) Impacted Specimens

Specimen I.D.	Cross Sectional Area		Ultimate Compression Strength		Strain at Ultimate Strength	Initial Compression Stiffness	
	[mm^2	(in^2)]	[MPa]	(ksi)]	[10^3 με]	[GPa	(10^6 psi)]
N-FS-1-8-5.0*	60.58	(0.094)	302.7+	(43.9)+	0.86	366.4	(53.1)
N-FS-2-2-5.0	59.78	(0.093)	550.8	(79.9)	1.19	486.1	(70.5)
N-FS-2-4-5.0	59.78	(0.093)	568.6	(82.5)	1.09	495.6	(71.9)
N-FS-3-3-5.0	59.97	(0.093)	598.8	(86.8)	1.27	486.6	(70.6)
N-FS-4-3-5.0	59.06	(0.092)	561.4	(81.4)	1.49	412.4	(59.8)
Average	59.83	(0.093)	516	(83)	1.18	449.4	(65.2)
Std. Dev.	0.54	(0.00)	121	(3)	0.23	57.3	(8.3)
Average	47.84	(0.093)	473	(67)	1.05	380.3	(55.2)
Std. Dev.	26.44	(0.04)	199	(36)	0.48	183.5	(26.6)
Chauvenet Limit	60.73	(0.09)	715.8	(87.6)	1.57	544.0	(78.9)
	-58.94	(0.09)	317.1	(77.7)	0.79	354.9	(51.5)

*Specimen eliminated using Chauvenet's criterion; italicized values not included in final average or standard deviation.
+ Properties used to eliminate specimen.

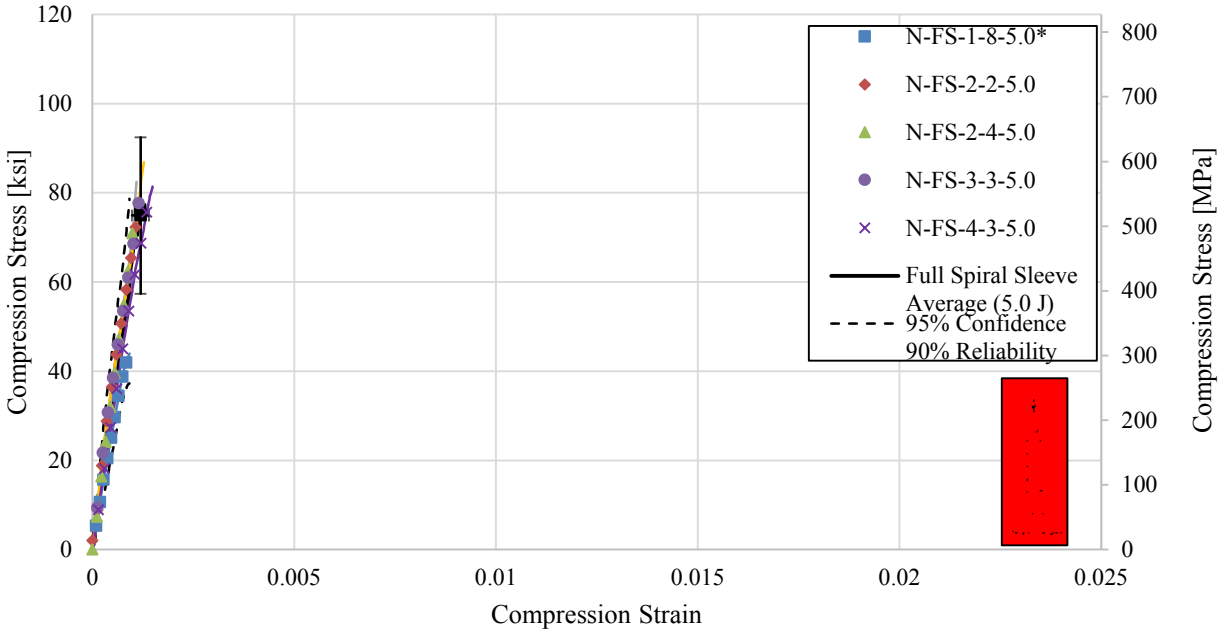

Figure 5.17 Stress-Strain Curves for Full Spiral, 5.0 J (3.7 ft-lbs) Impacted Specimens

Table 5.18 Summary of Compression Properties of Full Spiral, 7.5 J (5.6 ft-lbs) Impacted Specimens

Specimen I.D.	Cross Sectional Area		Ultimate Compression Strength		Strain at Ultimate Strength	Initial Compression Stiffness	
	[mm^2	(in^2)]	[MPa]	(ksi)]	[10^3 με]	[GPa	(10^6 psi)]
N-FS-1-3-7.5	60.58	(0.09)	231.1	(33.5)	0.28	693.1	(100.5)
N-FS-1-7-7.5	60.58	(0.09)	272.4	(39.5)	3.19	184.9	(26.8)
*N-FS-1-10-7.5**	*60.58*	*(0.09)*	*556.4+*	*(80.7)+*	*1.54*	*291.8*	*(42.3)*
N-FS-2-10-7.5	59.78	(0.00)	308.5	(44.7)	0.89	378.5	(54.9)
N-FS-4-5-7.5	59.06	(0.09)	258.3	(37.5)	0.18	1193.0	(173.0)
Average	60.11	(0.09)	325.4	(47.2)	1.22	548.3	(79.5)
Std. Dev.	0.68	(0.00)	132.1	(19.2)	1.23	407.2	(59.1)
Average	60.00	(0.09)	267.6	(38.8)	1.13	612.4	(88.8)
Std. Dev.	0.73	(0.00)	32.2	(4.7)	1.40	440.1	(63.8)
Chauvenet Limit	61.12	(0.09)	317.2	(46.0)	3.30	1290.2	(187.1)
	58.87	(0.09)	218.0	(31.6)	-1.03	-65.4	(-9.5)

*Specimen eliminated using Chauvenet's criterion; italicized values not included in final average or standard deviation.
+ Properties used to eliminate specimen.

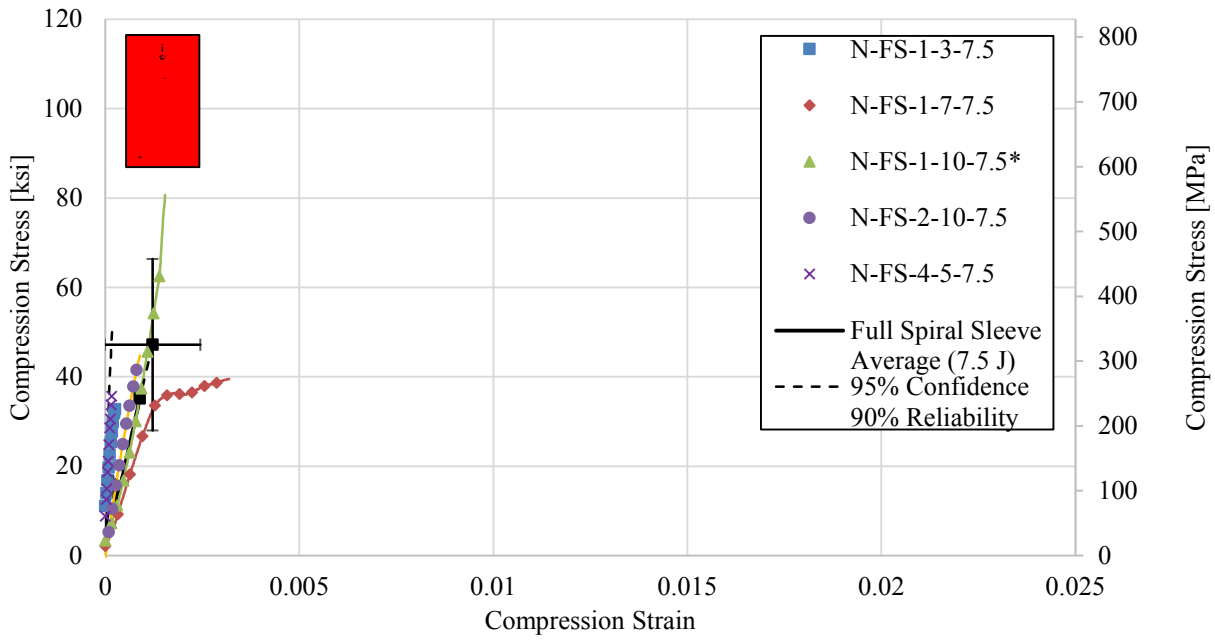

Figure 5.18 Stress-Strain Curves for Full Spiral, 7.5 J (5.6 ft-lbs) Impacted Specimens

The test results full spiral specimens impacted with 10 J (7.4 ft-lbs) are summarized in Table 5.19 and the stress-strain curves are shown in Figure 5.19. The test results full spiral specimens impacted with 15 J (11 ft-lbs) are summarized in Table 5.20 and the stress-strain curves are shown in Figure 5.20. After the initial test for full spiral specimens with 10 J (7.4 ft-lbs) impact, the compression modulus of Specimen N-FS-3-2-10 was higher than the Chauvenet maximum. Specimen N-FS-3-2-10 was an outlier and was therefore excluded from the final data set. After the initial test for full spiral specimens with 15 J (11 ft-lbs) impact, the compression modulus of Specimen N-FS-3-4-15 was higher than the Chauvenet maximum. Also, the ultimate compression strength for Specimen N-FS-3-4-15 was lower than the Chauvenet minimum. Specimen N-FS-3-4-15 was an outlier and was therefore excluded from the final data set. The stress-strain curve for Specimen N-FS-1-4-15 of the full spiral carbon/epoxy specimens impacted at 15 J (11 ft-lbs) fell 50.0% outside of Chauvenet's envelope. Specimen N-FS-1-4-15 was an outlier and was therefore excluded from the final data set.

Table 5.19 Summary of Compression Properties of Full Spiral, 10 J (7.4 ft-lbs) Impacted Specimens

Specimen I.D.	Cross Sectional Area		Ultimate Compression Strength		Strain at Ultimate Strength	Initial Compression Stiffness	
	[mm^2	(in^2)]	[MPa]	(ksi)]	[10^3 με]	[GPa	(10^6 psi)]
N-FS-1-9-10.0	60.58	(0.09)	205.2	(29.8)	7.93	-105.0	(-15.2)
N-FS-2-7-10.0	59.78	(0.09)	238.0	(34.5)	1.79	1653.4	(239.8)
N-FS-2-9-10.0	59.78	(0.09)	231.3	(33.5)	2.57	1196.0	(173.5)
*N-FS-3-2-10.0**	*59.97*	*(0.09)*	*248.8*	*(36.1)*	*0.36*	*8293.3+*	*(1202.8)+*
N-FS-3-6-10.0	59.97	(0.09)	273.6	(39.7)	1.14	2365.6	(343.1)
Average	60.01	(0.09)	239.4	(34.7)	2.76	2680.7	(388.8)
Std. Dev.	0.33	(0.00)	25.0	(3.6)	3.00	3264.2	(473.4)
Average	60.03	(0.09)	237.03	(34.38)	3.36	1277.51	(185.29)
Std. Dev.	0.38	(0.00)	28.18	(4.09)	3.10	1039.78	(150.81)
Chauvenet	60.61	(0.09)	280.4	(40.7)	8.17	2878.8	(417.5)
Limit	59.40	(0.09)	190.5	(27.6)	-1.76	-438.1	(-63.5)

*Specimen eliminated using Chauvenet's criterion; italicized values not included in final average or standard deviation.
+ Properties used to eliminate specimen.

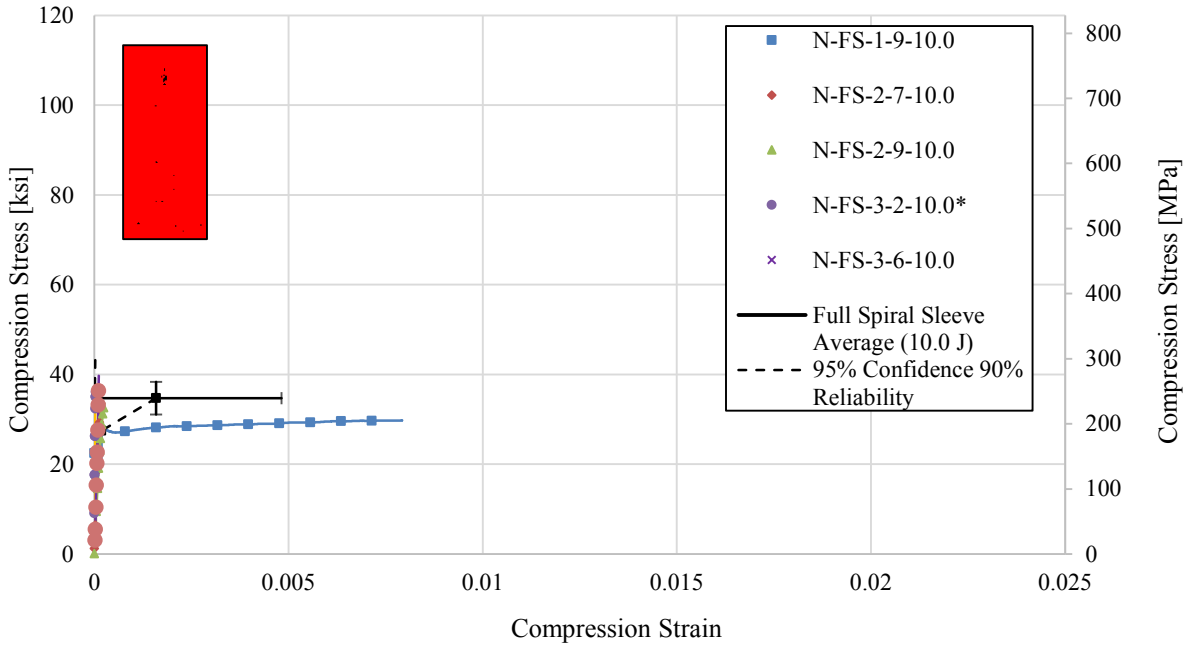

Figure 5.19 Stress-Strain Curves for Full Spiral, 10 J (7.4 ft-lbs) Impacted Specimens

Table 5.20 Summary of Compression Properties of Full Spiral, 15 J (11 ft-lbs) Impacted Specimens

Specimen I.D.	Cross Sectional Area		Ultimate Compression Strength		Strain at Ultimate Strength	Initial Compression Stiffness	
	[mm^2	(in^2)]	[MPa]	(ksi)]	[10^3 με]	[GPa	(10^6 psi)]
N-FS-1-4-15.0	60.58	(0.09)	199.6	(28.9)	0.36	70.1	(10.2)
N-FS-2-1-15.0	59.78	(0.09)	205.8	(29.8)	0.86	210.8	(30.6)
*N-FS-3-4-15.0**	*59.97*	*(0.09)*	*169.0*	*(24.5)*	*8.14*	*363.1+*	*(52.7)+*
N-FS-4-1-15.0	59.06	(0.09)	202.0	(29.3)	4.14	68.0	(9.9)
N-FS-5-1-15.0	57.41	(0.09)	207.4	(30.1)	3.43	210.0	(30.5)
Average	59.36	(0.09)	196.7	(28.5)	3.39	184.4	(26.7)
Std. Dev.	1.22	(0.00)	15.8	(2.3)	3.11	122.4	(17.7)
Average	59.20	(0.09)	203.7	(29.5)	2.20	139.7	(20.3)
Std. Dev.	1.35	(0.00)	3.6	(0.5)	1.87	81.6	(11.8)
Chauvenet Limit	31.28	(0.09)	209.2	(30.3)	5.08	265.4	(38.5)
	57.13	(0.09)	198.2	(28.7)	-0.68	14.0	(2.0)

*Specimen eliminated using Chauvenet's criterion; italicized values not included in final average or standard deviation.
+ Properties used to eliminate specimen.

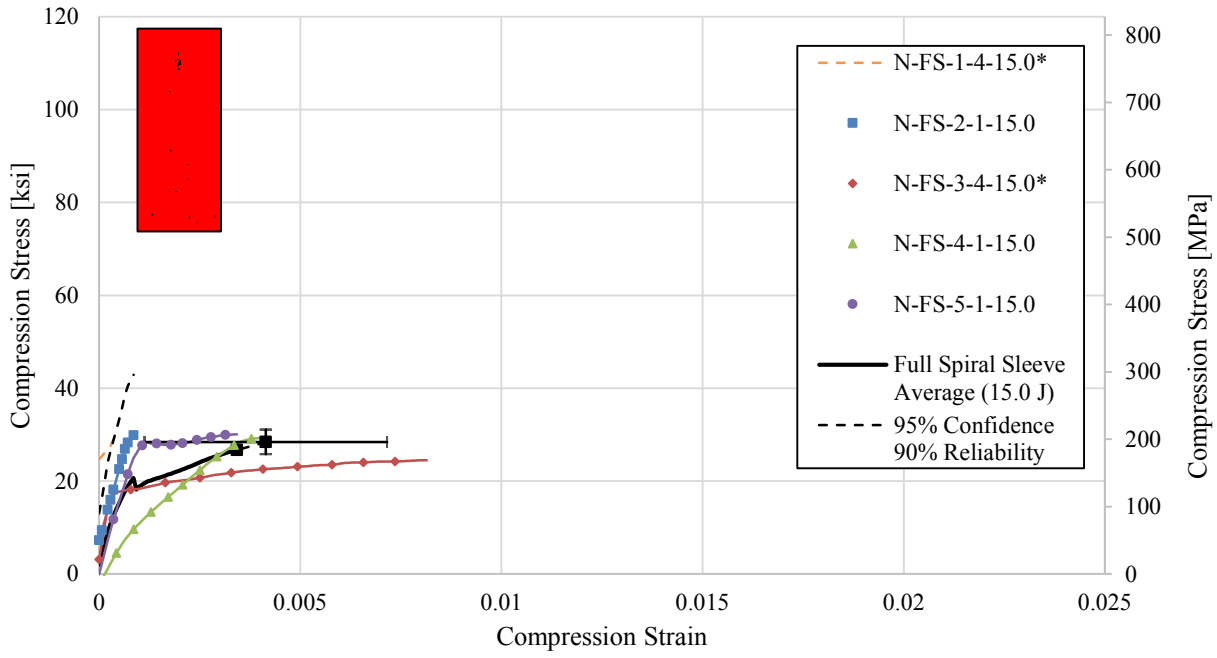

Figure 5.20 Stress-Strain Curves for Full Spiral, 15 J (11 ft-lbs) Impacted Specimens

The test results full spiral specimens impacted with 20 J (15 ft-lbs) are summarized in Table 5.21 and the stress-strain curves are shown in Figure 5.21.

Table 5.21 Summary of Compression Properties of Full Spiral, 20 J (15 ft-lbs) Impacted Specimens

Specimen I.D.	Cross Sectional Area		Ultimate Compression Strength		Strain at Ultimate Strength	Initial Compression Stiffness	
	[mm^2	(in^2)]	[MPa]	(ksi)]	[10^3 με]	[GPa	(10^6 psi)]
N-FS-1-1-20.0	60.58	(0.09)	173.2	(25.1)	1.57	223.0	(32.3)
N-FS-1-2-20.0	60.58	(0.09)	220.8	(32.0)	3.14	52.3	(7.6)
N-FS-1-6-20.0	60.58	(0.09)	160.6	(23.3)	6.43	120.8	(17.5)
N-FS-2-5-20.0	59.78	(0.09)	207.5	(30.1)	3.43	121.2	(17.6)
N-FS-2-8-20.0	59.78	(0.09)	175.2	(25.4)	0.64	140.2	(20.3)
Average	60.26	(0.09)	187.5	(27.2)	3.04	131.5	(19.1)
Std. Dev.	0.44	(0.00)	25.4	(3.7)	2.21	61.1	(8.9)
Chauvenet	60.98	(0.09)	229.4	(33.3)	6.69	232.3	(33.7)
Limit	59.54	(0.09)	145.5	(21.1)	-0.60	30.6	(4.4)

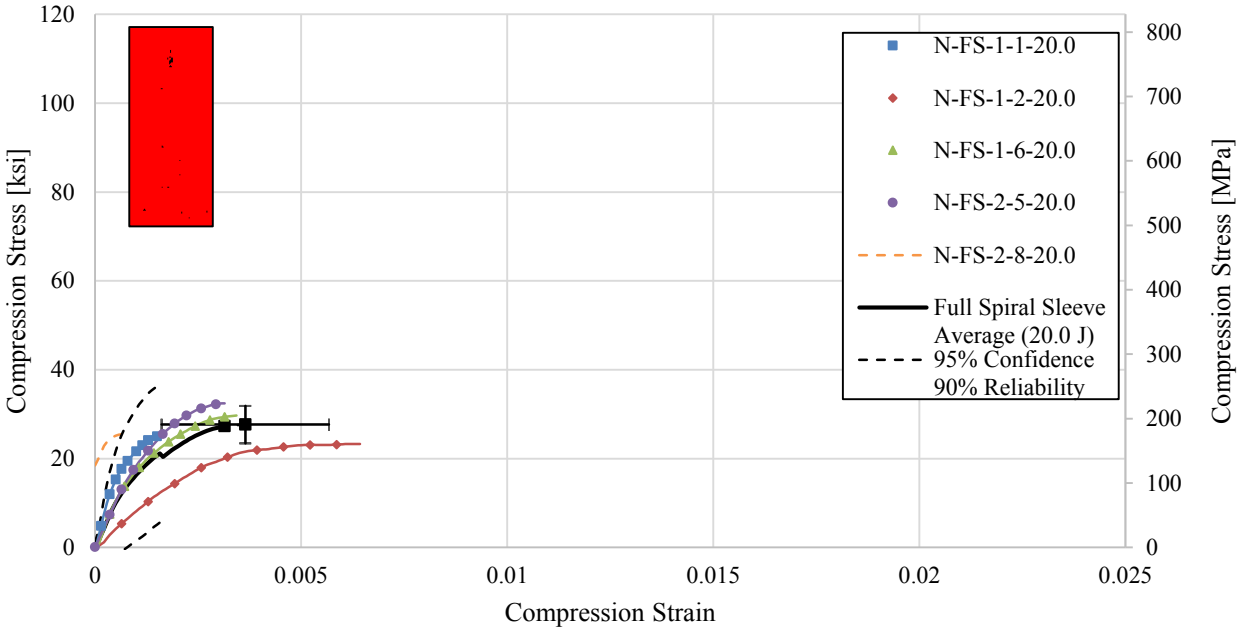

Figure 5.21 Stress-Strain Curves for Full Spiral, 20 J (15 ft-lbs) Impacted Specimens

5.5 Half Spiral Compression Test Results

The test results for undamaged half spiral carbon/epoxy specimens are summarized in Table 5.22 and the stress-strain curves are shown in Figure 5.22. The test results half spiral specimens impacted with 2.5 J (1.9 ft-lbs) are summarized in Table 5.23 and the stress-strain curves are shown in Figure 5.23. After the initial test for half spiral specimens with 2.5 J (1.9 ft-lbs) impact, the ultimate compression strength of Specimen N-HS-4-6-2.5 was higher than the Chauvenet maximum. Specimen N-HS-4-6-2.5 was an outlier and was an outlier and was therefore excluded from the final data set. The test results for half spiral specimens impacted with 5.0 J (3.7 ft-lbs) are summarized in Table 5.24 and the stress-strain curves are shown in Figure 5.24. The test results for half spiral specimens impacted with 7.5 J (5.6 ft-lbs) are summarized in Table 5.25 and the stress-strain curves are shown in Figure 5.25. After the initial test for half spiral specimens with 7.5 J (5.6 ft-lbs) impact, the ultimate compression strength of Specimen N-HS-2-10-7.5 was higher than the Chauvenet maximum. Specimen N-HS-2-10-7.5 was an outlier and was an outlier and was therefore excluded from the final data set.

Table 5.22 Summary of Compression Properties of Half Spiral, No Impact Specimens

Specimen I.D.	Cross Sectional Area		Ultimate Compression Strength		Strain at Ultimate Strength	Initial Compression Stiffness	
	[mm^2	(in^2)]	[MPa]	(ksi)]	[10^3 με]	[GPa	(10^6 psi)]
N-HS-1-1-0.0	57.42	(0.09)	895.6	(129.9)	2.37	399.3	(57.9)
N-HS-1-3-0.0	57.42	(0.09)	788.2	(114.3)	1.77	436.8	(63.3)
N-HS-1-5-0.0	57.42	(0.09)	746.5	(108.3)	1.81	398.6	(57.8)
N-HS-1-8-0.0	57.42	(0.09)	782.0	(113.4)	1.54	494.6	(71.7)
N-HS-2-2-0.0	57.43	(0.09)	896.4	(130.0)	1.78	529.6	(76.8)
Average	57.42	(0.09)	821.7	(119.2)	1.85	451.8	(65.5)
Std. Dev.	0.00	(0.00)	69.6	(10.1)	0.31	58.5	(8.5)
Chauvenet Limit	57.43	(0.09)	936.6	(135.8)	2.36	548.32	(79.5)
	57.42	(0.09)	706.8	(102.5)	1.34	355.23	(51.5)

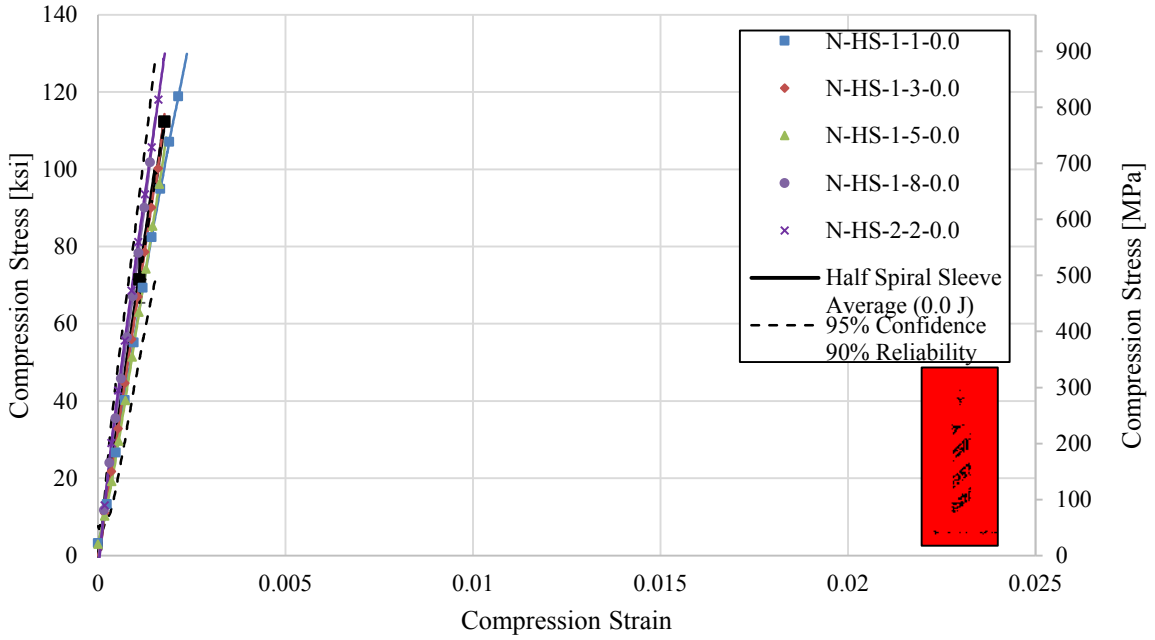

Figure 5.22 Stress-Strain Curves for Half Spiral, Non-Impacted Specimens

Table 5.23 Summary of Compression Properties of Half Spiral, 2.5 J (1.9 ft-lbs) Impacted Specimens

Specimen I.D.	Cross Sectional Area		Ultimate Compression Strength		Strain at Ultimate Strength	Initial Compression Stiffness	
	[mm^2	(in^2)]	[MPa]	(ksi)]	[10^3 με]	[GPa	(10^6 psi)]
N-HS-4-3-2.5	56.66	(0.090)	659.2	(95.6)	1.90	411.9	(59.7)
N-HS-4-4-2.5	56.66	(0.090)	694.1	(100.7)	1.36	496.2	(72.0)
*N-HS-4-6-2.5**	*56.66*	*(0.090)*	*779.7*	*(113.1)+*	*1.63*	*484.7*	*(70.3)*
N-HS-4-8-2.5	56.66	(0.090)	690.2	(100.1)	1.67	431.0	(62.5)
N-HS-4-9-2.5	56.66	(0.090)	675.8	(98.0)	1.81	373.0	(54.1)
Average	56.66	(0.090)	699.8	(101.5)	1.68	439.4	(63.7)
Std. Dev.	0.00	(0.00)	46.7	(6.8)	0.21	51.3	(7.4)
Average	56.66	(0.090)	679.80	(98.60)	1.69	428.03	(62.08)
Std. Dev.	0.00	(0.00)	15.85	(2.30)	0.24	51.48	(7.47)
Chauvenet	56.66	(0.09)	776.9	(112.7)	2.01	524.0	(76.0)
Limit	56.66	(0.09)	622.7	(90.3)	1.34	354.7	(51.5)

*Specimen eliminated using Chauvenet's criterion; italicized values not included in final average or standard deviation.
+ Properties used to eliminate specimen.

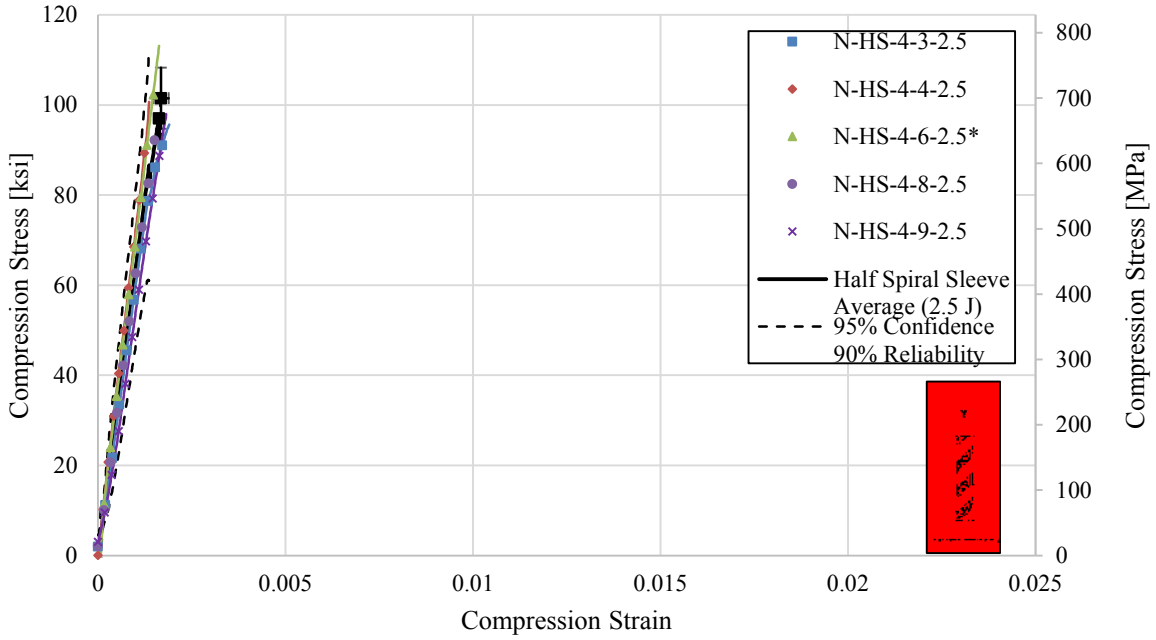

Figure 5.23 Stress-Strain Curves for Half Spiral, 2.5 J (1.9 ft-lbs) Impacted Specimens

Table 5.24 Summary of Compression Properties of Half Spiral, 5.0 J (3.7 ft-lbs) Impacted Specimens

Specimen I.D.	Cross Sectional Area		Ultimate Compression Strength		Strain at Ultimate Strength	Initial Compression Stiffness	
	[mm^2	(in^2)]	[MPa]	(ksi)]	[10^3 με]	[GPa	(10^6 psi)]
N-HS-4-5-5.0	56.66	(0.090)	284.3	(41.2)	0.93	325.3	(47.2)
N-HS-3-4-5.0	55.56	(0.087)	316.0	(45.8)	2.93	192.2	(27.9)
N-HS-3-8-5.0	55.56	(0.087)	299.0	(43.4)	2.21	156.7	(22.7)
N-HS-3-6-5.0	55.56	(0.087)	331.0	(48.0)	1.21	313.1	(45.4)
N-HS-3-7-5.0	55.56	(0.087)	318.5	(46.2)	0.64	537.0	(77.9)
Average	55.78	(0.088)	309.8	(44.9)	1.59	304.8	(44.2)
Std. Dev.	0.49	(0.00)	18.2	(2.6)	0.96	149.2	(21.6)
Chauvenet	56.59	(0.09)	339.9	(49.3)	3.16	551.0	(79.9)
Limit	54.97	(0.09)	279.7	(40.6)	0.01	58.7	(8.51)

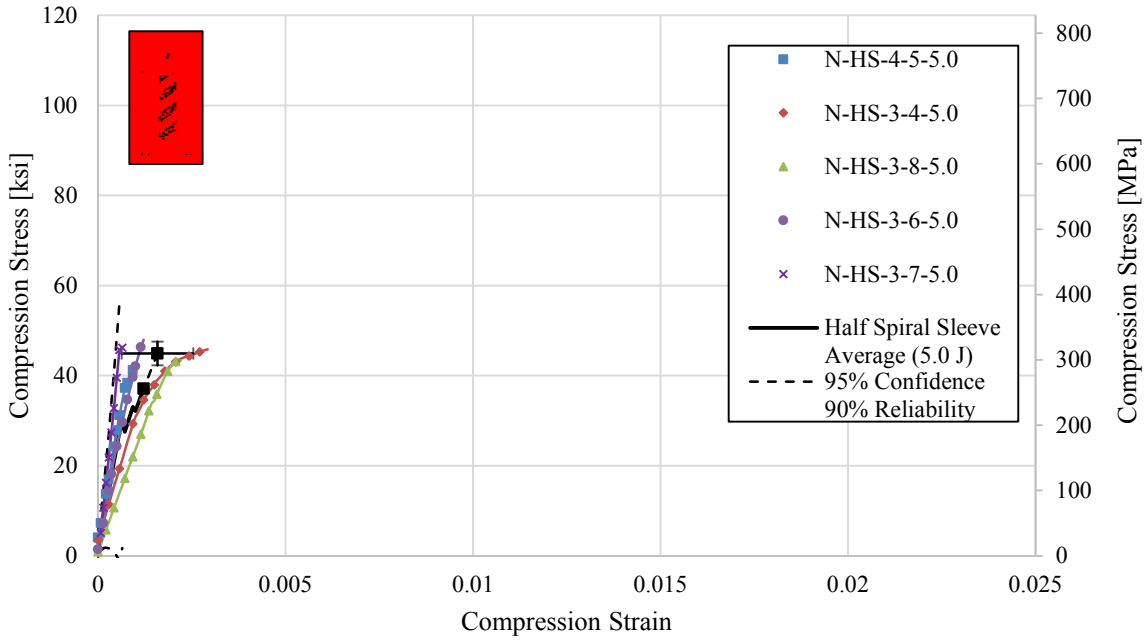

Figure 5.24 Stress-Strain Curves for Half Spiral, 5.0 J (3.7 ft-lbs) Impacted Specimens

Table 5.25 Summary of Compression Properties of Half Spiral, 7.5 J (5.6 ft-lbs) Impacted Specimens

Specimen I.D.	Cross Sectional Area		Ultimate Compression Strength		Strain at Ultimate Strength	Initial Compression Stiffness	
	[mm^2	(in^2)]	[MPa]	(ksi)]	[10^3 με]	[GPa	(10^6 psi)]
N-HS-2-9-7.5	57.43	(0.090)	244.7	(35.50	1.46	191.1	(27.7)
N-HS-2-10-7.5*	57.43	(0.090)	469.4+	(68.1)+	1.39	395.6	(57.4)
N-HS-3-3-7.5	55.56	(0.087)	217.3	(31.5)	3.14	174.6	(25.3)
N-HS-4-2-7.5	56.66	(0.090)	245.0	(35.5)	0.36	722.9	(104.8)
N-HS-4-7-7.5	56.66	(0.090)	253.1	(36.7)	0.46	605.5	(87.8)
Average	56.75	(0.089)	285.9	(41.5)	1.36	417.9	(60.6)
Std. Dev.	0.77	(0.00)	103.5	(15.0)	1.12	244.6	(35.5)
Average	56.58	(0.089)	240.03	(34.8)	1.36	423.53	(61.4)
Std. Dev.	0.77	(0.00)	15.63	(2.3)	1.29	282.05	(40.9)
Chauvenet Limit	58.01	(0.09)	456.6	(66.2)	3.21	821.5	(119.1)
	55.48	-(0.09)	115.2	(16.7)	-0.48	14.4	(2.1)

*Specimen eliminated using Chauvenet's criterion; italicized values not included in final average or standard deviation.
+ Properties used to eliminate specimen.

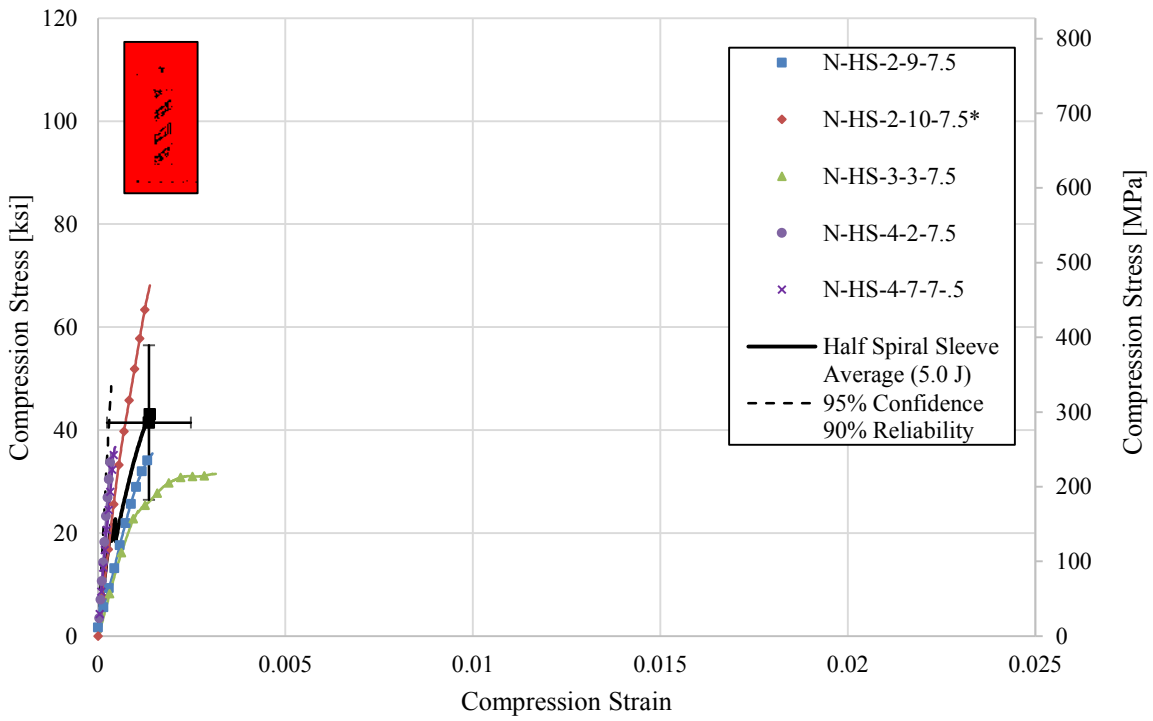

Figure 5.25 Stress-Strain Curves for Half Spiral, 7.5 J (5.6 ft-lbs) Impacted Specimens

The test results for half spiral carbon/epoxy specimens impacted with 10 J (7.4 ft-lbs) are summarized in Table 5.26 and the stress-strain curves are shown in Figure 5.26. After the initial test for half spiral specimens with 10 J (7.4 ft-lbs) impact, the compression modulus of specimen N-HS-4-10-10.0 was higher than the Chauvenet maximum. The stress-strain curve for Specimen N-HS-4-10-10.0 fell 30.8% outside of Chauvenet's envelope. Specimen N-HS-4-10-10.0 was an outlier and was therefore excluded from the final data set. The test results half spiral specimens impacted with 15 J (11 ft-lbs) are summarized in Table 5.27 and the stress-strain curves are shown in Figure 5.27.

Table 5.26 Summary of Compression Properties of Half Spiral, 10 J (7.4 ft-lbs) Impacted Specimens

Specimen I.D.	Cross Sectional Area		Ultimate Compression Strength		Strain at Ultimate Strength	Initial Compression Stiffness	
	[mm^2]	(in^2)]	[MPa]	(ksi)]	[10^3 με]	[GPa	(10^6 psi)]
N-HS-2-4-10.0	57.43	(0.090)	260.6	(37.8)	0.80	336.1	(48.8)
N-HS-2-6-10.0	57.43	(0.090)	273.7	(39.7)	0.73	324.5	(47.1)
N-HS-3-9-10.0	55.56	(0.087)	241.3	(35.0)	3.41	103.8	(15.1)
N-HS-3-10-10.0	55.56	(0.087)	274.6	(39.8)	0.99	368.7	(53.5)
*N-HS-4-10-10.0**	*56.66*	*(0.090)*	*219.2*	*(31.8)*	*0.74*	*25456.9+*	*(3692.2)+*
Average	56.53	(0.089)	253.9	(36.8)	1.33	5318.0	(771.3)
Std. Dev.	0.94	(0.00)	23.6	(3.4)	1.17	11258.5	(1632.9)
Average	56.49	(0.089)	262.56	(38.1)	1.48	283.27	(41.08)
Std. Dev.	1.08	(0.00)	15.53	(2.25)	1.29	121.12	(17.57)
Chauvenet	58.07	(0.09)	292.8	(42.5)	3.26	23894.5	(3465.6)
Limit	54.98	(0.09)	215.0	(31.2)	-0.59	-13258.5	(-1923.0)

*Specimen eliminated using Chauvenet's criterion; italicized values not included in final average or standard deviation.
+ Properties used to eliminate specimen.

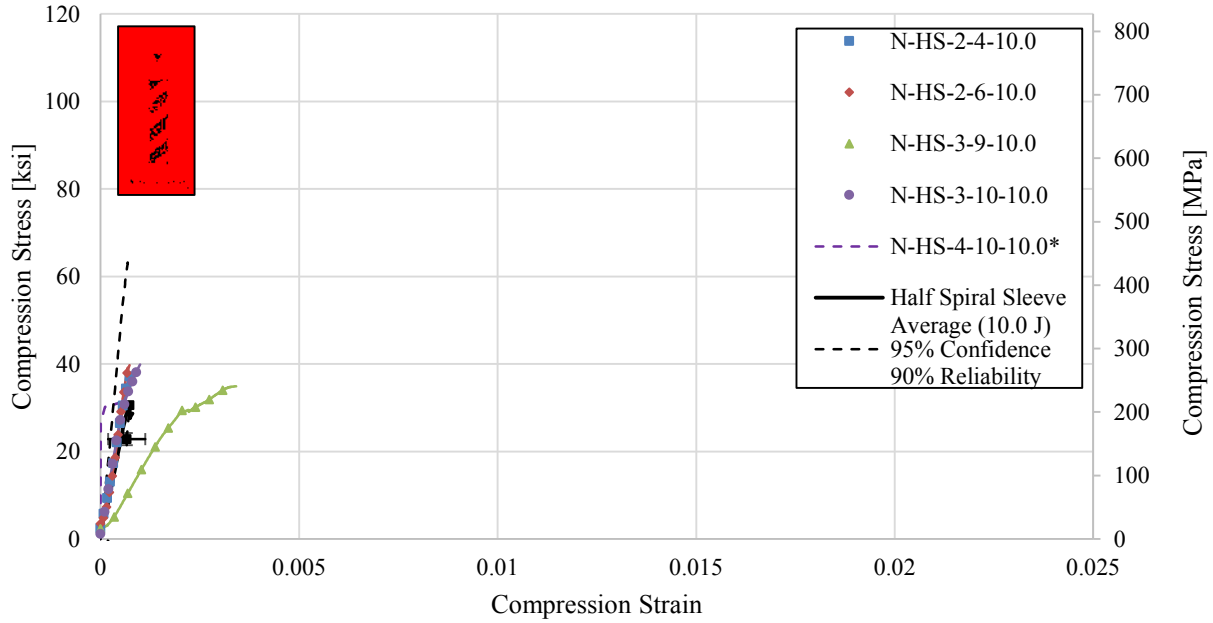

Figure 5.26 Stress-Strain Curves for Half Spiral, 10 J (7.4 ft-lbs) Impacted Specimens

Table 5.27 Summary of Compression Properties of Half Spiral, 15 J (11 ft-lbs) Impacted Specimens

Specimen I.D.	Cross Sectional Area		Ultimate Compression Strength		Strain at Ultimate Strength	Initial Compression Stiffness	
	[mm^2	(in^2)]	[MPa]	(ksi)]	[10^3 με]	[GPa	(10^6 psi)]
N-HS-2-3-15.0	57.43	(0.090)	145.3	(21.1)	5.86	36.1	(5.2)
N-HS-4-1-15.0	56.66	(0.090)	194.3	(28.2)	0.71	172.0	(25.0)
N-HS-3-2-15.0	55.56	(0.087)	242.8	(35.2)	2.36	161.6	(23.4)
N-HS-2-8-15.0	57.43	(0.090)	257.1	(37.3)	2.21	142.6	(20.7)
N-HS-1-10-15.0	57.42	(0.091)	160.1	(23.2)	3.21	288.8	(41.9)
Average	56.90	(0.089)	199.9	(29.0)	2.87	160.2	(23.2)
Std. Dev.	0.82	(0.00)	49.3	(7.1)	1.90	90.0	(13.0)
Chauvenet	58.25	(0.09)	281.2	(40.8)	6.00	308.7	(44.8)
Limit	55.55	(0.09)	118.7	(17.2)	-0.26	11.8	(1.71)

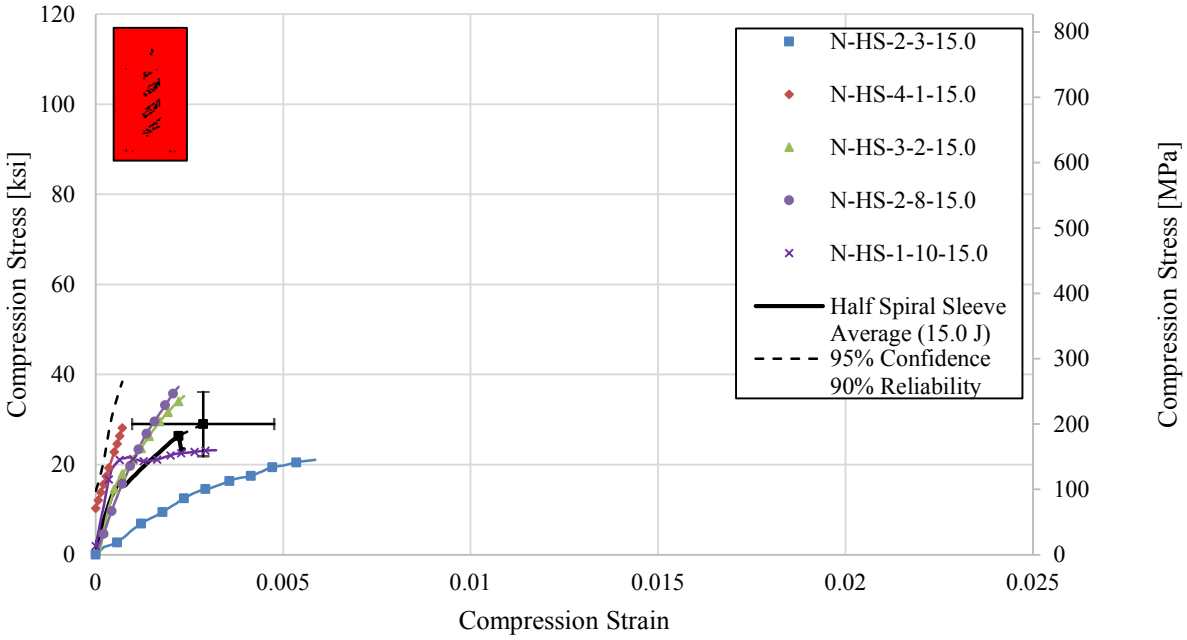

Figure 5.27 Stress-Strain Curves for Half Spiral, 15 J (11 ft-lbs) Impacted Specimens

The test results half spiral specimens impacted with 20 J (15 ft-lbs) are summarized in Table 3.28 and the stress-strain curves are shown in Figure 3.28.

Table 5.28 Summary of Compression Properties of Half Spiral, 20 J (15 ft-lbs) Impacted Specimens

Specimen I.D.	Cross Sectional Area		Ultimate Compression Strength		Strain at Ultimate Strength	Initial Compression Stiffness	
	[mm^2	(in^2)]	[MPa]	(ksi)]	[10^3 με]	[GPa	(10^6 psi)]
N-HS-1-9-20.0	57.42	(0.091)	144.4	(20.9)	4.86	92.4	(13.4)
N-HS-1-7-20.0	57.42	(0.091)	155.7	(22.6)	8.50	131.9	(19.1)
N-HS-1-6-20.0	57.42	(0.091)	177.8	(25.8)	2.86	153.3	(22.2)
N-HS-1-5-20.0	57.42	(0.091)	184.8	(26.8)	3.86	90.8	(13.2)
N-HS-1-2-20.0	57.42	(0.091)	212.8	(30.9)	2.36	153.6	(22.3)
Average	57.42	(0.091)	175.1	(25.4)	4.49	124.4	(18.0)
Std. Dev.	0.00	(0.00)	26.7	(3.9)	2.44	31.2	(4.5)
Chauvenet	57.42	(0.09)	219.1	(31.8)	8.51	175.9	(25.5)
Limit	57.42	(0.09)	131.1	(19.0)	0.46	72.9	(10.6)

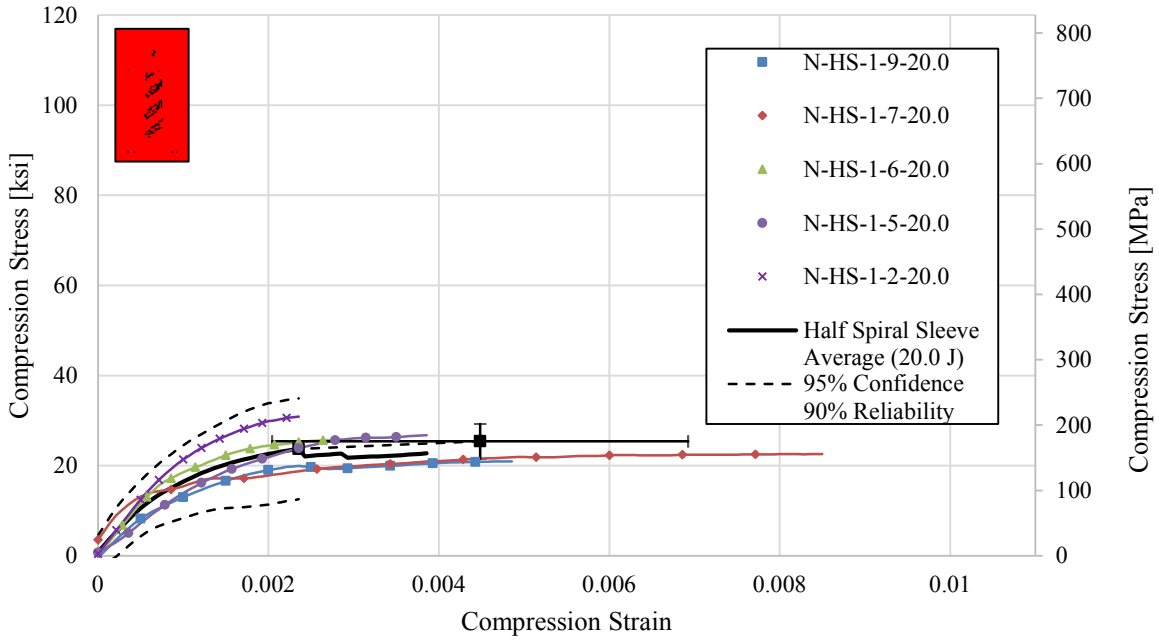

Figure 5.28 Stress-Strain Curves for Half Spiral, 20 J (15 ft-lbs) Impacted Specimens

5.6 Shrink Tape Compression Test Results

The test results for undamaged half spiral specimens are summarized in Table 5.29 and the stress-strain curves are shown in Figure 5.29. The stress-strain curve for Specimen ST-1-2-0.0 of the no impact specimens fell 24.9% outside of Chauvenet's envelope. Specimen ST-1-2-0.0 was an outlier and was therefore excluded from the final data set. The test results for shrink tape carbon/epoxy specimens impacted with 2.5 J (1.9 ft-lbs) are summarized in Table 5.30 and the stress-strain curves are shown in Figure 5.30. The stress-strain curve for Specimen ST-3-3-2.5 of the 2.5 J (1.9 ft-lbs) impacted specimens fell 15.4% outside of Chauvenet's envelope. Specimen ST-3-3-2.5 was an outlier and was therefore excluded from the final data set.

Table 5.29 Summary of Compression Properties of Shrink Tape, Non-Impacted Specimens

Specimen I.D.	Cross Sectional Area		Ultimate Compression Strength		Strain at Ultimate Strength	Initial Compression Stiffness	
	[mm^2	(in^2)]	[MPa]	(ksi)]	[10^3 με]	[GPa	(10^6 psi)]
ST-1-2-0.0	55.91	(0.087)	924.6	(134.1)	1.81	494.6	(71.7)
ST-1-9-0.0	55.91	(0.087)	931.0	(135.0)	1.65	619.2	(89.8)
ST-4-4-0.0	55.54	(0.085)	1029.2	(149.3)	2.47	431.4	(62.6)
ST-4-9-0.0	55.54	(0.085)	915.0	(132.7)	2.18	444.3	(64.4)
ST-4-11-0.0	55.54	(0.085)	755.7	(109.6)	2.01	391.6	(56.8)
Average	55.69	(0.086)	911.1	(132.1)	2.02	476.2	(69.1)
Std. Dev.	0.20	(0.00)	98.3	(14.3)	0.32	88.0	(12.8)
Chauvenet Limit	56.03	(0.09)	1073.4	(155.7)	2.55	621.4	(90.1)
	55.36	(0.09)	748.8	(108.6)	1.49	331.0	(48.0)

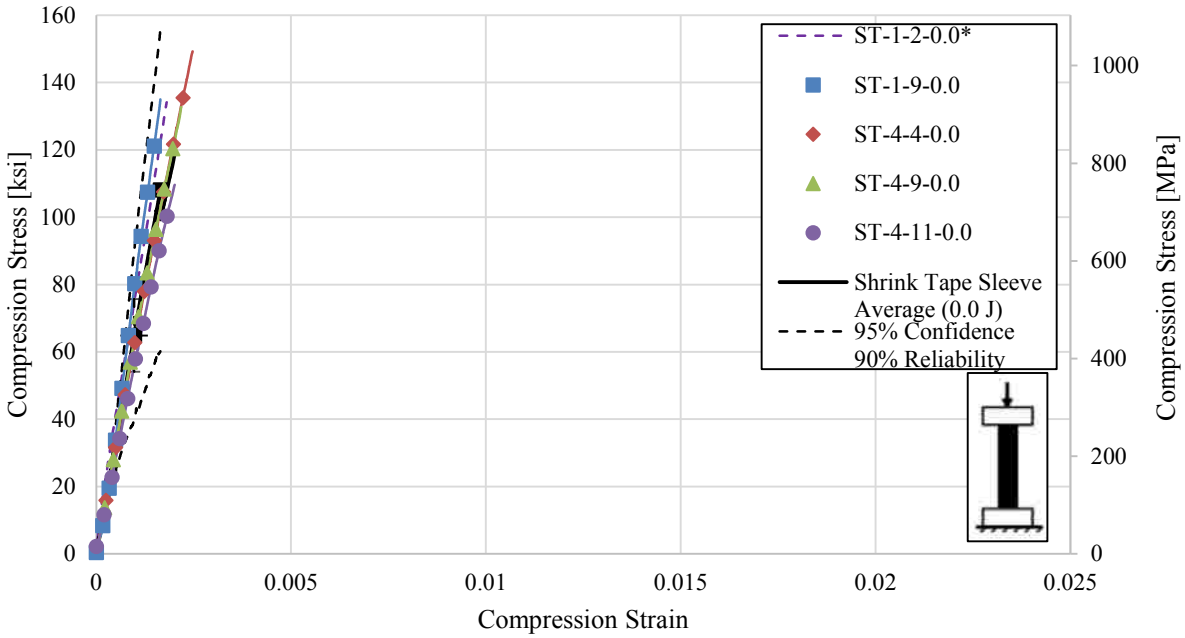

Figure 5.29 Stress-Strain Curves for Shrink Tape, Non-Impacted Specimens

Table 5.30 Summary of Compression Properties of Shrink Tape, 2.5 J (1.9 ft-lbs) Impacted Specimens

Specimen I.D.	Cross Sectional Area		Ultimate Compression Strength		Strain at Ultimate Strength	Initial Compression Stiffness	
	[mm^2	(in^2)]	[MPa]	(ksi)]	[10^3 με]	[GPa	(10^6 psi)]
ST-2-1-2.5	57.53	(0.087)	406.4	(58.9)	1.09	378.3	(54.9)
ST-2-11-2.5	57.53	(0.087)	549.9	(79.8)	1.09	539.4	(78.2)
ST-3-2-2.5	57.25	(0.087)	372.7	(54.1)	0.78	425.3	(61.7)
ST-3-3-2.5	57.25	(0.087)	398.7	(57.8)	1.36	331.9	(48.1)
ST-1-1-2.5	55.91	(0.087)	486.2	(70.5)	0.99	467.8	(67.9)
Average	57.10	(0.087)	442.8	(64.2)	1.06	428.6	(62.2)
Std. Dev.	0.68	(0.00)	73.4	(10.6)	0.21	80.1	(11.6)
Chauvenet	58.21	(0.09)	563.9	(81.8)	1.41	560.8	(81.3)
Limit	55.98	(0.09)	321.7	(46.7)	0.72	296.3	(43.0)

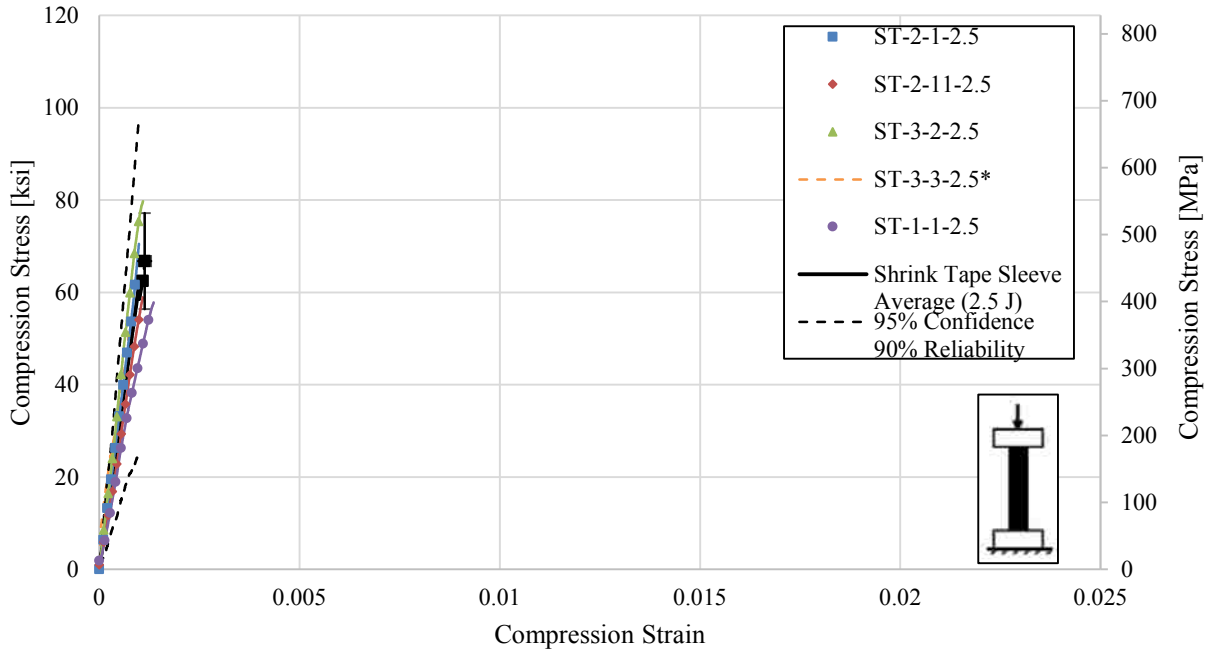

Figure 5.30 Stress-Strain Curves for Shrink Tape, 2.5 J (1.9 ft-lbs) Impacted Specimens

The test results for shrink tape specimens impacted with 5.0 J (3.7 ft-lbs) are summarized in Table 5.31 and the stress-strain curves are shown in Figure 5.31. The test results for shrink tape specimens impacted with 7.5 J (5.6 ft-lbs) are summarized in Table 5.32 and the stress-strain curves are shown in Figure 5.32. The stress-strain curve for specimen ST-2-4-7.5 of the 7.5 J (5.6 ft-lbs) impacted specimens fell 100% outside of Chauvenet's envelope. Specimen ST-2-4-7.5 was an outlier and was therefore excluded from the final data set The test results for shrink tape specimens impacted with 10 J (7.4 ft-lbs) are summarized in Table 5.33 and the stress-strain curves are shown in Figure 5.33. After the initial test for shrink tape specimens with 10 J (7.4 ft-lbs) impact, the compression modulus of Specimen ST-1-4-10.0 was higher than the Chauvenet maximum. Specimen ST-1-4-10.0 was an outlier and was therefore excluded from the final data set. The test results for shrink tape specimens impacted with 15 J (11 ft-lbs) are summarized in Table 5.34 and the stress-strain curves are shown in Figure 5.34. The compression modulus of

Specimen ST-2-9-15.0 for shrink tape specimens with 15 J (11 ft-lbs) impact was higher than the Chauvenet maximum. Specimen ST-2-9-15.0 was an outlier and was therefore excluded from the final data set.

Table 5.31 Summary of Compression Properties of Shrink Tape, 5.0 J (3.7 ft-lbs) Impacted Specimens

Specimen I.D.	Cross Sectional Area		Ultimate Compression Strength		Strain at Ultimate Strength	Initial Compression Stiffness	
	[mm^2	(in^2)]	[MPa]	(ksi)]	[10^3 με]	[GPa	(10^6 psi)]
ST-1-7-5.0	55.91	(0.087)	212.0	(30.7)	1.60	239.0	(34.7)
ST-2-6-5.0	57.53	(0.087)	219.5	(31.8)	2.11	171.2	(24.8)
ST-3-6-5.0	57.25	(0.087)	381.4	(55.3)	1.46	272.4	(39.5)
ST-3-11-5.0	57.25	(0.087)	279.5	(40.5)	1.11	244.0	(35.4)
ST-4-6-5.0	55.54	(0.085)	251.8	(36.5)	1.20	335.2	(48.6)
Average	56.70	(0.087)	268.8	(39.0)	1.50	252.4	(36.6)
Std. Dev.	0.90	(0.00)	68.4	(9.9)	0.40	59.4	(8.6)
Chauvenet	58.18	(0.09)	381.8	(55.4)	2.15	350.3	(50.8)
Limit	55.21	(0.09)	155.9	(22.6)	0.84	154.4	(22.4)

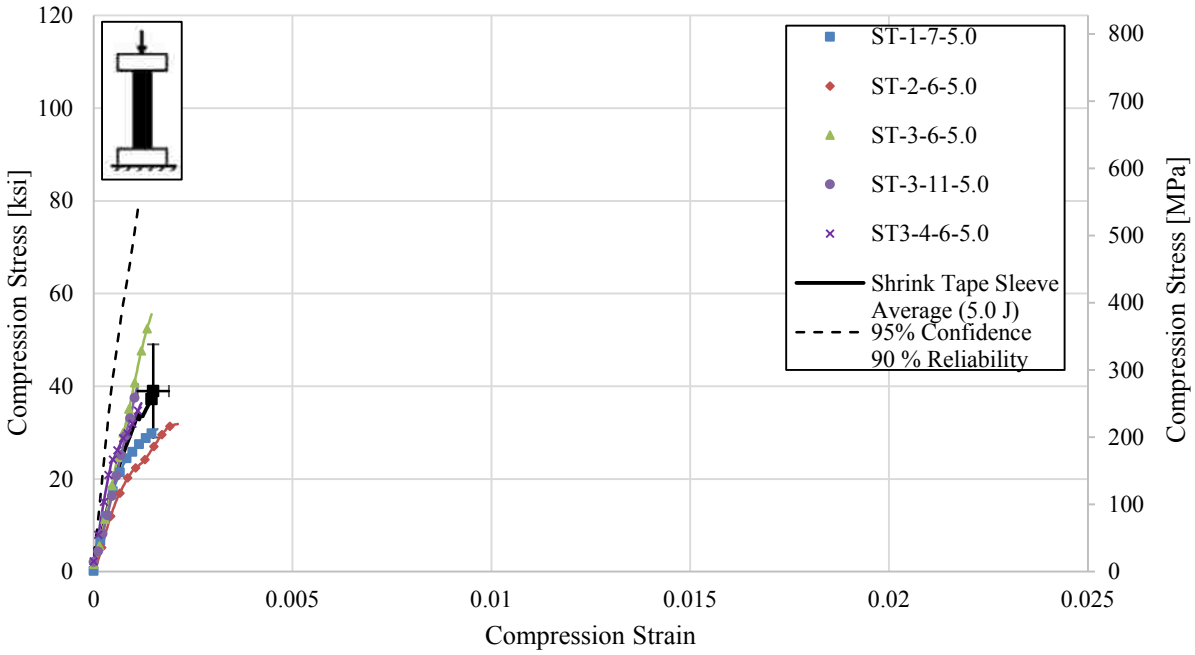

Figure 5.31 Stress-Strain Curves for Shrink Tape, 5.0 J (3.7 ft-lbs) Impacted Specimens

Table 5.32 Summary of Compression Properties of Shrink Tape, 7.5 J (5.6 ft-lbs) Impacted Specimens

Specimen I.D.	Cross Sectional Area		Ultimate Compression Strength		Strain at Ultimate Strength	Initial Compression Stiffness	
	[mm^2	(in^2)]	[MPa]	(ksi)]	[10^3 με]	[GPa	(10^6 psi)]
ST-2-2-7.5	57.53	(0.087)	236.5	(34.3)	3.64	81.9	(11.9)
ST-2-4-7.5	57.53	(0.087)	245.3	(35.6)	0.43	350.5	(50.8)
ST-2-8-7.5	57.53	(0.087)	140.2	(20.3)	6.14	67.3	(9.8)
ST-3-9-7.5	57.25	(0.087)	180.6	(26.2)	2.29	217.7	(31.6)
ST-3-10-7.5	57.25	(0.087)	200.9	(29.1)	2.21	238.3	(34.6)
Average	57.42	(0.087)	200.7	(29.1)	2.94	191.1	(27.7)
Std. Dev.	0.16	(0.00)	42.8	(6.2)	2.12	117.9	(17.1)
Chauvenet	57.68	(0.09)	271.4	(39.4)	6.44	385.7	(55.94)
Limit	57.16	(0.09)	130.0	(18.9)	-0.56	-3.41	(-0.49)

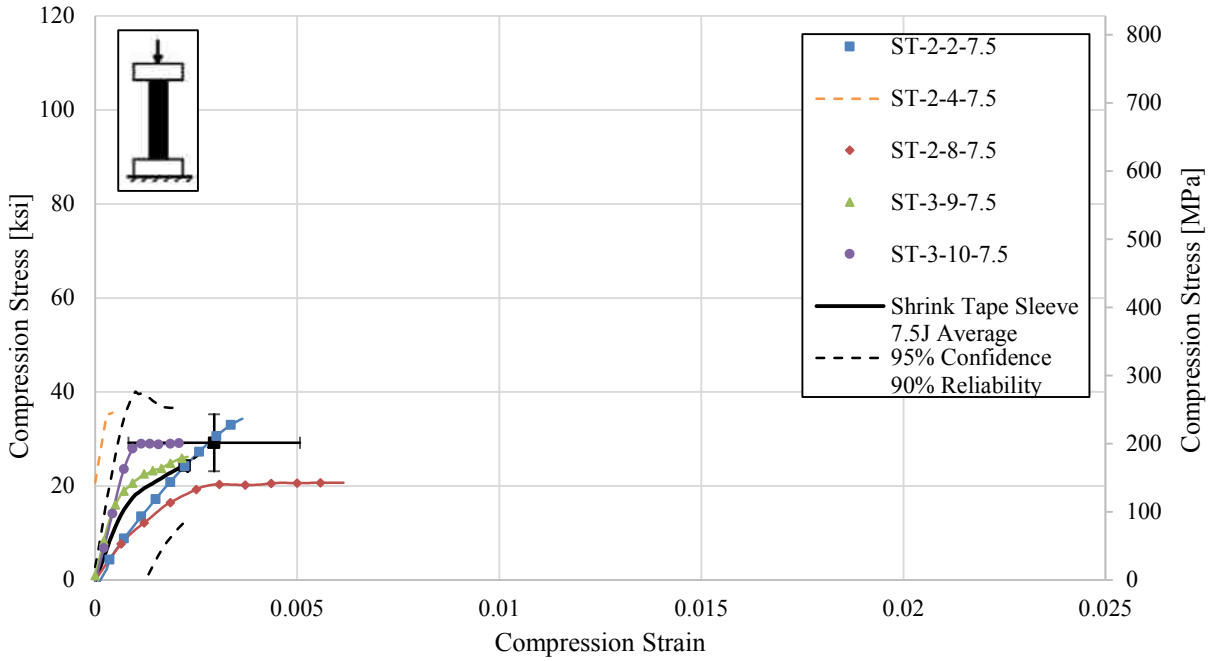

Figure 5.32 Stress-Strain Curves for Shrink Tape, 7.5 J (5.6 ft-lbs) Impacted Specimens

Table 5.33 Summary of Compression Properties of Shrink Tape, 10 J (7.4 ft-lbs) Impacted Specimens

Specimen I.D.	Cross Sectional Area		Ultimate Compression Strength		Strain at Ultimate Strength	Initial Compression Stiffness	
	[mm^2	(in^2)]	[MPa]	(ksi)]	[10^3 με]	[GPa	(10^6 psi)]
ST-1-3-10.0	55.91	(0.087)	151.6	(22.0)	7.21	71.7	(10.4)
*ST-1-4-10.0**	*55.91*	*(0.087)*	*164.8*	*(23.9)*	*3.07*	*375.9+*	*(54.5)+*
ST-2-7-10.0	57.53	(0.087)	168.2	(24.4)	2.93	61.6	(8.9)
ST-3-1-10.0	57.25	(0.087)	176.3	(25.6)	5.00	51.7	(7.5)
ST-3-4-10.0	55.54	(0.087)	169.7	(24.6)	3.07	151.8	(22.0)
Average	56.43	(0.087)	166.1	(24.1)	4.26	142.5	(20.7)
Std. Dev.	0.89	(0.00)	9.1	(1.3)	1.86	136.4	(19.8)
Average	56.56	(0.087)	166.5	(24.1)	4.55	84.2	(12.2)
Std. Dev.	0.98	(0.00)	10.5	(1.5)	2.01	45.8	(6.6)
Chauvenet Limit	57.91	(0.09)	167.0	(24.2)	7.33	168.1	(24.4)
	54.96	(0.09)	113.1	(16.4)	1.18	-16.9	(-2.5)

*Specimen eliminated using Chauvenet's criterion; italicized values not included in final average or standard deviation.
+ Properties used to eliminate specimen.

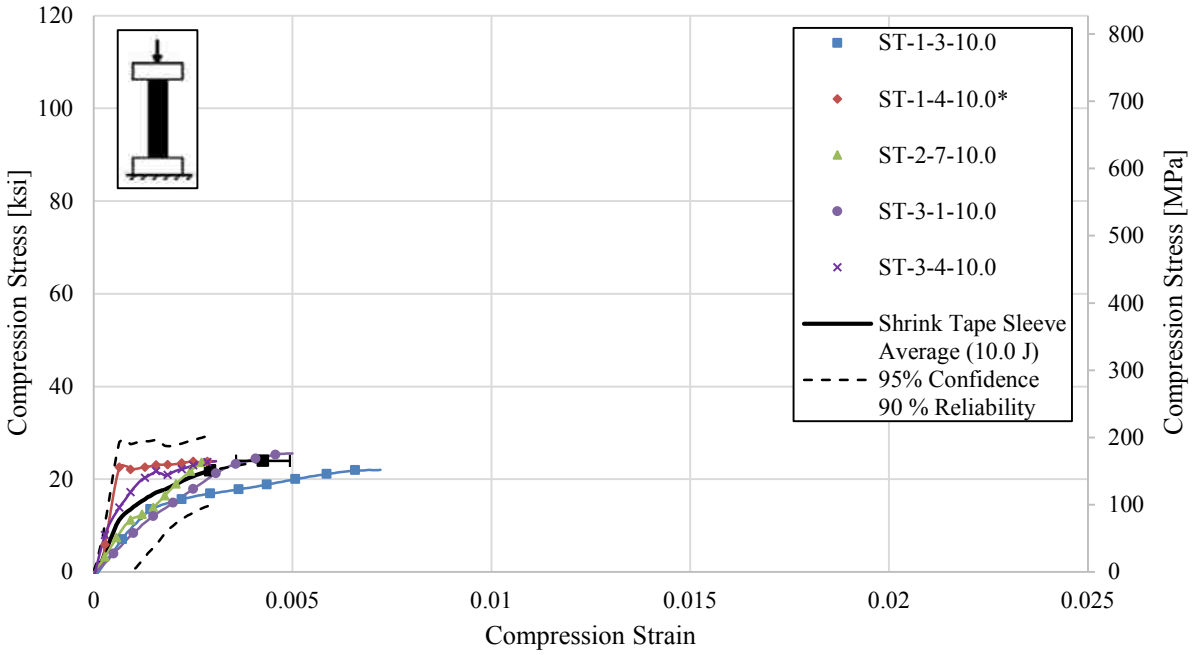

Figure 5.33 Stress-Strain Curves for Shrink Tape, 10 J (7.4 ft-lbs) Impacted Specimens

Table 5.34 Summary of Compression Properties of Shrink Tape, 15 J (11 ft-lbs) Impacted Specimens

Specimen I.D.	Cross Sectional Area		Ultimate Compression Strength		Strain at Ultimate Strength	Initial Compression Stiffness	
	[mm^2	(in^2)]	[MPa]	(ksi)]	[10^3 με]	[GPa	(10^6 psi)]
ST-2-5-15.0	57.53	(0.087)	115.5	(16.7)	6.21	48.6	(7.0)
*ST-2-9-15.0**	*57.53*	*(0.087)*	*149.5*	*(21.7)*	*3.07*	*168.8+*	*(24.5)+*
ST-2-10-15.0	57.53	(0.087)	155.0	(22.5)	7.07	41.6	(6.0)
ST-4-2-15.0	55.54	(0.085)	148.8	(21.6)	5.07	86.7	(12.6)
ST-5-1-15.0	55.54	(0.087)	131.4	(19.1)	6.79	32.3	(4.7)
Average	56.74	(0.087)	140.0	(20.3)	5.64	75.6	(11.0)
Std. Dev.	1.09	(0.00)	16.3	(2.4)	1.63	56.1	(8.1)
Average	56.54	(0.087)	137.7	(20.0)	6.29	52.3	(7.6)
Std. Dev.	1.15	(0.00)	17.8	(2.6)	0.88	23.9	(3.5)
Chauvenet Limit	58.54	(0.09)	167.0	(24.2)	8.33	168.1	(24.4)
	-54.94	(0.09)	113.1	(16.4)	2.96	-16.9	(-2.5)

*Specimen eliminated using Chauvenet's criterion; italicized values not included in final average or standard deviation.
+ Properties used to eliminate specimen.

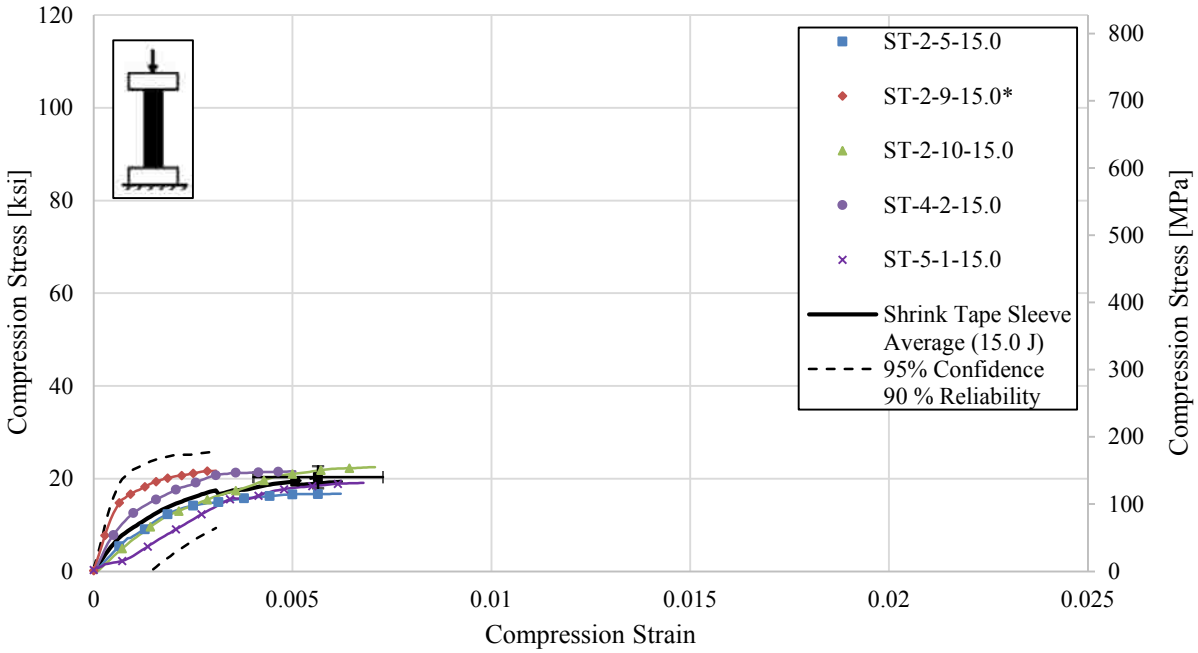

Figure 5.34 Stress-Strain Curves for Shrink Tape, 15 J (11 ft-lbs) Impacted Specimens

The test results for shrink tape specimens impacted with 20 J (15 ft-lbs) are summarized in Table 5.35 and the stress-strain curves are shown in Figure 5.35.

Table 5.35 Summary of Compression Properties of Shrink Tape, 20 J (15 ft-lbs) Impacted Specimens

Specimen I.D.	Cross Sectional Area		Ultimate Compression Strength		Strain at Ultimate Strength	Initial Compression Stiffness	
	[mm^2	(in^2)]	[MPa]	(ksi)]	[10^3 με]	[GPa	(10^6 psi)]
ST-2-5-20.0	57.53	(0.087)	118.4	(17.2)	9.07	44.7	(6.5)
ST-2-9-20.0	57.53	(0.087)	129.2	(18.7)	4.50	117.4	(17.0)
ST-2-10-20.0	57.53	(0.087)	123.9	(18.0)	6.71	189.3	(27.5)
ST-4-2-20.0	55.54	(0.085)	82.2	(11.9)	6.93	51.0	(7.4)
ST-5-1-20.0	55.54	(0.087)	80.6	(11.7)	18.86	72.7	(10.5)
Average	56.74	(0.087)	106.9	(15.5)	9.21	95.0	(13.8)
Std. Dev.	1.09	(0.00)	23.6	(3.4)	5.63	59.9	(8.7)
Chauvenet	58.54	(0.09)	145.8	(21.1)	18.50	193.9	(28.1)
Limit	54.94	(0.09)	68.0	(9.9)	-0.07	-3.8	(-0.6)

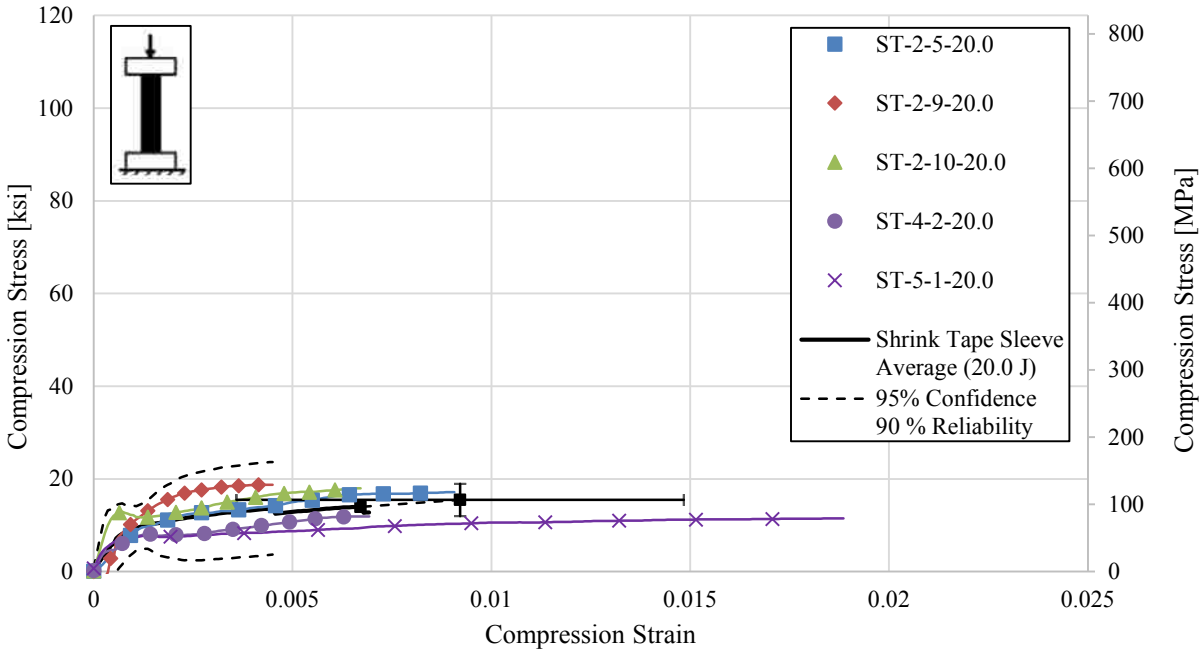

Figure 5.35 Stress-Strain Curves for Shrink Tape, 20 J (15 ft-lbs) Impacted Specimens

6 COMPARISON OF COMPRESSION STRESS-STRAIN BEHAVIOR

In this chapter, the influences of the impact energy and sleeve configurations on the stress-strain behavior are presented. All 35 curves, representing the averages of each configuration, are compared to unveil the overall trends of how the stress-strain behavior is affected by sleeve configuration (type, material, and coverage), and impact energy. Figure 6.1 shows the average stress-strain curves for the 35 configurations (five sleeve configurations at each of the seven impact energy levels).

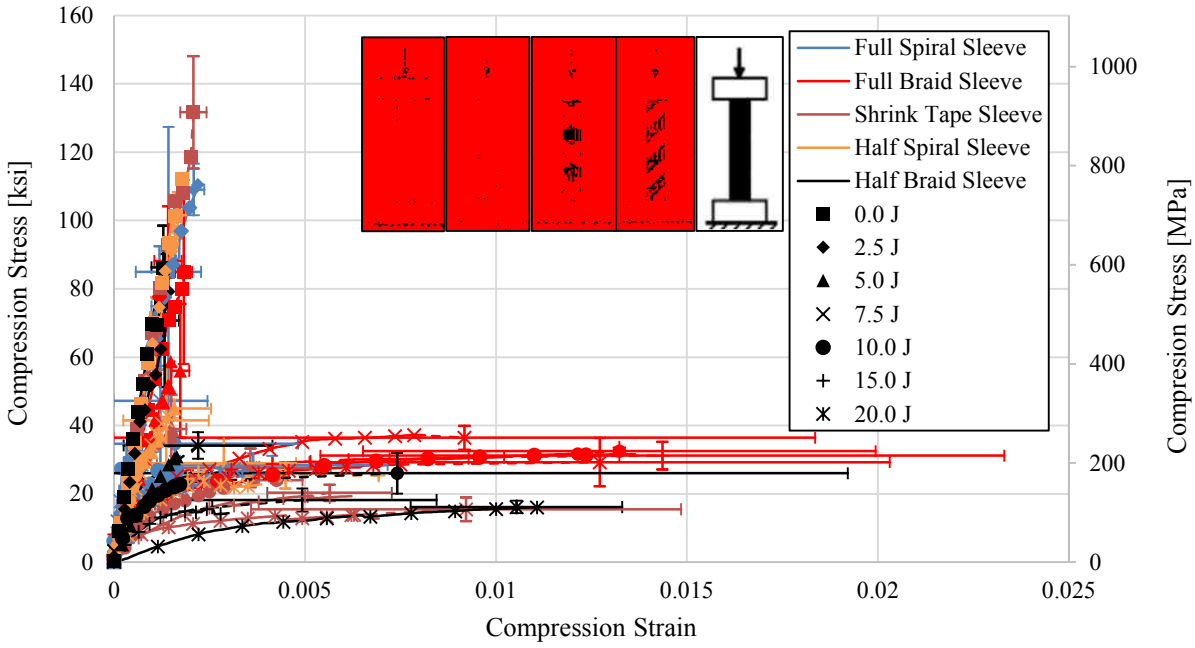

Figure 6.1 Average Stress-Strain Curves for All Test Configurations

All configurations exhibited a significant degradation in stiffness and strength due to impact energies of at least 5.0 J (3.7 ft-lbs).

6.1 Influence of Impact Energy on Stress-Strain Curves for Each Sleeve Configuration

Stress-strain curves for full braid, half braid, full spiral, half spiral, and shrink tape configurations are shown in Figure 6.2, Figure 6.3, Figure 6.4, Figure 6.5, and Figure 6.6, respectively. The test results for full braid, half braid, full spiral, half spiral, and shrink tape specimens are summarized in Tables 6.1-6.6, respectively. The compression modulus and ultimate compression strength decrease with increasing impact energy for each configuration. For each of the five sleeve configurations, there was an approximate 70% decrease in strength when impacted with 5.0 J (3.7 ft-lbs) of energy.

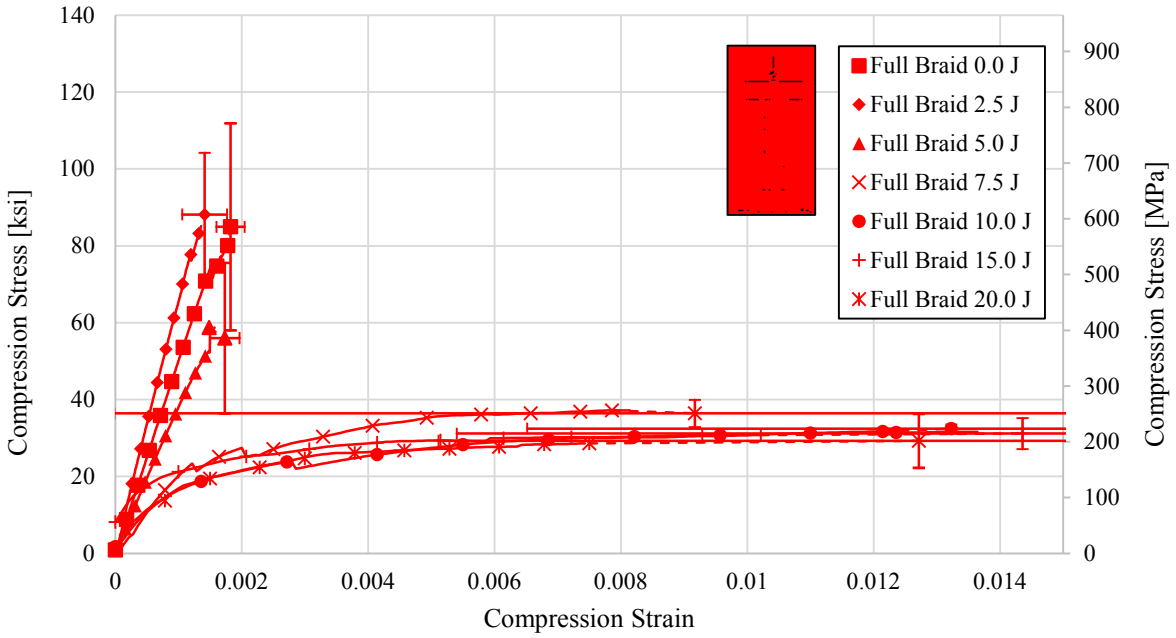

Figure 6.2 Average Stress-Strain Curves of Full Braid Sleeves

Table 6.1 Summary of Average Compression Properties for Full Braid Sleeves

Impact Energy	Average Compression Young's Modulus			Average Strain at Ultimate Strength		Average ultimate Compression Strength		
	[GPa	(10^6 psi)]	Diff.	[10^3 με]	Diff.	[MPa	(ksi)]	Diff
Undamaged	397.2	57.6	-	1.77	-	674.2	97.8	-
2.5 J (1.9 ft-lbs)	458.8	66.5	15%	1.41	-20%	607.7	88.1	-10%
5.0 J (3.7 ft-lbs)	265.6	38.5	-33%	1.77	0%	385.8	56.0	-43%
7.5 J (5.6 ft-lbs)	152.5	22.1	-62%	3.51	98%	240.7	34.9	-64%
10 J (7.4 ft-lbs)	188.4	27.3	-53%	8.01	353%	227.0	32.9	-66%
15 J (11 ft-lbs)	150.2	21.8	-62%	13.46	660%	207.3	30.1	-69%
20 J (15 ft-lbs)	123.5	17.9	-69%	12.71	618%	201.8	29.3	-70%

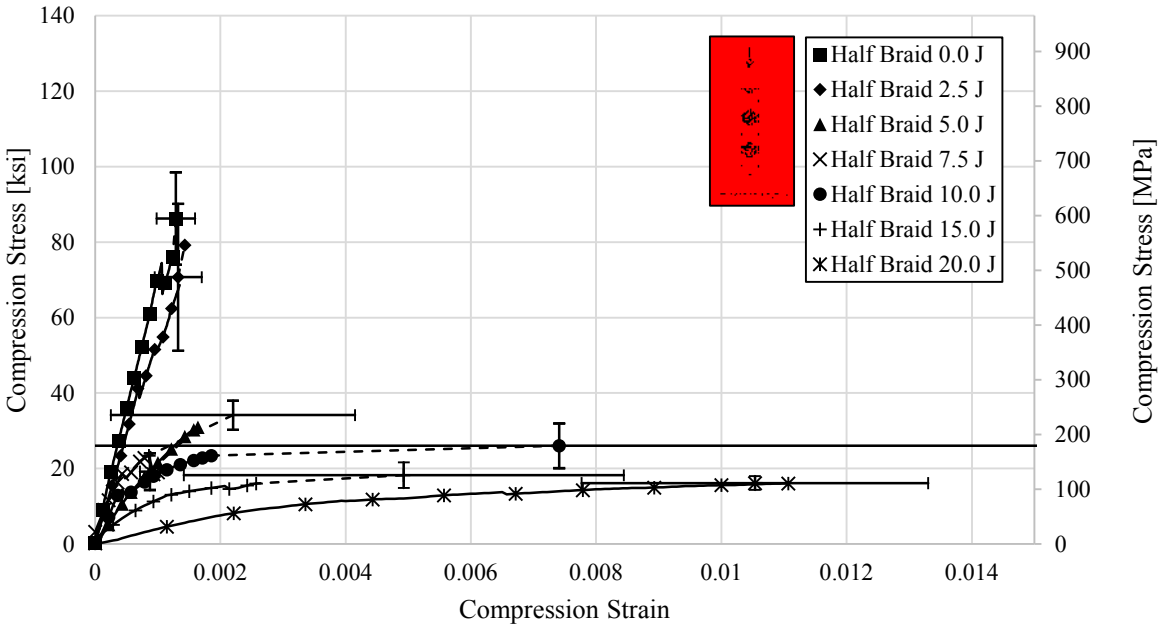

Figure 6.3 Average Stress-Strain Curves of Half Braid Sleeves

Table 6.2 Summary of Average Compression Properties for Half Braid Sleeves

Impact Energy	Average Compression Young's Modulus			Average Strain at Ultimate Strength		Average ultimate Compression Strength		
	[GPa	(10^6 psi)]	Diff.	[10^3 με]	Diff.	[MPa	(ksi)]	Diff
Undamaged	503.1	73.0	-	1.29	-	594.9	86.3	-
2.5 J (1.9 ft-lbs)	400.0	58.0	-21%	1.33	3%	487.5	70.7	-18%
5.0 J (3.7 ft-lbs)	130.6	18.9	-74%	1.89	47%	203.8	29.6	-66%
7.5 J (5.6 ft-lbs)	280.7	40.7	-44%	2.20	71%	235.5	34.2	-60%
10 J (7.4 ft-lbs)	185.4	26.9	-63%	5.99	364%	186.7	27.1	-69%
15 J (11 ft-lbs)	79.1	11.5	-84%	4.93	282%	125.6	18.2	-79%
20 J (15 ft-lbs)	25.5	3.7	-95%	10.54	717%	111.3	16.1	-81%

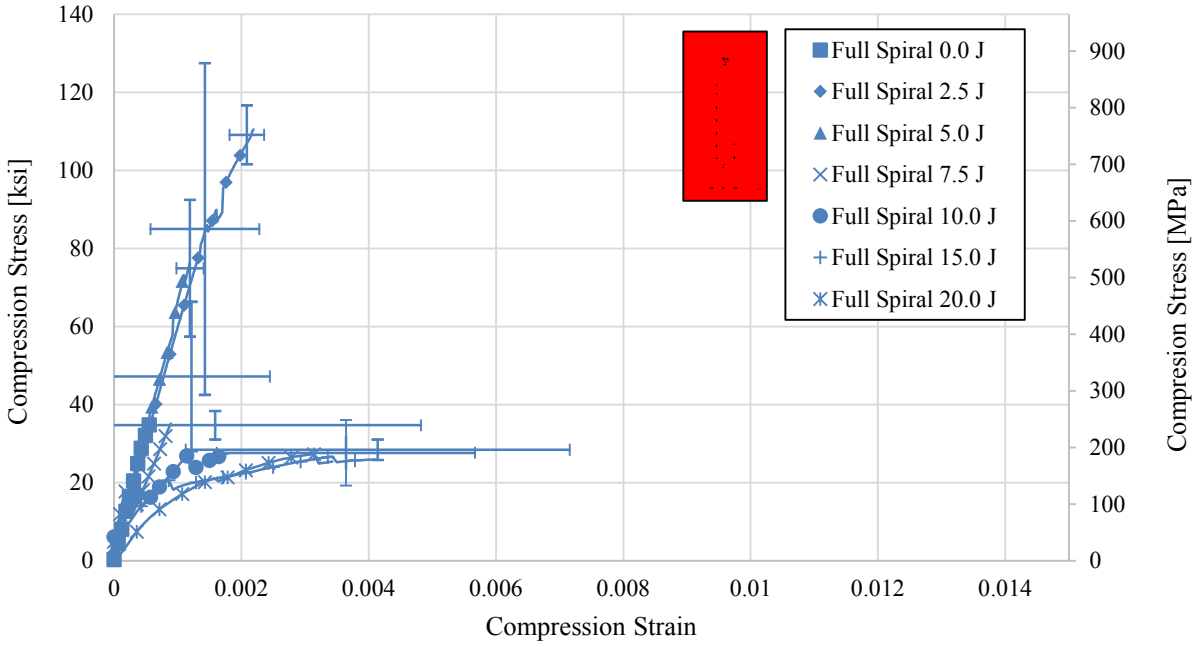

Figure 6.4 Average Stress-Strain Curves of Full Spiral Sleeves

Table 6.3 Summary of Average Compression Properties for Full Spiral Sleeves

Impact Energy	Average Compression Young's Modulus			Average Strain at Ultimate Strength		Average ultimate Compression Strength		
	[GPa	(10^6 psi)]	Diff.	[10^3 με]	Diff.	[MPa	(ksi)]	Diff
Undamaged	454.5	65.9	-	14.25	-	585.5	84.9	-
2.5 J (1.9 ft-lbs)	427.1	61.9	-6%	20.62	45%	733.2	106.3	25%
5.0 J (3.7 ft-lbs)	380.3	55.2	-16%	1.05	-93%	473.0	67.0	-21%
7.5 J (5.6 ft-lbs)	612.4	88.8	35%	1.13	-92%	267.6	38.8	-54%
10 J (7.4 ft-lbs)	1277.5	185.3	181%	3.36	-76%	237.0	34.4	-60%
15 J (11 ft-lbs)	139.7	20.3	-69%	2.20	-85%	203.7	29.5	-65%
20 J (15 ft-lbs)	131.5	19.1	-71%	3.04	-79%	187.5	27.2	-68%

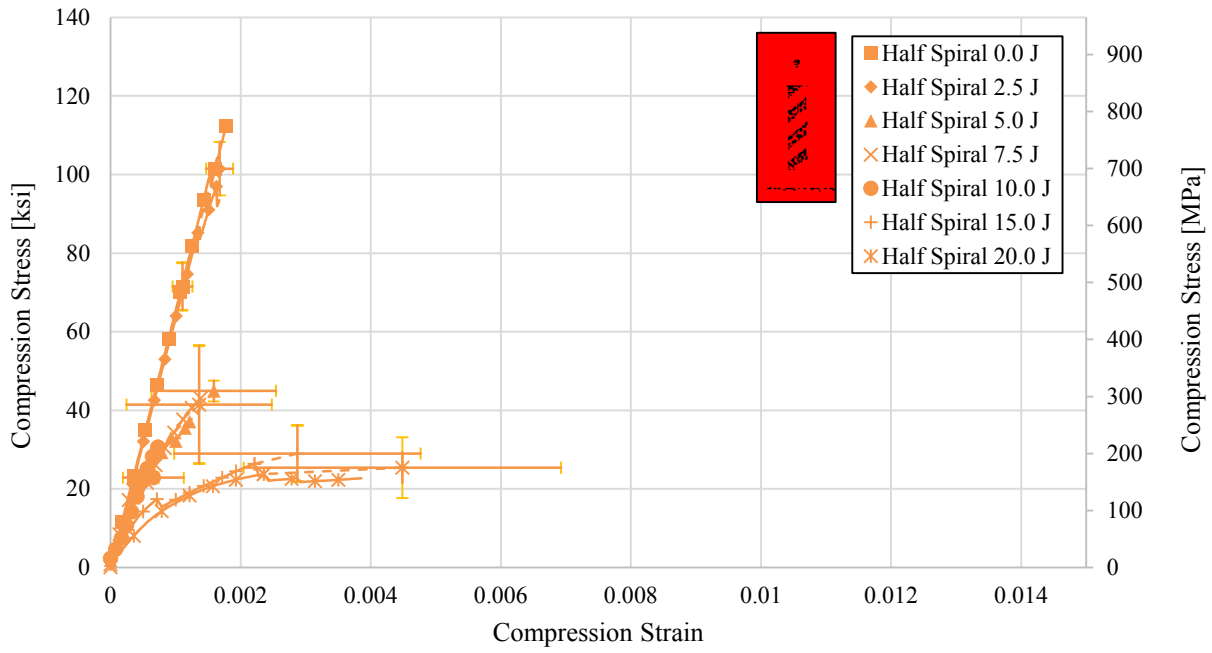

Figure 6.5 Average Stress-Strain Curves of Half Spiral Sleeves

Table 6.4 Summary of Average Compression Properties for Half Spiral Sleeves

Impact Energy	Average Compression Young's Modulus			Average Strain at Ultimate Strength		Average ultimate Compression Strength		
	[GPa	(10^6 psi)]	Diff.	[10^3 με]	Diff.	[MPa	(ksi)]	Diff
Undamaged	451.8	65.5	-	1.85	-	821.7	119.2	-
2.5 J (1.9 ft-lbs)	428.0	62.1	-5%	1.69	-9%	679.8	98.6	-17%
5.0 J (3.7 ft-lbs)	304.8	44.2	-33%	1.59	-14%	309.8	44.9	-62%
7.5 J (5.6 ft-lbs)	423.5	61.4	-6%	1.36	-26%	240.0	34.8	-71%
10 J (7.4 ft-lbs)	283.3	41.1	-37%	1.48	-20%	262.6	38.1	-68%
15 J (11 ft-lbs)	451.8	65.5	0%	2.87	55%	199.9	29.0	-76%
20 J (15 ft-lbs)	124.4	18.0	-73%	4.49	143%	175.1	25.4	-79%

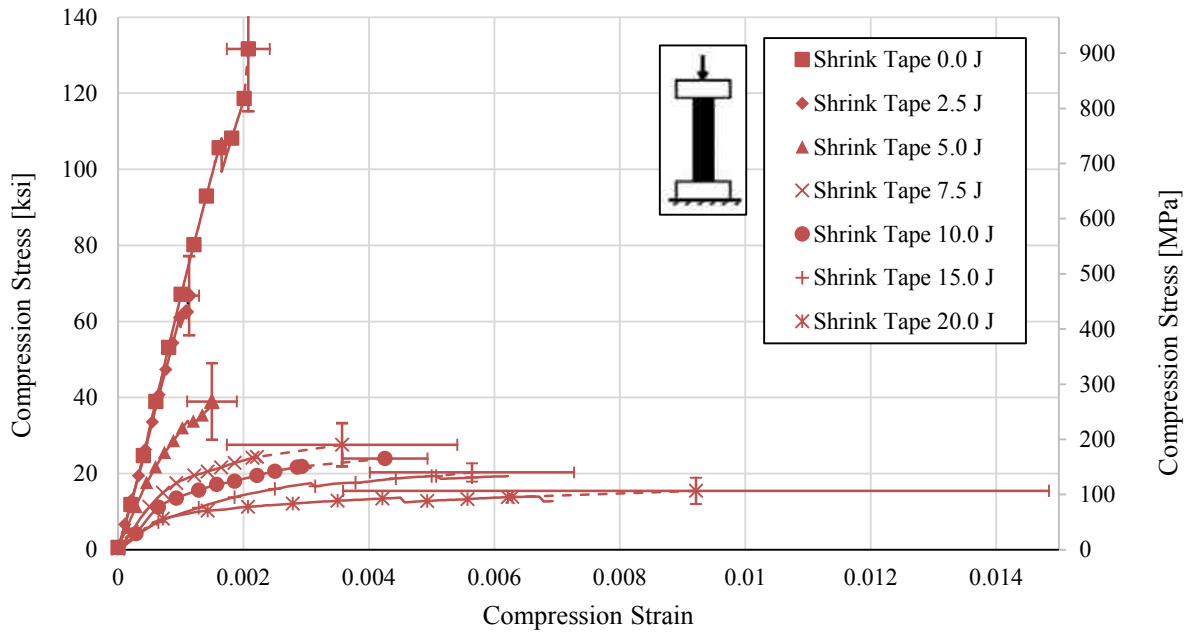

Figure 6.6 Average Stress-Strain Curves for Shrink Tape Sleeves

Table 6.5 Summary of Average Compression Properties for Shrink Tape Sleeves

Impact Energy	Average Compression Young's Modulus			Average Strain at Ultimate Strength		Average ultimate Compression Strength		
	[GPa	(10^6 psi)]	Diff.	[10^3 με]	Diff.	[MPa	(ksi)]	Diff
Undamaged	476.2	69.1	-	2.02	-	911.1	132.1	-
2.5 J (1.9 ft-lbs)	428.6	62.2	-10%	1.06	-48%	442.8	64.2	-51%
5.0 J (3.7 ft-lbs)	252.4	36.6	-47%	1.50	-26%	268.8	39.0	-70%
7.5 J (5.6 ft-lbs)	191.1	27.7	-60%	2.94	46%	200.7	29.1	-78%
10 J (7.4 ft-lbs)	84.2	12.2	-82%	4.55	125%	166.5	24.1	-82%
15 J (11 ft-lbs)	52.3	7.6	-89%	6.29	211%	137.7	20.0	-85%
20 J (15 ft-lbs)	95.0	13.8	-80%	9.21	356%	106.9	15.5	-88%

6.2 Influence of Sleeve Configuration on Stress-Strain Curves for Each Impact Energy

The influences of sleeve type and coverage for different impact energy levels (0.0 J (0.0 ft-lbs), 2.5 J (1.9 ft-lbs), 5.0 J (3.7 ft-lbs), 7.5 J (5.6 ft-lbs), 10 J (7.4 ft-lbs), 15 J (11 ft-lbs), and 20 J (15-ft-lbs)) are illustrated in Figures 6.7 through 6.13, respectively. Sleeve type and coverage make no significant difference in compression strength for non-impacted specimens as exemplified by Figure 6.7.

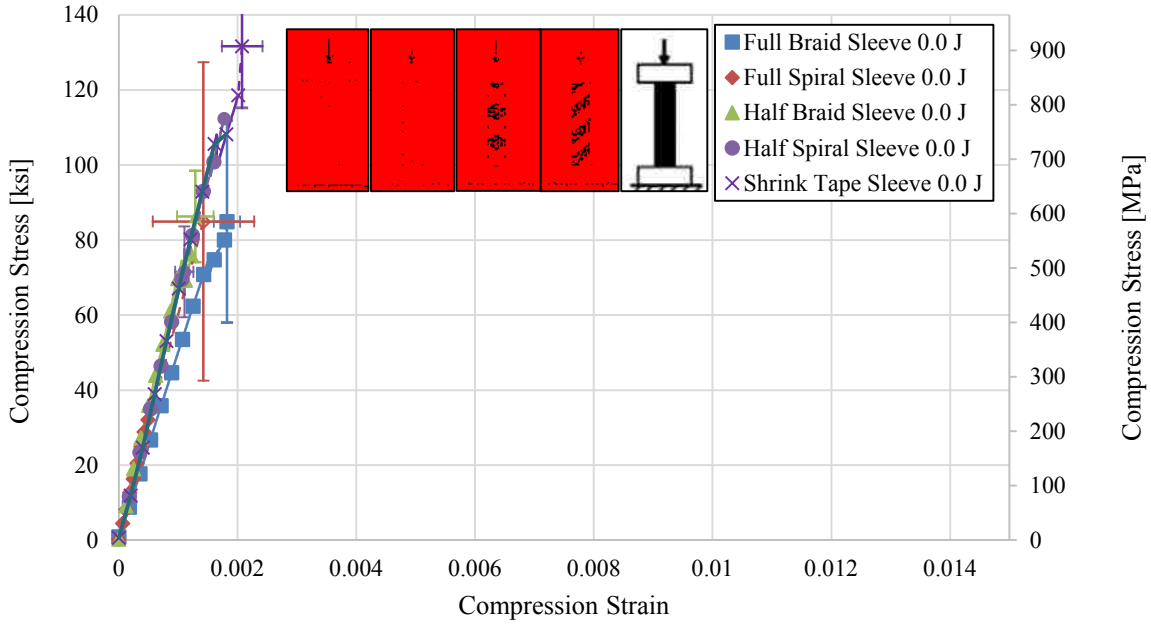

Figure 6.7 Average Stress-Strain Curves of Non-Impacted Specimens

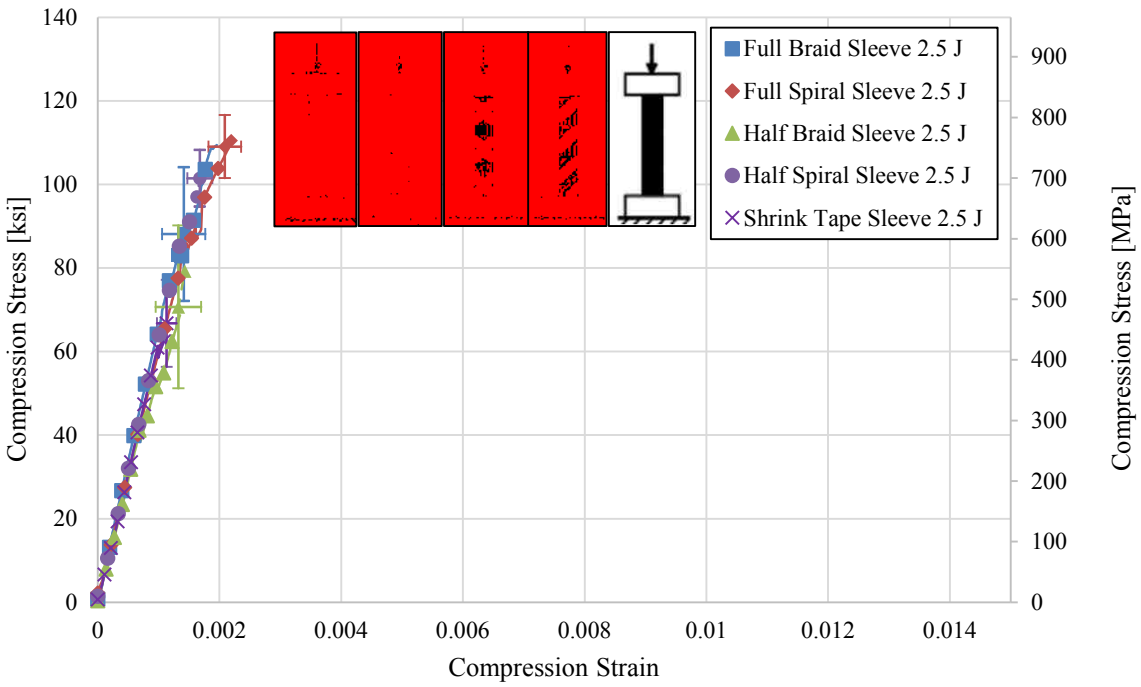

Figure 6.8 Average Stress-Strain Curves of 2.5 J (1.9 ft-lbs) Impacted Specimens

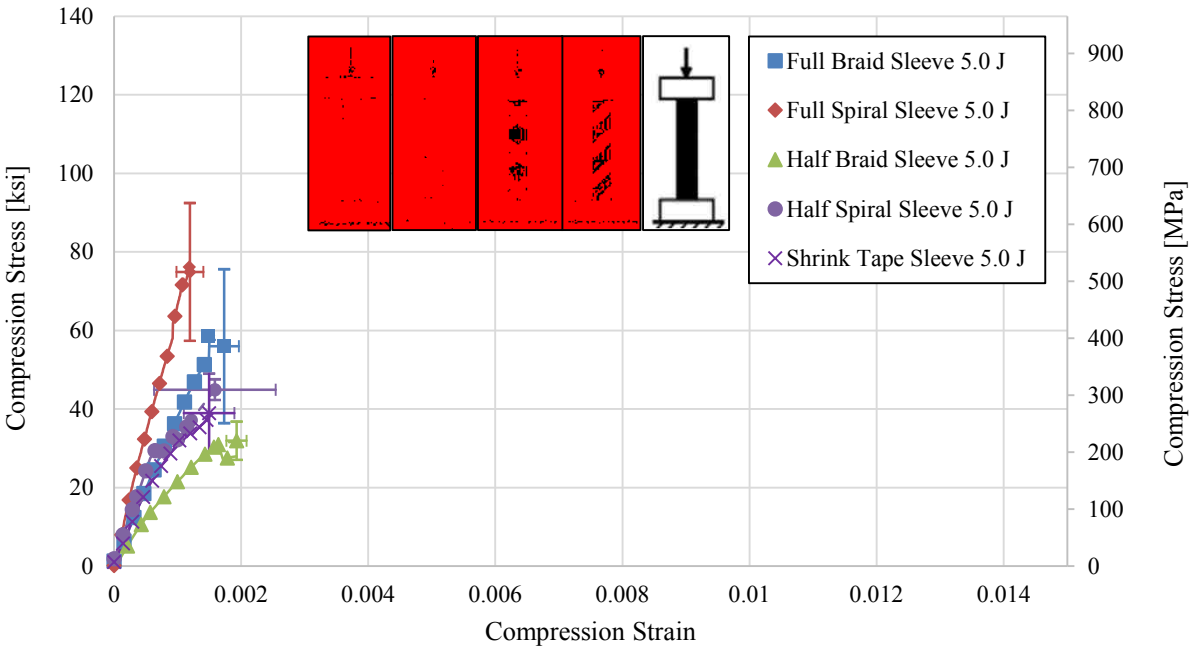

Figure 6.9 Average Stress-Strain Curves of 5.0 J (3.7 ft-lbs) Impacted Specimens

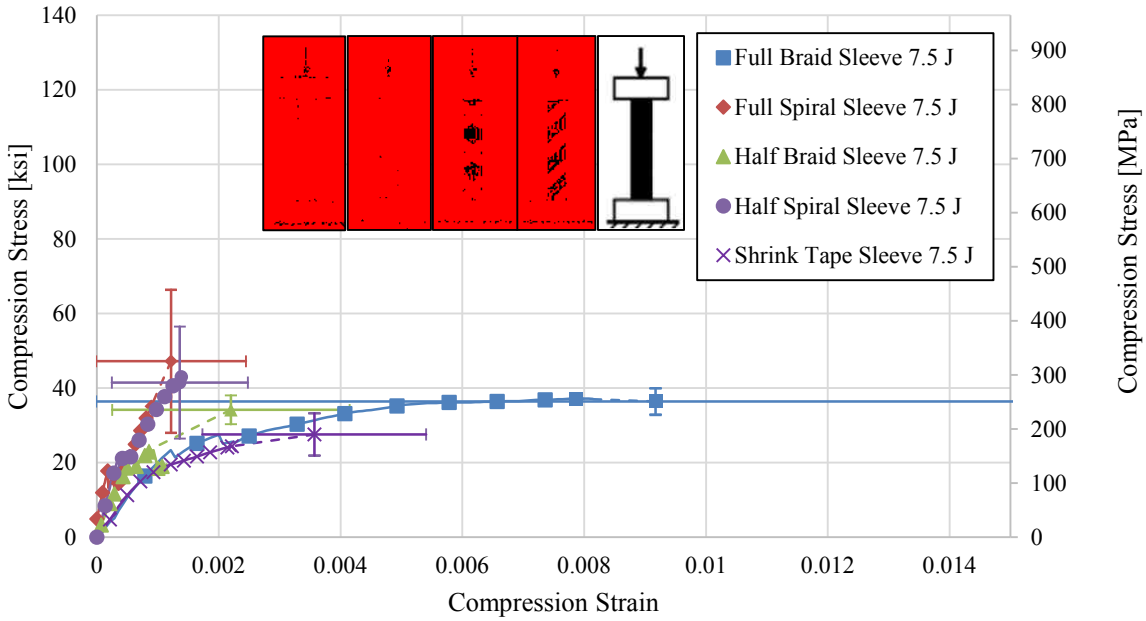

Figure 6.10 Average Stress-Strain Curves of 7.5 J (5.6 ft-lbs) Impacted Specimens

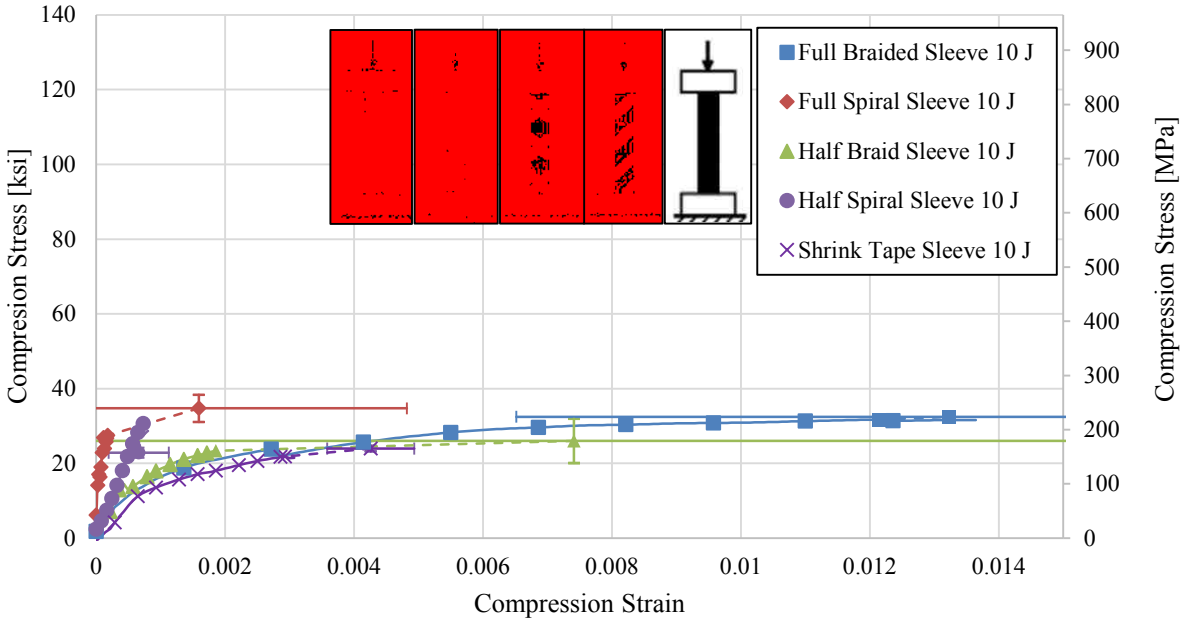

Figure 6.11 Average Stress-Strain Curves of 10 J (7.4 ft-lbs) Impacted Specimens

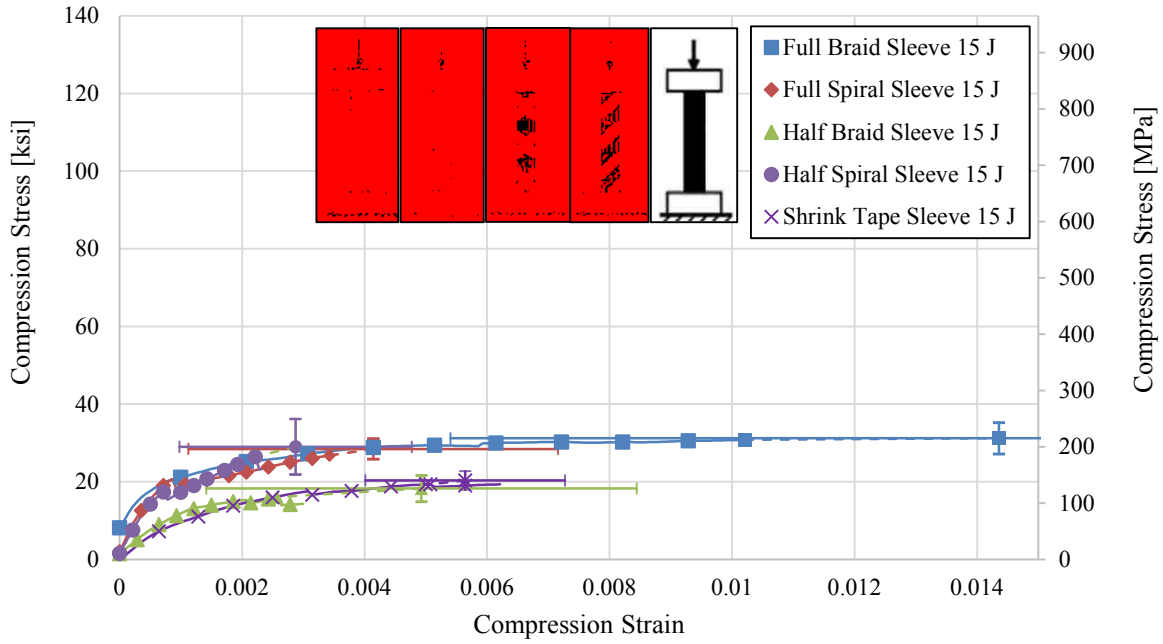

Figure 6.12 Average Stress-Strain Curves of 15 J (11 ft-lbs) Impacted Specimens

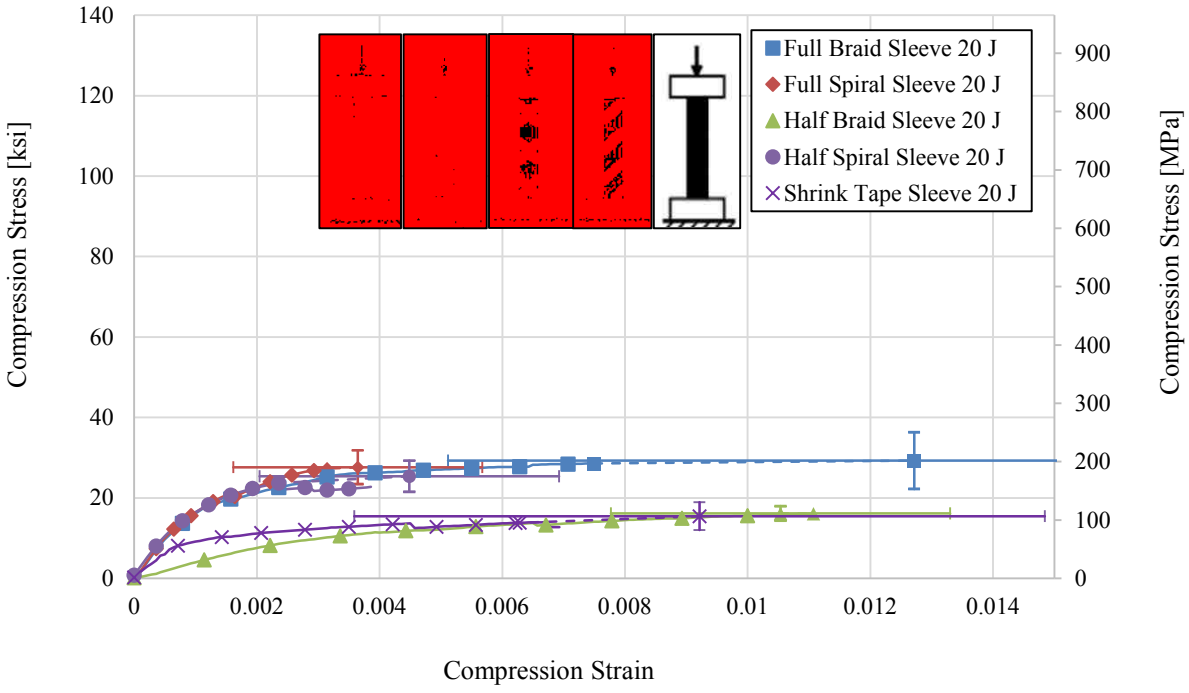

Figure 6.13 Average Stress-Strain Curves of 20 J (15 ft-lbs) Impacted Specimens

Figure 6.14 and Figure 6.15 show the influence of sleeve type and impact energy for different coverage (full and half), respectively.

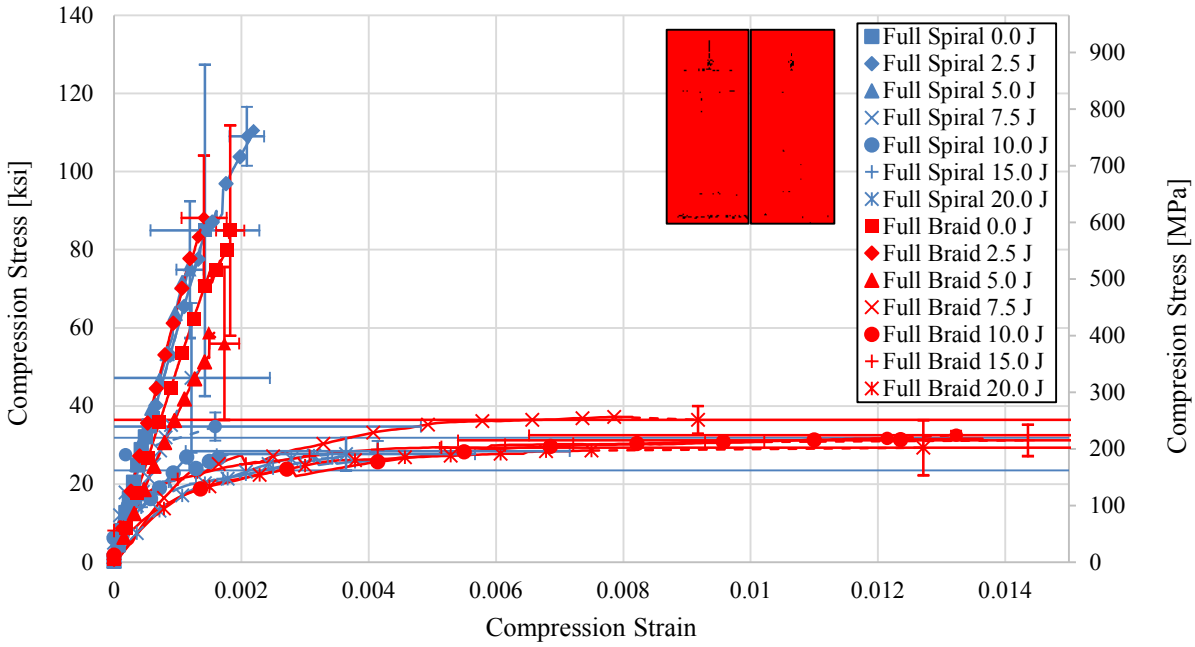

Figure 6.14 Average Stress-Strain Curves for Full Sleeve Specimens

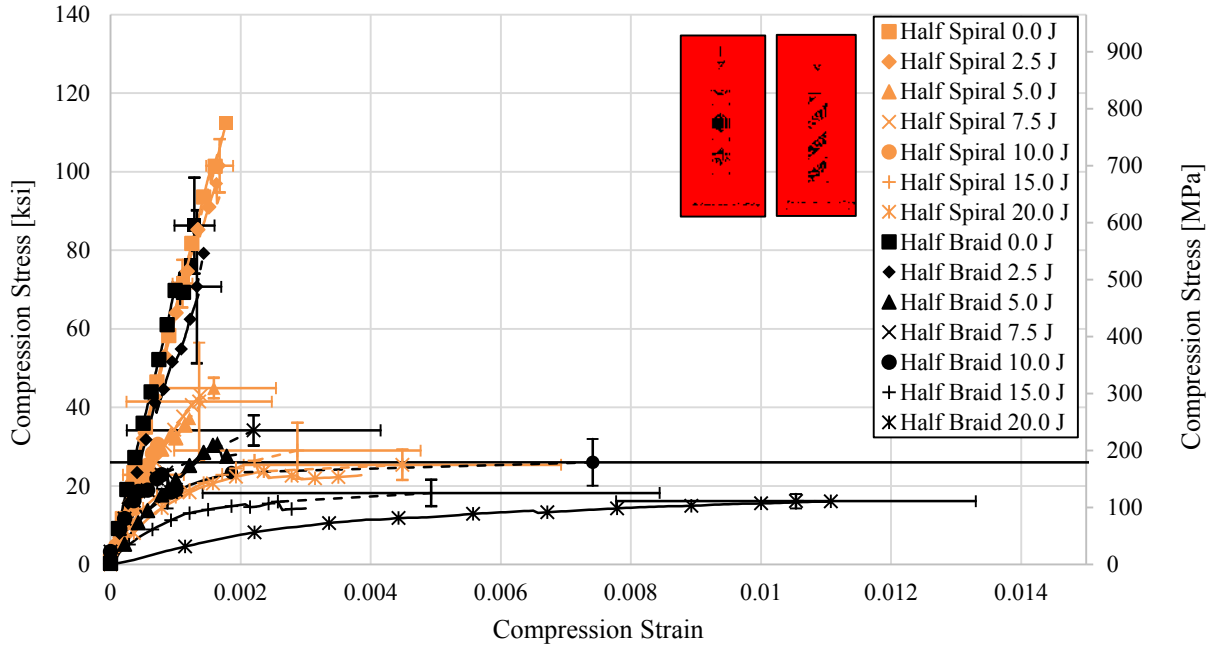

Figure 6.15 Average Stress-Strain Curves for Half Sleeve Specimens

6.3 Influence of Coverage and Impact Energy for Different Sleeve Types

Figure 6.16 and Figure 6.17 show the influence of coverage and impact levels for different sleeve types (braid and spiral).

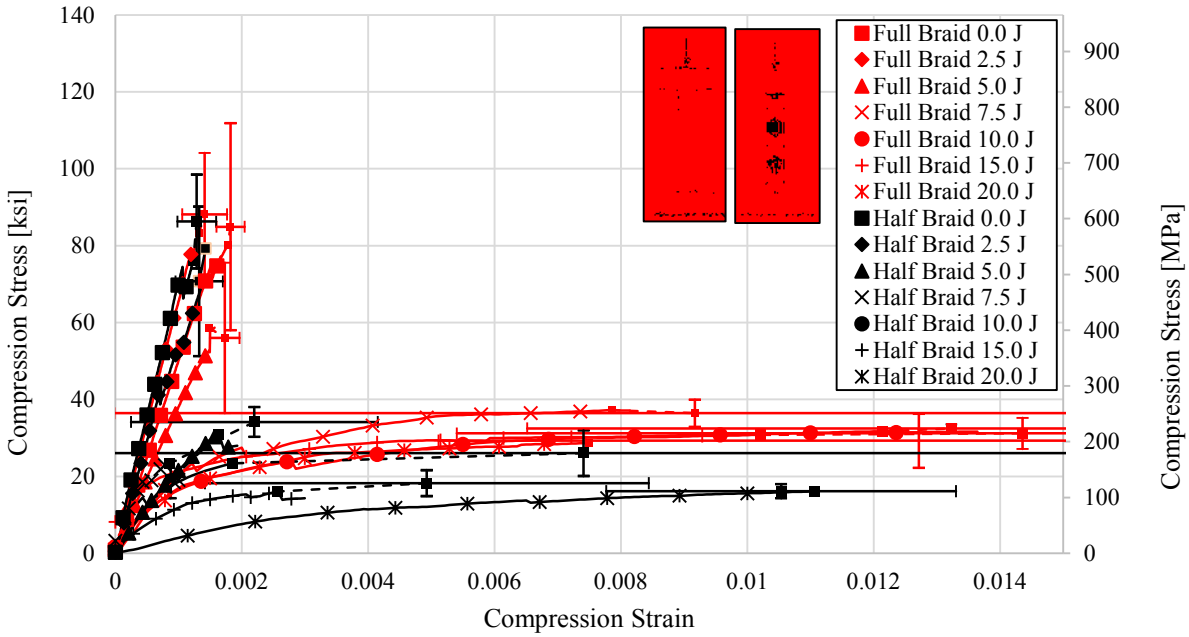

Figure 6.16 Average Stress-Strain Curves for Braided Sleeves Specimens

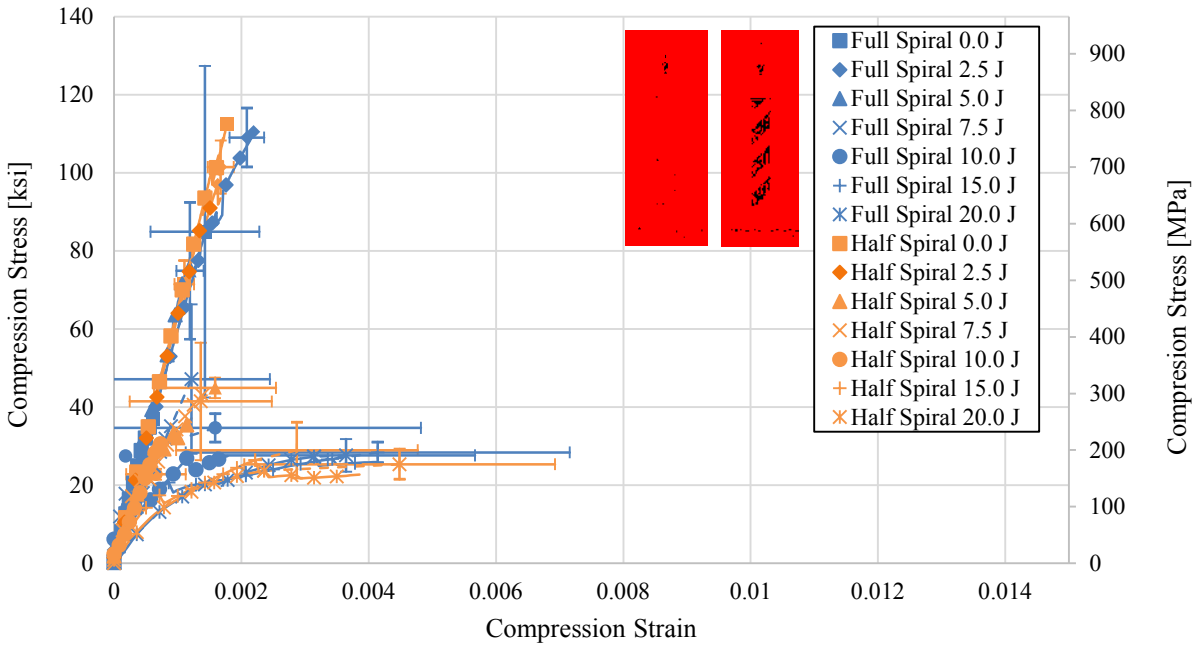

Figure 6.17 Average Stress-Strain Curves for Spiral Specimens

7 DISCUSSION OF COMPRESSION STRENGTH AFTER IMPACT

This chapter discusses the significance of the damage tolerance results for the various sleeve configurations. To illustrate the effect of sleeve type (braid vs. spiral) and coverage (full vs. half), the differences in compression modulus and strength between configurations (in percentages) are normalized to undamaged specimen. For example, -5% means that the performance of the configuration represented exhibited 5% lower value. In the figures, the error bars represent ±1 standard deviation. The relative difference in modulus and ultimate strength of are examined. These comparisons help in defining the effect that impact energy has on residual strength.

7.1 Effect of Impact Energy on Residual Strength

7.1.1 Influence of Sleeve Type

To examine the influence of sleeve type, Figure 7.1 was created by combining results of all braided sleeves (full and half), and all spiral sleeves (full and half), respectively. This approach allows comparison of just the sleeve type. The stress-strain curves indicate a very significant reduction in strength for damaged configurations. The plot also shows a decreasing compression modulus with increasing impact energy, indicated by the shift of slopes to the right. The slopes of the curves at each impact energy level is lower for braided sleeves relative to spiral sleeves above

5.0 J (3.7 ft-lbs) impact, suggesting that the sleeve type does have a slight impact on stiffness at each impact energy level. A summary of the relative difference between braided and spiral sleeves is shown in Table 7.1. With no impact, there is roughly a 20% difference in both modulus and ultimate strength between the braided and spiral sleeve types. Furthermore, for 5.0 J (ft-lbs) and greater, compression modulus is greatly affected by sleeve type, as shown by a difference of upwards of 250% between braided and spiral sleeve types. These results are not consistent with previous research. This inconsistency may be due to the unsymmetric braiding pattern which pulled the carbon/epoxy core against the inside wall of the tube, causing the exterior fibers to fray. The braid pattern may also have led the tows to not be straight which could explain the increase in difference between the stiffness as impact energy increases. The spiral sleeves had a much higher compression stiffness than the braided sleeves. The difference between the spiral and braided compression stiffness generally increased with increase impact energy. Spiral sleeves have a higher compression strength for impact energies less than 15 J (11 ft-lbs). At 15 J (11 ft-lbs) and 20 J (15 ft-lbs), the braided sleeves exhibited a larger compression strength than the spiral. These differences are significant given that it is uncommon for composites to have greater than a ±10% variation in mechanical properties [1] [9]. These differences are most likely due to difference in manufacturing processes for braided and spiral sleeves. In summary, a significant difference in strength was observed for the spiral and braided sleeve types.

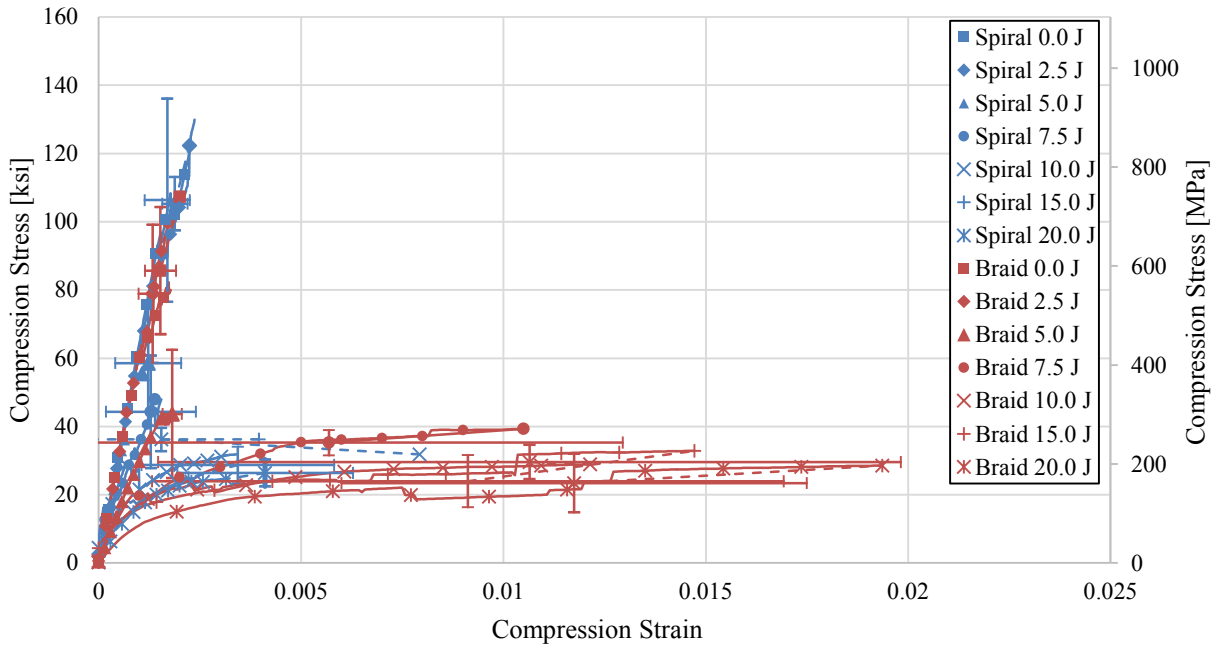

Figure 7.1 Stress-Strain Curves for Combined Spiral and Braided Sleeves

Table 7.1 Average Compression Young's Modulus, Strain at Ultimate Strength, and Compression Strength for Braided and Spiral Sleeves

Impact Energy	Sleeve Type	Average Compression Young's Modulus			Average Strain at Ultimate Strength		Average Ultimate Compression Strength		
		[GPa	(10^6 psi)]	Diff.	[10^3 με]	Diff.	[MPa	(ksi)]	Diff.
Undamaged	All Braid	368.0	(53.4)		2.01		740.2	(107.4)	
	All Spiral	438.8	(63.6)	19%	2.37	18%	895.6	(129.9)	21%
2.5 J (1.9 ft-lbs)	All Braid	408.0	(59.2)		1.71		689.0	(99.9)	
	All Spiral	420.6	(61.0)	3%	2.24	31%	843.2	(122.3)	22%
5.0 J (3.7 ft-lbs)	All Braid	209.5	(30.4)		1.57		292.9	(42.5)	
	All Spiral	389.7	(56.5)	86%	1.07	-32%	382.1	(55.4)	30%
7.5 J (5.6 ft-lbs)	All Braid	82.2	(11.9)		10.50		271.4	(39.4)	
	All Spiral	232.2	(33.7)	183%	1.39	-87%	330.6	(47.9)	22%
10 J (7.4 ft-lbs)	All Braid	108.5	(15.7)		12.14		199.4	(28.9)	
	All Spiral	262.0	(38.0)	142%	7.93	-35%	219.4	(31.8)	10%
15 J (11 ft-lbs)	All Braid	50.9	(7.4)		14.71		226.7	(32.9)	
	All Spiral	178.9	(25.9)	251%	2.21	-85%	171.9	(24.9)	-24%
20 J (15 ft-lbs)	All Braid	42.0	(6.1)		19.36		196.8	(28.5)	
	All Spiral	119.8	(17.4)	185%	3.14	-84%	169.8	(24.6)	-14%

7.1.2 Influence of Sleeve Coverage

To illustrate the effect of sleeve coverage (full vs. half), independent of the sleeve type, Figure 7.2 was created by combining the results from full braid and spiral sleeve samples, and half braid and spiral sleeve samples, isolating the influence of the sleeve coverage. The stress-strain curves indicate a significant reduction in strength for damaged configurations. The plot also show a decrease in compression modulus with increasing impact energy, indicated by the shift of slopes to the right. A summary of the relative difference between full and half sleeve coverage is shown in Table 7.2. At no impact there is little difference in modulus, and ultimate strength between full and half sleeve coverage, as illustrated by the less than 16% difference. Impacted specimens with half coverage had significantly lower modulus with upwards of 76% difference for 10 J (7.4 ft-lbs) impact. While the ultimate strength of the half coverage was typically lower than that of full coverage, for 10 J (7.4 ft-lbs) impact, half coverage had higher ultimate strength as illustrated by a 13% difference. In summary, half coverage sleeves have a lower compression modulus and typically have a lower ultimate strength than specimens with full coverage sleeves, as concluded in previous related research.

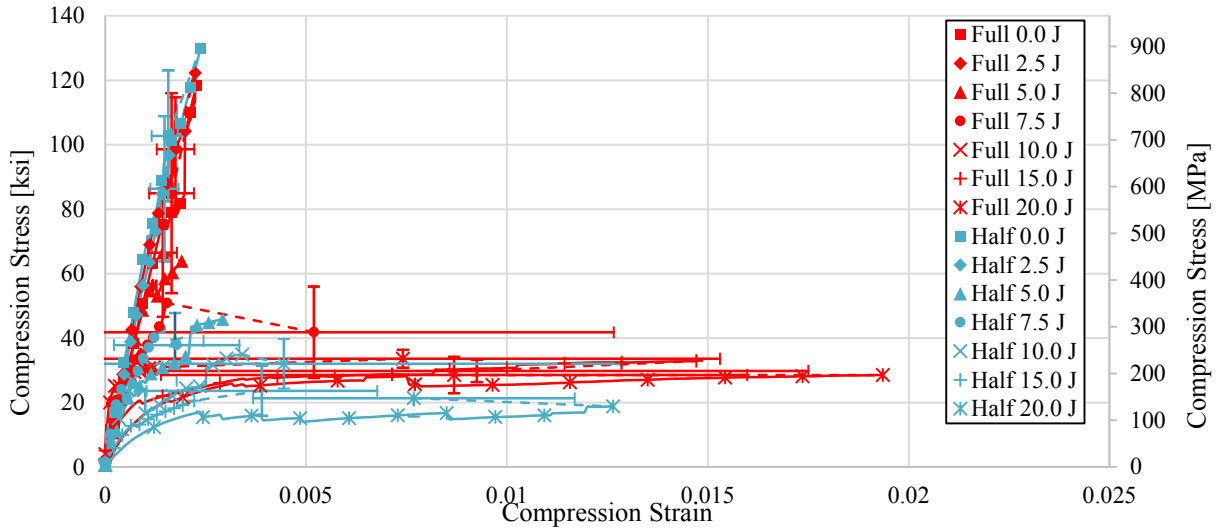

Figure 7.2 Stress-Strain Curves for Combined Half and Full Sleeves

Table 7.2 Average Compression Young's Modulus, Strain at Ultimate Strength, and Compression Strength for Spiral and Full Sleeves

Impact Energy	Sleeve Coverage	Average Compression Young's Modulus			Average Strain at Ultimate Strength		Average ultimate Compression Strength		
		[GPa	(10^6 psi)]	Diff.	[10^3 με]	Diff.	[MPa	(ksi)]	Diff
Undamaged	Full	362.9	(52.6)		2.26		816.6	(118.4)	
	Half	421.3	(61.1)	16%	2.37	5%	895.6	(129.9)	10%
2.5 J (1.9 ft-lbs)	Full	423.0	(61.4)		2.24		843.2	(122.3)	
	Half	399.5	(57.9)	-6%	1.63	-27%	668.8	(97.0)	-21%
5.0 J (3.7 ft-lbs)	Full	366.5	(53.2)		1.91		440.1	(63.8)	
	Half	169.3	(24.6)	-54%	2.93	54%	316.0	(45.8)	-28%
7.5 J (5.6 ft-lbs)	Full	297.0	(43.1)		1.54		350.5	(50.8)	
	Half	228.6	(33.2)	-23%	1.39	-10%	296.8	(43.1)	-15%
10 J (7.4 ft-lbs)	Full	1129	(163.8)		1.21		213.2	(30.9)	
	Half	270.4	(39.2)	-76%	3.41	181%	240.6	(34.9)	13%
15 J (11 ft-lbs)	Full	138.1	(20.0)		14.71		226.7	(32.9)	
	Half	124.8	(18.1)	-10%	2.21	-85%	141.8	(20.6)	-37%
20 J (15 ft-lbs)	Full	111.4	(16.2)		19.36		196.8	(28.5)	
	Half	70.4	(10.2)	-37%	12.64	-35%	129.7	(18.8)	-34%

7.1.3 Influence of Sleeve Material

To illustrate the effect of sleeve material (Nomex Thread vs. Shrink Tape), independent of the sleeve type, Figure 7.3 was created by combining the results from full braid and spiral sleeve samples comparing them with Shrink Tape samples. This combination of results approach allows comparison of just the sleeve material since the Shrink Tape covered the full length of each specimen. The stress-strain curves indicate a significant reduction in strength for damaged configurations. The plot also show a decrease in compression modulus with increasing impact energy, indicated by the shift of slopes to the right. A summary of the relative difference between Nomex Thread and Shrink Tape sleeve material is shown in Table 7.3. At no impact there is virtually no difference in ultimate strength between Nomex Thread and Shrink Tape sleeve, as

illustrated by a 0% difference. Impacted specimens with Shrink Tape sleeves; however, exhibited significantly lower ultimate strength with an average of 44% difference for each energy level. While Shrink Tape started with a higher compression modulus for no impact, as the impact energy increased, the compression modulus for Shrink Tape was significantly lower than the Nomex Thread with the maximum difference being 90% at 10 J (7.4 ft-lbs). Shrink Tape had the highest undamaged compressive stress of all sleeve types. This was due to the higher level of consolidation and which lead to a higher fiber volume fraction than Nomex Thread sleeves. In summary, while undamaged Shrink Tape had higher compression modulus and similar ultimate strength than Nomex Thread, as impact energy increased, the compression modulus and ultimate strength was significantly lower for Shrink Tape than for Nomex Thread.

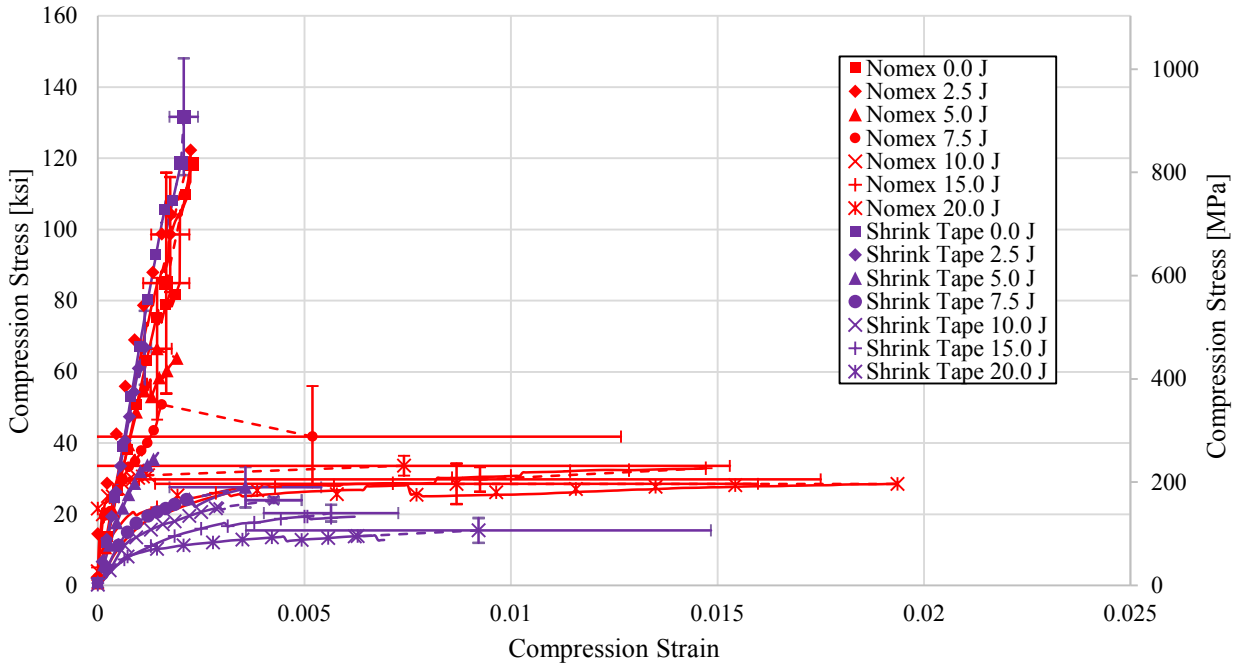

Figure 7.3 Stress-Strain Curves for Combined Half and Full Sleeves

Table 7.3 Average Compression Young's Modulus, Strain at Ultimate Strength, and Compression Strength for Shrink Tape and Nomex Thread Sleeves

Impact Energy	Sleeve Material	Average Compression Young's Modulus			Average Strain at Ultimate Strength		Average ultimate Compression Strength		
		[GPa	(10^6 psi)]	Diff.	[10^3 με]	Diff.	[MPa	(ksi)]	Diff.
Undamaged	Nomex Thread	362.9	-52.6		2.26		816.6	-118.4	
	Shrink Tape	471.3	-68.4	30%	2.01	-11%	911.1	-118.6	12%
2.5 J	Nomex Thread	423	-61.4		2.24		843.2	-122.3	
(1.9 ft-lbs)	Shrink Tape	428.3	-62.1	1%	1.09	-51%	442.8	-62.5	-47%
5.0 J	Nomex Thread	366.5	-53.2		1.91		440.1	-63.8	
(3.7 ft-lbs)	Shrink Tape	240.3	-34.8	-34%	1.46	-24%	268.8	-37.2	-39%
7.5 J	Nomex Thread	297	-43.1		1.54		350.5	-50.8	
(5.6 ft-lbs)	Shrink Tape	150.9	-21.9	-49%	2.21	44%	200.7	-24.4	-43%
10 J	Nomex Thread	1129.4	-163.8		1.21		213.2	-30.9	
(7.4 ft-lbs)	Shrink Tape	110.9	-16.1	-90%	2.93	141%	166.5	-21.9	-22%
15 J	Nomex Thread	138.1	-20		14.71		226.7	-32.9	
(11 ft-lbs)	Shrink Tape	55.4	-8	-60%	5.07	-66%	137.7	-19.3	-39%
20 J	Nomex Thread	111.4	-16.2		19.36		196.8	-28.5	
(15 ft-lbs)	Shrink Tape	74.6	-10.8	-33%	6.71	-65%	106.9	-14	-46%

7.1.4 Influence of Impact Energy

A plot of the compression strength as a function of impact energy was prepared to illustrate the effect of impact energy on compression strength, as a function of sleeve type and coverage. Figure 7.4 compares trends of all sleeve configurations (shrink tape, full braid, full spiral, half braid, and half spiral) at each impact level (0.0 J (0.0 ft-lbs), 2.5 J (1.9 ft-lbs), 5.0 J (3.7 ft-lbs), 7.5 J (5.6 ft-lbs), 10 J (7.4 ft-lbs), 15 J (11 ft-lbs), and 20 J (15 ft-lbs)). The dashed trend lines simply connect the averages of each sleeve configuration and should not be used for extrapolation. This plot shows that 2.5 J (1.9 ft-lbs) of impact energy significantly affects the ultimate strength of configurations and subsequently show an insignificant difference in strength with specimens 10 J (7.4 ft-lbs) of impact energy and higher. Configurations impacted with 10 J (7.4 ft-lbs) of energy

show that the coverage material does matter; i.e., shrink tape has the lowest average residual compressive stress of all the sleeve configurations.

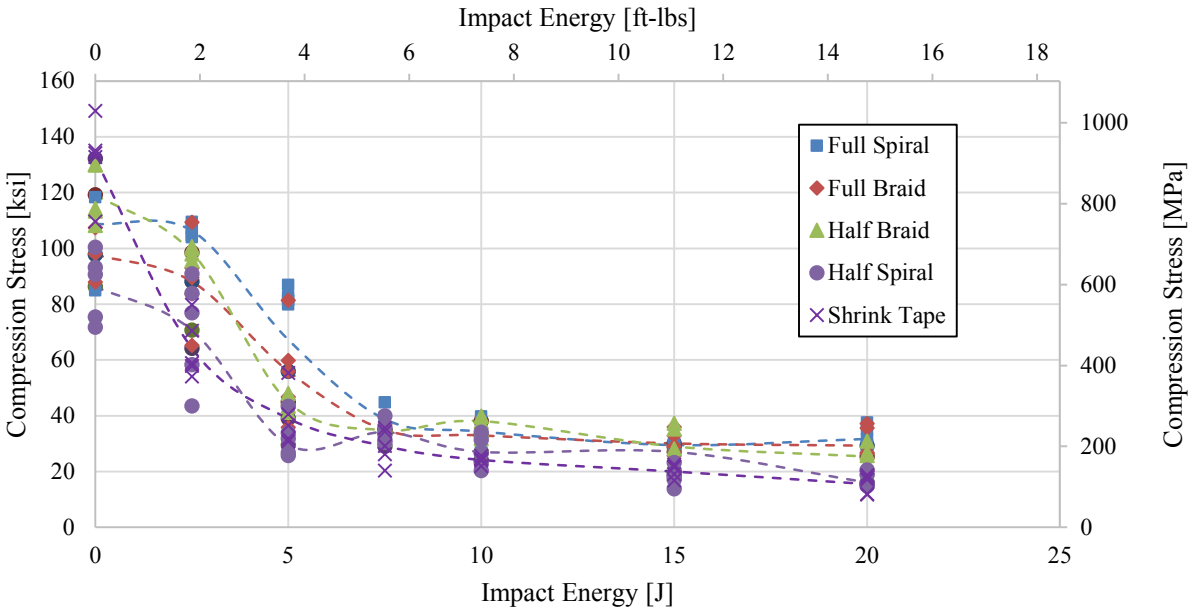

Figure 7.4 Compression Strength vs. Impact Energy for All Sleeve Types

7.2 Comparison to Past Results

The tables in this section compare the damage tolerance characteristics of carbon/epoxy composites of the current research and previous results. The percentages in each row represent a percentage difference in strength of a particular configuration, relative to the corresponding undamaged configuration.

7.2.1 Comparison of the Influence of Sleeve Type

Table 7.5 compares the compression strength difference of carbon configurations impacted with (0 J (1.1 ft-lbs), 5.0 J (3.7 ft-lbs) and 10 J (7.4 ft-lbs)) relative to undamaged configurations, isolating just the sleeve type (braid and spiral). As expected, the compression strength decreases with increasing impact energy. There was a significant difference in undamaged compression

strength between past and current research, with a difference of 23% for braided specimens. Interestingly, there was no significant difference for undamaged spiral sleeves. For low impact energy (5.0 J (3.7 ft-lbs)), braided sleeves from current research had an insignificantly higher compression strength than past research while the spiral had a 31% higher compression strength than spiral specimens from past research. For high impact energy (10 J (7.4 ft-lbs)), there was a difference of less than 10% in the compression strength for spiral whereas braided sleeves had 12% lower strength. The difference for braided specimens was most likely due to complications in the manufacturing process.

Table 7.4 Relative Difference in Compression Strength of Carbon Epoxy Composites with Braided and Spiral Sleeves

Impact Energy	Sleeve Type	Ultimate Compression Strength				
		Current Research		Previous Research		
		[MPa	(ksi)]	[MPa	(ksi)]	Diff.
Undamaged	All Braid	740	(107)	960	(139)	-23%
	All Spiral	896	(130)	931	(135)	-4%
5.0 J (3.7 ft-lbs)	All Braid	293	(43)	276	(40)	8%
	All Spiral	382	(55)	288	(42)	31%
10 J (7.4 ft-lbs)	All Braid	199	(29)	231	(33)	-12%
	All Spiral	219	(32)	217	(31)	3%

7.2.2 Comparison of the Influence of Sleeve Coverage

Table 7.4 compares compression strength difference of the current and previous research by examining just the sleeve coverage (full and half). As expected, compression strength decreases with increasing impact energy level. For both sleeve types, the ultimate compression stress for undamaged specimens are lower than previous research by roughly 9%. For low energy impact (5.0 J (3.7 ft-lbs)); however, the current research for both sleeve types is higher than for previous

research as exhibited by a maximum 49% difference. For high energy impact (10 J (7.4 ft-lbs)), full sleeves for the current research exhibited a lower ultimate compressive stress than prior research while half sleeves exhibited higher compressive stress.

Table 7.5 Relative Difference in Compression Strength of Carbon Epoxy Composites with Full and Half Coverages

Impact Energy	Sleeve Coverage	Ultimate Compression Strength				
		Current Research		Previous Research		
		[MPa	(ksi)]	[MPa	(ksi)]	Diff.
Undamaged	Full	817	(118)	915	(133)	-11%
	Half	896	(130)	976	(142)	-8%
5.0 J (3.7 ft-lbs)	Full	440	(64)	294	(43)	49%
	Half	316	(46)	271	(39)	18%
10 J (7.4 ft-lbs)	Full	213	(31)	270	(39)	-21%
	Half	241	(35)	171	(25)	40%

7.2.3 Comparison of the Influence of Sleeve Material

Table 7.6 compares the compression strength difference of carbon configurations impacted with (0 J (0.0 ft-lbs), 5.0 J (3.7 ft-lbs) and 10 J (7.4 ft-lbs)), isolating just the sleeve material (Nomex Thread, Kevlar, Shrink Tape). As expected, the compression strength decreases with increasing impact energy. There was a significant difference in undamaged compression strength between past and current research with a difference of roughly 13% for both Nomex Thread and Shrink Tape. For low impact energy (5.0 J (3.7 ft-lbs)), Shrink Tape sleeves had a significantly higher compression strength with a 56% difference compared to Kevlar while the Nomex Thread had less than 10% difference when compared to Kevlar. For high impact energy (10 J (7.4 ft-lbs)), there was less than 10% difference in the compression strength for Shrink Tape compared to Kevlar sleeves whereas Nomex Thread sleeves had 32% lower strength than Kevlar sleeves.

Overall, Shrink Tape and Nomex Thread specimens typically had similar or lower compression strength than the previous specimens consolidated with Kevlar with the same damage.

Table 7.6 Relative Difference in Compression Strength of Carbon Epoxy Composites with Nomex Thread, Shrink Tape, and Kevlar Sleeves

Impact Energy	Sleeve Material	Ultimate Compression Strength [MPa	(ksi)]	Diff
Undamaged	Kevlar	946	137	-
	Shrink Tape	911	132	-4%
	Nomex Thread	818	119	-13%
5.0 J (3.7 ft-lbs)	Kevlar	282	41	-
	Shrink Tape	269	39	-5%
	Nomex Thread	257	37	-9%
10.0 J (7.4 ft-lbs)	Kevlar	224	32	-
	Shrink Tape	167	24	-26%
	Nomex Thread	151	22	-33%

8 DISCUSSION OF MICRO-CT RESULTS

8.1 Effect of Impact Energy on Crack Area and Overall Crack Volume

8.1.1 Influence of Sleeve Type

To examine the influence of sleeve type, Figure 8.1 was created by combining the micro-CT results of all braided sleeves (full and half), and all spiral sleeves (full and half), respectively. This approach allows comparison of just the sleeve type. The crack area curves indicate a significant increase in the peak crack area and overall crack volume for damaged configurations. The curves also show that for both spiral and braided sleeves, the peak crack area is larger for 15 J (11 ft-lbs) than for 20 J (15 ft-lbs). This shows that after a certain level of impact energy, a higher impact doesn't increase the peak crack area. A summary of the relative difference between braided and spiral sleeves for carbon/epoxy composites is shown in Table 7.1. At 2.5 J (1.9 ft-lbs) impact spiral sleeves have roughly 20% increase in peak crack area and overall crack volume. As impact energy increases; however, the peak crack area for braided sleeves is significantly higher than spiral sleeves. There is not as clear a pattern with overall crack volume. This shows that the cracks are more dispersed over the length of the specimen for spiral sleeves while as the cracks for the braided sleeves are more localized.

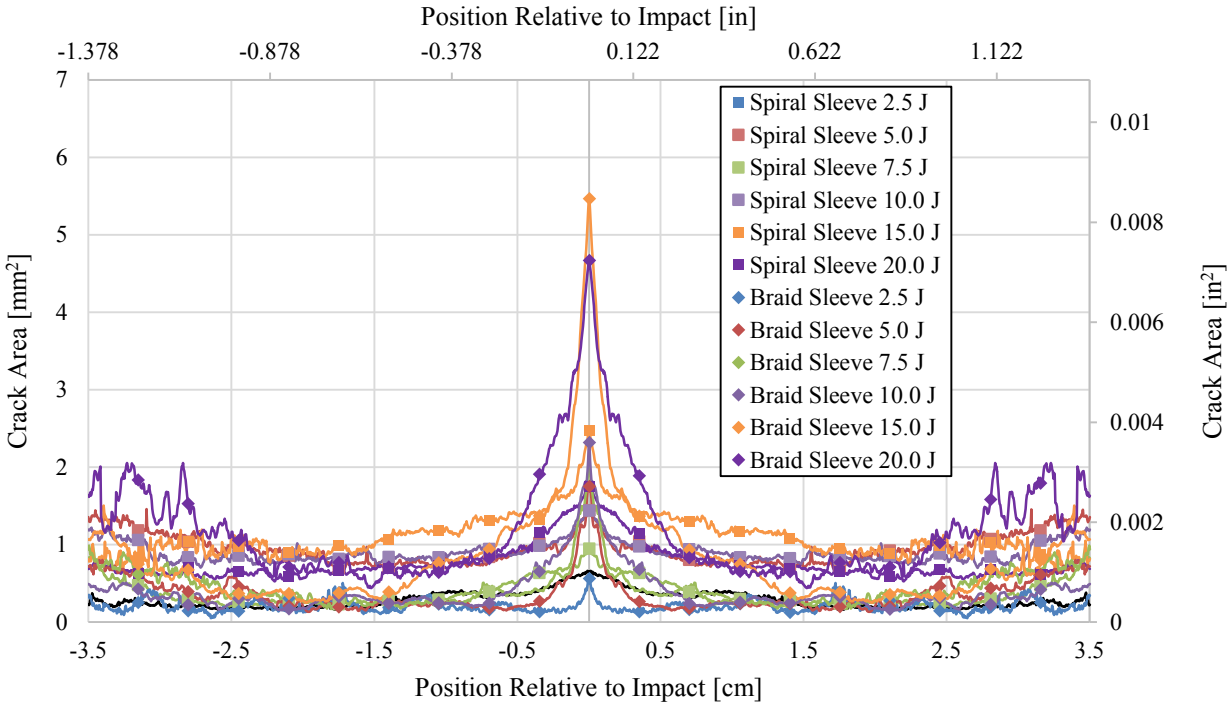

Figure 8.1 Average Crack Area as a Function of Distance from the Point of Impact for Spiral and Braided Sleeve Types

Table 8.1 Average Peak Crack Area and Overall Crack Volume for Spiral and Braided Sleeve Types

Impact Energy	Sleeve Type	Peak Crack Area			Overall Crack Volume		
		mm^2	(10^3 in^2)	Diff.	mm^3	(10^6 in^3)	Diff.
0.0 J (0.0 ft-lbs)	Spiral	0.00	(0.00)	0%	0.00	(0.00)	0%
	Braid	0.00	(0.00)		0.00	(0.00)	
2.5 J (1.9 ft-lbs)	Spiral	0.66	(1.01)	-14%	20.0	(1.22)	-27%
	Braid	0.57	(0.88)		14.5	(0.89)	
5.0 J (3.7 ft-lbs)	Spiral	1.44	(2.23)	22%	66.4	(4.05)	-62%
	Braid	1.75	(2.72)		25.4	(1.55)	
7.5 J (5.6 ft-lbs)	Spiral	0.95	(1.47)	113%	26.7	(1.63)	20%
	Braid	2.03	(3.14)		32.0	(1.95)	
10 J (7.4 ft-lbs)	Spiral	1.44	(2.23)	61%	63.3	(3.86)	-57%
	Braid	2.32	(3.60)		27.4	(1.67)	
15 J (11 ft-lbs)	Spiral	2.48	(3.84)	120%	77.5	(4.73)	-26%
	Braid	5.46	(8.47)		57.3	(3.50)	
20 J (15 ft-lbs)	Spiral	1.74	(2.70)	168%	53.8	(3.28)	56%
	Braid	4.67	(7.23)		84.1	(5.13)	

8.1.2 Influence of Sleeve Coverage

To illustrate the effect of sleeve coverage (full vs. half), independent of the sleeve type, Figure 8.2 was created by combining the results from full braid and spiral sleeve samples, and half braid and spiral sleeve samples. This combination of results approach allows comparison of just the sleeve coverage. The crack area curves indicate a significant increase in crack peak area and crack volume as impact energy increases. A summary of the relative difference between full and half sleeve coverage configurations is shown in Table 8.2. Aside from 5.0 J (3.7 ft-lbs), the peak crack area for half coverage sleeves is significantly higher than for full coverage sleeves. For lower energy levels, (2.5 J (1.9 ft-lbs) and 5.0 J (3.7 ft-lbs)) the overall crack volume of half coverage is significantly higher than that of full coverage sleeves with a 32% increase. However, for mid-level impact energy (7.5 J (5.6 ft-lbs), 10 J (7.4 ft-lbs), and 15 J (11 ft-lbs)), while the overall crack volume for half coverage is still larger than that of full coverage, the difference not as significant at only 10%. For high impact energy (20 J (15 ft-lbs)), there is no significant difference in the overall crack volume between half and full coverage sleeves. In summary, the peak crack area is typically significantly higher for half coverage than for full coverage, and as impact energy increases, the difference in the overall crack volume between half and full coverage decreases.

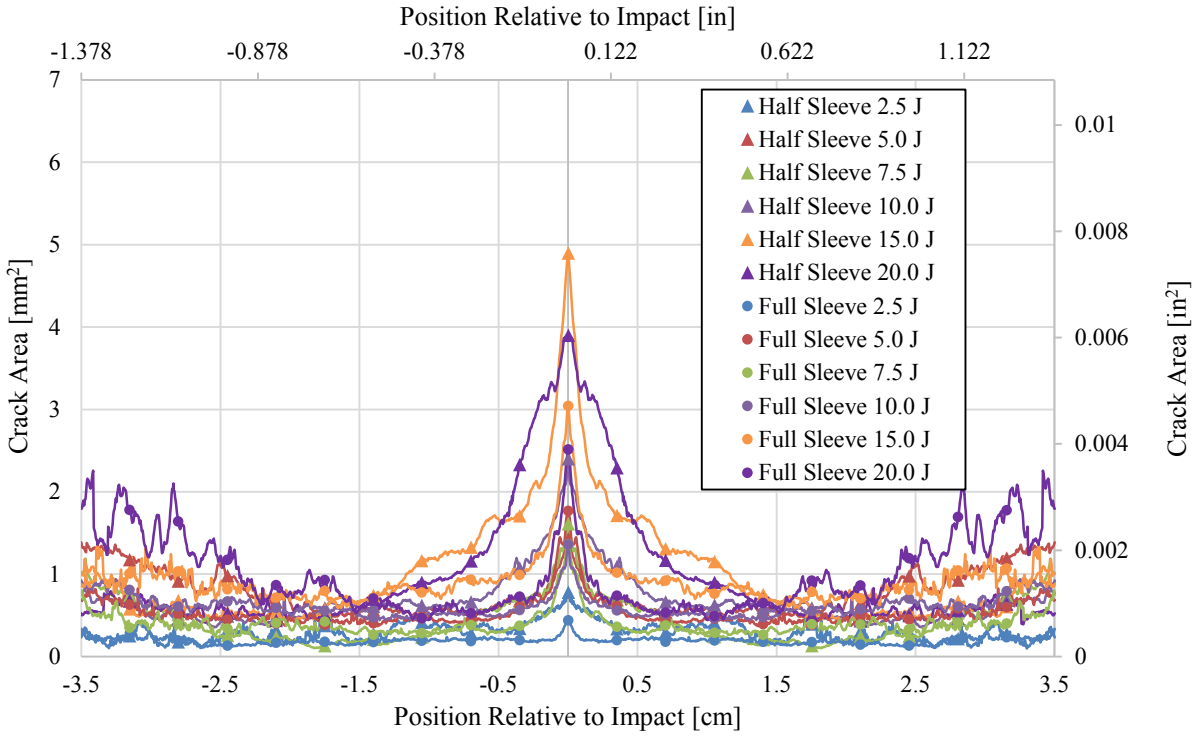

Figure 8.2 Average Crack Area as a Function of Distance from the Point of Impact for Half and Full Sleeve Types

Table 8.2 Average Peak Crack Area and Overall Crack Volume for Half and Full Sleeve Types

Impact Energy	Sleeve Coverage	Peak Crack Area			Overall Crack Volume		
		mm^2	(10^3 in^2)	Diff.	mm^3	(10^6 in^3)	Diff.
0.0 J (0.0 ft-lbs)	Half	0.00	(0.00)	0%	0.00	(0.00)	0%
	Full	0.00	(0.00)		0.00	(0.00)	
2.5 J (1.9 ft-lbs)	Half	0.78	(1.21)	-44%	20.5	(1.26)	-32%
	Full	0.44	(0.68)		13.9	(0.85)	
5.0 J (3.7 ft-lbs)	Half	1.43	(2.21)	24%	54.5	(3.33)	-32%
	Full	1.77	(2.74)		37.3	(2.28)	
7.5 J (5.6 ft-lbs)	Half	1.62	(2.50)	-16%	310	(1.89)	-10%
	Full	1.36	(2.11)		27.8	(1.69)	
10 J (7.4 ft-lbs)	Half	2.40	(3.72)	-43%	47.7	(2.91)	-10%
	Full	1.36	(2.11)		43.0	(2.63)	
15 J (11 ft-lbs)	Half	4.90	(7.60)	-38%	70.7	(4.31)	-9%
	Full	3.04	(4.71)		64.1	(3.91)	
20 J (15 ft-lbs)	Half	3.90	(6.04)	-36%	68.3	(4.17)	2%
	Full	2.51	(3.90)		69.6	(4.25)	

8.1.3 Influence of Sleeve Material

To illustrate the effect of sleeve material (Nomex Thread vs. Shrink Tape), independent of the sleeve type, Figure 8.3 was created by combining the results from full braid and spiral sleeve samples and comparing them with Shrink Tape samples. This combination of results approach allows comparison of just the sleeve material since the Shrink Tape covered the full length of each specimen. The stress-strain curves indicate a significant increase in peak crack area and crack volume as impact energy increases. A summary of the relative difference between Nomex Thread and Shrink Tape sleeve material configurations is shown in Table 8.3. For 2.5 J (1.9 ft-lbs) and 5.0 J (3.7 ft-lbs) impact, there is no significant difference in peak crack area. For higher impact energy there is a significant difference in peak crack area. With the exception of 5.0 J (3.7 ft-lbs), the overall crack volume for Shrink Tape is significantly higher than for the Nomex Thread sleeve material.

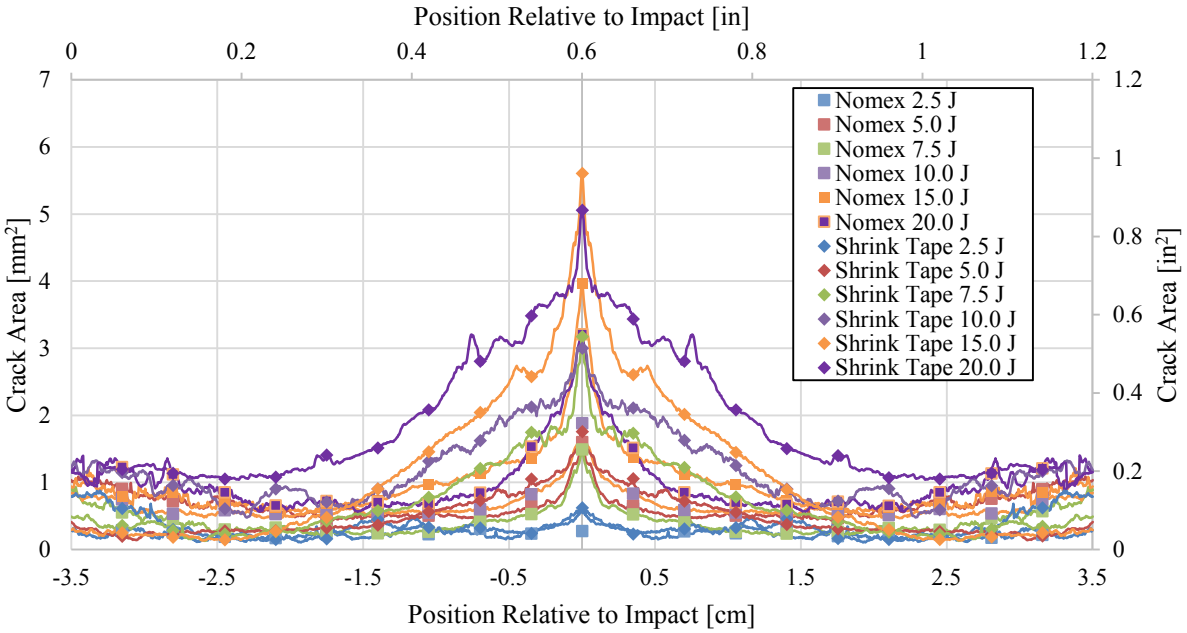

Figure 8.3 Average Crack Area as a Function of Distance from the Point of Impact for Nomex Thread and Shrink Tape Sleeve Types

Table 8.3 Peak Crack Area and Overall Crack Volume for Nomex Thread and Shrink Tape Sleeve Types

Impact Energy	Sleeve Material	Peak Crack Area			Overall Crack Volume		
		mm^2	(10^3 in^2)	Diff.	mm^3	(10^3 in^3)	Diff.
0.0 J (0.0 ft-lbs)	Nomex Thread	0.00	(0.00)	0%	0.00	(0.00)	0%
	Shrink Tape	0.00	(0.00)	0%	0.00	(0.00)	0%
2.5 J (1.9 ft-lbs)	Nomex Thread	0.61	(0.95)	2%	17.25	(1.05)	41%
	Shrink Tape	0.62	(0.96)		24.32	(1.48)	
5.0 J (3.7 ft-lbs)	Nomex Thread	1.60	(2.48)	10%	45.90	(2.80)	-27%
	Shrink Tape	1.75	(2.72)		33.32	(2.03)	
7.5 J (5.6 ft-lbs)	Nomex Thread	1.49	(2.31)	113%	29.36	(1.79)	66%
	Shrink Tape	3.17	(4.92)		48.63	(2.97)	
10 J (7.4 ft-lbs)	Nomex Thread	1.88	(2.91)	60%	45.36	(2.77)	86%
	Shrink Tape	3.00	(4.65)		84.17	(5.14)	
15 J (11 ft-lbs)	Nomex Thread	3.97	(6.16)	41%	67.39	(4.11)	12%
	Shrink Tape	5.61	(8.69)		75.31	(4.60)	
20 J (15 ft-lbs)	Nomex Thread	3.21	(4.97)	58%	68.90	(4.21)	87%
	Shrink Tape	5.06	(7.84)		129.17	(7.88)	

8.1.4 Influence of Impact Energy

Plots of the peak crack area and the overall crack volume as a function of impact energy was prepared to illustrate the effect of impact energy on peak crack area and overall crack volume, as a function of sleeve type and coverage. Figures 8.4-8.9 compare trends of all sleeve configurations (shrink tape, full braid, full spiral, half braid, and half spiral) at each impact level (0.0 J (0.0 ft-lbs), 2.5 J (1.9 ft-lbs), 5.0 J (3.7 ft-lbs), 7.5 J (5.6 ft-lbs), 10 J (7.4 ft-lbs), 15 J (11 ft-lbs), and 20 J (15 ft-lbs)) for peak crack area and overall crack volume, respectively. The dashed lines in Figures 8.4 and 8.6 simply connect the averages of each sleeve configuration and should not be used for extrapolation. Figure 8.4 shows that as impact energy increases, peak crack area generally increases up to 15 J (11 ft-lbs). Beyond 15 J (11 ft-lbs), the peak crack area decreases which shows that after a certain point, an increase in impact energy does not cause a significant increase in damage. This data is almost bimodal in that there is a bump in peak crack area around

5.0-7.5 J (3.7-5.6 ft-lbs) and then another bump at 15 J (11 ft-lbs). Further in depth analysis of the crack area is recommended to further understand this behavior. Figure 8.7 shows a more linear increase in overall crack volume as impact energy increases for shrink tape sleeves, however it exhibits a similar bimodal increase for the Nomex Thread sleeves as was seen with peak crack area.

Figures 8.5 and 8.8 are similar to 8.4 and 8.7, respectively; however, the dashed lines are replaced with linear trendlines. Tables 8.4 and 8.5 list the slopes of the trendlines for each sleeve configuration. The peak crack area increases at a similar rate for shrink tape and half braid specimens. Full spiral has the lowest slope which shows that sleeve type and coverage has an impact on how much damage is inflicted in the specimens. A similar trend can be seen with overall crack volume with the exception of the braided sleeves which are switched. Full spiral still has the lowest increase in crack volume with increasing impact energy of all sleeve types. For both peak crack area and overall crack volume, the slope for Shrink Tape sleeves is roughly double that of full and half spiral sleeves. Also, there is a roughly 80% difference in slope between half and full spiral sleeves.

Figures 8.6 and 8.9 are similar for 8.4 and 8.7, respectively; however, the dashed lines are replaced with third degree polynomial trend lines. Similar to the linear trendlines, the peak crack area increases at a similar rate for shrink tape and half braid specimens with increasing impact energy followed by full braid, half spiral, and full spiral. This shows that sleeve type and coverage do have an impact on how much damage is inflicted in the specimens. A similar trend can be seen with overall crack volume with the exception of full spiral which is due to a large jump in crack volume at 20 J (15 ft-lbs) impact energy. Prior to that last point, the same trend that was seen for peak crack area was exhibited.

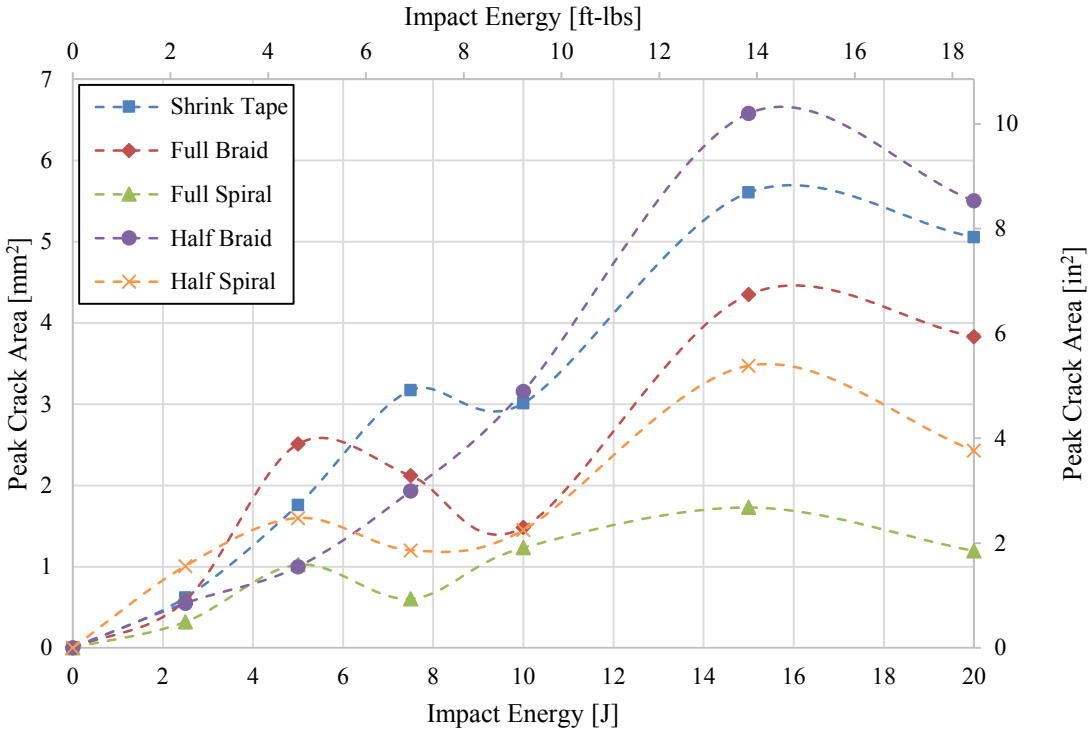

Figure 8.4 Average Peak Crack Area vs. Impact Energy for All Sleeve Types with Best Fit Lines

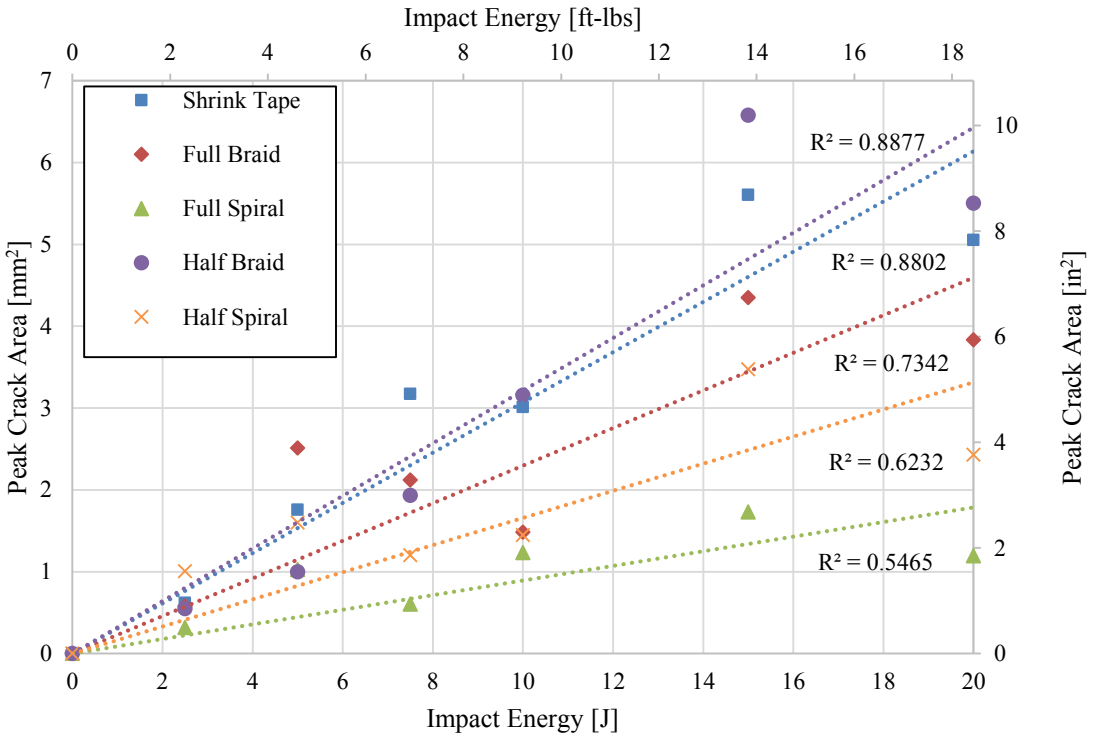

Figure 8.5 Linear Trendlines for Average Peak Crack Area vs. Impact Energy for All Sleeve Types

Table 8.4 Slopes of Linear Trendlines for Average Peak Crack Area vs. Impact Energy for All Sleeve Types

Sleeve	Slope
Full Braid	0.23
Half Braid	0.32
Full Spiral	0.09
Half Spiral	0.17
Shrink Tape	0.31

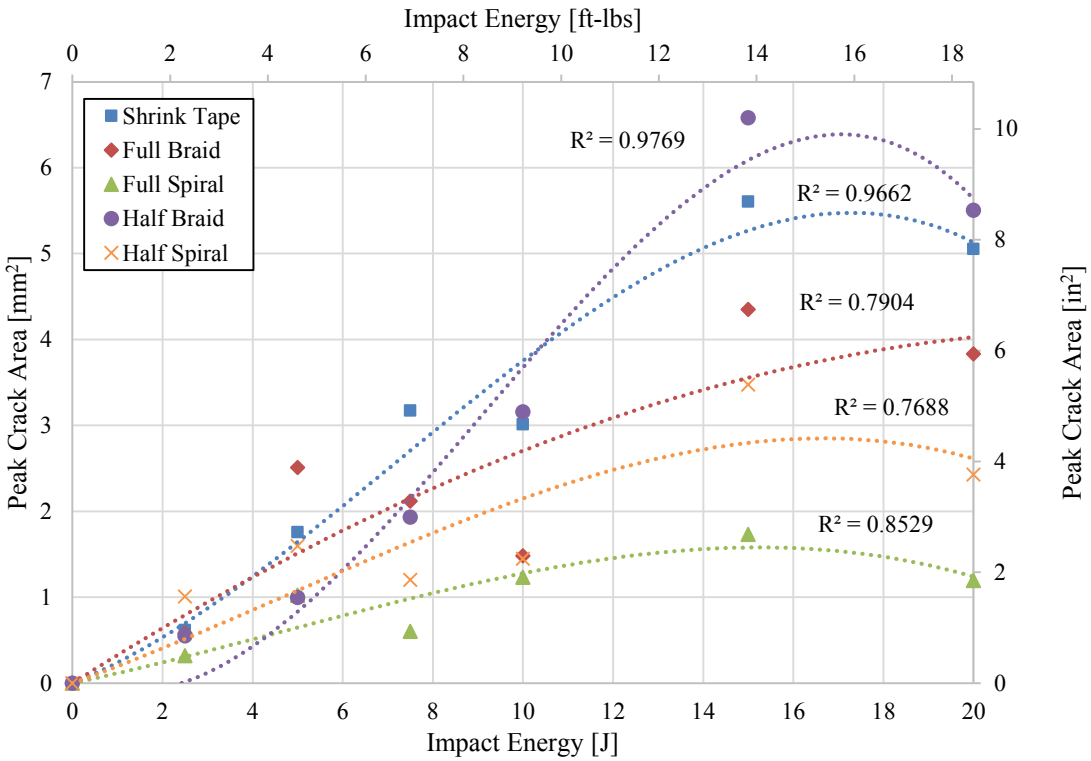

Figure 8.6 Nonlinear Trendlines for Average Peak Crack Area vs. Impact Energy for All Sleeve Types

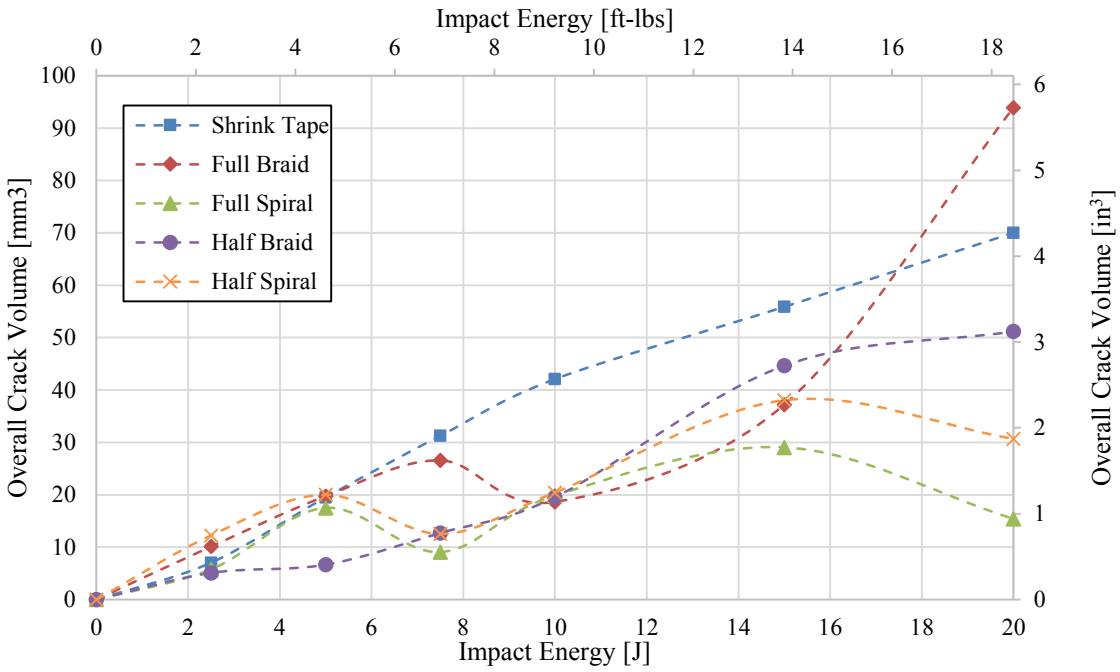

Figure 8.7 Average Overall Crack Volume vs. Impact Energy for All Sleeve Types with Best Fit Lines

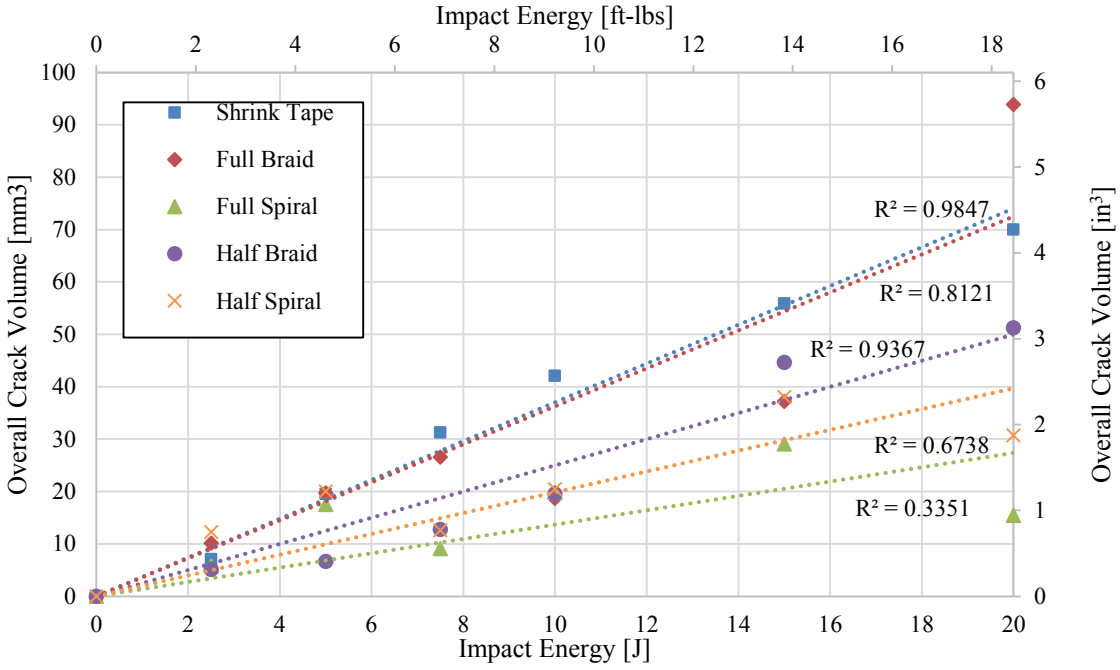

Figure 8.8 Linear Trendlines for Average Overall Crack Volume vs. Impact Energy for All Sleeve Types

Table 8.5 Slopes of Linear Trendlines for Average Overall Crack Volume vs. Impact Energy for All Sleeve Types

Sleeve	Slope
Full Braid	3.6
Half Braid	2.5
Full Spiral	1.4
Half Spiral	2.0
Shrink Tape	3.7

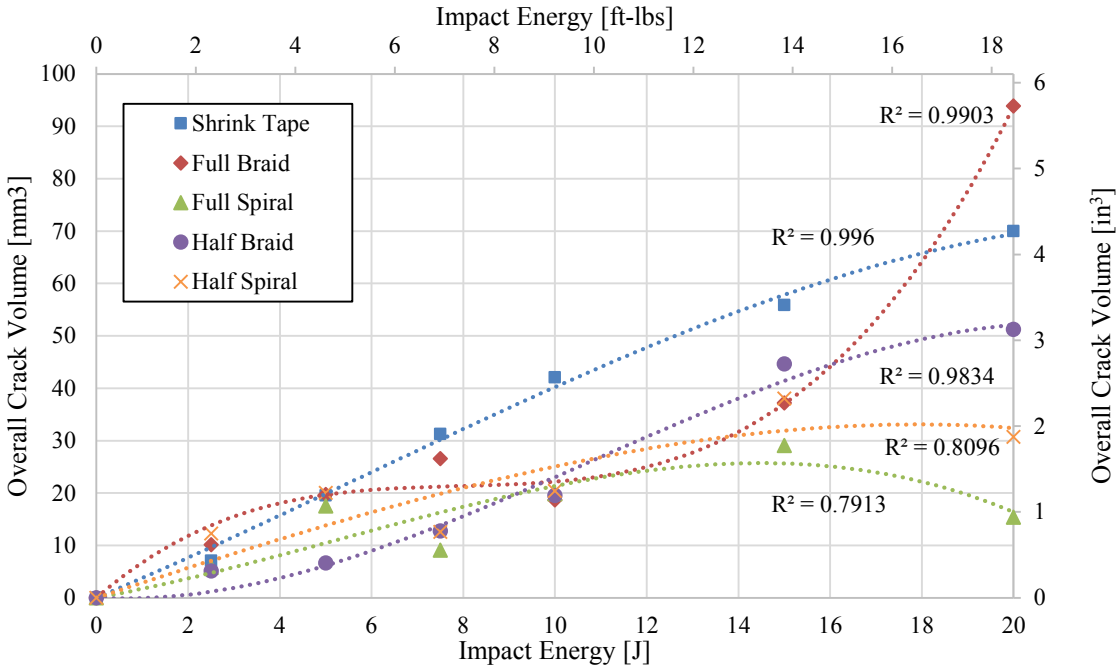

Figure 8.9 Nonlinear Trendlines for Average Overall Crack Volume vs. Impact Energy for All Sleeve Types

8.2 Effect of Peak Crack Area and Overall Crack Volume on Residual Strength

8.2.1 Influence of Sleeve Type

To examine the influence of sleeve type, Figure 8.10 and Figure 8.11 were created by comparing the residual compressive strength vs. the peak crack area and overall crack volumes; respectively, for all braided sleeves (full and half), and all spiral sleeves (full and half). This approach allows comparison of just the sleeve type. Lines have been added to Figures 8.10 and 8.11 to show the general trend that damage has on residual strength for each sleeve type. The slope of the trend lines for peak crack area are very similar, indicating that braided sleeves and spiral sleeves have a similar correlation between increase in peak crack area and decrease in residual strength. For crack volume; however, the slope is much steeper for spiral sleeves than for braided sleeves, indicating that a smaller increase is overall crack volume has a larger impact on residual strength for spiral sleeves than for braided sleeves.

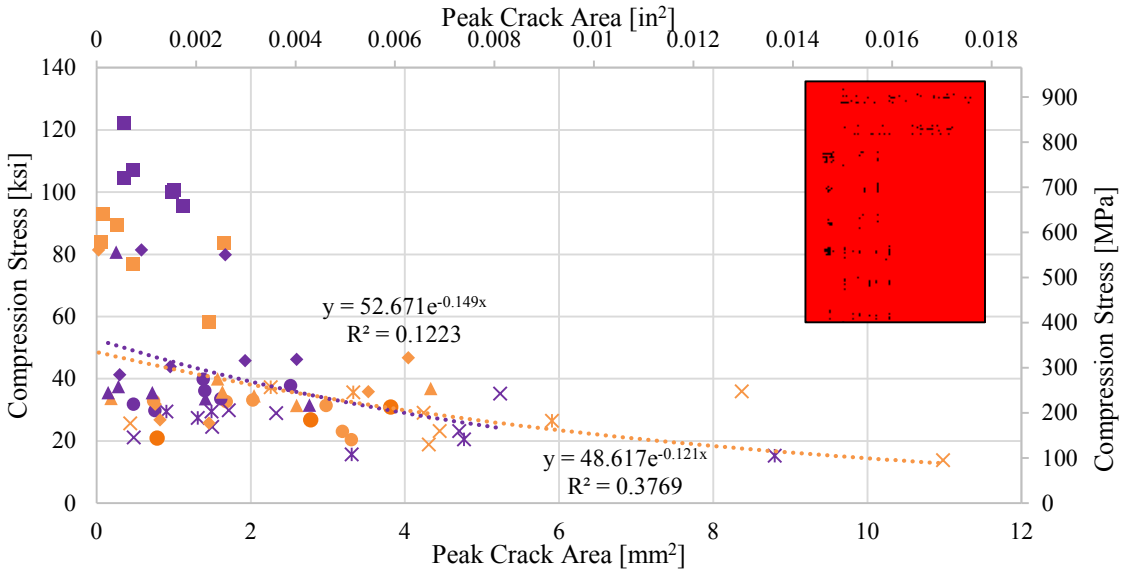

Figure 8.10 Peak Crack Area vs. Ultimate Compressive Stress for Braided and Spiral Sleeves

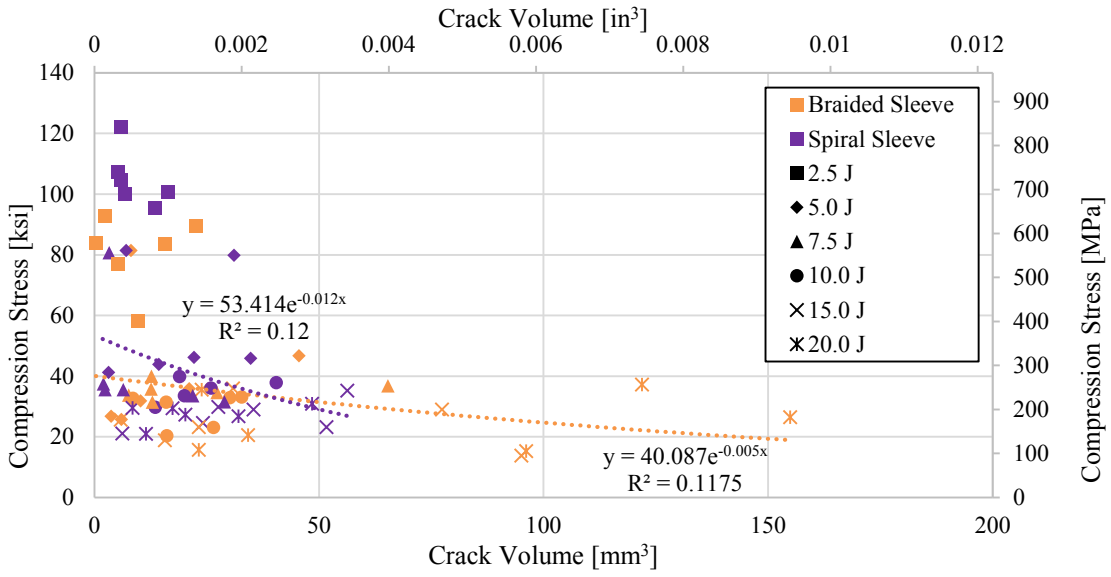

Figure 8.11 Overall Crack Volume vs. Ultimate Compressive Stress for Braided and Spiral Sleeves

8.2.2 Influence of Sleeve Coverage

To examine the influence of sleeve coverage, Figure 8.12 and Figure 8.13 were created by comparing the residual compressive strength vs. the peak crack area and overall crack volumes, respectively, for all full sleeves (braid and spiral), and all half sleeves (braid and spiral). This approach allows comparison of just the sleeve coverage. Lines have been added to Figures 8.12 and 8.13 to show the general trend that damage has on residual strength relative to sleeve coverage. The slopes of the trend lines for peak crack area are very similar, indicating that full sleeves and half sleeves have a similar correlation between increase in peak crack area and decrease in residual strength. The trend lines are offset from each other; however, with full sleeves being higher. This indicates that with the same amount of internal damage, full sleeves retain a higher residual strength. A similar trend can be seen for overall crack volume.

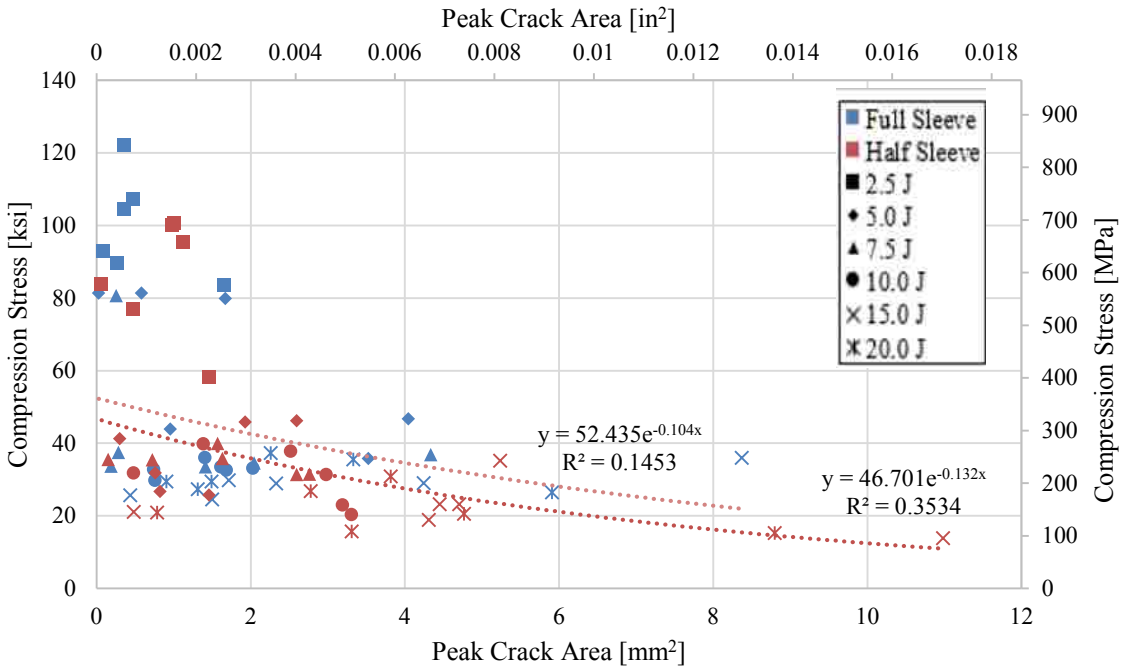

Figure 8.12 Peak Crack Area vs. Ultimate Compressive Stress for Full and Half Sleeves

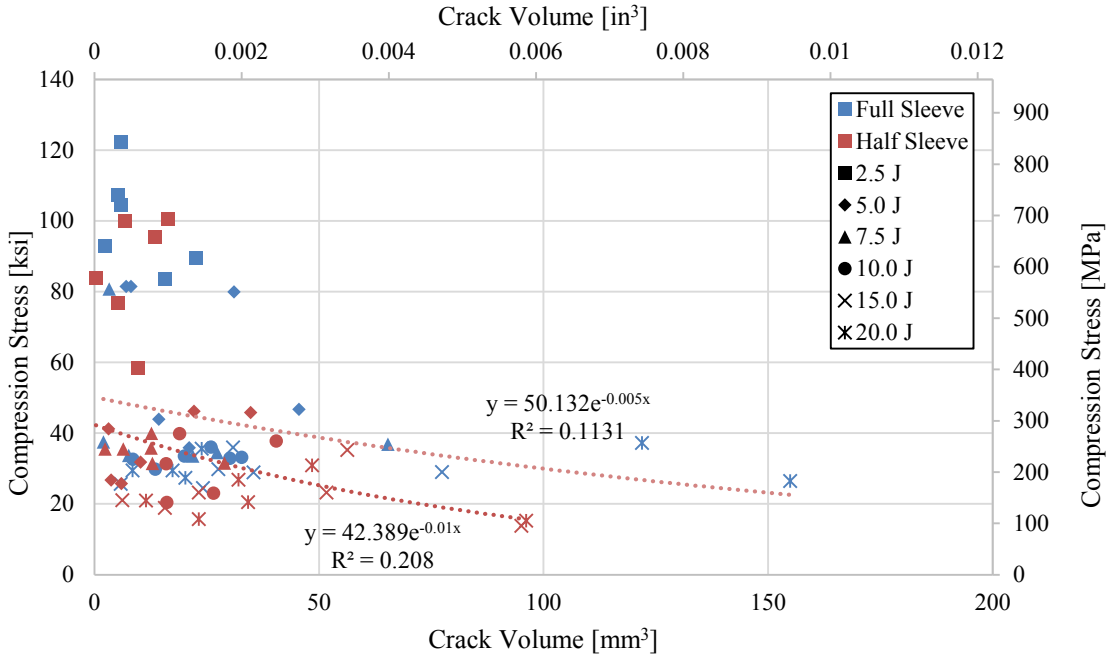

Figure 8.13 Overall Crack Volume vs. Ultimate Compressive Stress for Full and Half Sleeves

8.2.3 Influence of Sleeve Material

To examine the influence of sleeve material, Figure 8.14 and Figure 8.15 were created by comparing the residual compressive strength vs. the peak crack area and overall crack volumes, respectively, for Nomex Thread sleeves (full spiral and full braid), and Shrink Tape sleeves. This approach allows comparison of just the sleeve material. Lines have been added to Figure 8.14 and Figure 8.15 to show the general trend that damage has on residual strength relative to sleeve material. The slope of the trend line for Shrink Tape is steeper than that of Nomex Thread for both peak crack area and overall crack volume. This indicates that a smaller increase is damage has a larger impact on residual strength for Shrink Tape sleeves than for Nomex Thread sleeves.

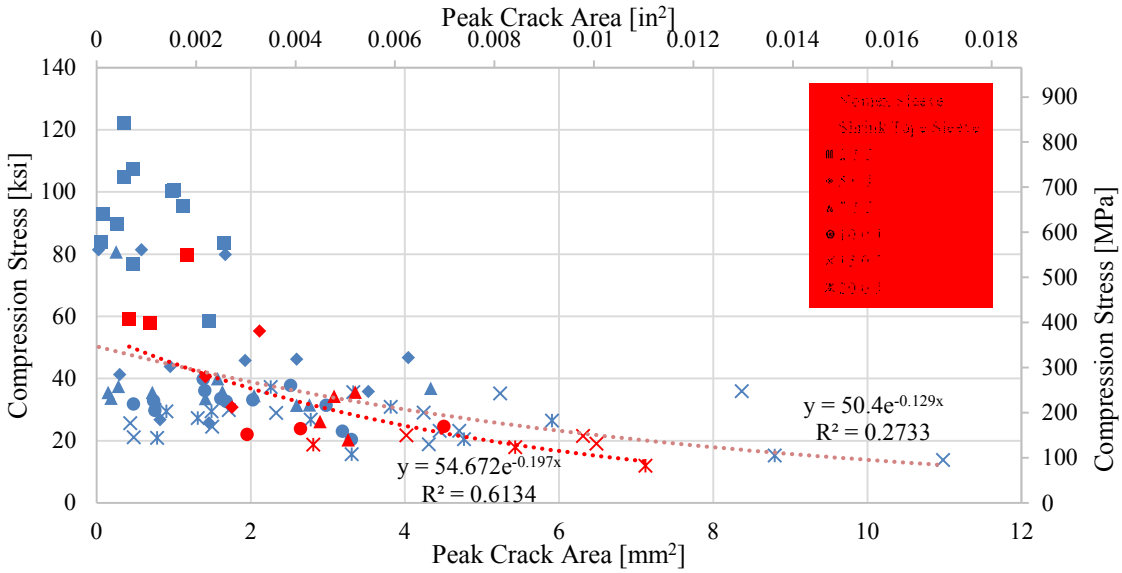

Figure 8.14 Peak Crack Area vs. Ultimate Compressive Stress for Nomex Thread and Shrink Tape Sleeves

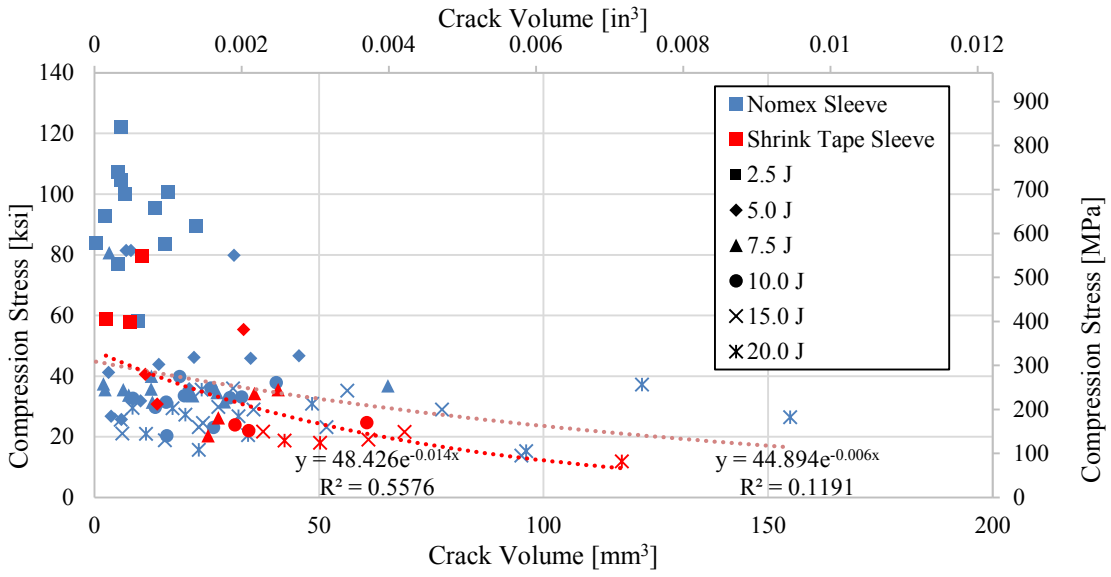

Figure 8.15 Overall Crack Volume vs. Ultimate Compressive Stress for Nomex Thread and Shrink Tape Sleeves

8.3 Effect of Impact Energy on Peak Crack Area and Overall Crack Volume for Lower Energy Levels

Since there is an insignificant difference in strength with specimens impacted with 10 J (7.4 ft-lbs) of impact energy and higher, the following section zooms in on specimens impacted with 7.5 J (5.6 ft-lbs) and lower. This will provide a clearer picture of how internal damage affects residual strength.

8.3.1 Influence of Sleeve Type at Lower Energy Levels

To examine the influence of sleeve type for lower energy levels, Figure 8.16 was created in a similar manner as Figure 8.1. The crack area curves indicate a significant increase in the peak crack area and overall crack volume for configurations damaged at lower impact energy. A summary of the relative difference between braided and spiral sleeves for composites is shown in

Table 8.6. As impact energy increases; the difference between the braided sleeve and the spiral increases. There is not as clear a pattern with overall crack volume.

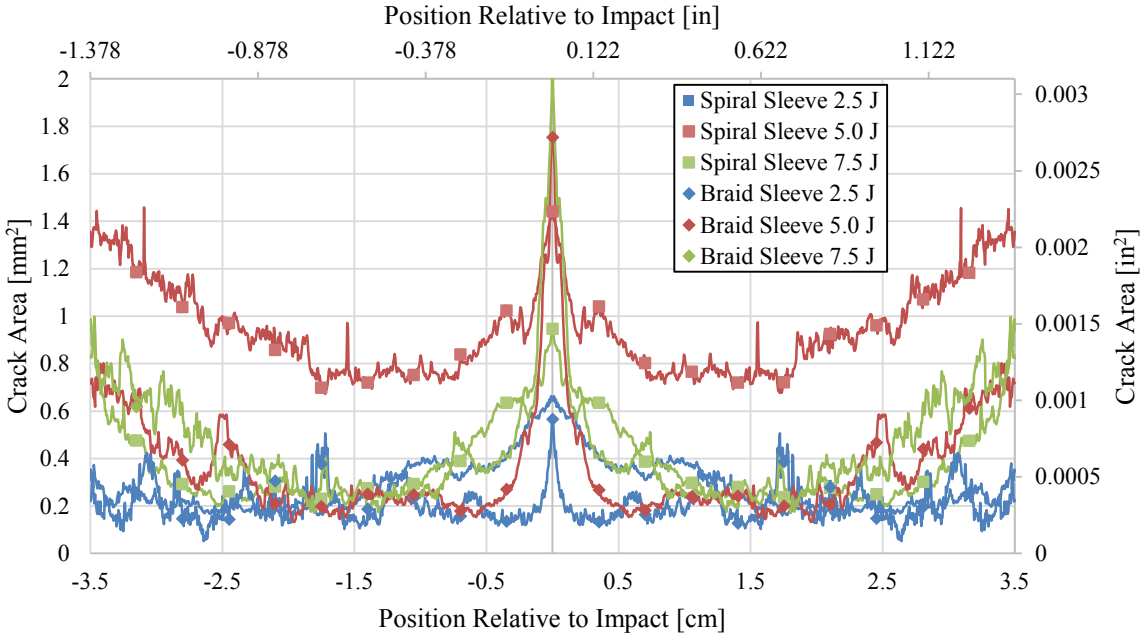

Figure 8.16 Average Crack Area as a Function of Distance from the Point of Impact for Spiral and Braided Sleeve Types for Lower Impact Energies

Table 8.6 Average Peak Crack Area and Overall Crack Volume for Spiral and Braided Sleeve Types for Lower Impact Energies

Impact Energy	Sleeve Type	Peak Crack Area			Overall Crack Volume		
		mm^2	(10^3 in^2)	Diff.	mm^3	(10^6 in^3)	Diff.
0.0 J (0.0 ft-lbs)	Spiral	0.00	(0.00)	0%	0.00	(0.00)	0%
	Braid	0.00	(0.00)		0.00	(0.00)	
2.5 J (1.9 ft-lbs)	Spiral	0.66	(1.01)	-14%	20.0	(1.22)	-27%
	Braid	0.57	(0.88)		14.5	(0.89)	
5.0 J (3.7 ft-lbs)	Spiral	1.44	(2.23)	22%	66.4	(4.05)	-62%
	Braid	1.75	(2.72)		25.4	(1.55)	
7.5 J (5.6 ft-lbs)	Spiral	0.95	(1.47)	113%	26.7	(1.63)	20%
	Braid	2.03	(3.14)		32.0	(1.95)	

To examine the influence of sleeve type for the lower energy levels, Figure 8.17 and Figure 8.18 were created by comparing the residual compressive strength vs. the peak crack area and overall crack volumes, respectively, for all braided sleeves (full and half), and all spiral sleeves (full and half). Lines have been added to Figures 8.17 and 8.18 to show the general trend that damage has on residual strength for each sleeve type. For crack volume and peak crack area the slope is much steeper for spiral sleeves than for braided sleeves, indicating that a smaller increase in overall crack volume has a larger impact on residual strength for spiral sleeves than for braided sleeves. This is a similar trend for the overall crack volume for all impact energy levels.

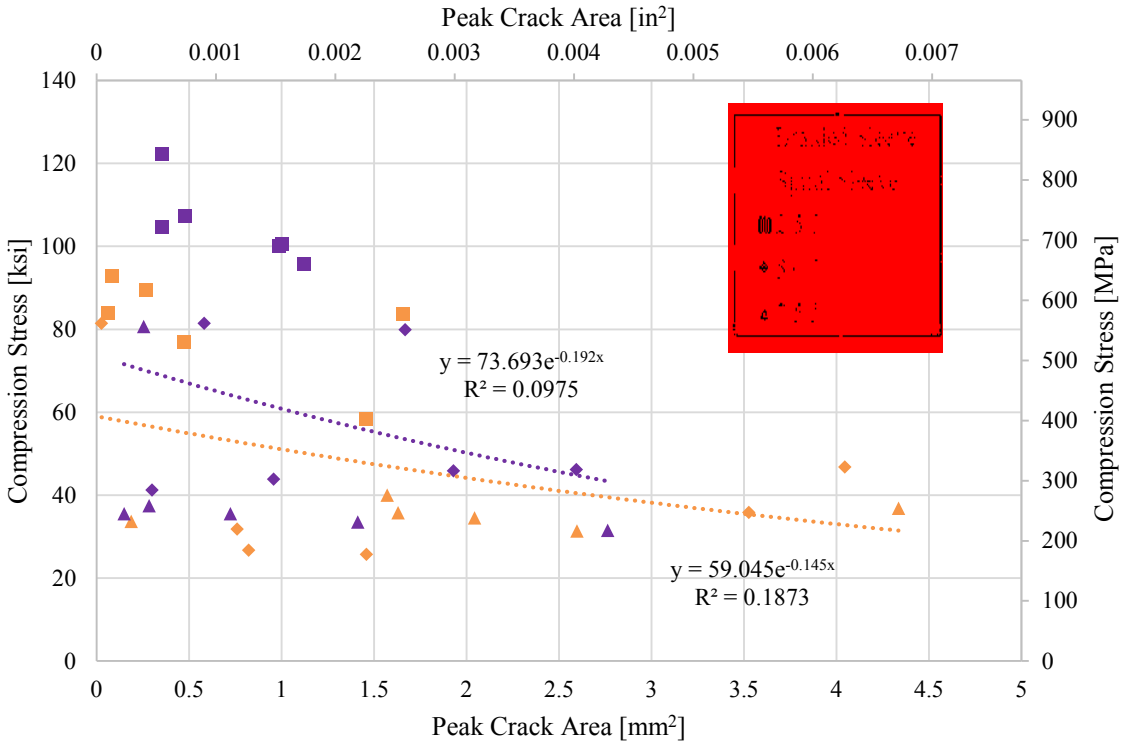

Figure 8.17 Peak Crack Area vs. Ultimate Compressive Stress for Braided and Spiral Sleeves for Lower Energy Levels

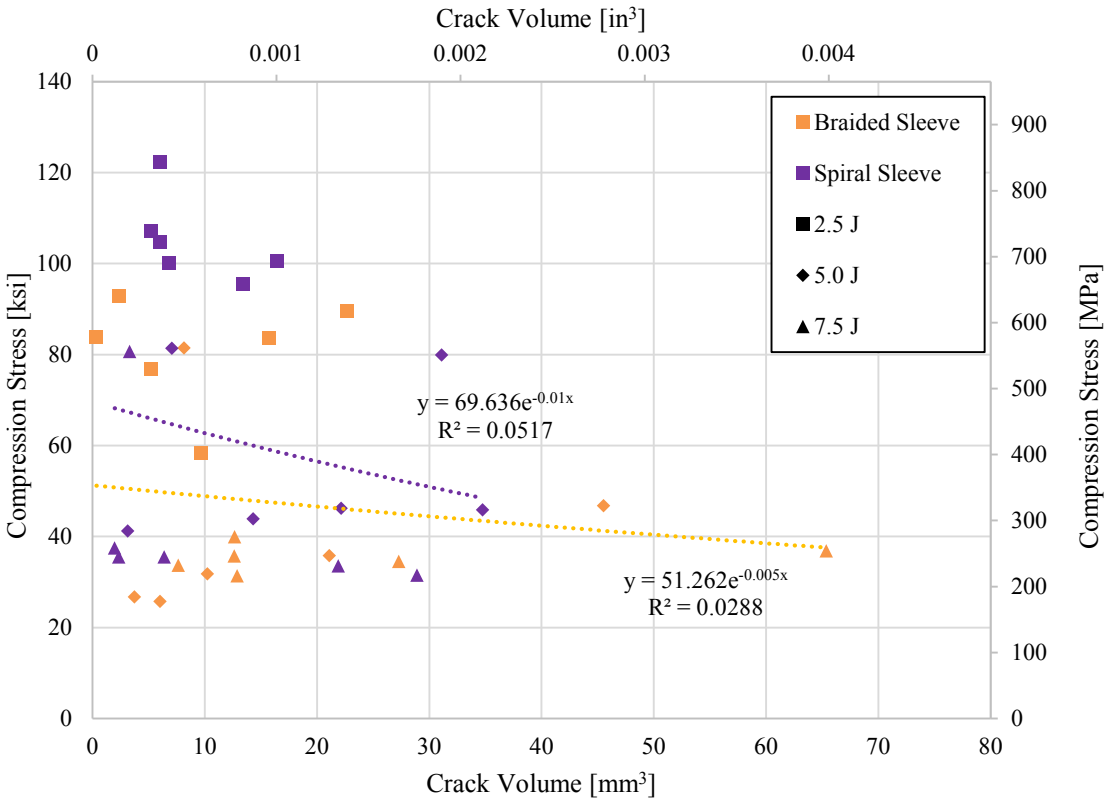

Figure 8.18 Overall Crack Volume vs. Ultimate Compressive Stress for Braided and Spiral Sleeves for Lower Energy Levels

8.3.2 Influence of Sleeve Coverage at Lower Energy Levels

To illustrate the effect of sleeve coverage (full vs. half), independent of the sleeve type, Figure 8.19 was created in a manner similar to Figure 8.2. The crack area curves indicate a significant increase in crack peak area and crack volume as impact energy increases. A summary of the relative difference between full and half sleeve coverage configurations is shown in Table 8.7. Aside from 5.0 J (3.7 ft-lbs), the peak crack area for half coverage sleeves is significantly higher than for full coverage sleeves. For lower energy levels, the overall crack volume of half coverage is significantly higher than that of full coverage sleeves. In summary, the peak crack area is typically significantly higher for half coverage than for full coverage for the lower energy levels.

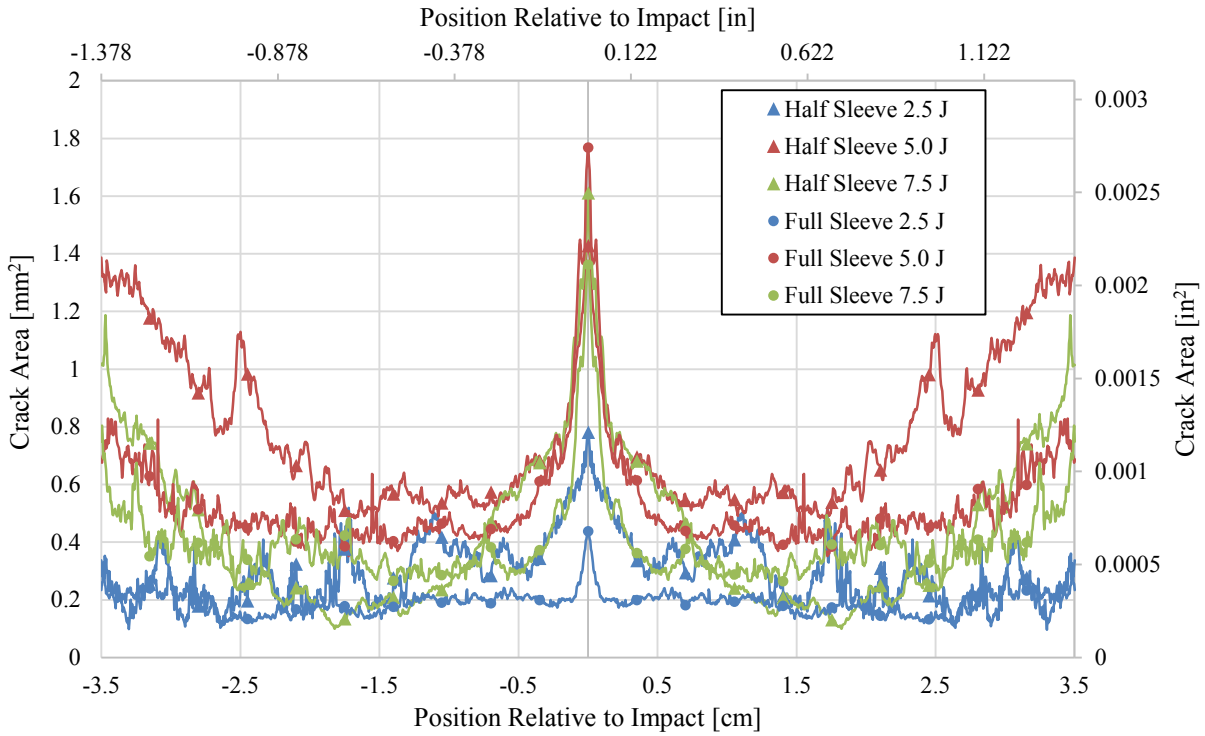

Figure 8.19 Average Crack Area as a Function of Distance from the Point of Impact for Half and Full Sleeve Types for Lower Impact Energies

Table 8.7 Average Peak Crack Area and Overall Crack Volume for Half and Full Sleeve Types Lower Impact Energies

Impact Energy	Sleeve Coverage	Peak Crack Area			Overall Crack Volume		
		mm^2	(10^3 in^2)	Diff.	mm^3	(10^6 in^3)	Diff.
0.0 J (0.0 ft-lbs)	Half	0.00	(0.00)	0%	0.00	(0.00)	0%
	Full	0.00	(0.00)		0.00	(0.00)	
2.5 J (1.9 ft-lbs)	Half	0.78	(1.21)	-44%	20.5	(1.26)	-32%
	Full	0.44	(0.68)		13.9	(0.85)	
5.0 J (3.7 ft-lbs)	Half	1.43	(2.21)	24%	54.5	(3.33)	-32%
	Full	1.77	(2.74)		37.3	(2.28)	
7.5 J (5.6 ft-lbs)	Half	1.62	(2.50)	-16%	310	(1.89)	-10%
	Full	1.36	(2.11)		27.8	(1.69)	

To examine the influence of sleeve coverage for lower energy levels, Figure 8.20 and Figure 8.21 were created by comparing the residual compressive strength vs. the peak crack area and overall crack volumes, respectively, for all full sleeves (braid and spiral), and all half sleeves (braid and spiral). Lines have been added to Figures 8.20 and 8.21 to show the general trend that damage has on residual strength relative to sleeve coverage. The slopes of the trend lines for peak crack area are very similar, indicating that full sleeves and half sleeves have a similar correlation between increase in peak crack area and decrease in residual strength. The trend lines are offset from each other; however, with full sleeves being higher. This is similar to the trend lines for all impact energy levels. This indicates that with the same amount of internal damage, full sleeves retain a higher residual strength. The slopes are different for full and half sleeves for overall crack volume which is different from the trend for all impact energy levels. For half spiral, there is not a significant correlation between increase in peak crack area and crack volume and decrease in residual strength.

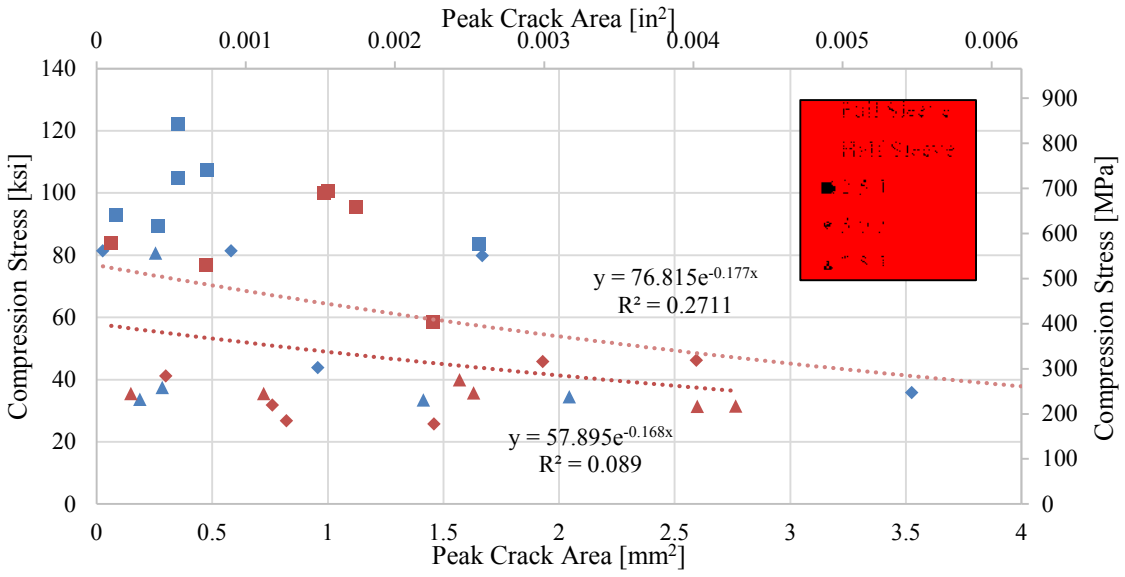

Figure 8.20 Peak Crack Area vs. Ultimate Compressive Stress for Full and Half Sleeves for Lower Energy Levels

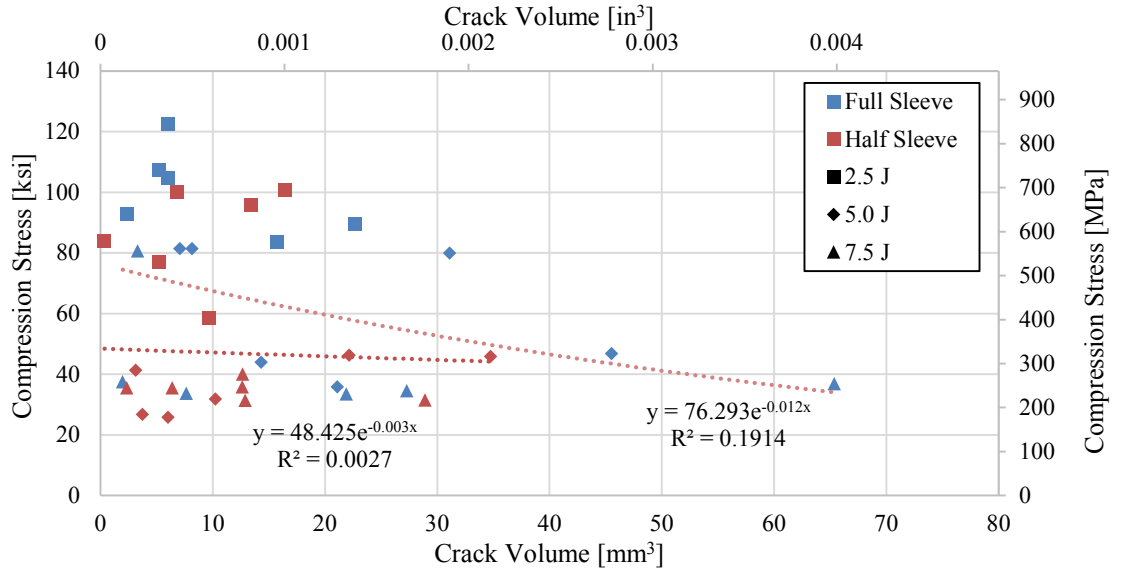

Figure 8.21 Overall Crack Volume vs. Ultimate Compressive Stress for Full and Half Sleeves for Lower Energy Levels

8.3.3 Influence of Sleeve Material at Lower Energy Levels

To illustrate the effect of sleeve material (Nomex Thread vs. Shrink Tape), independent of the sleeve type for the lower impact energy levels, Figure 8.22 was created by combining the results from full braid and spiral sleeve samples and comparing them with Shrink Tape samples.

The crack area curves indicate a significant increase in peak crack area and crack volume as impact energy increases. A summary of the relative difference between Nomex Thread and Shrink Tape sleeve material configurations for the lower energy levels is shown in Table 8.8. For 2.5 J (1.9 ft-lbs) and 5.0 J (3.7 ft-lbs) impact, there is no significant difference in peak crack area. For 7.5 J (5.6 ft-lbs) energy there is a significant difference in peak crack area. With the exception of 5.0 J (3.7 ft-lbs), the overall crack volume for Shrink Tape is significantly higher than for the Nomex Thread sleeve material.

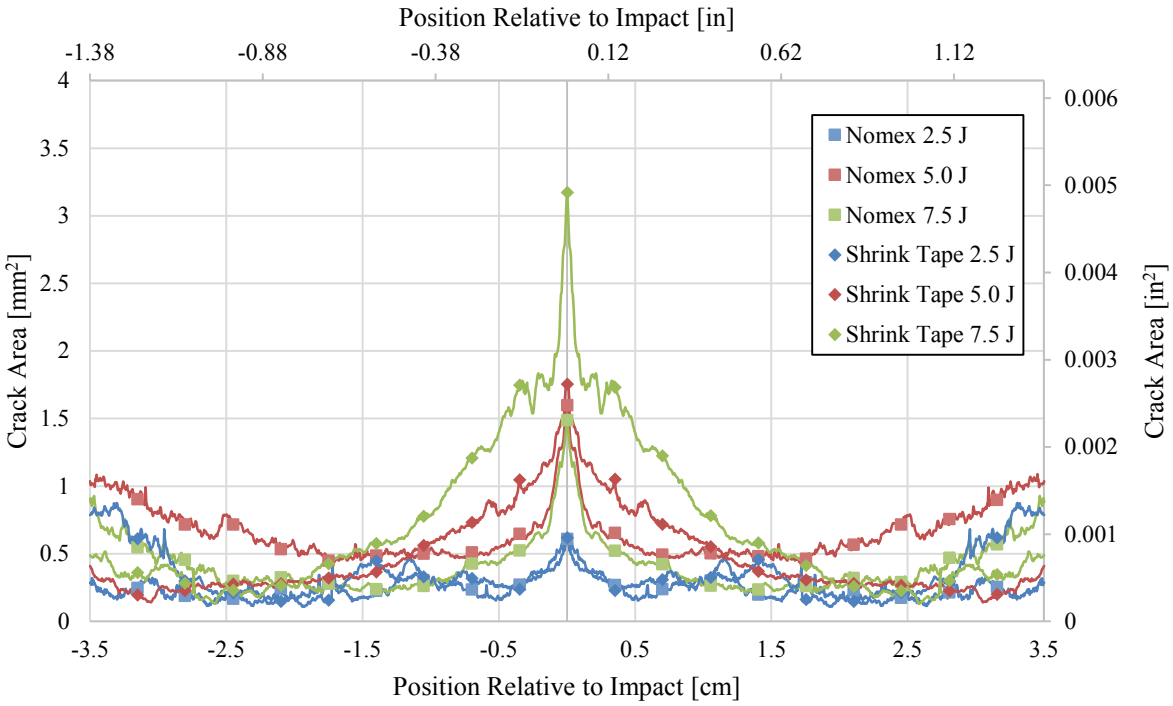

Figure 8.22 Average Crack Area as a Function of Distance from the Point of Impact for Nomex Thread and Shrink Tape Sleeve Types for Lower Impact Energies

Table 8.8 Average Peak Crack Area and Overall Crack Volume for Nomex Thread and Shrink Tape Sleeve Types for Lower Impact Energies

Impact Energy	Sleeve Material	Peak Crack Area			Overall Crack Volume		
		mm^2	(10^3 in^2)	Diff.	mm^3	(10^3 in^3)	Diff.
0.0 J (0.0 ft-lbs)	Nomex Thread	0.00	(0.00)	0%	0.00	(0.00)	0%
	Shrink Tape	0.00	(0.00)		0.00	(0.00)	
2.5 J (1.9 ft-lbs)	Nomex Thread	0.61	(0.95)	2%	17.25	(1.05)	41%
	Shrink Tape	0.62	(0.96)		24.32	(1.48)	
5.0 J (3.7 ft-lbs)	Nomex Thread	1.60	(2.48)	10%	45.90	(2.80)	-27%
	Shrink Tape	1.75	(2.72)		33.32	(2.03)	
7.5 J (5.6 ft-lbs)	Nomex Thread	1.49	(2.31)	113%	29.36	(1.79)	66%
	Shrink Tape	3.17	(4.92)		48.63	(2.97)	

To examine the influence of sleeve material, Figure 8.23 and Figure 8.24 were created by comparing the residual compressive strength vs. the peak crack area and overall crack volumes, respectively, for Nomex Thread sleeves (full spiral and full braid), and Shrink Tape sleeves. Lines have been added to Figures 8.23 and 8.24 to show the general trend that damage has on residual strength relative to sleeve material. Similar to the trend lines for all impact energy levels, the slope of the trend line for Shrink Tape is steeper than that of Nomex Thread for both peak crack area and overall crack volume. This indicates that a smaller increase is damage has a larger impact on residual strength for Shrink Tape sleeves than for Nomex Thread sleeves for the lower impact energy.

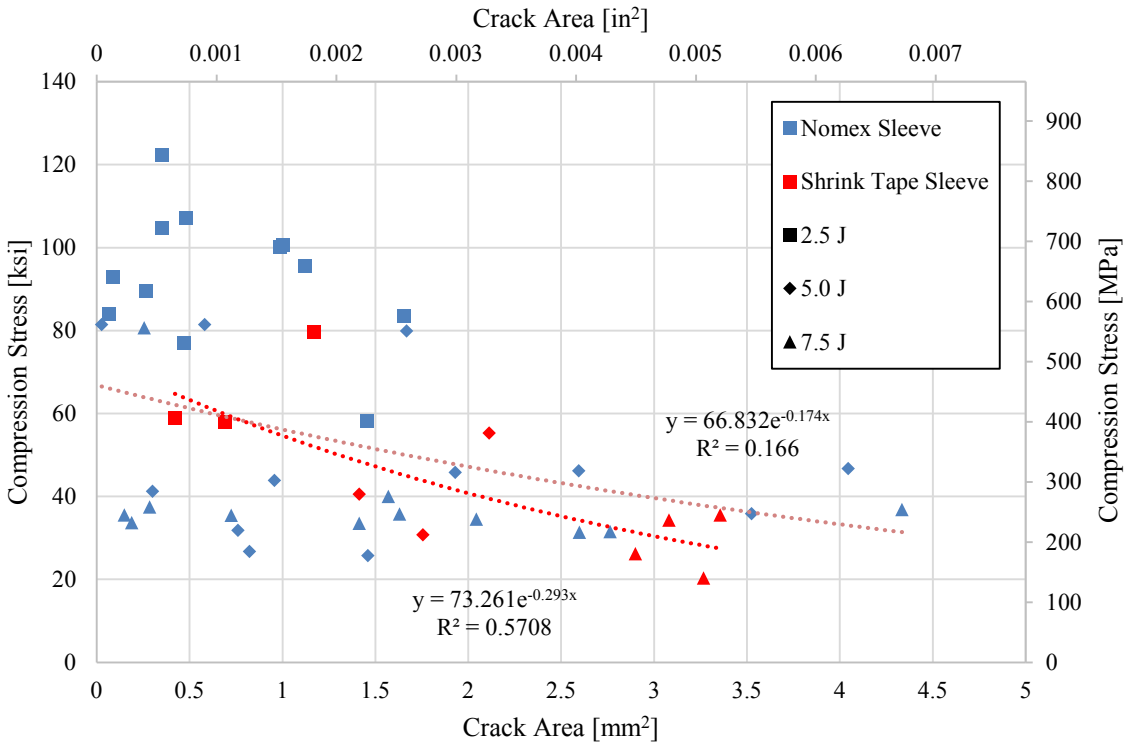

Figure 8.23 Peak Crack Area vs. Ultimate Compressive Stress for Nomex Thread and Shrink Tape Sleeves for Lower Energy Levels

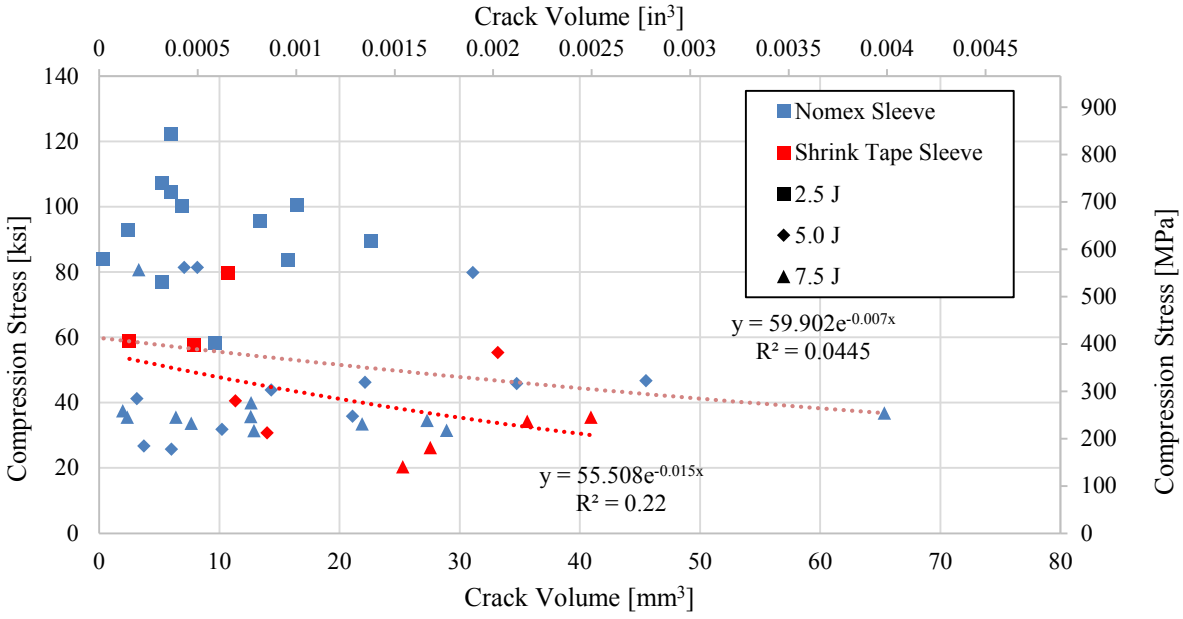

Figure 8.24 Overall Crack Volume vs. Ultimate Compressive Stress for Nomex Thread and Shrink Tape Sleeves for Lower Energy Levels

8.3.4 Influence of Impact Energy at Lower Energy Levels

Plots of the peak crack area and the overall crack volume as a function of the lower impact energy were prepared to illustrate the effect of impact energy on peak crack area and overall crack volume, as a function of sleeve type and coverage. Figures 8.25-8.30 compare trends of all sleeve configurations (shrink tape, full braid, full spiral, half braid, and half spiral) at each of the lower impact levels (0.0 J (0.0 ft-lbs), 2.5 J (1.9 ft-lbs), 5.0 J (3.7 ft-lbs), 7.5 J (5.6 ft-lbs)) for peak crack area and overall crack volume. Figure 8.25 shows that as impact energy increases, peak crack area generally increases. Shrink Tape has the most linear increase in peak crack area as impact energy increases. Full braid, full spiral, and half spiral all reach their maximum peak crack area at 5.0 J (3.7 ft-lbs). Figure 8.28 shows a similar trend as that of peak crack area for the spiral sleeves as well as the shrink tape. For overall crack volume, half braid sleeve has the lowest slope.

Figures 8.26 and 8.29 are similar to 8.25 and 8.28, respectively; however, the dashed lines are replaced with linear trendlines. Tables 8.9 and 8.10 list the slopes of the trendlines for each sleeve configuration. The same trends for all energy levels can be seen for the lower energy levels. Shrink Tape and half braid have the highest slopes, followed by full braid, half spiral, and full spiral. Similarly to all energy levels, the braids are switched for overall crack volume. This shows that spiral had the greatest resistance to damage as quantified by peak crack area and overall crack volume. The slope of the Shrink Tape trendline is roughly double that of full and half spiral which is similar to the results for all energy levels. There is a roughly 80% increase in slope between full and half spirals.

Figures 8.27 and 8.30 are similar to 8.25 and 8.28, respectively; however, the dashed lines are replaced with third degree polynomial trendlines. A similar pattern as that seen in Figure 8.5 can been seen in Figure 8.27, where shrink tape has largest the slope, followed by full braid, half

spiral, and full spiral. The only difference is half braid which has a low slope at the lowest energy levels that gradually increases with increased impact energy. Overall crack volume has a similar order as with peak crack area with the exception of half braid, which has the lowest slope that doesn't increase very much between 0.0 J (0.0 ft-lbs) and 7.5 J (5.6 ft-lbs).

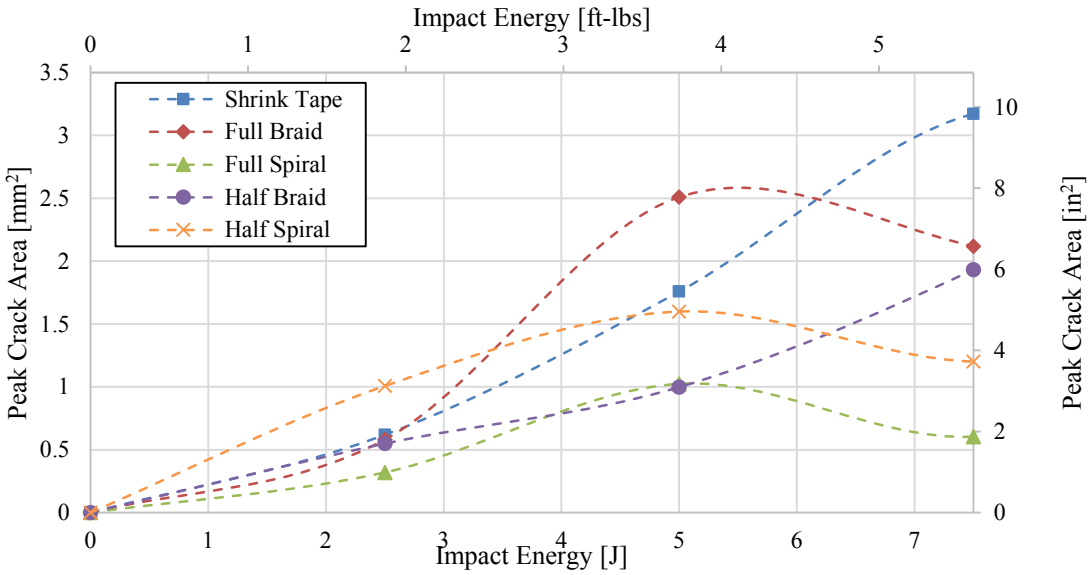

Figure 8.25 Best Fit Lines for Average Peak Crack Area vs. Lower Impact Energy for All Sleeve Types

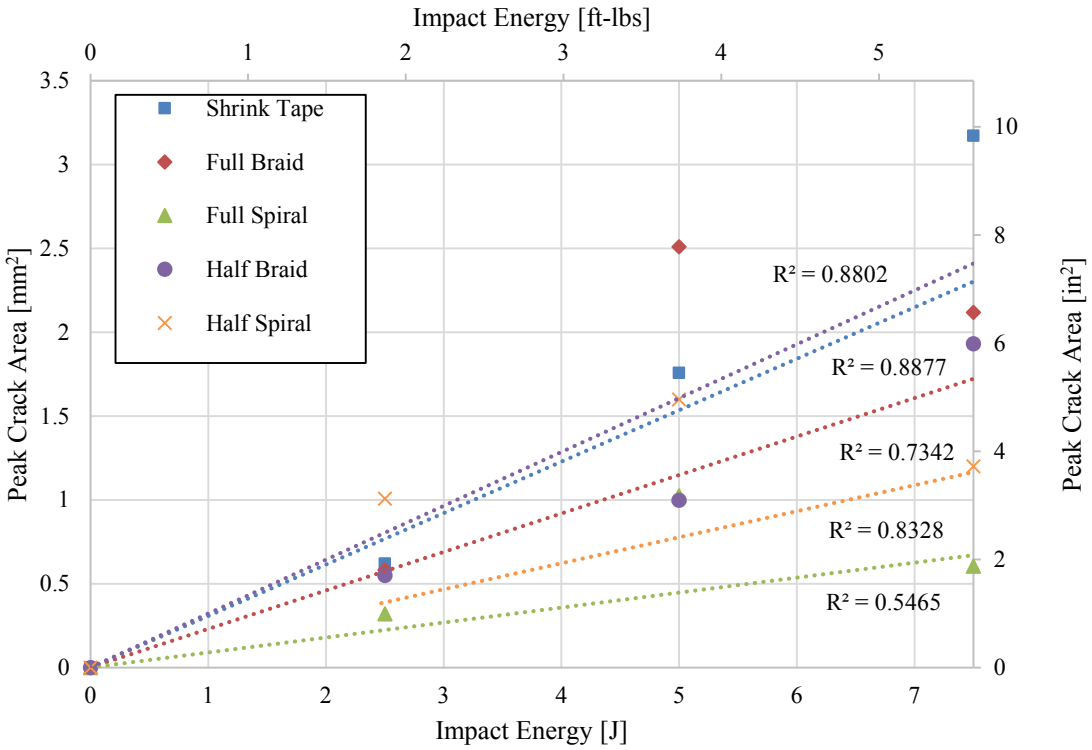

Figure 8.26 Linear Trendlines for Average Peak Crack Area vs. Impact Energy for All Sleeve Types

Table 8.9 Slopes of Linear Trendlines for Average Peak Crack Area vs. Impact Energy for All Sleeve Types for Lower Energy Levels

Sleeve	Slope
Full Braid	0.34
Half Braid	0.24
Full Spiral	0.12
Half Spiral	0.22
Shrink Tape	0.39

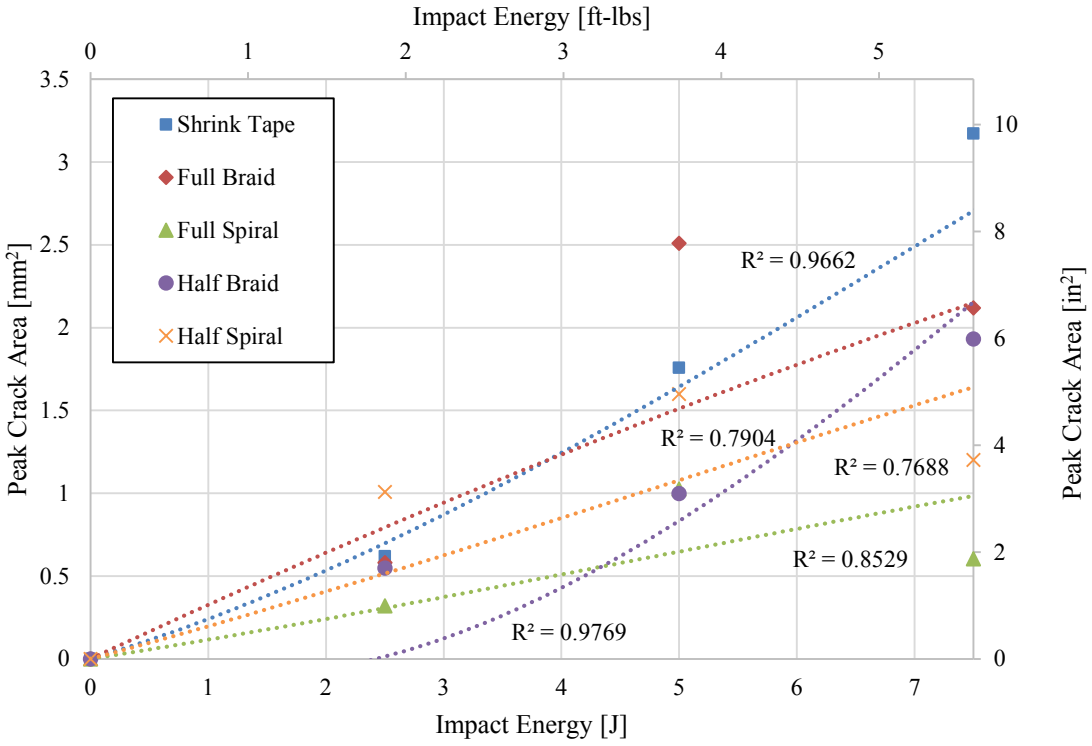

Figure 8.27 Nonlinear Trendlines for Average Peak Crack Area vs. Lower Impact Energy for All Sleeve Types

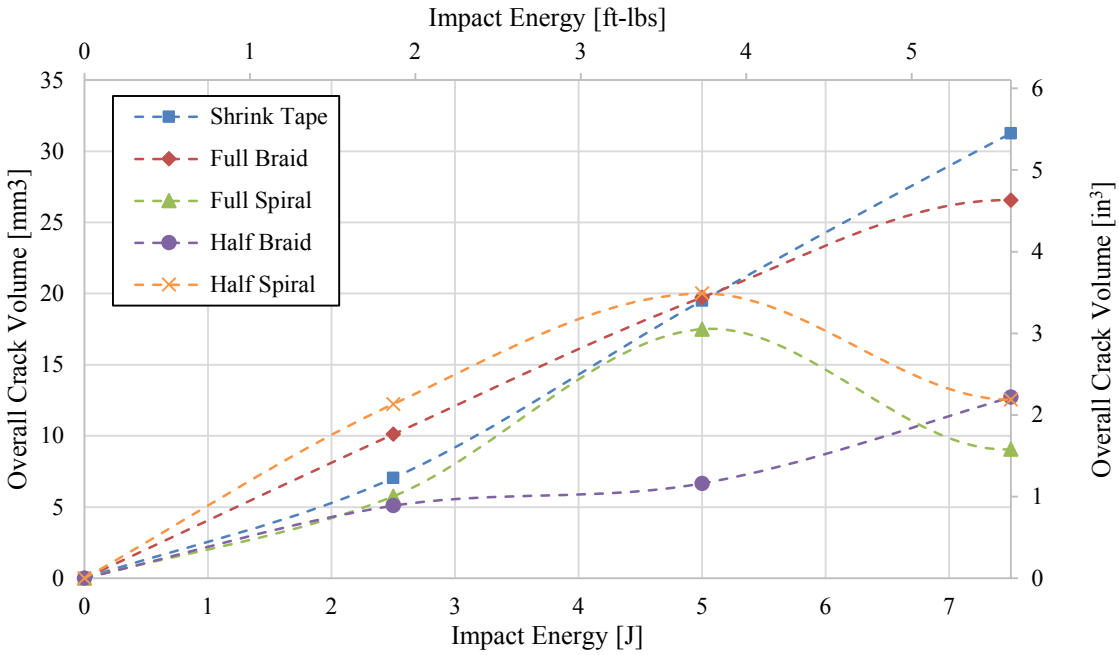

Figure 8.28 Best Fit Lines for Average Overall Crack Volume vs. Lower Impact Energy for All Sleeve Types

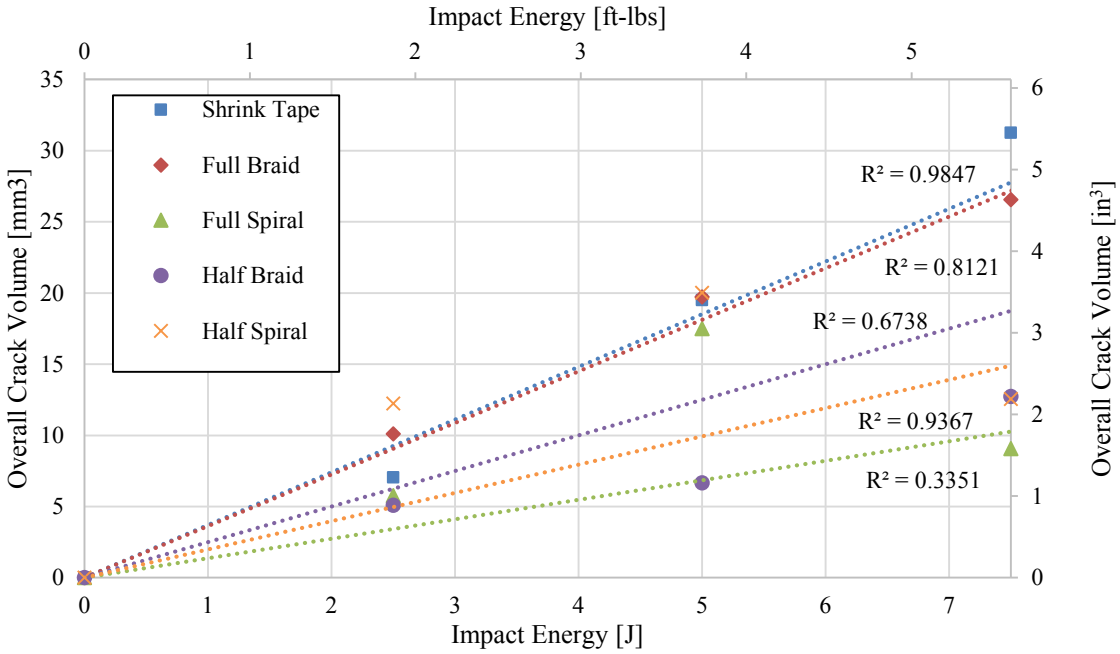

Figure 8.29 Linear Trendlines for Average Overall Crack Volume vs. Impact Energy for All Sleeve Types

Table 8.10 Slopes of Linear Trendlines for Average Overall Crack Volume vs. Impact Energy for All Sleeve Types for Lower Energy Levels

Sleeve	Slope
Full Braid	3.7
Half Braid	1.6
Full Spiral	1.9
Half Spiral	2.6
Shrink Tape	4.0

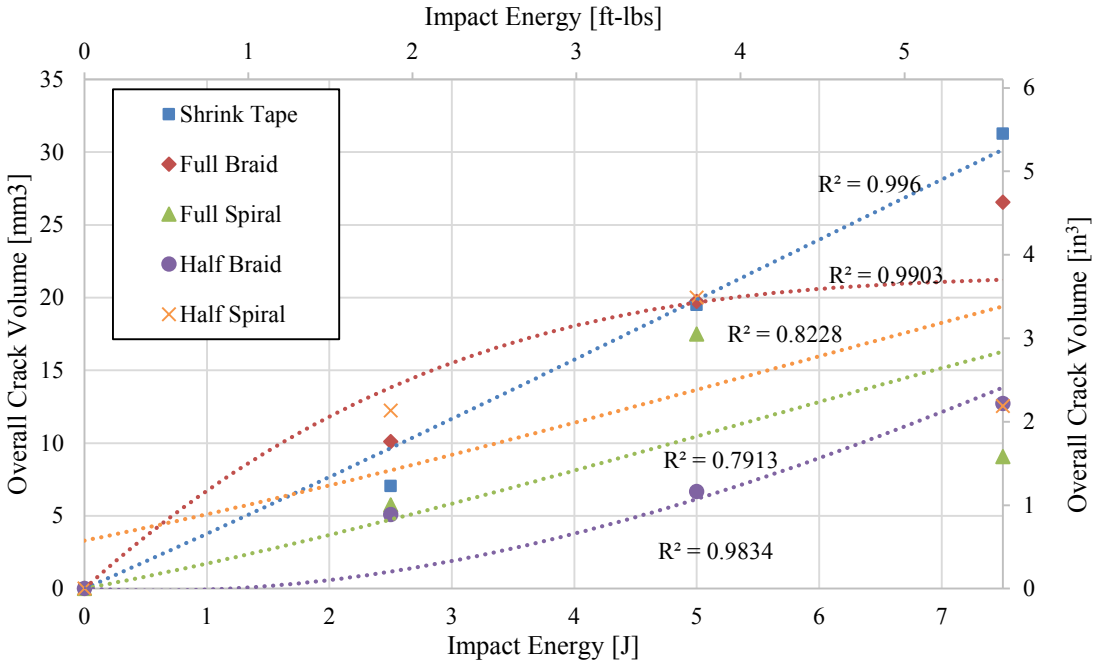

Figure 8.30 Nonlinear Trendlines for Average Overall Crack Volume vs. Lower Impact Energy for All Sleeve Types

9 CONCLUSIONS

This chapter presents general conclusions reached in the current research, and describes recommendations for future research. Micro-CT scans were completed to quantify the internal damage and compression tests were conducted to quantify the damage tolerance of unidirectional carbon fiber epoxy composite rods consolidated with various Nomex Thread and Shrink Tape sleeve configurations. The rod elements represent individual members of IsoTruss structures. Test variables include impact energy levels, sleeve type, sleeve material, and sleeve coverage.

9.1 General Conclusions

1. Nomex Thread sleeves are better at protecting the composite elements from damage than Shrink Tape sleeves. Both sleeves were comparable to Kevlar at no and low impact energy but yielded significantly lower compression strength at higher impact energy.
2. As impact energy increases, the peak crack area and overall crack volume increases. Shrink Tape sleeves increase in peak crack area and overall crack volume an average of twice as much as spiral Nomex Thread sleeves. There was on average an 80% increase in peak crack area and overall crack volume as impact energy increased between half and full sleeves.
3. There is a low correlation between decrease in residual strength as peak crack area and overall crack volume increase for the lower energy levels.

4. Peak crack area and overall crack volume can give a general idea of how much internal damage there is in a sample.

9.2 Conclusions Drawn from Comparison to Past Results

In general, the conclusions from related research by Allen and Sika [2] [3] on basalt/epoxy, carbon fiber/epoxy, and fiberglass/epoxy composites are equally applicable to carbon fiber epoxy composites. The comparison of conclusions drawn in the current research are as follows:

1. Co-curing dry fiber over unidirectional fiber/epoxy composites effectively consolidates the core materials. Shrink Tape is also an effective method for consolidating the core materials.
2. Unlike previous research, when undamaged, the ultimate compression strength and compression stiffness are affected by sleeve type (braid or spiral) for carbon/epoxy composites. This was most likely due to manufacturing anomalies.
3. Similar to Kevlar sleeves, increasing Nomex Thread sleeve coverage increases the damage tolerance of carbon composites.
4. Similar to past results, ultimate compression strength and compression stiffness after impact decrease with increasing impact energy levels.

9.3 Recommendations for Future Results

1. A stronger string than Nomex Thread should be used for consolidation. Kevlar has the necessary tensile strength, but it frays, so a different consolidation material should be identified. Alternatively, a better way to prevent the Kevlar from fraying should be investigated.
2. The bobbins should be cleaned and modified to improve the fiber release mechanism. The tension on the current bobbins would increase causing the Nomex Thread to break periodically,

slowing down the manufacturing process and causing the braided sleeves to be inconsistent, resulting in rough surfaces.

3. The bobbins could be modified further so that they can be used to apply Shrink Tape in more complex patterns (i.e., braided).
4. New braiding patterns should be developed that are more symmetric so that the core material does not get pulled into the side of the tube resulting in fraying.
5. Micro-CT scans should be performed prior to impact to compare the damage before and after impact.
6. A more in-depth analysis of the micro-CT scan images should be performed to get a better sense of the quantity of cracks and crack propagation, delaminations, and other forms of damage.
7. Micro-CT testing should be performed on specimens with different core materials (basalt, fiberglass, etc.)
8. Synchrotron radiation computed tomography (SRCT) or computed laminography (SRCL) could be used to get scans with the highest image quality, allowing damage micromechanisms to be studied in detail.

REFERENCES

[1] Strong, A. and Jensen, D., (2002), "The Ultimate Composite Structure," Composites Fabrication, pp. 22–27, Aug. 2002.

[2] Allen, D. (2011), "Damage Tolerance of Unidirectional Basalt Composites Encased in an Aramid Sleeve," M.S. Thesis, Brigham Young University, Provo, Utah.

[3] Sika, C. (2012), "Damage Tolerance of Unidirectional Carbon and Fiberglass Composites with Aramid Sleeves," M.S. Thesis, Brigham Young University, Provo, Utah.

[4] Embley, M. (2011), "Damage Tolerance of Buckling-Critical Unidirectional Carbon, Fiberglass, and Basalt Fiber Composites in Co-Cured Aramid Sleeves," M.S. Thesis, Brigham Young University, Provo, Utah.

[5] Kesler, S. (2006), "Consolidation and Interweaving of Composite Members by a Continuous Manufacturing Process," M.S. Thesis, Brigham Young University, Provo, Utah.

[6] Winkel, L. (2001), "Parametric Investigation of IsoTruss™ Geometry Using Linear Finite Element Analysis," M.S. Thesis, Brigham Young University, Provo, Utah.

[7] Scoresby, B. (2003), "Low Velocity Longitudinal and Radial Impact of IsoTruss™ Grid Structures," M.S. Thesis, Brigham Young University, Provo, Utah.

[8] McCune, A. (2001), "Tension and Compression of Carbon/Epoxy IsoTruss™ Grid Structures," M.S. Thesis, Brigham Young University, Provo, Utah.

[9] Stoutis, C. (2000), "Compression Testing of Pultruded Carbon Fibre-Epoxy Cylindrical Rods," Journal of Materials Science, Vol. 34, pp. 3441-3446.

[10] Hansen, S. (2004), "Influence of Consolidation and Interweaving on Compression Behavior of IsoTruss® Structures," M.S. Thesis, Brigham Young University, Provo, Utah.

[11] Wisnom, M. 1999 "Suppression of Splitting and Impact Sensitivity of Unidirectional Carbon-Fibre Composite Rods Using Tensioned Overwind," Composites Part A: Applied Science and Manufacturing, Vol. 30, No. 5, 1999, p. 661-665.

[12] Sika, C. A., D. W. Jensen, C. Garvin, and M. J. Jensen. 2012. "Compression Strength After Impact of Unidirectional Fiberglass Rods Consolidated with Aramid Sleeves," Proceedings of the 53rd AIAA/ASME/ASCE/ASC Structures, Structural Dynamics and Materials Conference, AIAA, Honolulu, HI, 11 pp., Apr. 23-26, 2012.

[13] Allen, D., D. Jensen, M. Embley, C. Garvin, and M. Jensen. 2011. "Compression Strength After Impact of Basalt Fiber Members in an Aramid Sleeve," SAMPE TECH Conference, Fort Worth, TX, Oct. 2011, 12 pp.

[14] Bull, D.J., Helfen, L., Sinclair, I., Spearing, S.M., Baumbach, T., "A Comparison of Multi-Scale 3D X-ray Tomographic Inspection Techniques for Assessing Carbon Fibre Composite Impact Damage," Composites Science and Technology 75 (2013) 55-61.

[15] Wright, P., Fu, X., Sinclair, I., Speaing, S.M., "Ultra High Resolution Computed Tomography of Damage in Notched Carbon Fiber-Epoxy Composites," Engineering Materials and Surface Engineering, School of Engineering Sciences University of Southampton, Southampton, SO17 1BJ, UK.

[16] Crupi, V., Epasto, G., Guglielmino, E., "Computed Tomography Analysis of Damage in Composites Subjected to Impact Loading," Department of Industrial Chemistry and Materials Engineering, University of Messina, Messina, Italy.

[17] TCR Composites (2013). "UF3369 TCRTM Resin Technical Data Sheet," Revision 13 http://www.tcrcomposites.com/pdfs/resindata/uf3369_v11_912.pdf

[18] The Thread Exchange (2016). "Nomex™ Thread Buying Guide," http://www.thethreadexchange.com/miva/merchant.mvc?Screen=CTGY&Store_Code=TTE&Category_Code=about_the_thread_exchange#

[19] Dunstone (2016). "Hi Shrink Tape," http://www.shrinktape.com/products/hi-shrink-tape/hi-shrink-tape.aspx

[20] Center for Quantitative Cancer Imaging (2016). "Pre-clinical Imaging," https://healthcare.utah.edu/huntsmancancerinstitute/research/center-for-quantitative-cancer-imaging/resources/pre-clinical-imaging.php

[21] Natrella, M.G., "Engineering Design Handbook: Experimental Statistics," U.S. Army Material Command, 1969.

[22] Embley, M. D., D. W. Jensen, D. N. Allen, C. Garvin, and M. J. Jensen, "Buckling Strength of Damaged Unidirectional Basalt Composite Rods with Braid Sleeves," Proceedings of the SAMPE TECH 2011 Conference, SAMPE, Fort Worth, TX, 15 pp., Oct. 17-20, 2011.

[23] Jensen, M. J., D. W. Jensen, and A. D. Howcroft. 2010. "Continuous Manufacturing of Cylindrical Composite Lattice Structures," Recent Advances in Textile Composites (Proceedings of the 10th International Conference on Textile Composites-EXCOMP10), edited by Christophe Binetruy and Francois Boussu, DEStech Publications, Inc., 4th Quarter/Autumn, October 2010, pp. 80-87.

[24] Asay, B., "Bending Behavior of Carbon/Epoxy Composite IsoBeam Structures," M.S. Thesis, Brigham Young University, Provo, Utah.

[25] Jensen, D. W. 2000. "A Glimpse Into the World of Innovative Composite IsoTrussTM Grid Structures," SAMPE Journal, Vol. 36, No. 5, Sep./Oct. 2000 pp.8-16.

[26] Jensen, D. W. 2004. "Manufacturing Small Diameter IsoTruss® Lattice Structures for Mountain Bike Frames," The 15th SICOMP Conference on Manufacturing and Design of Composites, Sarohus, Gothenburg, Sweden, Sep. 27–28, 2004.

[27] Jensen, D. W. 2010. "Automated Continuous Manufacturing of Composite Grid Structures," ABSTRACTS, The 21st Annual International SICOMP Conference on Manufacturing and Design of Composites, Swerea SICOMP, June 2010, 2 pp..

[28] Jensen, D. W. 2010. "Using External Robots Instead of Internal Mandrels to Produce Composite Lattice Structures," Recent Advances in Textile Composites (Proceedings of the 10th International Conference on Textile Composites—TEXCOMP10), edited by Christophe Binetruy and Francois Boussu, DEStech Publications, Inc., 4th Quarter/Autumn, October 2010, pp. 88-94.

[29] Kesler, S. L. and D. W. Jensen. 2007. "Consolidation and Interweaving of Composite Members by a Continuous Manufacturing Process," Digital Proceedings of the 6th International Conference on Composite Science and Technology, Durban, South Africa, ISBN: 1-86840-642-3, Jan. 22-24, 2007, 15 pp..

[30] Hansen, S. M. and D. W. Jensen. 2004. "Influence of Consolidation and Interweaving On Compression Behavior of IsoTruss™ Structures," Proceedings of the Design and Nature 2004 Conference, Rhodes, Greece, Jun. 28–30, 2004. Also published in Transactions of Wessex Institute, online, ISSN: 1744-7151.

[31] Allen, D. N., D. W. Jensen, M. D. Embley, and M. J. Jensen, "Influence of Braided Sleeves on the Impact Damage of Cylindrical Unidirectional Elements," Proceedings of the 18TH International Conference on Composite Materials, International Committee on Composite Materials, www.iccm-central.org/index.htm, Jeju, Korea Republic, 6 pp., Aug. 21-26, 2011.

[32] Embley, M. D., D. W. Jensen, C. Garvin, and M. J. Jensen. 2012. "Influence of Consolidating Sleeves and Geometric Scale on Buckling After Impact of Basalt Columns," Proceedings of the 53rd AIAA/ASME/ASCE/ASC Structures, Structural Dynamics and Materials Conference, AIAA, Honolulu, HI, 11 pp., Apr. 23-26, 2012.

[33] Hartness, J., P. Sjoblom, T. Cordell. 1988. "On Low-Velocity Impact Testing of Composite Materials." Journal of Composite Materials, Vol. 22, No. 1, 1988, pp. 30-52.

[34] Stanford, L., and Jensen, D. "Correlating Impact, Micro-CT Inspection, and Residual Strength of Carbon/Epoxy Rods," 57th AIAA/ASCE/AHS/ASC Structures, Structural Dynamics, and Materials Converece, AIAA SciTech, (AIAA 2016-2183), 14 pp. http://dx.doi.org/10.2514/6.2016-2183

[35] Jensen, D. W., C. A. Sika, K. Hinds, and M. J. Jensen, "Compression Strength After Impact of Unidirectional Carbon/Epoxy Rods Consolidated with Aramid Sleeves," Proceedings of the ASC 28th Technical Conference, ASC, State College, PA, 14 pp., Sep. 9-11, 2013.

[36] Jensen, M. J., A. D. Howcroft, and D. W. Jensen, "Design of an IsoTruss Aircraft Strut," Proceedings of the SAMPE TECH 2011 Conference, SAMPE, Long Beach, CA, 8 pp., May 23-26, 2011.

[37] Jensen, D. and Hinds, K., (2015). "Shear-Dominated Bending Behavior of Carbon/Epoxy Composite Lattice IsoBeam Structures", 20th International Conference on Composite Materials, July 2015.

[38] Jensen, D. W. and M. E. Rackliffe, "Ultra-Lightweight IsoTruss™ Grid Structures," Experimental Techniques and Design in Composite Materials 6, University of Padova, Vicenza, Italy, p. 53, Jun. 18–20, 2003.

[39] Jensen, D. W. and A. M. McCune, "Axial Performance of IsoTruss Grid Structures," Proceedings of the 8th Annual International Conference on Composites Engineering, Tenerife, Canary Islands, Spain, International Community for Composites Engineering and College of Engineering, University of New Orleans, New Orleans, LA, pp. 399–400, Aug. 5–11, 2001.

APPENDIX A. PICTURES OF SPECIMENS AFTER FAILURE

Appendix A contains failure pictures of all tested specimens investigated in this research. Figure A.1 and Figure A.2 show full braided and half braided sleeves of carbon/epoxy elements, respectively. Full and half spiral carbon specimens are shown in Figure A.3 and Figure A.4, respectively. Figure A.5 show shrink tape sleeves of carbon/epoxy elements.

Figure A.1: Pictures of Half Braid Specimens After Failure

FB 1-5-20

FB 3-6-20

FB 2-2-7.5

FB 3-5-20

FB 4-6-2.5

FB 5-2-10

FB 4-5-15

FB 3-9-20

FB 4-8-5

FB 3-7-0

FB 1-4-7.5

FB 2-1-15

FB 2-3-7.5

FB 3-4-0

FB 4-10-2.5

FB 1-6-10

FB 2-4-15

FB 1-1-15

FB 4-4-5

FB 4-2-20

FB 4-3-2.5

FB 3-8-10

FB 4-9-5

FB 1-3-7.5

FB 5-1-2.5

FB 2-6-15

FB 3-2-10

FB 3-1-7.5

FB 4-7-0

Figure A.2 Pictures of Full Braid Specimens After Failure

FB 2-5-10

FB 3-3-15

Figure A.2 (cont.): Pictures of Full Braid Specimens After Failure

Figure A.3: Pictures of Half Spiral Specimens After Failure

HS 4-2-7.5

HS 4-1-15

HS 4-3-2.5

HS 4-4-2.5

HS 3-6-5

HS 4-8-2.5

HS 1-1-0

HS 1-2-20

HS 1-3-0

HS 1-5-20

Figure A.3 (cont.): Pictures of Half Spiral Specimens After Failure

HS 1-6-20

HS 1-7-20

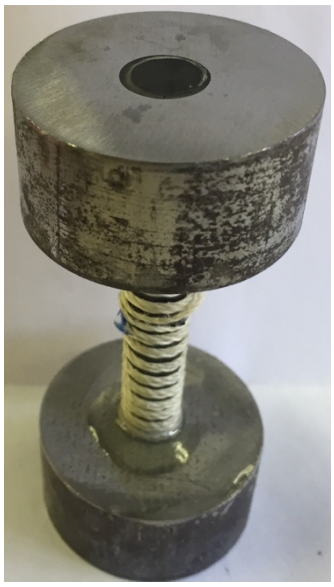

HS 1-9-20

HS 1-10-15

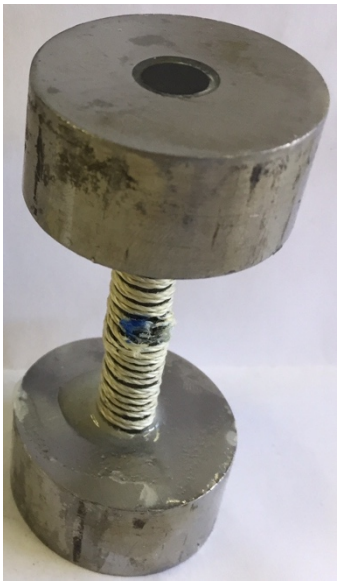

HS 4-4-5

HS 4-9-2.5

HS 4-6-2.5

Figure A.3: Pictures of Half Spiral Specimens After Failure

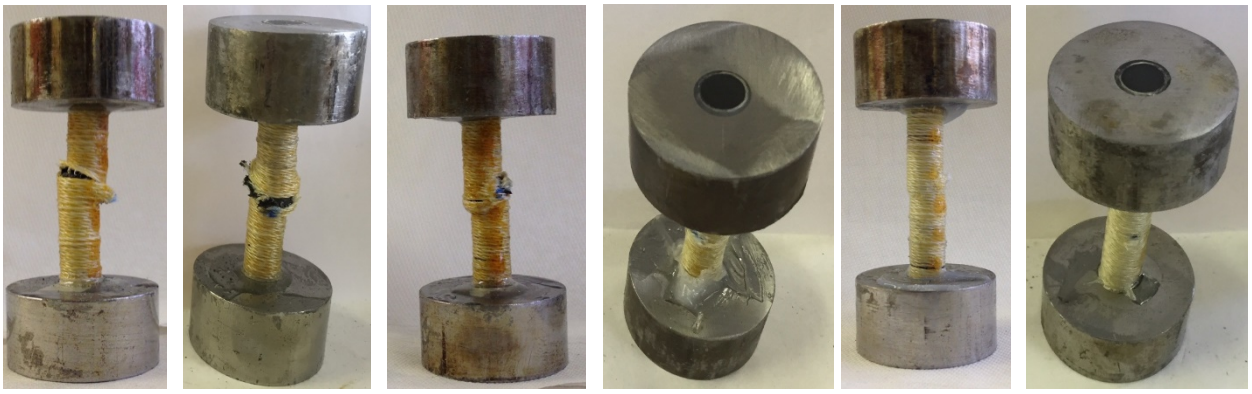

FS 1-3-7.5 FS 1-4-15 FS 1-7-7.5 FS 1-10-7.5 FS 2-2-5 FS 2-3-0

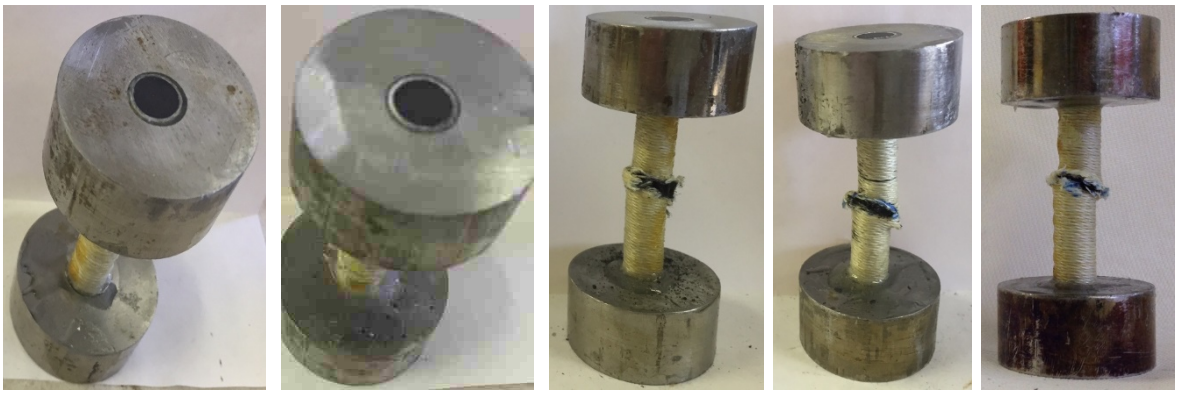

FS 2-4-5 FS 2-6-0 FS 2-7-10 FS 2-9-10 FS 2-10-7.5

FS 3-2-10 FS 3-5-2.5 FS 3-6-10 FS 3-8-2.5

Figure A.4: Pictures of Full Spiral Specimens After Failure

FS 4-4-0 **FS 4-5-7.5**

Figure A.4 (cont.): Pictures of Full Spiral Specimens After Failure

ST 1-1-0

ST 1-1-7.5

ST 1-3-10

ST 4-10-15

ST 1-4-10

ST 1-6-15

ST 1-7-15

ST 1-8-15

Figure A.5: Pictures of Shrink Tape Specimens After Failure

ST 2-1-0

ST 2-1-2.5

ST 2-2-7.5

ST 3-11-5

ST 2-2-7.5

ST 2-4-7.5

ST 2-5-20

ST 3-1-10

Figure A.5 (cont.): Pictures of Shrink Tape Specimens After Failure

ST 2-6-5

ST 2-7-10

ST 2-8-0

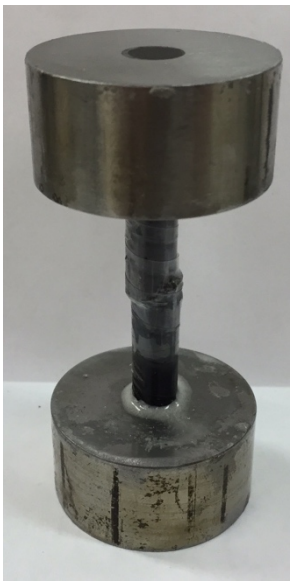

ST 2-11-2.5

ST 2-8-2.5

ST 2-9-20

ST 4-2-20

Figure A.5 (cont.): Pictures of Shrink Tape Specimens After Failure

ST 2-10-20

ST 3-2-2.5

ST 3-1-10

ST 3-2-2.5

ST 3-3-2.5

Figure A.5 (cont.): Pictures of Shrink Tape Specimens After Failure

ST 3-4-10

ST 3-6-5

ST 3-5-15

ST 3-11-5

ST 3-7-15

ST 4-9-0

Figure A.5 (cont.): Pictures of Shrink Tape Specimens After Failure

ST 3-9-15

ST 4-6-5

ST 4-6-5

ST 3-9-7.5

ST 4-4-0

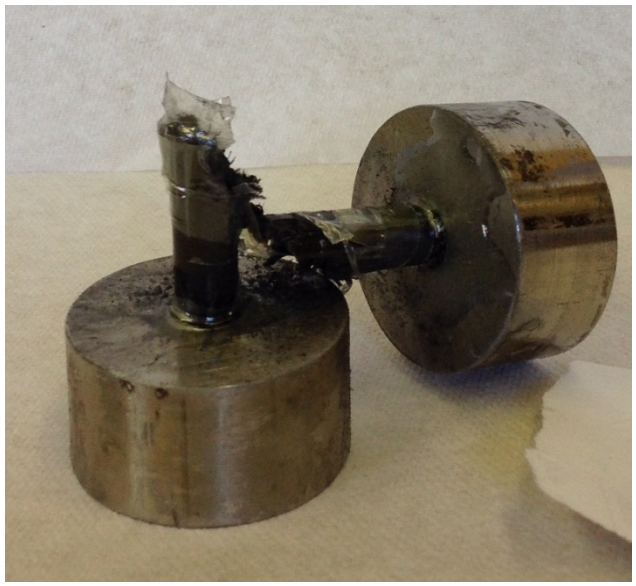

ST 5-1-20

Figure A.5 (cont.): Pictures of Shrink Tape Specimens After Failure

APPENDIX B. CROSS-SECTIONAL AREAS

Appendix B contains cross-sectional area microscopic and micro-CT measurements for specimens in this research. Cross-sectional areas for full braid, half braid, full spiral, half spiral, and shrink tape sleeve are shown in Table B.1-Table B.5, respectively.

Table B.1: Cross-Sectional Area Measurements for Specimens with Full Braided Sleeves

Specimen I.D.	Microscope Area		Micro-CT Area							
			Area 1		Area 2		Area 3		Micro-CT Average	
	[mm^2]	[in^2)]	[mm^2]	[in^2)]	[mm^2]	[in^2)]	[mm^2]	[in^2)]	[mm^2]	[in^2)]
N-FB-1-2			51.99	0.0806	52.21	0.0809	50.06	0.0776	51.42	0.0797
N-FB-1-3	53.87	0.0835							-	-
N-FB-1-4			49.25	0.0763	47.47	0.0736	52.92	0.082	49.88	0.0773
N-FB-1-5			52.96	0.0821	53.55	0.083	55.34	0.0858	53.95	0.0836
N-FB-1-6			51.42	0.0797	50.96	0.079	52.55	0.0815	51.64	0.0801
N-FB-2-3	56.12	0.087	53.57	0.083	52.53	0.0814	52.39	0.0812	52.83	0.0819
N-FB-2-4			50.76	0.0787	49.04	0.076	50.32	0.078	50.04	0.0776
N-FB-2-5			56.55	0.0877	54.33	0.0842	57.52	0.0891	56.13	0.0870
N-FB-2-6			49.75	0.0771	52.89	0.082	53.85	0.0835	52.16	0.0809
N-FB-3-1			51.83	0.0803	51.49	0.0798	52.89	0.082	52.07	0.0807
N-FB-3-5			52.07	0.0807	50.31	0.078	51.55	0.0799	51.31	0.0795
N-FB-3-6			49.06	0.076	49	0.076	52.79	0.0818	50.28	0.0779
N-FB-3-7	50.7	0.0786							-	-
N-FB-3-8			51.8	0.0803	52.46	0.0813	50.91	0.0789	51.72	0.0802
N-FB-4-2			50.04	0.0776	50.78	0.0787	49.94	0.0774	50.25	0.0779
N-FB-4-3			53.55	0.083	53.8	0.0834	53.63	0.0831	53.66	0.0832
N-FB-4-4			55.43	0.0859	54.45	0.0844	58.56	0.0908	56.15	0.0870
N-FB-4-8			51.91	0.0805	52.03	0.0806	51.58	0.08	51.84	0.0804
N-FB-4-9	53.33	0.0827							-	-
N-FB-4-10			52.52	0.0814	51.82	0.0803	52.98	0.0821	52.44	0.0813
N-FB-5-2	56.17	0.0871	49.13	0.0761	51.7	0.0801	52.75	0.0818	51.19	0.0793

Table B.2: Cross-Sectional Area Measurements for Specimens with Half Braided Sleeves

Specimen I.D.	Microscope Area		Micro-CT Area							
			Area 1		Area 2		Area 3		Micro-CT Average	
	[mm^2]	[in^2)]	[mm^2]	[in^2)]	[mm^2]	[in^2)]	[mm^2]	[in^2)]	[mm^2]	[in^2)]
N-HB-1-2			53.61	0.0831	50.87	0.0789	51.39	0.0797	51.96	0.0806
N-HB-1-3			48.43	0.0751	50.9	0.0789	50.97	0.079	50.10	0.0777
N-HB-1-5			48.79	0.0756	55.01	0.0853	51.65	0.0801	51.82	0.0803
N-HB-1-6			52.13	0.0808	50.51	0.0783	53.18	0.0824	51.94	0.0805
N-HB-1-7			55.94	0.0867	52.01	0.0806	53.16	0.0824	53.70	0.0832
N-HB-1-8	51.48	0.0798	51.74	0.0802	50.15	0.0777	51.04	0.0791	50.98	0.0790
N-HB-1-9			54.29	0.0842	52.66	0.0816	52.7	0.0817	53.22	0.0825
N-HB-1-10			54.47	0.0844	52.55	0.0815	53	0.0822	53.34	0.0827
N-HB-2-1			52.16	0.0808	52.38	0.0812	52.15	0.0808	52.23	0.0809
N-HB-2-2			53.71	0.0833	54.44	0.0844	53.14	0.0824	53.76	0.0834
N-HB-2-3			51.89	0.0804	50.01	0.0775	52.38	0.0812	51.43	0.0797
N-HB-2-4	53.73	0.0833	51.27	0.0795	53.22	0.0825	52.99	0.0821	52.49	0.0814
N-HB-2-6			52.58	0.0815	53.92	0.0836	54.6	0.0846	53.70	0.0832
N-HB-2-7			59.54	0.0923	59.95	0.0929	63.45	0.0984	60.98	0.0945
N-HB-3-3	52.59	0.0815	51.86	0.0804	52.7	0.0817	52.87	0.082	52.48	0.0814
N-HB-3-11			49.82	0.0772	52.33	0.0811	54.91	0.0851	52.35	0.0811
N-HB-4-2			52.63	0.0816	51.23	0.0794	52.33	0.0811	52.06	0.0807
N-HB-4-5	55.59	0.0862	53.04	0.0822	53.48	0.0829	52.92	0.082	53.15	0.0824

Table B.3: Cross-Sectional Area Measurements for Specimens with Full Spiral Sleeves

Specimen I.D.	Microscope Area		Micro-CT Area							
			Area 1		Area 2		Area 3		Micro-CT Average	
	[mm^2	(in^2)]	[mm^2	(in^2)]	[mm^2	(in^2)]	[mm^2	(in^2)]	[mm^2	(in^2)]
N-FS-1-1	57.71	0.0895	60.91	0.0944	61.07	0.0947	60.65	0.0940	60.88	0.0944
N-FS-1-3			60.66	0.0940	60.66	0.0940	61.52	0.0954	60.95	0.0945
N-FS-1-4			61.23	0.0949	59.91	0.0929	61.27	0.0950	60.80	0.0943
N-FS-1-6			60.24	0.0934	59.36	0.0920	60.44	0.0937	60.01	0.0930
N-FS-1-8			60.59	0.0939	59.27	0.0919	61.66	0.0956	60.51	0.0938
N-FS-1-9			61.65	0.0956	58.95	0.0914	60.86	0.0943	60.49	0.0938
N-FS-1-10			61.47	0.0953	60.18	0.0933	61.94	0.0960	61.20	0.0949
N-FS-2-1			58.81	0.0912	60.66	0.0940	61.11	0.0947	60.19	0.0933
N-FS-2-2			59.93	0.0929	61.31	0.0950	60.47	0.0937	60.57	0.0939
N-FS-2-5	57.9	0.0898							-	-
N-FS-2-8			61.15	0.0948	60.39	0.0936	60.13	0.0932	60.56	0.0939
N-FS-2-9			59.62	0.0924	60.13	0.0932	59.27	0.0919	59.67	0.0925
N-FS-3-1			59.32	0.0919	59.81	0.0927	60.44	0.0937	59.86	0.0928
N-FS-3-2			61.31	0.0950	59.94	0.0929	61.12	0.0947	60.79	0.0942
N-FS-3-4			59.57	0.0923	59.89	0.0928	60.67	0.0940	60.04	0.0930
N-FS-3-5			59.06	0.0915	59.82	0.0927	61.13	0.0947	60.00	0.0930
N-FS-3-8	57.89	0.0897	60.02	0.0930	59.33	0.0920	59.33	0.0920	59.56	0.0923
N-FS-4-1	57.4	0.089							-	-
N-FS-4-3			61.67	0.0956	60.82	0.0943	59.66	0.0925	60.72	0.0941
N-FS-5-1	57.41	0.089							-	-

Table B.4: Cross-Sectional Area Measurements for Specimens with Shrink Tape Sleeves

Specimen I.D.	Microscope Area		Micro-CT Area							
			Area 1		Area 2		Area 3		Micro-CT Average	
	[mm^2	(in^2)]	[mm^2	(in^2)]	[mm^2	(in^2)]	[mm^2	(in^2)]	[mm^2	(in^2)]
N-HS-1-2			58.48	0.0906	59.12	0.0916	58.05	0.09	58.55	0.0907
N-HS-1-5	58.97	0.0914							-	-
N-HS-1-9			56.8	0.088	57.34	0.0889	58.85	0.0912	57.66	0.0894
N-HS-1-10			53.96	0.0836	54.43	0.0844	55.15	0.0855	54.51	0.0845
N-HS-2-3			58.41	0.0905	58.23	0.0903	57.91	0.0898	58.18	0.0902
N-HS-2-4			56.24	0.0872	57.82	0.0896	58.51	0.0907	57.52	0.0892
N-HS-2-8	57.86	0.0897							-	-
N-HS-2-9			56.51	0.0876	55.43	0.0859	56.52	0.0876	56.15	0.0870
N-HS-3-2			58.18	0.0902	57.11	0.0885	56.96	0.0883	57.42	0.0890
N-HS-3-3	56.36	0.0874	57.97	0.0898	58.56	0.0908	59.05	0.0915	58.53	0.0907
N-HS-3-4			58.27	0.0903	57.95	0.0898	58.83	0.0912	58.35	0.0904
N-HS-3-7			58.62	0.0909	59.6	0.0924	60.62	0.094	59.61	0.0924
N-HS-3-10			58.13	0.0901	57.43	0.089	59.95	0.0929	58.50	0.0907
N-HS-4-1			55.14	0.0855	54.86	0.085	55.51	0.086	55.17	0.0855
N-HS-4-2			59.29	0.0919	57.68	0.0894	59.56	0.0923	58.84	0.0912
N-HS-4-3			57.34	0.0889	58.63	0.0909	61.9	0.096	59.29	0.0919
N-HS-4-4			62.55	0.0969	59.92	0.0929	60.94	0.0945	61.14	0.0948
N-HS-4-5			59.92	0.0929	58.98	0.0914	59.52	0.0923	59.47	0.0922
N-HS-4-8	58.29	0.0904	62.82	0.0974	62.55	0.0969	58.64	0.0909	61.34	0.0951

Table B.5: Cross-Sectional Area Measurements for Specimens with Shrink Tape Sleeves

Specimen I.D.	Microscope Area		Micro-CT Area							
			Area 1		Area 2		Area 3		Average	
	[mm^2	(in^2)]	[mm^2	(in^2)]	[mm^2	(in^2)]	[mm^2	(in^2)]	[mm^2	(in^2)]
ST-2-1			56.46	0.0875	58.68	0.0909	57.71	0.0895	57.62	0.0893
ST-2-11			57.88	0.0897	55.57	0.0861	56.26	0.0872	56.57	0.0877
ST-3-3	56.02	0.0868	58.01	0.0899	58.03	0.0899	57.38	0.0889	57.36	0.0889
ST-1-7	56.06	0.0869	56.97	0.0883	56.71	0.0879	55.8	0.0865	56.39	0.0874
ST-3-6			57.44	0.089	56.5	0.0876	58.34	0.0904	57.43	0.089
ST-3-11			58.66	0.0909	59.29	0.0919	55.14	0.0855	57.69	0.0894
ST-2-2			58.59	0.0908	57.2	0.0887	58.36	0.0905	58.05	0.09
ST-2-5			59.29	0.0919	59.31	0.0919	58.58	0.0908	59.06	0.0915
ST-3-9			56.75	0.088	57.38	0.0889	58.64	0.0909	57.59	0.0893
ST-2-8			53.99	0.0837	58.34	0.0904	58.68	0.0909	57	0.0883
ST-1-3			56.47	0.0875	56.4	0.0874	57.05	0.0884	56.64	0.0878
ST-3-4			54.57	0.0846	55.18	0.0855	58.35	0.0904	56.04	0.0869
ST-1-4			53.97	0.0836	56.15	0.087	56.75	0.088	55.62	0.0862
ST-3-7			56.77	0.088	57.37	0.0889	57.99	0.0899	57.38	0.0889
ST-1-8			53.65	0.0832	55.49	0.086	55.5	0.086	54.88	0.0851
ST-4-10	54.57	0.0846	55.83	0.0865	55.21	0.0856	56.75	0.088	55.59	0.0862
ST-1-10			55.83	0.0865	55.85	0.0866	56.46	0.0875	56.05	0.0869
ST-4-2			55.34	0.0858	55.8	0.0865	55.35	0.0858	55.5	0.086
ST-2-9	56.28	0.0872	55.16	0.0855	57.22	0.0887	58.99	0.0914	56.91	0.0882

APPENDIX C. MICROSCOPIC MEASUREMENTS

A summary of the measured void ratios and fiber volume fractions with the respective averages and standard deviations for full braid, full spiral, half braid, half spiral, and shrink tape, specimens are given in Table C.1 through C.5, respectively. Photographs that were used by the PAX-it computer software to find the measured void ratio (50x magnification) and measured fiber volume fraction (500x magnification) at three separate areas of the end of a representative specimen from each batch for full braid, full spiral, half braid, half spiral, and shrink tape specimens are given in Figures C.1-C.22, respectively.

Table C.1: Summary of Microscopic Measurements of Full Braided Specimens

Batch	Area	Average Measured Void Ratio [%]	Average Measured Fiber Volume Fraction [%]
1	1	0.04	64.7
	2	0.07	65.4
	3	0.09	60.4
2	1	0.06	66.9
	2	0.09	55.9
	3	0.07	60.9
3	1	0.03	65.5
	2	0.03	67.9
	3	0.05	57.2
4	1	0.08	61.5
	2	0.11	60.9
	3	0.10	67.6
5	1	0.04	71.6
	2	0.03	68.8
	3	0.03	71.9
Average		0.06	64.5
St. Dev.		0.03	4.9

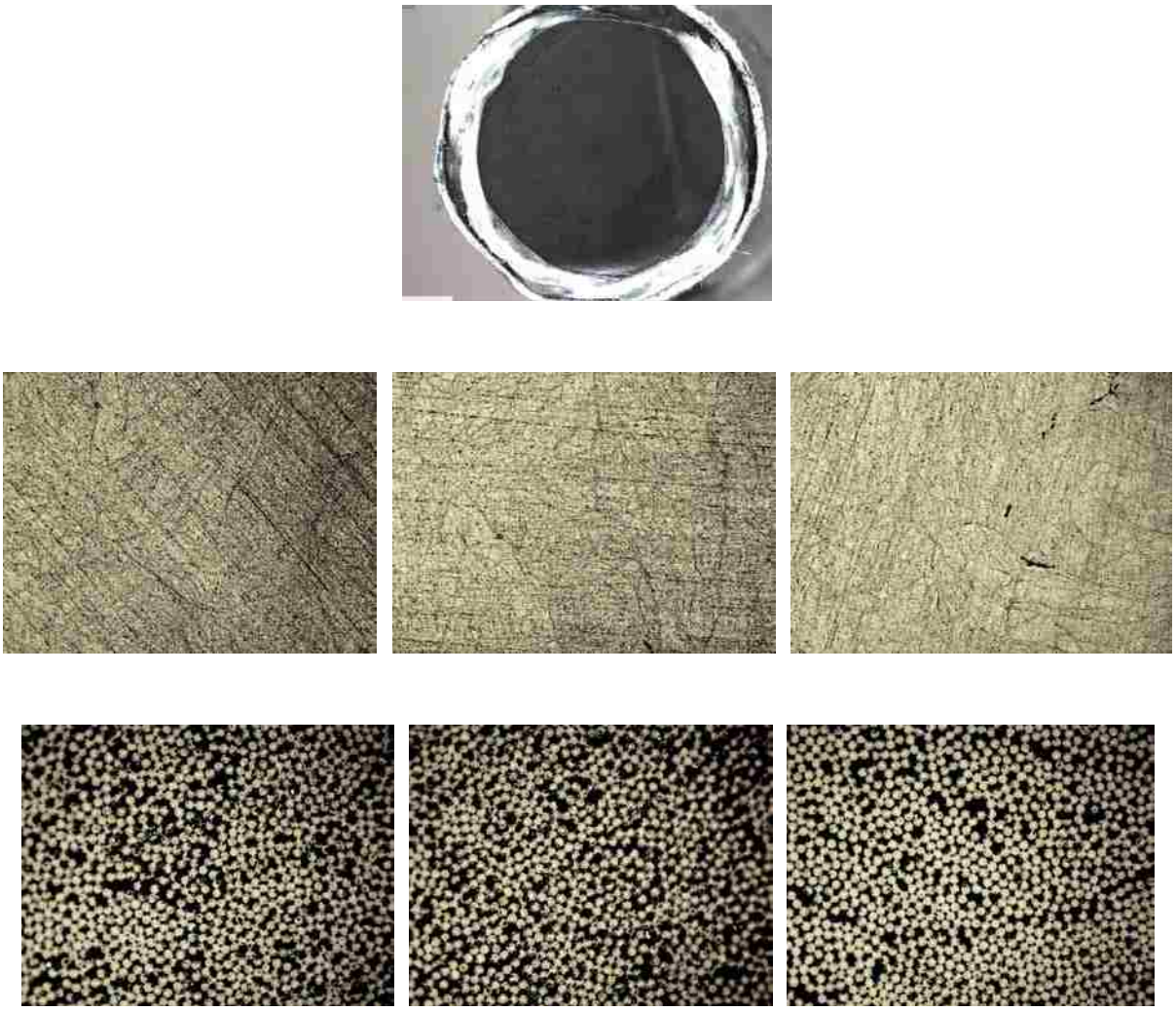

Figure C.1: FB-1-3-7.5 at 10x Magnification (top), 50x Magnification (middle), and 500x Magnification (bottom)

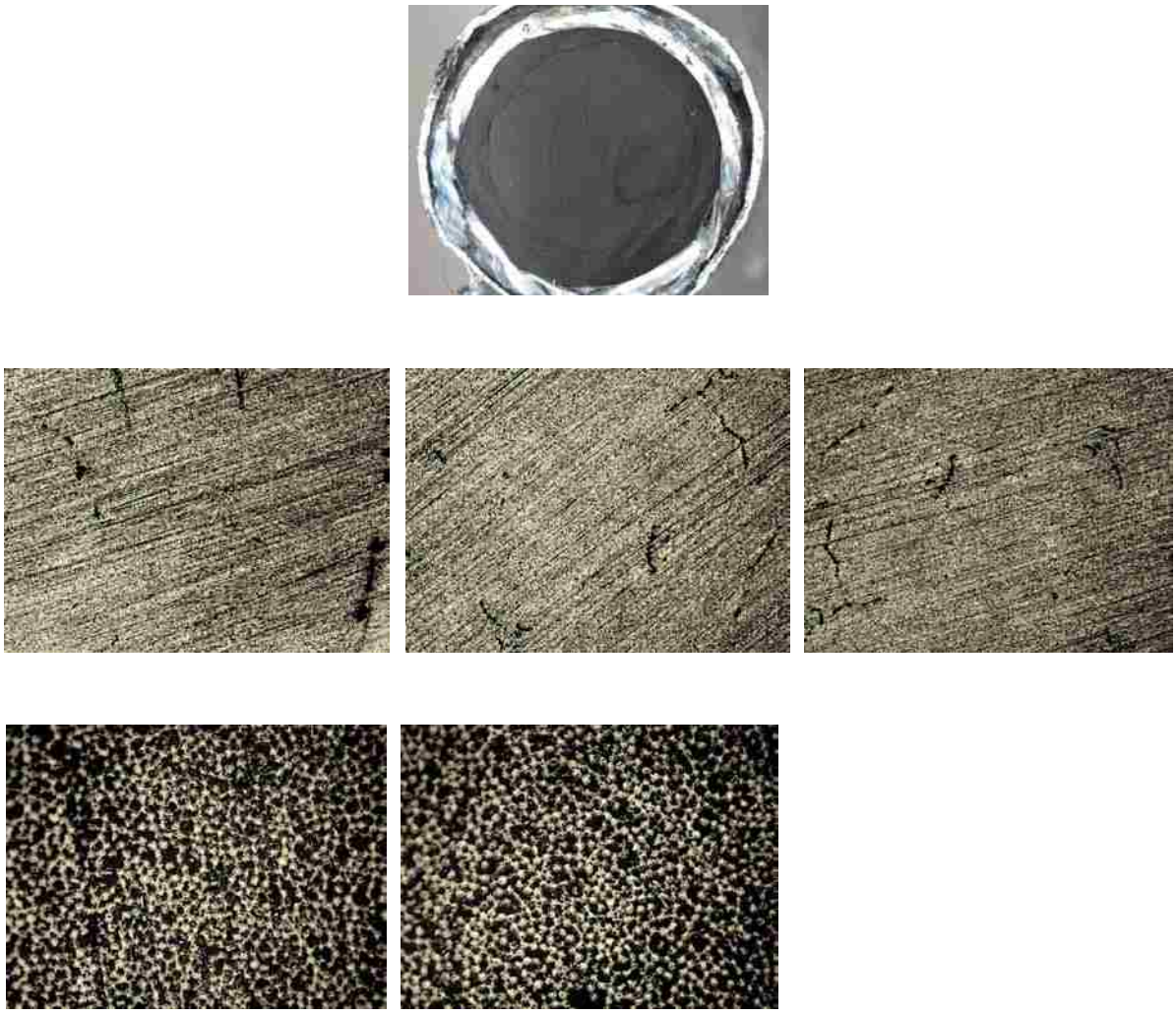

Figure C.2: FB-2-3-7.5 at 10x Magnification (top), 50x Magnification (middle), and 500x Magnification (bottom)

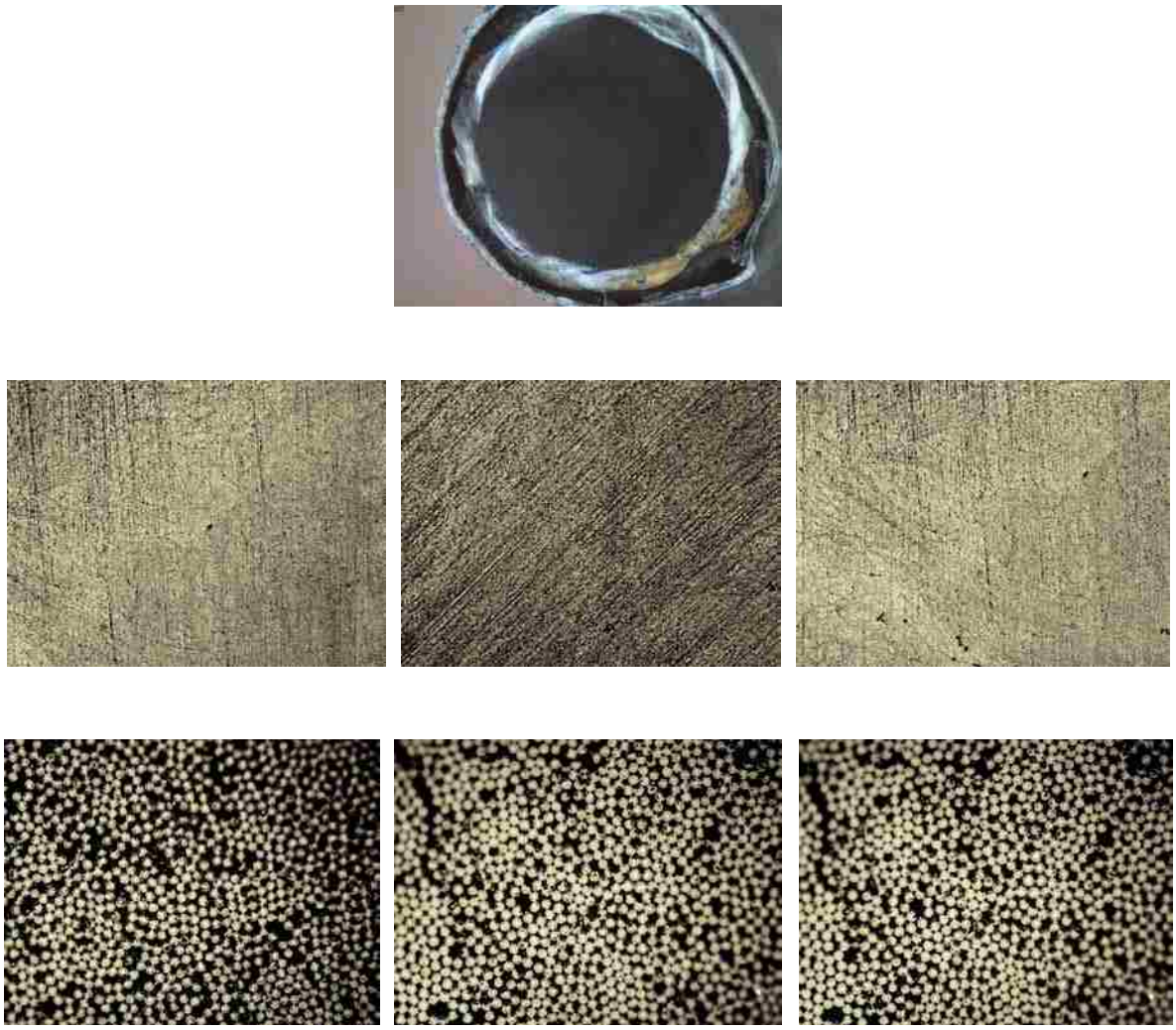

Figure C.3: FB-3-7-0 at 10x Magnification (top), 50x Magnification (middle), and 500x Magnification (bottom)

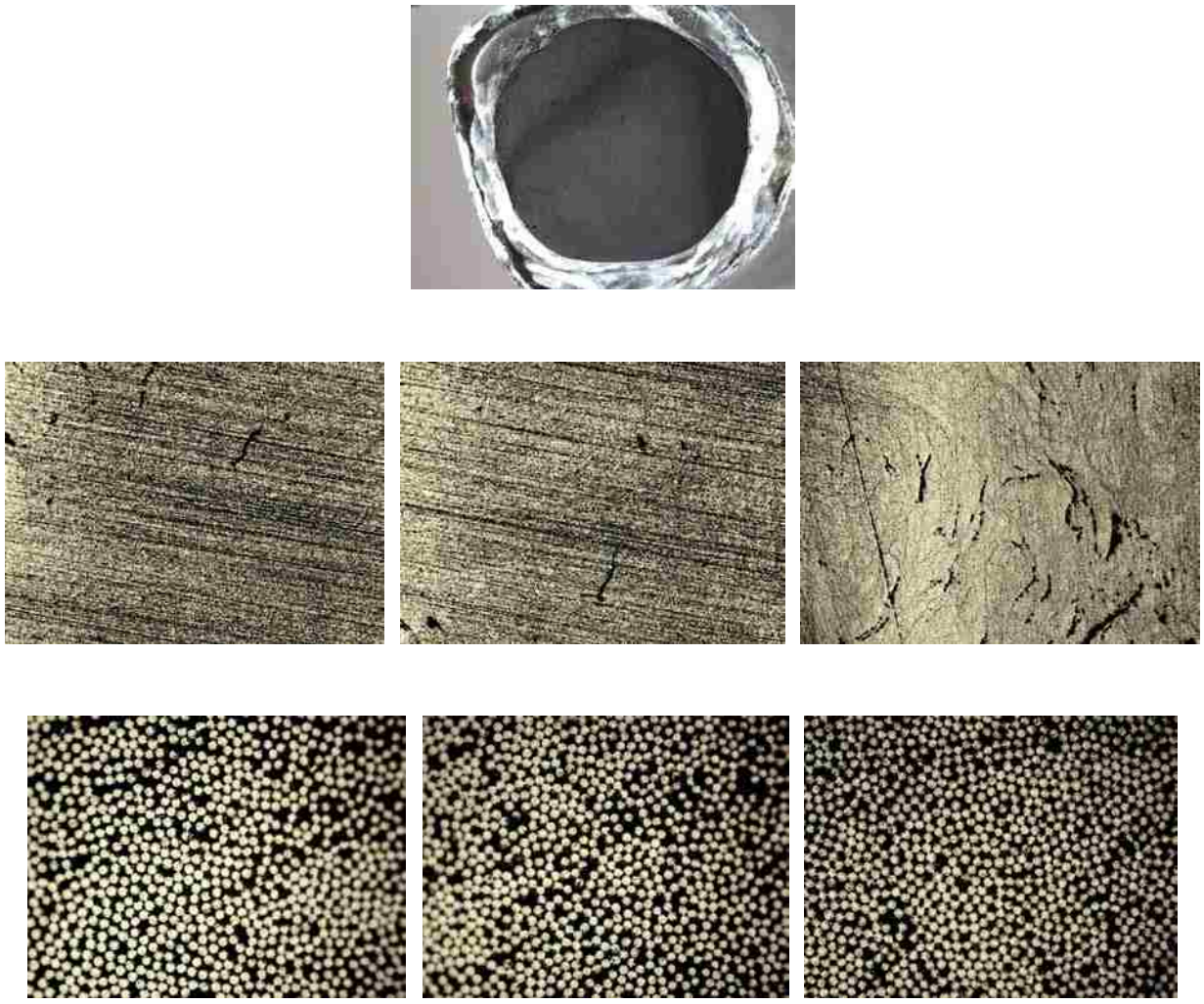

Figure C.4: FB-4-9-5 at 10x Magnification (top), 50x Magnification (middle), and 500x Magnification (bottom)

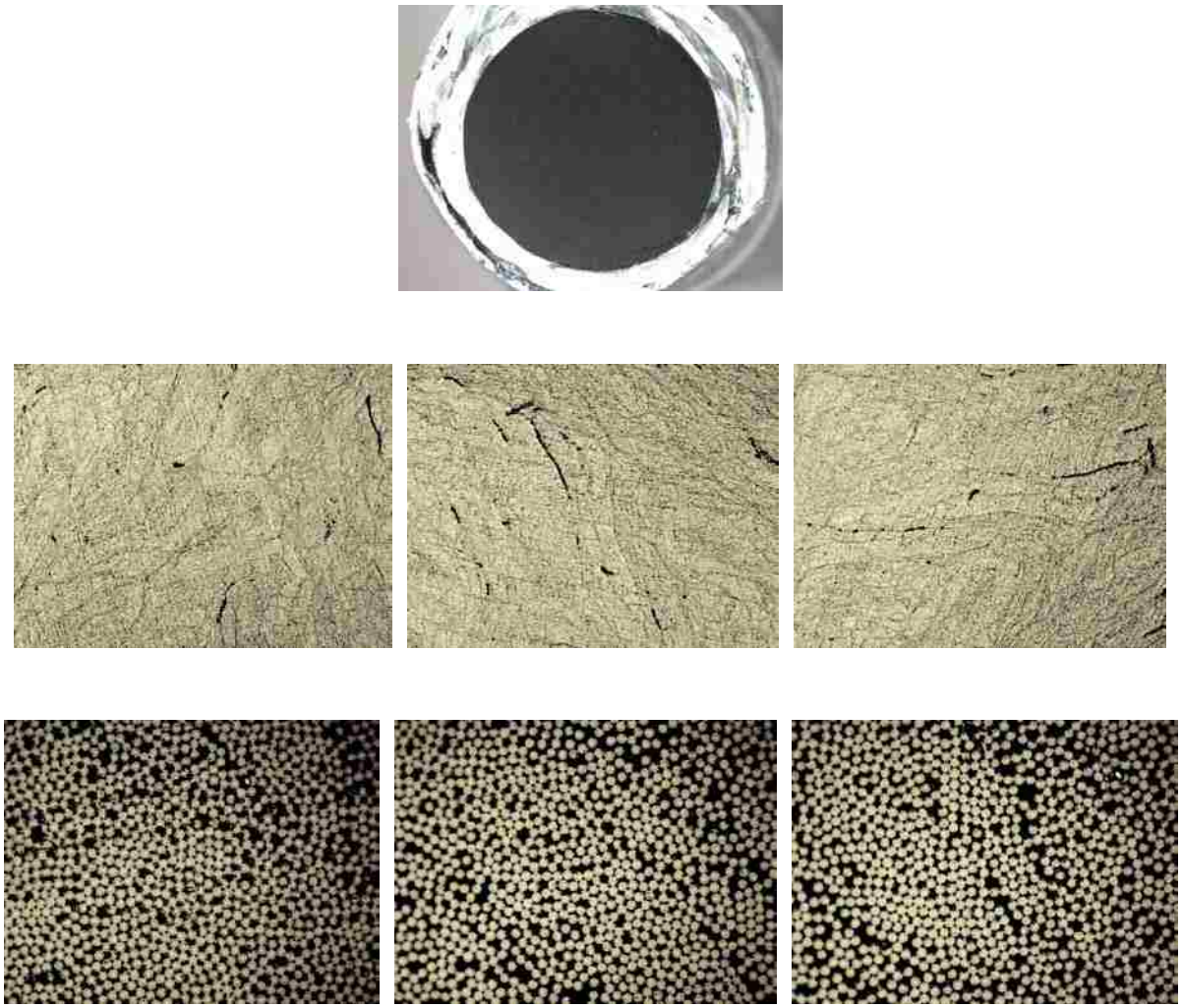

Figure C.5: FB-5-2-10 at 10x Magnification (top), 50x Magnification (middle), and 500x Magnification (bottom)

Table C.2: Summary of Microscopic Measurements of Full Spiral Specimens

Batch	Area	Average Measured Void Ratio [%]	Average Measured Fiber Volume Fraction [%]
1	1	0.07	60.0
	2	0.07	57.8
	3	0.10	58.2
2	1	0.11	64.6
	2	0.12	65.9
	3	0.10	59.8
3	1	0.06	68.3
	2	0.13	67.8
	3	0.07	59.0
4	1	0.05	65.1
	2	0.07	65.6
	3	0.04	69.1
5	1	0.08	60.0
	2	0.10	60.8
	3	0.13	66.5
Average		0.09	63.2
St. Dev.		0.03	4.0

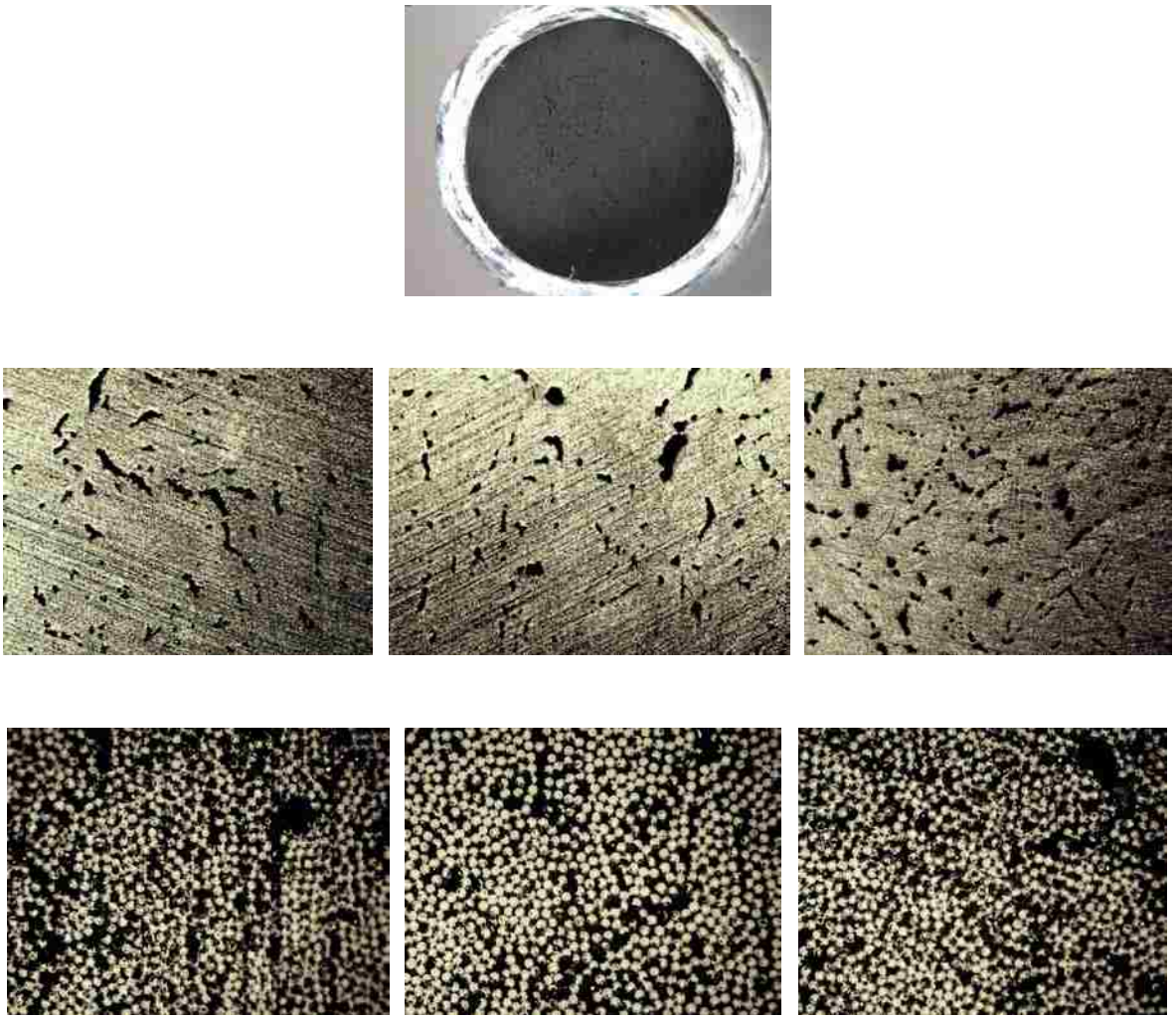

Figure C.6: FS-1-1-20 at 10x Magnification (top), 50x Magnification (middle), and 500x Magnification (bottom)

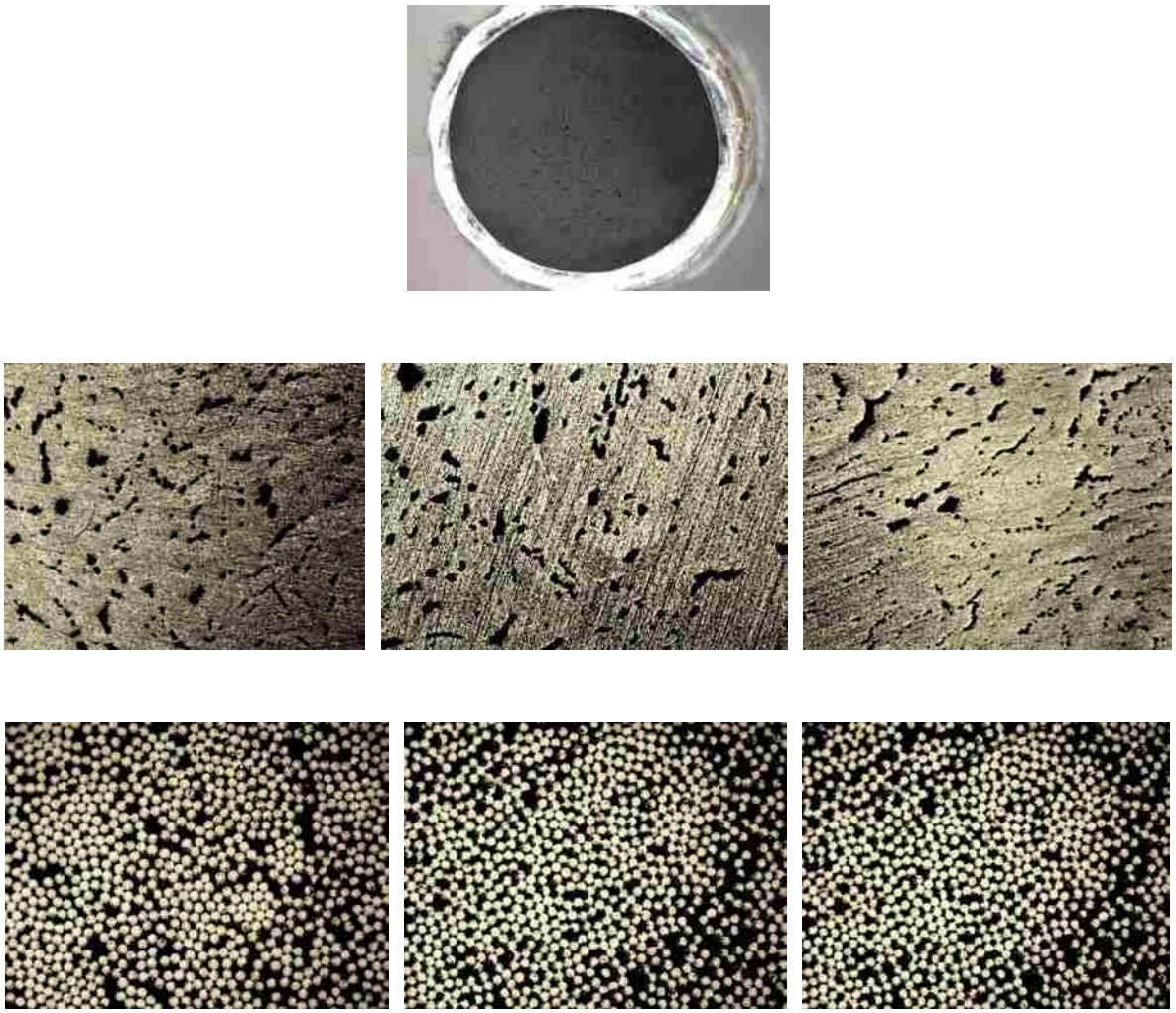

Figure C.7: FS-2-5-20 at 10x Magnification (top), 50x Magnification (middle), and 500x Magnification (bottom)

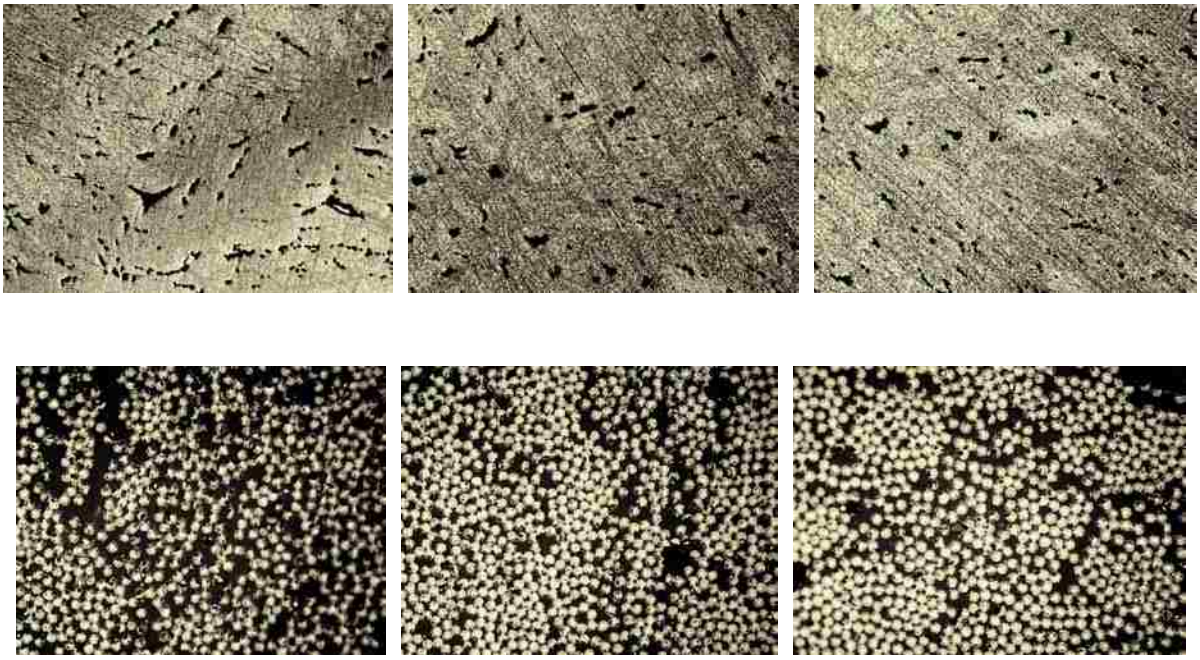

Figure C.8: FS-3-8-2.5 at 10x Magnification (top), 50x Magnification (middle), and 500x Magnification (bottom)

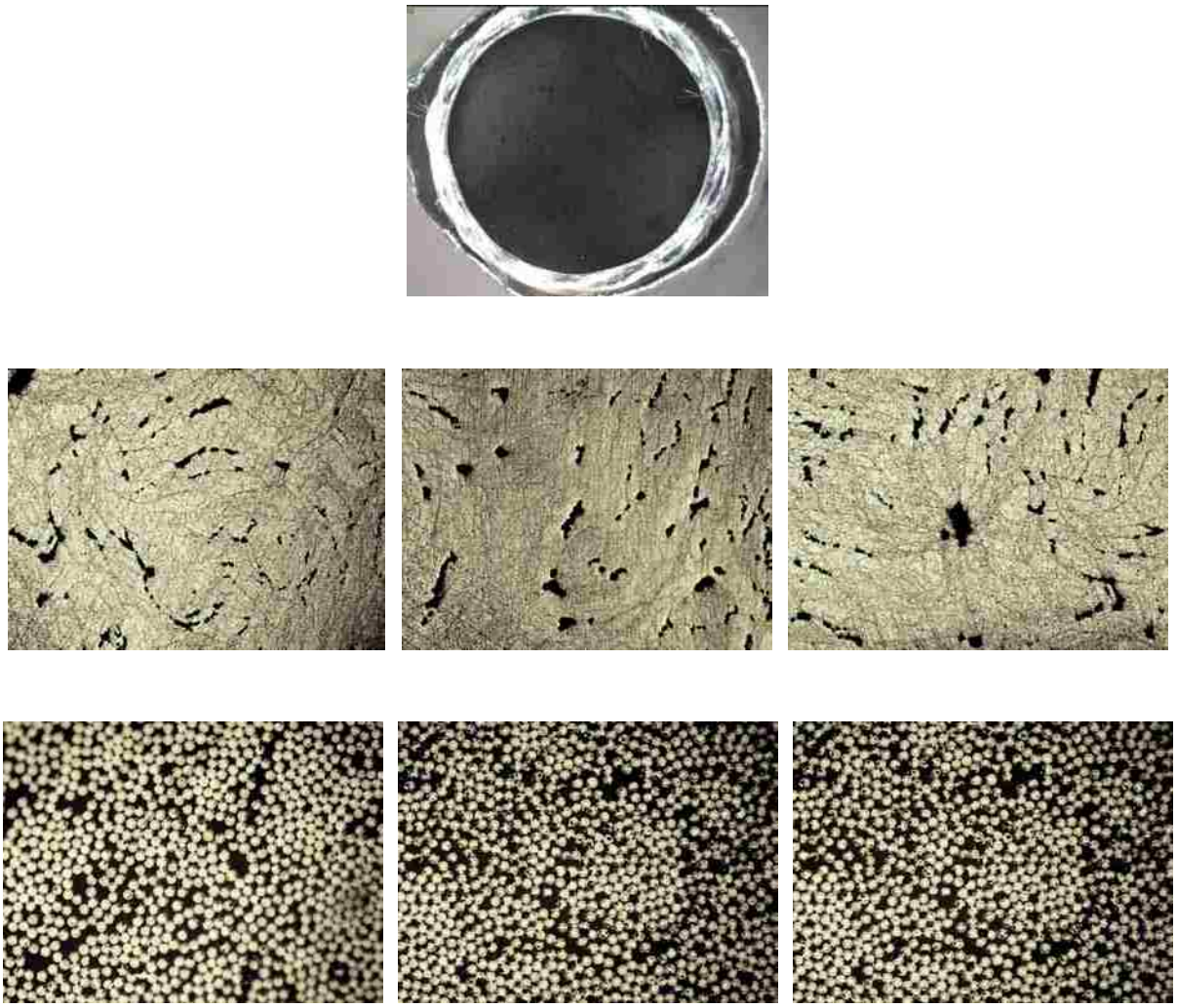

Figure C.9: FS-4-1-15 at 10x Magnification (top), 50x Magnification (middle), and 500x Magnification bottom)

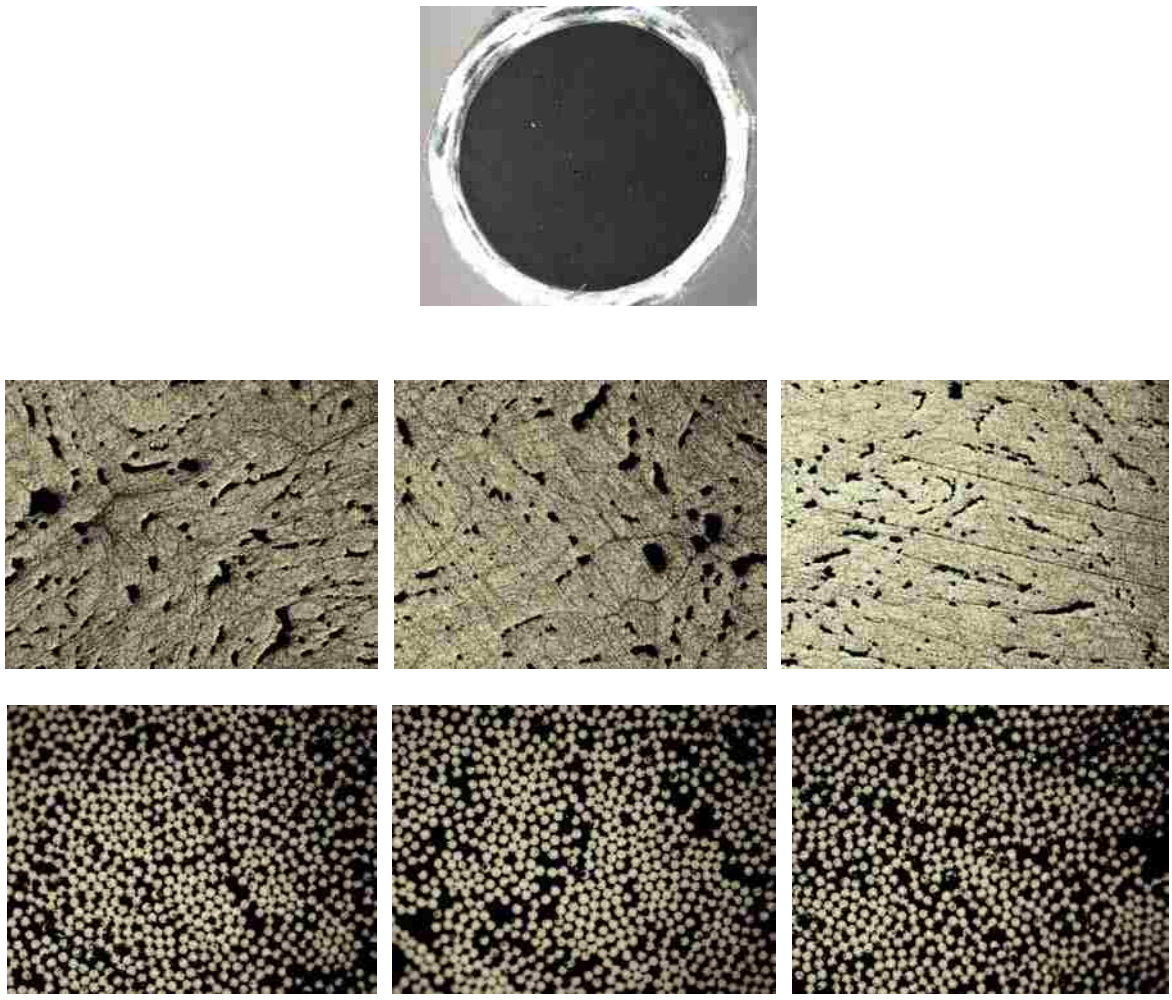

Figure C.10: FS-5-1-15 at 10x Magnification (top), 50x Magnification (middle), and 500x Magnification (bottom)

Table C.3: Summary of Microscopic Measurements of Half Braided Specimens

Batch	Area	Average Measured Void Ratio [%]	Average Measured Fiber Volume Fraction [%]
1	1	0.02	60.5
	2	0.09	56.8
	3	0.03	54.8
2	1	0.03	61.2
	2	0.02	61.0
	3	0.04	63.3
3	1	0.01	61.0
	2	0.01	71.2
	3	0.02	64.6
4	1	0.08	63.3
	2	0.04	63.6
	3	0.09	63.2
Average		0.04	62.0
St. Dev.		0.03	4.1

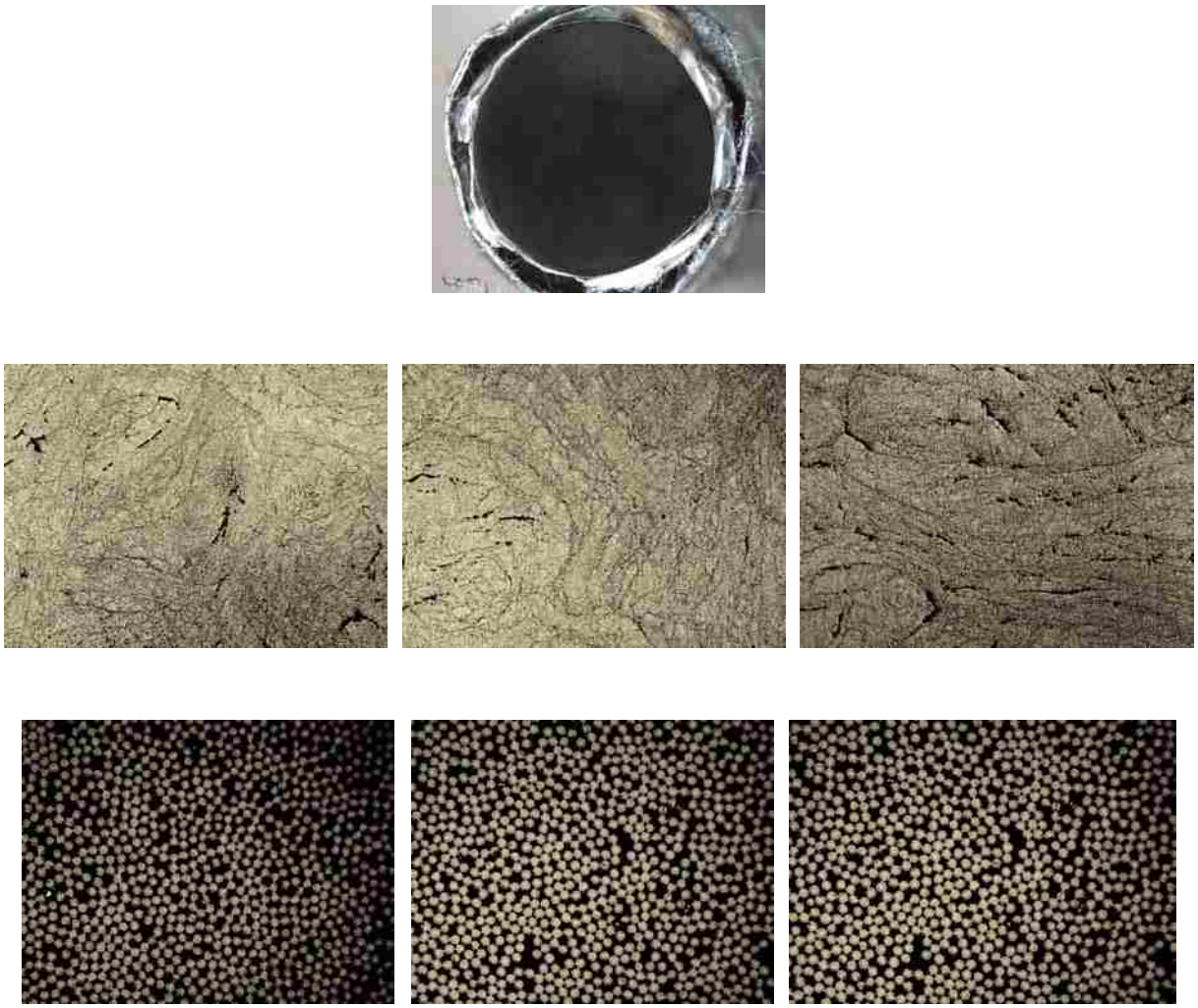

Figure C.11: HB-1-8-2.5 at 10x Magnification (top), 50x Magnification (middle), and 500x Magnification (bottom)

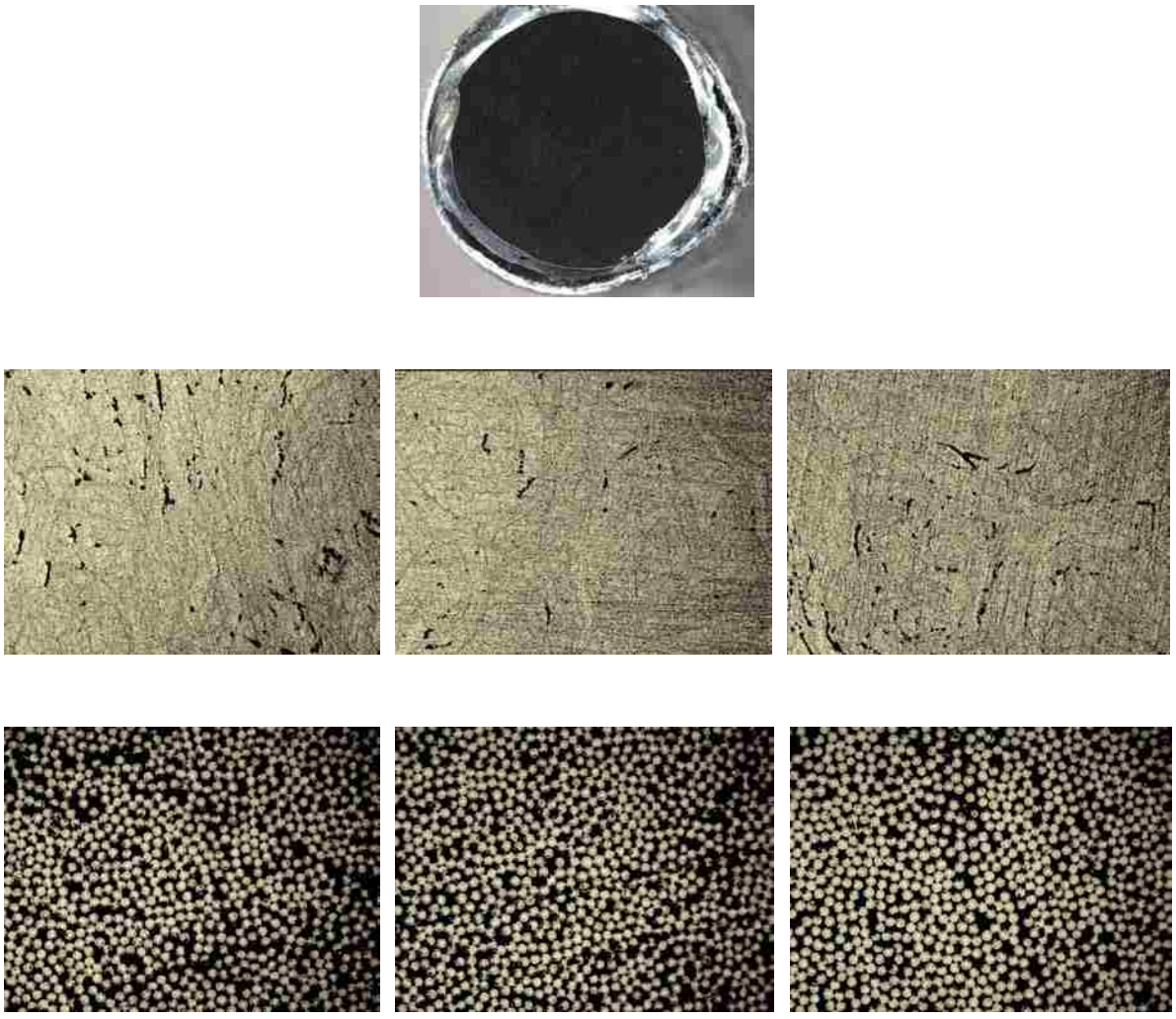

Figure C.12: HB-2-4-5 at 10x Magnification (top), 50x Magnification (middle), and 500x Magnification (bottom)

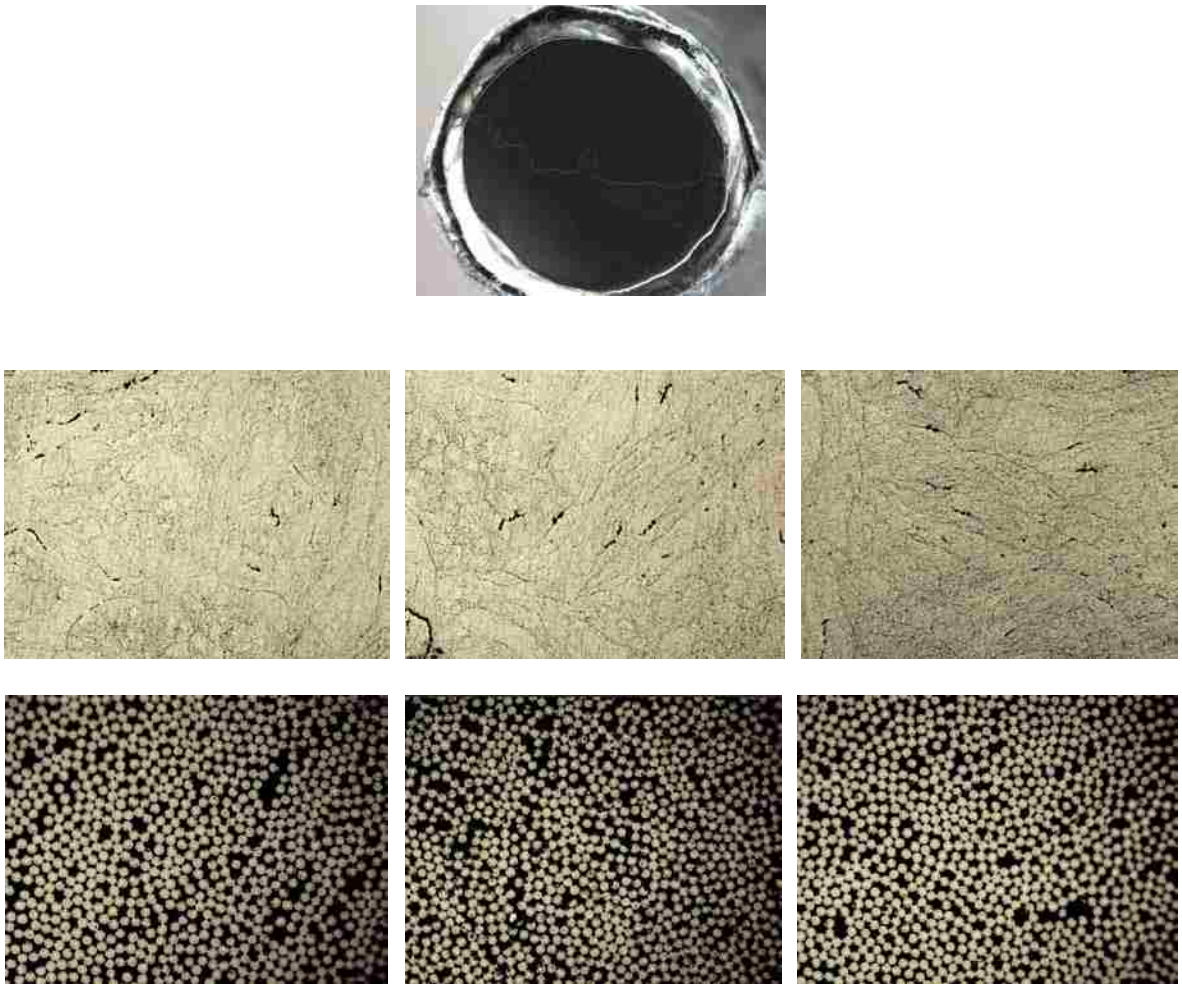

Figure C.13: HB-3-3-15 at 10x Magnification (top), 50x Magnification (middle), and 500x Magnification (bottom)

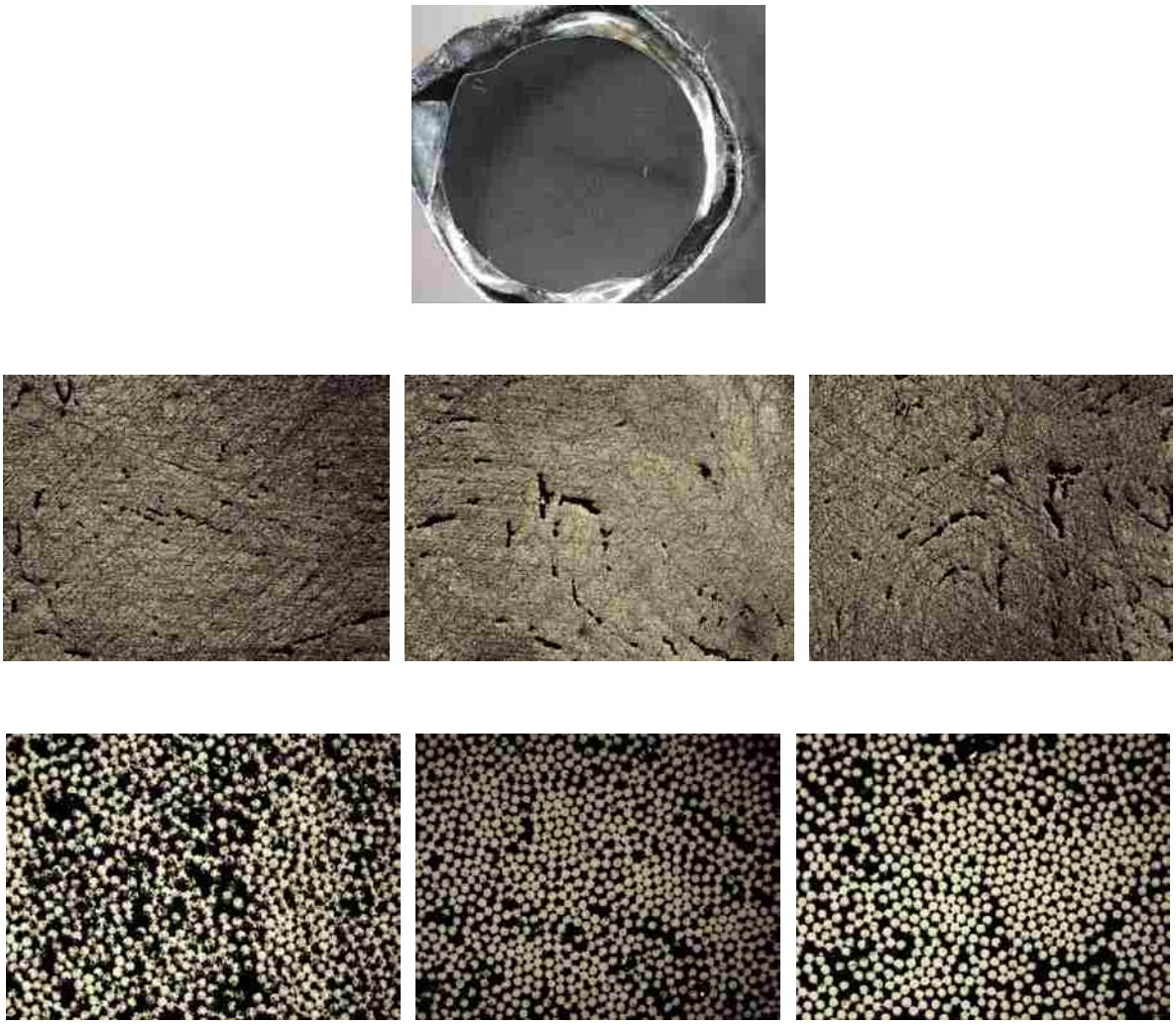

Figure C.14: HB-4-5-20 at 10x Magnification (top), 50x Magnification (middle), and 500x Magnification (bottom)

Table C.4: Summary of Microscopic Measurements of Half Spiral Specimens

Batch	Area	Average Measured Void Ratio [%]	Average Measured Fiber Volume Fraction [%]
1	1	0.08	55.9
	2	0.18	69.0
	3	0.10	67.4
2	1	0.08	57.0
	2	0.05	63.3
	3	0.10	63.8
3	1	0.06	62.8
	2	0.05	53.4
	3	0.04	64.2
4	1	0.05	68.4
	2	0.06	67.8
	3	0.07	66.1
Average		0.08	63.3
St. Dev.		0.04	5.2

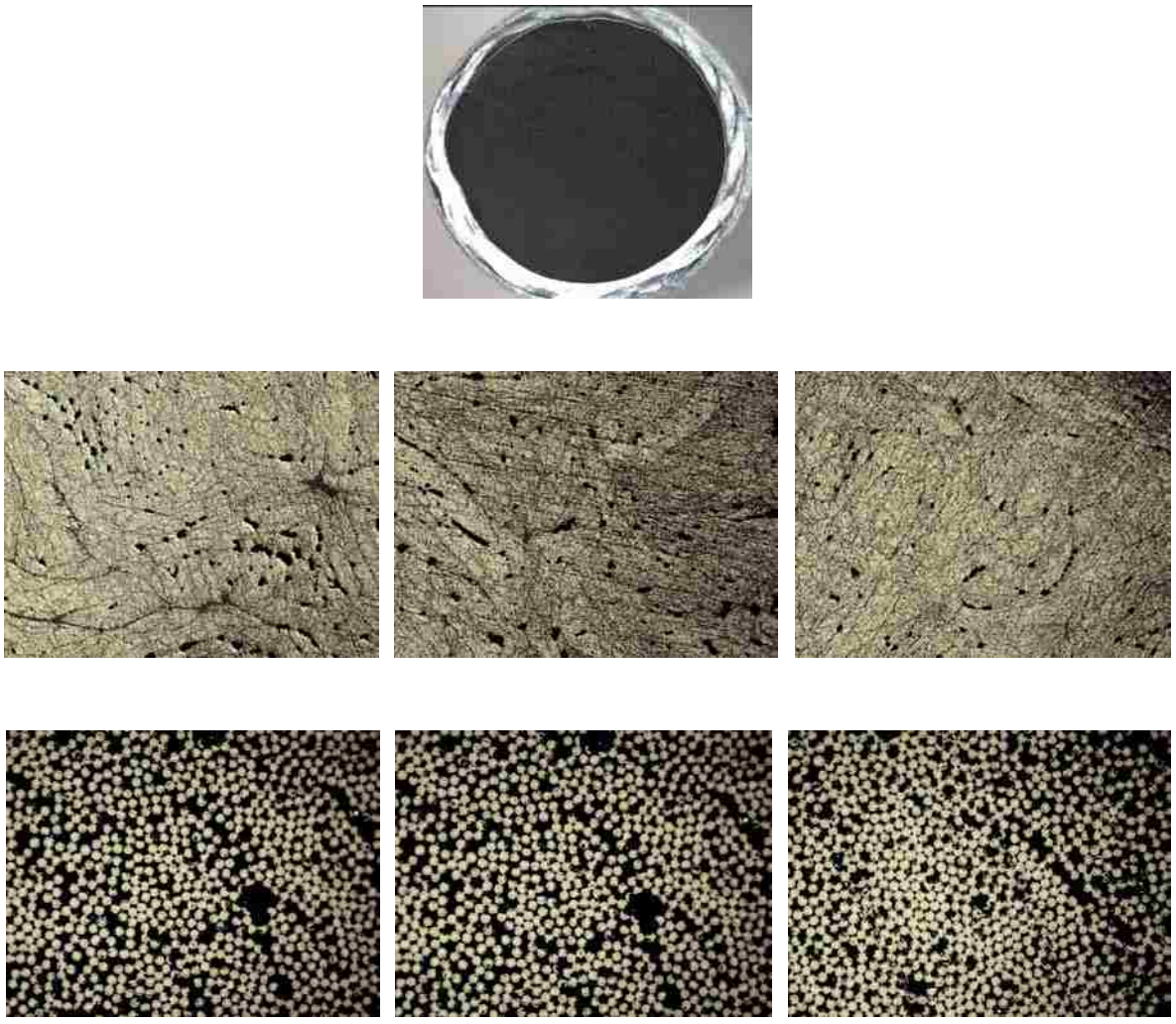

Figure C.15: HS-1-5-0 at 10x Magnification (top), 50x Magnification (middle), and 500x Magnification (bottom)

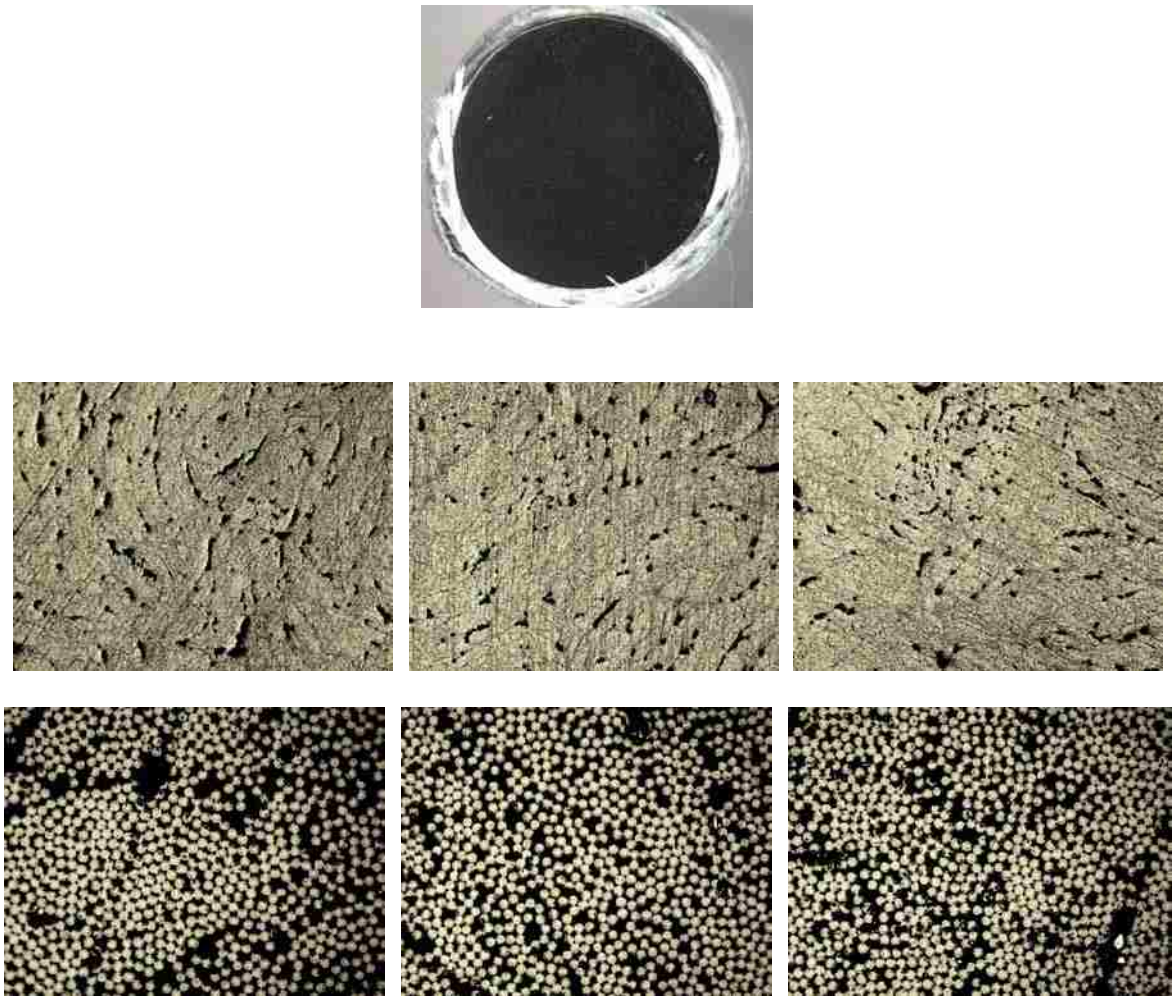

Figure C.16: HS-2-8-15 at 10x Magnification (top), 50x Magnification (middle), and 500x Magnification (bottom)

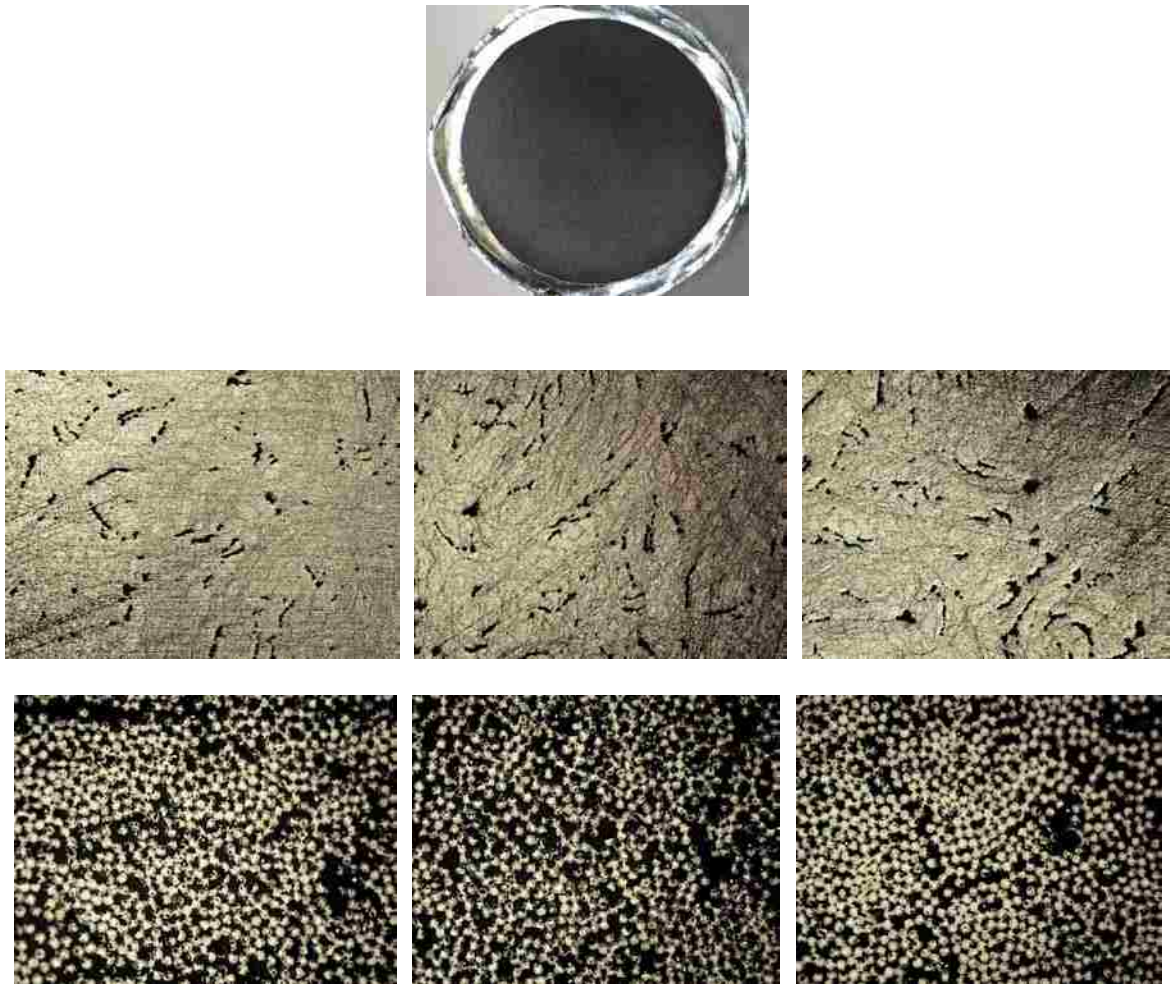

Figure C.17: HS-3-3-7.5 at 10x Magnification (top), 50x Magnification (middle), and 500x Magnification (bottom)

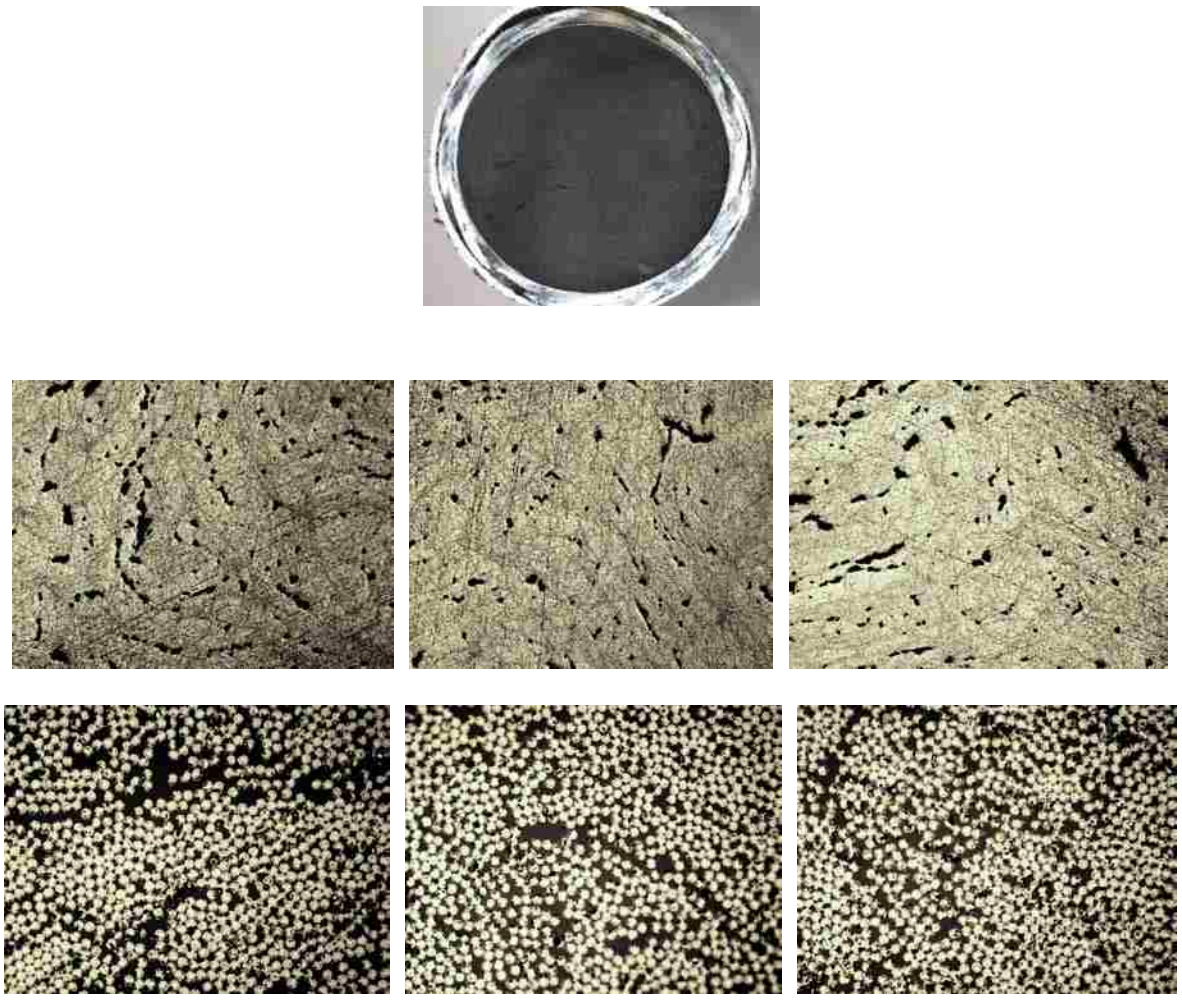

Figure C.18: HS-4-7-7.5 at 10x Magnification (top), 50x Magnification (middle), and 500x Magnification (bottom)

Table C.5: Summary of Microscopic Measurements of Shrink Tape Specimens

Batch	Area	Average Measured Void Ratio [%]	Average Measured Fiber Volume Fraction [%]
1	1	0.06	59.0
	2	0.06	64.0
	3	0.10	66.8
2	1	0.01	63.2
	2	0.02	64.1
	3	0.02	65.2
3	1	0.01	65.6
	2	0.01	61.6
	3	0.02	60.5
4	1	0.10	62.8
	2	0.04	61.1
	3	0.04	61.8
Average		0.04	66.0
St. Dev.		0.03	2.3

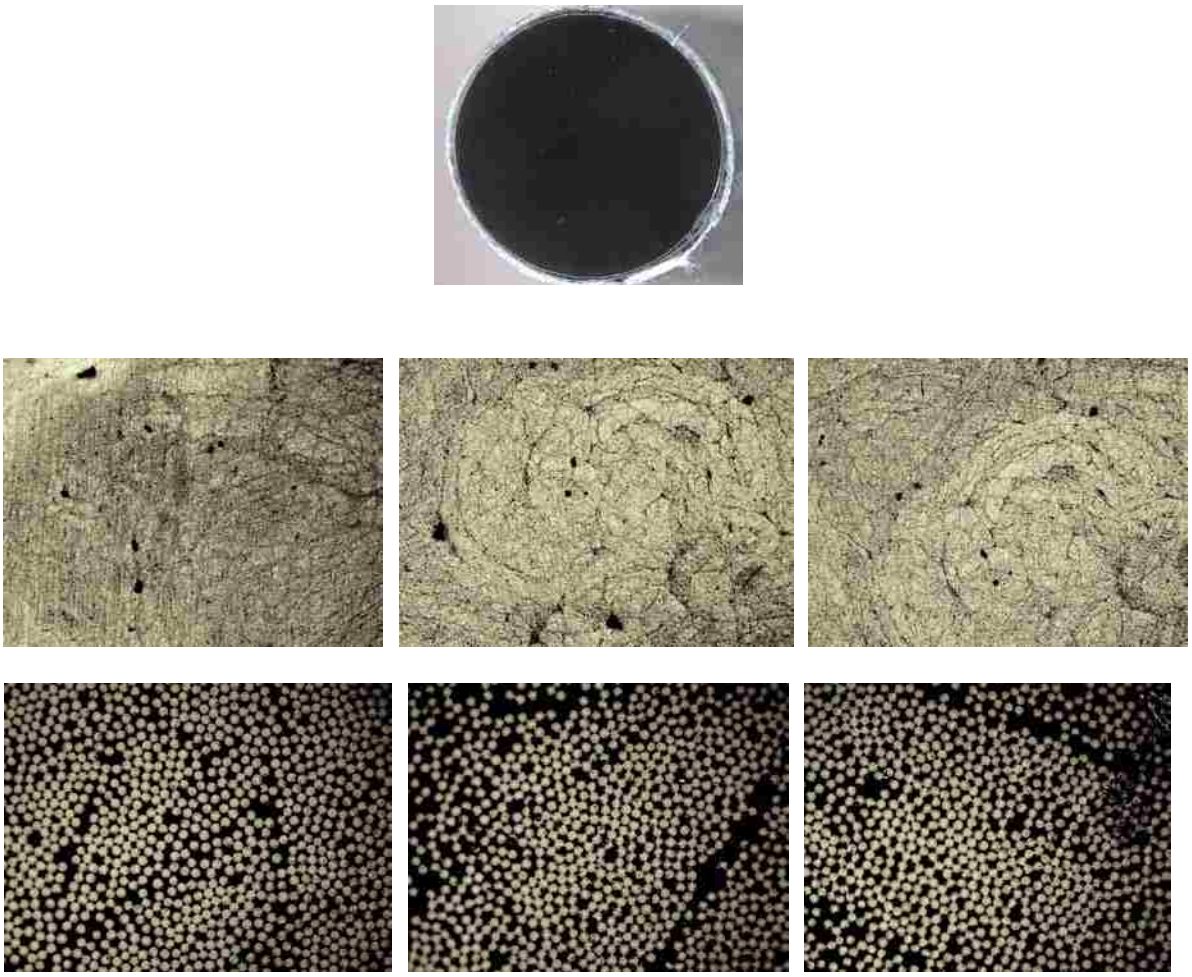

Figure C.19: ST-1-7-5 at 10x Magnification (top), 50x Magnification (middle), and 500x Magnification (bottom)

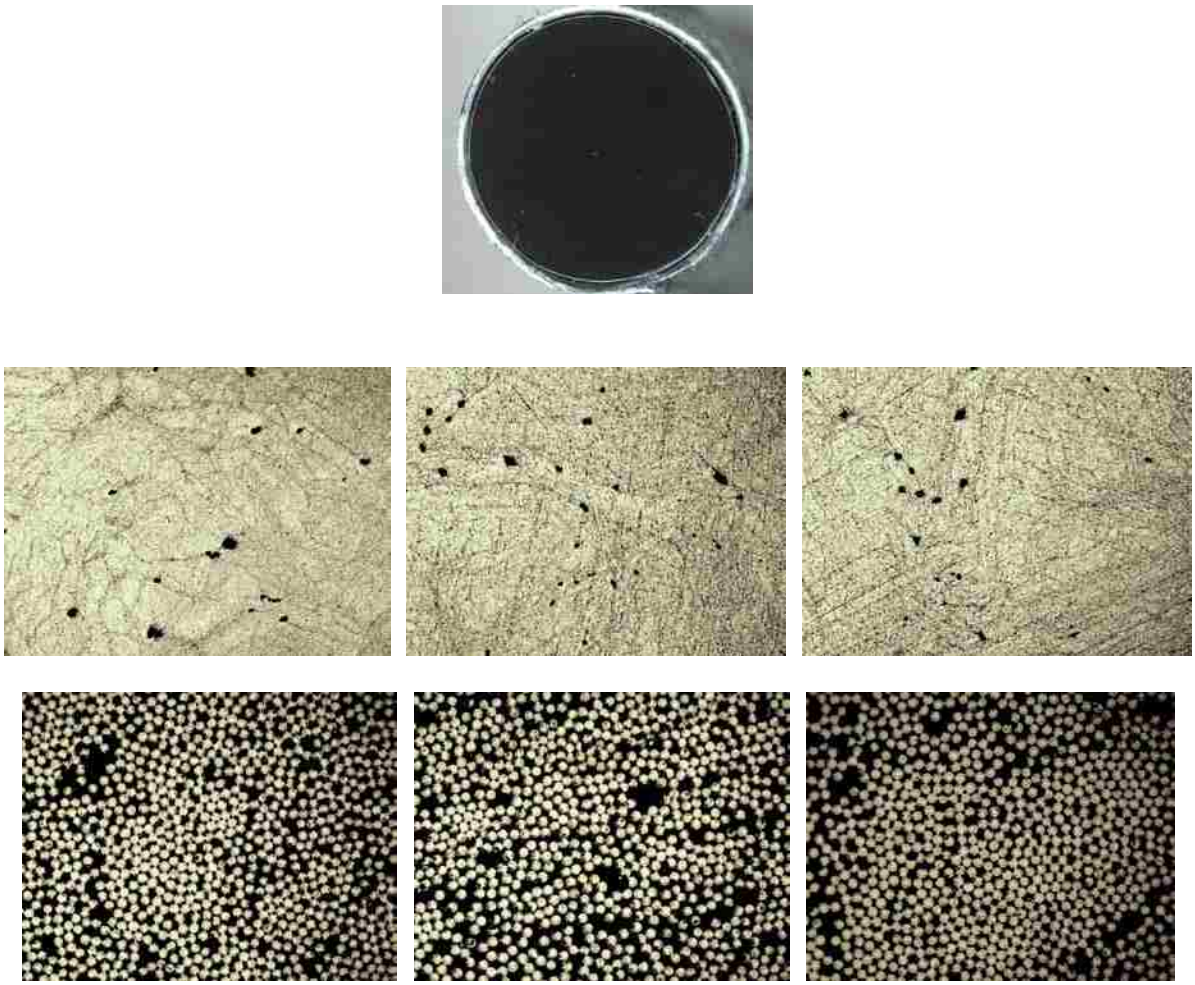

Figure C.20: ST-2-9-20 at 10x Magnification (top), 50x Magnification (middle), and 500x Magnification (bottom)

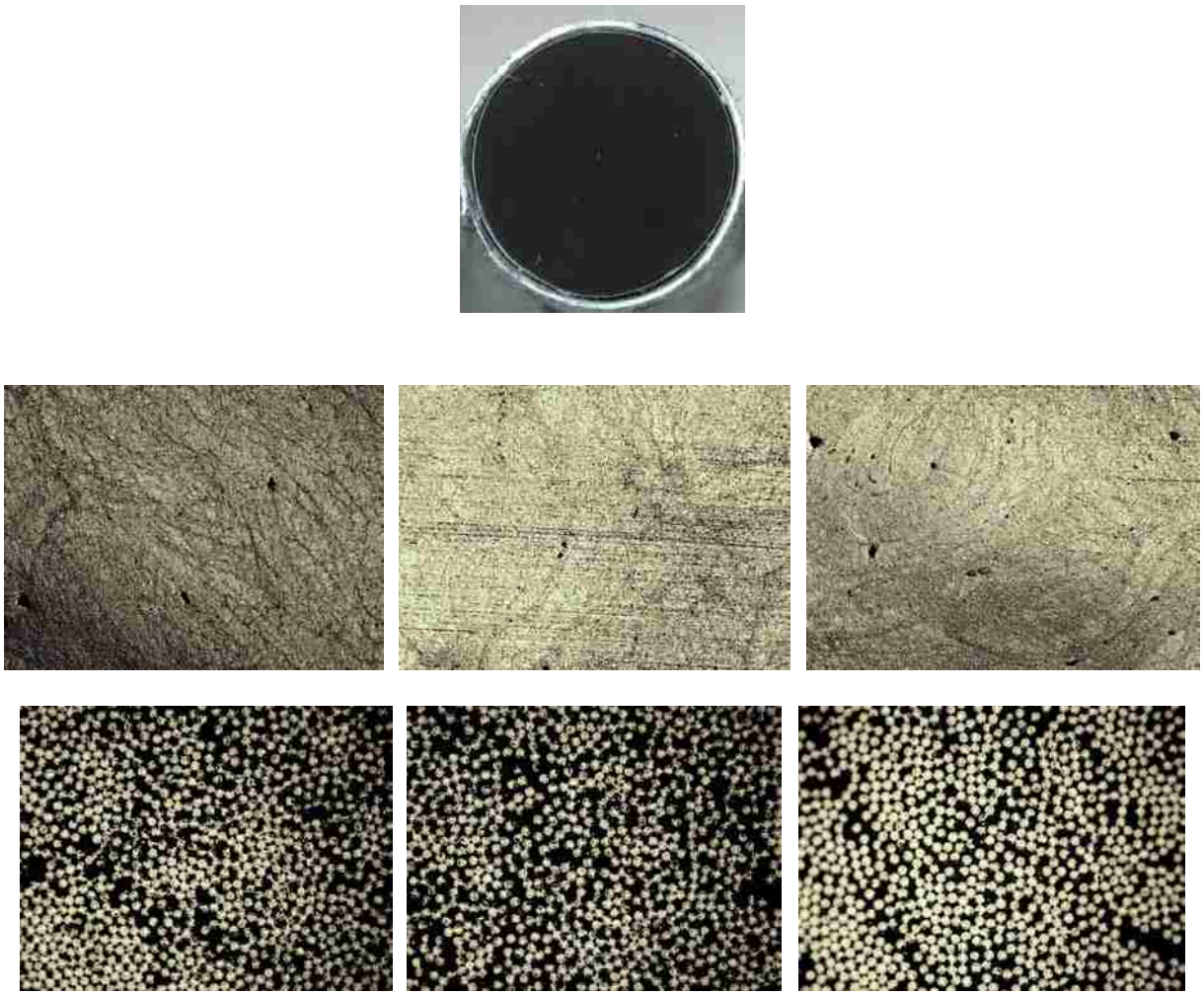

Figure C.21: ST-3-5-15 at 10x Magnification (top), 50x Magnification (middle), and 500x Magnification (bottom)

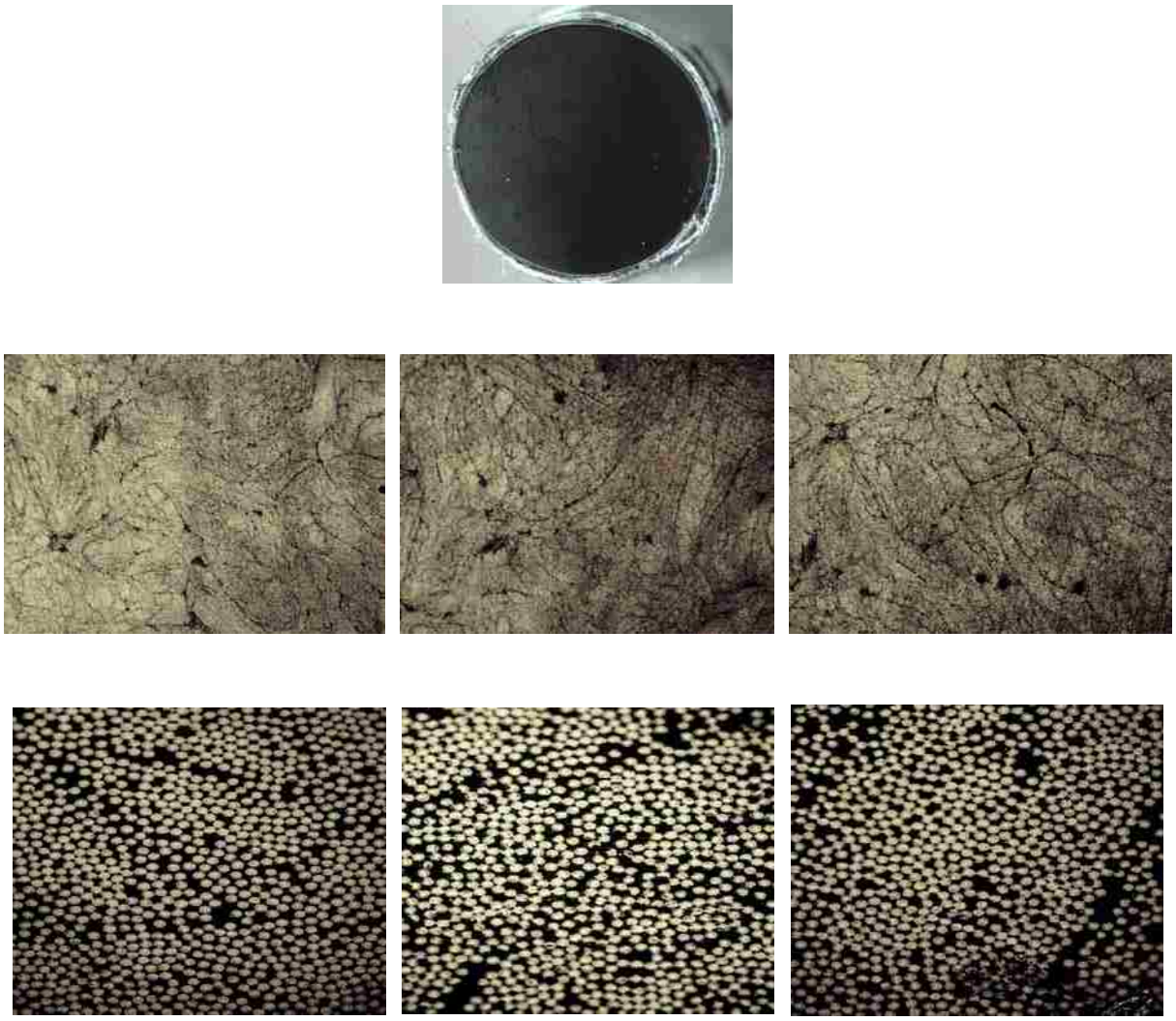

Figure C.22: ST-4-10-15 at 10x Magnification (top), 50x Magnification (middle), and 500x Magnification (bottom)